National Aeronautics and
Space Administration

NOT MEASUREMENT
SENSITIVE

NASA-HDBK-7005
MARCH 13, 2001

DYNAMIC ENVIRONMENTAL CRITERIA

NASA TECHNICAL HANDBOOK

FOREWORD

This handbook is approved for use by NASA Headquarters and all field centers and is intended to provide a common framework for consistent practices across NASA programs.

A concerted effort is underway within the NASA engineering community, under the cognizance of the NASA Office of the Chief Engineer, to promote more consistent practices across the NASA centers in the areas of dynamics and structures design and test criteria for spacecraft and payloads. This effort has resulted in NASA standards in the fields of structural design and test factors of safety, loads analyses, vibroacoustic test criteria, and pyroshock test criteria. A parallel effort, also funded by the Office of the Chief Engineer, was undertaken by the Jet Propulsion Laboratory and its contractors to summarize and assess mission dynamic environments, state-of-the-art procedures for predicting the dynamic excitations or loads induced by those environments and the structural responses to those excitations, and for establishing dynamics criteria with appropriate margins for the design and testing of a spacecraft and its components, along with the equipment and procedures used for testing. Contributions were made to this handbook by many members of the aerospace dynamics community; those contributions are gratefully acknowledged.

Requests for information, corrections, or additions to this handbook should be directed to the Mechanical Systems Engineering and Research Division, Section 352, Jet Propulsion Laboratory, 4800 Oak Grove Dr., Pasadena, CA 91109. Requests for general information concerning technical standards should be sent to the NASA Technical Standards Program Office, ED41, MSFC, AL, 35812 (telephone 256-544-2448). This and other NASA standards may be viewed and downloaded, free-of-charge, from our NASA Standards Homepage: http://standards.nasa.gov

(Original Signed By)

W. Brian Keegan
Chief Engineer

AUTHORS

Harry Himelblau
Dennis L. Kern
Jet Propulsion Laboratory
California Institute of Technology
4800 Oak Grove Drive
Pasadena, CA 91109-8099

Jerome E. Manning
Cambridge Collaborative, Inc.
689 Concord Avenue
Cambridge, MA 02138-1002

Allan G. Piersol
Piersol Engineering Company
23021 Brenford Street
Woodland Hills, CA 01364-4830

Sheldon Rubin
Rubin Engineering Company
3531 Alana Drive
Sherman Oaks, CA 91403-4708

TABLE OF CONTENTS

TABLE OF CONTENTS (CONT"D)

TABLE OF CONTENTS (CONT"D)

TABLE OF CONTENTS (CONT'D)

TABLE OF CONTENTS (CONT'D)

TABLE OF CONTENTS (CONT'D)

TABLE OF CONTENTS (CONT'D)

LIST OF FIGURES

LIST OF FIGURES (CONT'D)

LIST OF TABLES

This Page Left Blank Intentionally

LIST OF SYMBOLS

a	crack length, coefficient
A	area
A(f)	Fourier transform of acceleration response
b	slope parameter for fatigue curve
B	damping matrix, bandwidth
c	damping coefficient, material coefficient
c_0	speed of sound
C	damping coefficient matrix, cost, general coefficient
D	diameter, total distance
DI	directivity index
E	energy
$E_{xx}(f)$	energy spectral density function of x(t)
f	frequency in Hz
f_B	center frequency of bandwidth B
f_n	natural frequency in Hz
F	thrust, vector force, interface force
FF	fill factor
$F_x(f)$	Fourier spectrum of x(t)
g	grams, gravity unit
G	elastic flexibility matrix
G_{oa}	Guyan reduction matrix
$G_{xx}(f)$	autospectral density function of x(t)
$G_{xx}(k_n)$	wave-number spectral density function of x(δ)
$G_{xy}(f)$	cross-spectral density function between x(t) and y(t)
$h_{xy}(t)$	impulse response function between x(t) and y(t)
T_X	time to first crossing of level X
H	clearance distance
$H_{xy}(f)$	frequency response function between x(t) and y(t)
$j_{ik}^2(f)$	cross-acceptance function
$j_i^2(f)$	joint acceptance function
k	stiffness, coefficient, index
k_n	wave-number
$k_{n,\beta,\gamma}$	tolerance factor
K	stiffness matrix, crest ratio
L	load transfer matrix, distance
LD	deterministic induced load
LM	mechanically induced load
LR	random induced load
$L_x(f_i)$	sound pressure level in dB
L_W	sound power level in dB
m	mass, meters
M	Mach number, mass matrix
M(f)	dynamic mass
n	sample size, index
N	number of cycles to failure
p(t)	pressure time history
P	period
Pa	Pascals
$P_x(f_k)$	line (linear) spectrum of x(t)
q	flight dynamic pressure, generalized coordinate
Q	quality factor = 1/(2ζ)
Q(t)	modal forces
r	multiplier, frequency ratio
R	Reynolds Number
s	seconds
s_y	sample standard deviation of y

LIST OF SYMBOLS (CONT'D)

S	stress
$S(f_n,\zeta)$	shock response spectrum
T	time duration, averaging time
T_F	time to failure
u	unit
U	free-stream velocity
v	unit
V	velocity
V_r	ratio of volumes
w	surface weight density
W	sound power in watts
$W(f_B)$	sound power spectrum in watts
W(f)	apparent weight
X(f,T)	finite Fourier transform
$\overline{y}$	sample average of y
z_α	percentage point of standardized, normal distribution
Z(f)	impedance function
α	probability, (1 - β)
β	fractional portion
δ	boundary layer thickness, spatial variable
δ^*	boundary layer displacement thickness
Δf	frequency increment
ΔK	stress-intensity factor range
Δt	time interval
Δx	separation distance along x axis
Δy	separation distance along y axis
ϕ	normal mode shape
Φ	normal mode shape matrix
γ	confidence coefficient
$\gamma^2_{xy}(f)$	coherence function between x(t) and y(t)
η	loss factor
Λ	modal frequency vector
μ_x	mean value of x(t)
ν^+_x	number of upward crossings per unit time of level x
ν^+_0	number of upward crossings per unit time of zero
Π	power
ρ	correlation coefficient, density
σ_x	standard deviation of x(t)
τ	transmission coefficient, time delay
σ	standard deviation, radiation efficiency
ω	circular frequency
Ω^2	Squared circular natural frequency matrix
ψ_x	rms value of x(t)
ζ	damping ratio

LIST OF ABBREVIATIONS

AFB	Air Force Base
BEM	boundary element method
CDR	critical design review
CLA	critical loads analysis
CQC	complete quadratic combination
DOD	Department of Defense
DOF	degrees-of-freedom
DFL	distribution-free tolerance limits
ETL	empirical tolerance limits
FEM	finite element method
FLSC	flexible linear shaped charge
FPL	fluctuating pressure level
FRF	frequency response function
LM	mechanically induced loads
LRS	limit response spectrum
LTM	load transfer matrix
MAC	mass acceleration curve
MMAC	modal mass acceleration curve
MDF	mild detonating fuse
MEE	maximum expected environment
MIPS	mechanical impact pyroshock simulation
MUF	modal uncertainty factor
NPL	normal prediction limit
NTL	normal tolerance limit
PDR	preliminary design review
PSD	power spectral density
RF	radio frequency
RS	response spectrum
SEA	statistical energy analysis
S-N	stress versus number of cycles to failure
SRB	solid rocket booster
SRS	shock response spectrum
SRSS	square root of sum of squares
SSM	Space Station Module
TBL	turbulent boundary layer
VLC	verification load cycle
VMSS	virtual mode synthesis and simulation

This Page Left Blank Intentionally

DYNAMIC ENVIRONMENTAL CRITERIA

1. INTRODUCTION

A “watershed” period of aerospace research and development occurred during the decade of the 1960s, often referred to as the Apollo era, providing major advances to the fields of structural dynamics and aeroacoustics. Toward the end of this era, efforts were made to document and summarize these developments [1.1 – 1.9]. Since then, many improvements and a few significant breakthroughs have been made to these technologies including:

a. improved finite element method (FEM) modeling techniques
b. extension of FEM techniques to higher frequencies
c. better dynamics load analysis methods
d. more realistic methods of representing structural damping
e. improved methods for comparing the results of dynamic analyses and flight data
f. extension of statistical energy analysis (SEA) to transient conditions
g. better estimates of SEA coupling loss factors
h. application of the boundary element method (BEM) to acoustic analyses
i. development of fill factors for acoustic cavity analysis
j. widespread access to computerized dynamic databases
k. increased usage of digital data acquisition and analysis systems
l. avoidance of dynamic measurement problems through improved knowledge
m. improved transducer designs and data acquisition systems covering wider frequency ranges
n. improved knowledge of pyroshock measurement problems and limitations
o. development of nonstationary random data analysis techniques
p. better statistical data evaluation methods
q. more applications of multi-channel analyses
r. improved modal test and data processing techniques
s. better shock, vibration, and acoustic test facilities and/or control systems
t. utilization of force limiting in vibration testing
u. more realistic simulations of transient loads instead of sine sweep and dwell vibration testing.

Note that these improvements have been achieved over a wide frequency range that covers the spectra for virtually all spacecraft excitations from liquid sloshing in tanks (generally below 5 Hz) to pyroshocks (up to 100 kHz).

1.1 Purpose. The purpose of this handbook is to summarize and assess the following:

a. The dynamic environments that a spacecraft might be exposed to during its service life from the completion of its manufacture to the completion of its mission.

b. The state-of-the-art procedures for predicting the dynamic excitations (loads) produced by the dynamic environments.

c. The state-of-the-art procedures for predicting the structural responses to the dynamic excitations.

d. The state of the art procedures for establishing dynamic criteria with appropriate margins for the design and testing of a spacecraft and its components.

e. The equipment and procedures used to test a spacecraft and its components.

Although written primarily for spacecraft, many sections of the handbook may be useful for launch vehicle, aircraft, and ground transportation vehicle applications. The handbook covers a broad range of topics within the fields of aerospace structural dynamics and aeroacoustics. However, the guidelines provided herein do not encompass all the engineering and management details necessary to successfully implement a spacecraft dynamics loads design and verification program. An extensive reference list at the end of each section is provided to assist the user in addressing these details.

1.2 Handbook Organization. This handbook is organized into ten sections, including this introduction. Section 2 presents basic definitions of terms used throughout the handbook, and Section 3 outlines the relationships between dynamic environments and mission events for spacecraft. Section 4 details current procedures for the prediction of dynamic excitations, while Section 5 covers the prediction of structural responses. Various procedures for computing maximum expected environments and associated durations are presented in Sections 6 and 7, respectively. Section 8 summarizes the formulation of design criteria during the preliminary and final design stages, and the design and test margins for dynamic loads environments. Sections 9 and 10 cover general testing considerations and the performance of tests, respectively.

1.3 REFERENCES:

1.1 Potter, R. C., and Crocker, M. J., “Acoustic Prediction Methods for Rocket Engines, Including the Effects of Clustered Engines and Deflected Exhaust Flow,” *NASA CR-566*, Oct. 1966.

1.2 Sutherland, L. C., “Sonic and Vibration Environments for Ground Facilities - A Design Manual,” *NASA CR-61636,* 644 pp, Mar. 1968 (NASA Acc. N76-71920).

1.3 Archer, J. S., “Natural Vibration Modal Analysis,” *NASA SP-8012,* Sept. 1968.

1.4 Barnoski, R. L., Piersol, A. G., Van Der Laan, W. F., White, P. H., and Winter, E. F., “Summary of Random Vibration Prediction Procedures,” *NASA CR-1302,* Apr. 1969.

1.5 Himelblau, H., Fuller, C. M., and Scharton, T. D., “Assessment of Space Vehicle Aeroacoustic Noise-Induced Vibration Prediction, Design, Analysis and Testing,” *NASA CR-1596,* July l970.

1.6 Rubin, S., “Prevention of Coupled Structure-Propulsion Instability (Pogo),” NASA SP-8055, Oct. 1970.

1.7 Kacena, W. J., McGrath, M. B., Engelsgjerd, I. K., and Rader, W. P., “Aerospace Systems Pyrotechnic Shock Data,” Vol. I through VII, *NASA CR-116437,-116450,-116401,-116402,-116403,-116406,-116019,* Mar. 1970 (NASA Acc. N71-17900 through 5-19250),

1.8 Robertson, J. E., “Prediction of In-Flight Fluctuating Pressure Environments Including Protuberance Induced Flow,” *NASA CR-119947,* Mar. 1971 (NASA Acc. N71-36677).

1.9 Eldred, K. M., “Acoustic Loads Generated by the Propulsion System,” *NASA SP-8072,* June 1971.

This Page Left Blank Intentionally

2. DEFINITIONS

To facilitate a full understanding of the material presented in later sections, certain terms used routinely throughout this handbook are defined in this section. These definitions are grouped under three topics: (a) types of dynamic environments, (b) descriptions of dynamic environments, and (c) level of assembly of hardware exposed to dynamic environments.

2.1 Types of Dynamic Environments. Dynamic environments include all phenomena that produce fluctuating excitations (also called forcing functions or dynamic loads) that act on a spacecraft and/or its constituent components. The excitations may occur physically as either an applied force or an input motion, and may be either internally or externally induced. Examples of internally induced excitations include, (a) imbalance of rotating parts, (b) operation of mechanisms, (c) coupling misalignment in the assembly of hardware, (d) magnetic, aero- or hydrodynamic forces within the unit, (e) sloshing of liquid propellants in tanks, and (f) torque variations due to an uneven supply or demand of power. Since internally induced excitations are strongly related to the specific design and function of a component, they cannot be easily dealt with in the context of the general treatment intended for this handbook. However, the importance of internally induced excitations should not be overlooked. Examples of external excitations are those occurring due to handling, transportation, launch, ascent, operation in space, and, in some cases, planetary entry and landing (including the Earth).

To facilitate data analysis and testing procedures, dynamic environments are commonly classified as being deterministic, random, or a mixture of both. They also are usually classified as being stationary, nonstationary, or transient in character.

2.1.1 Deterministic Dynamic Environments. A deterministic dynamic environment is one that produces an excitation with the same time history each time the environment occurs. It follows that the instantaneous value of the excitation at any time t can be specified in advance, within reasonable experimental error, based upon a single previous measurement of the excitation. Deterministic dynamic environments are generally produced by relatively well understood and well-characterized physical processes and, hence, deterministic methods are commonly used to describe and predict the excitations and responses produced by such environments. In this regard, deterministic environments may be mathematically expressed as a function of time, x(t), by a periodic or a nonperiodic (transient) time history signal. Examples of these signals are shown in Figure 2.1. Alternatively, the Fourier transformation X(f) of the signal x(t) may be used to describe the deterministic dynamic environment in the frequency domain, as discussed later in Section 2.2.

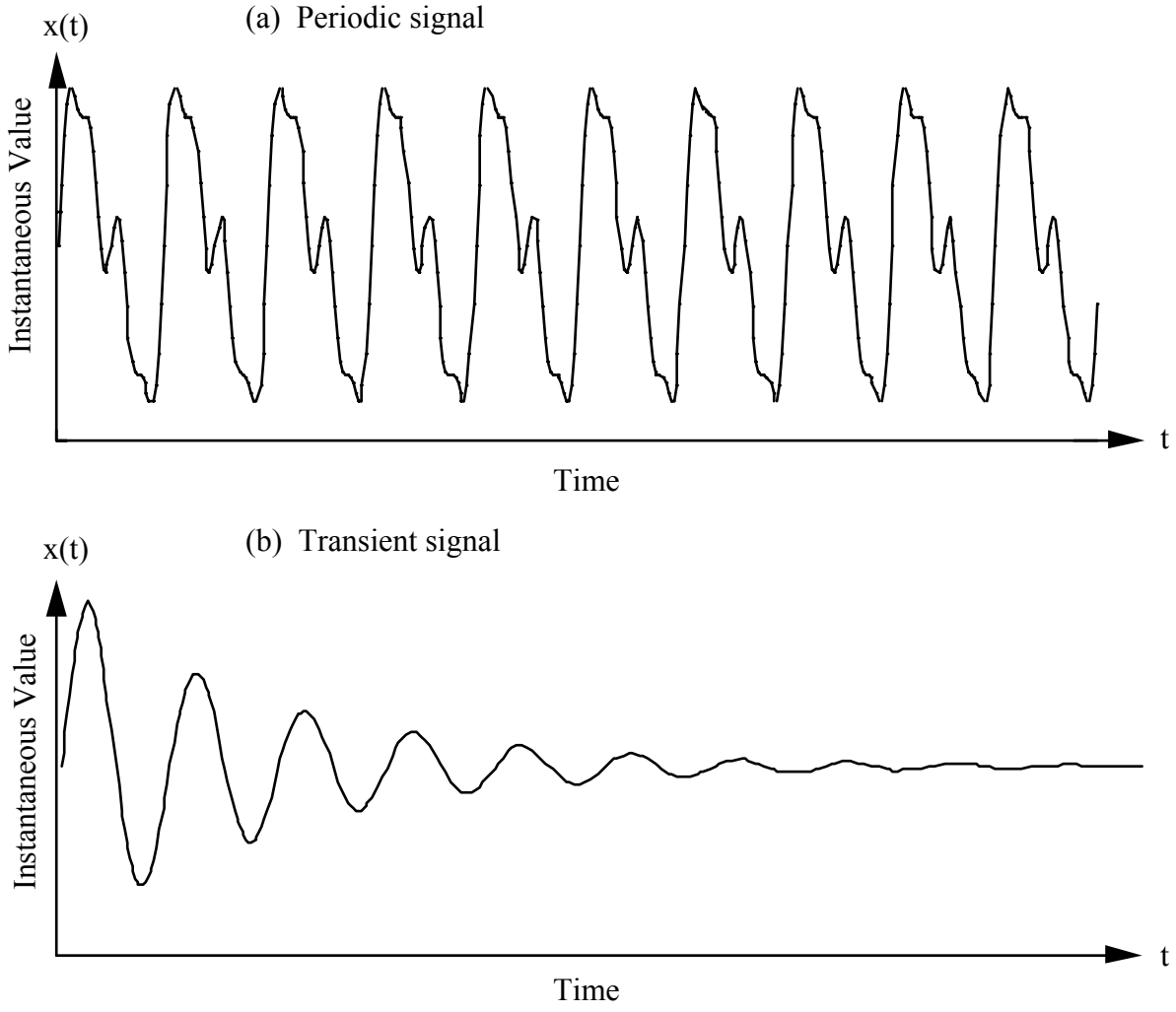

FIGURE 2.1. Illustration of Periodic and Transient Deterministic Signals.

2.1.2 Random Dynamic Environments. A random dynamic environment is one where the average properties of the time history signal characterizing the environment (e.g., the mean and standard deviation) might be the same each time the environment occurs, but the exact time history signal is not the same and, hence, the exact value of the signal at a specific time t cannot be predicted in advance based upon a previous measurement of the environment. The aerodynamic noise generated by a high velocity air flow in a pipe is an example. Commonly, a dynamic environment is a mixture of a deterministic component and a random component. Figure 2.2 shows examples of signals representing a purely random environment and a mixture of a periodic (deterministic) and a random environment, where the periodic component is as shown in Figure 2.1(a).

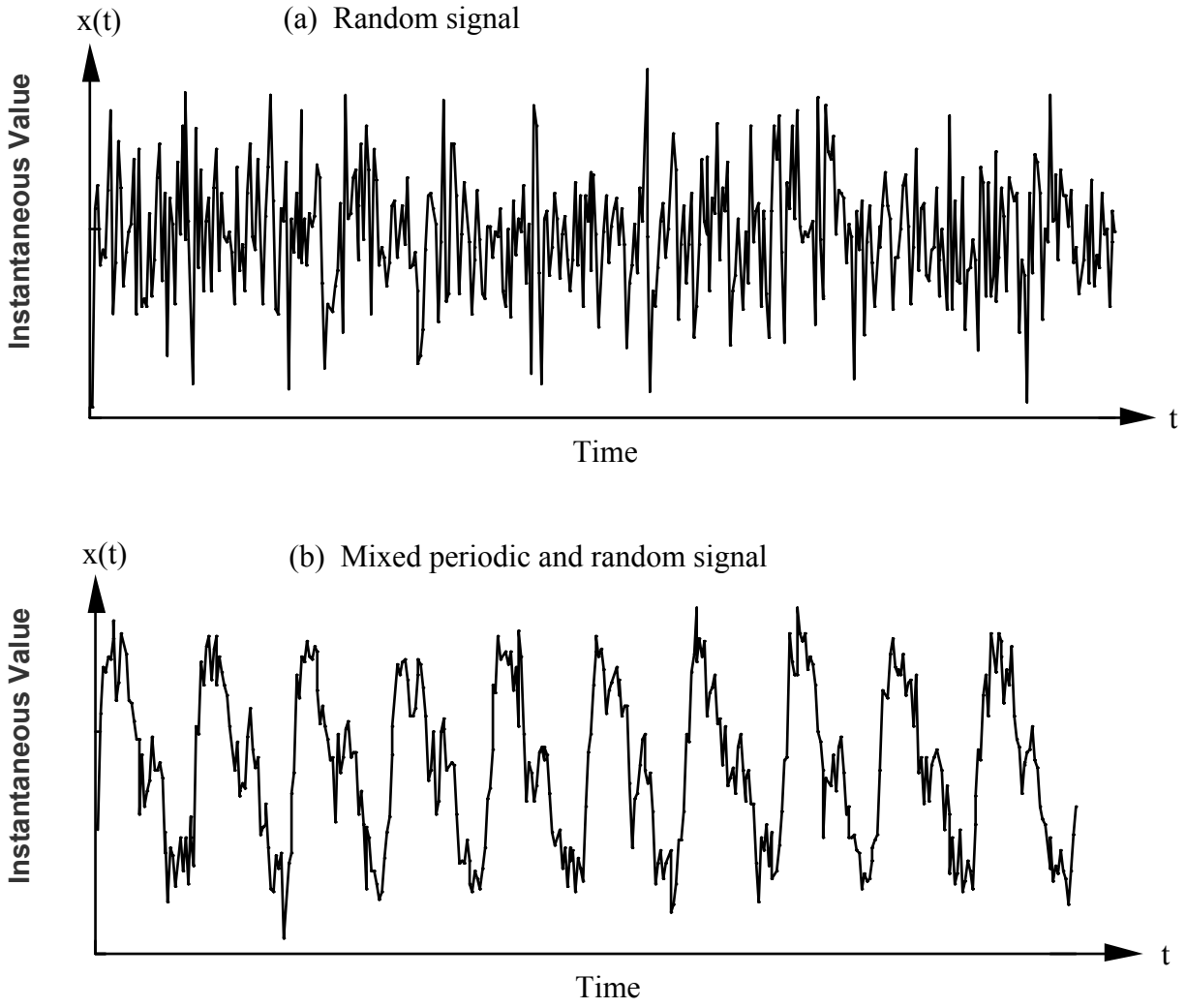

FIGURE 2.2. Illustration of Random and Mixed Deterministic-Random Signals.

A random dynamic environment is said to be either “time-invariant” or “time-varying,” depending on whether the average properties of all time history signals representing the environment do or do not vary with time, at least over the time interval of interest. Time-invariant random signals are usually referred to as “stationary” signals. When one or more of the average properties of the random signal representing the environment varies with time, the environment is said to be time-varying. Most dynamic environments experienced by a space vehicle during the launch phase are time-varying. From both a data analysis and an engineering applications viewpoint, it is convenient to divide random, time-varying environments into two categories, namely, nonstationary and transient. A random environment is said to be nonstationary if the signals representing the environment are ongoing, but have at least one average property that varies with time, e.g., the aerodynamic noise over the exterior of a space vehicle whose rms value varies during ascent through the atmosphere. An environment is said to be transient if the signals representing the environment have a clear beginning and end, and a relatively short duration compared to the decay time of the impulse response function (see Section 2.2.12) of the structures subjected to the transient environment, e.g., a rocket motor ignition overpressure, or a pyrotechnic event. Typical examples of signals representing nonstationary and transient random

dynamic environments are shown in Figure 2.3. Further details and distinctions between nonstationary and transient environments are discussed in Section 2.2.

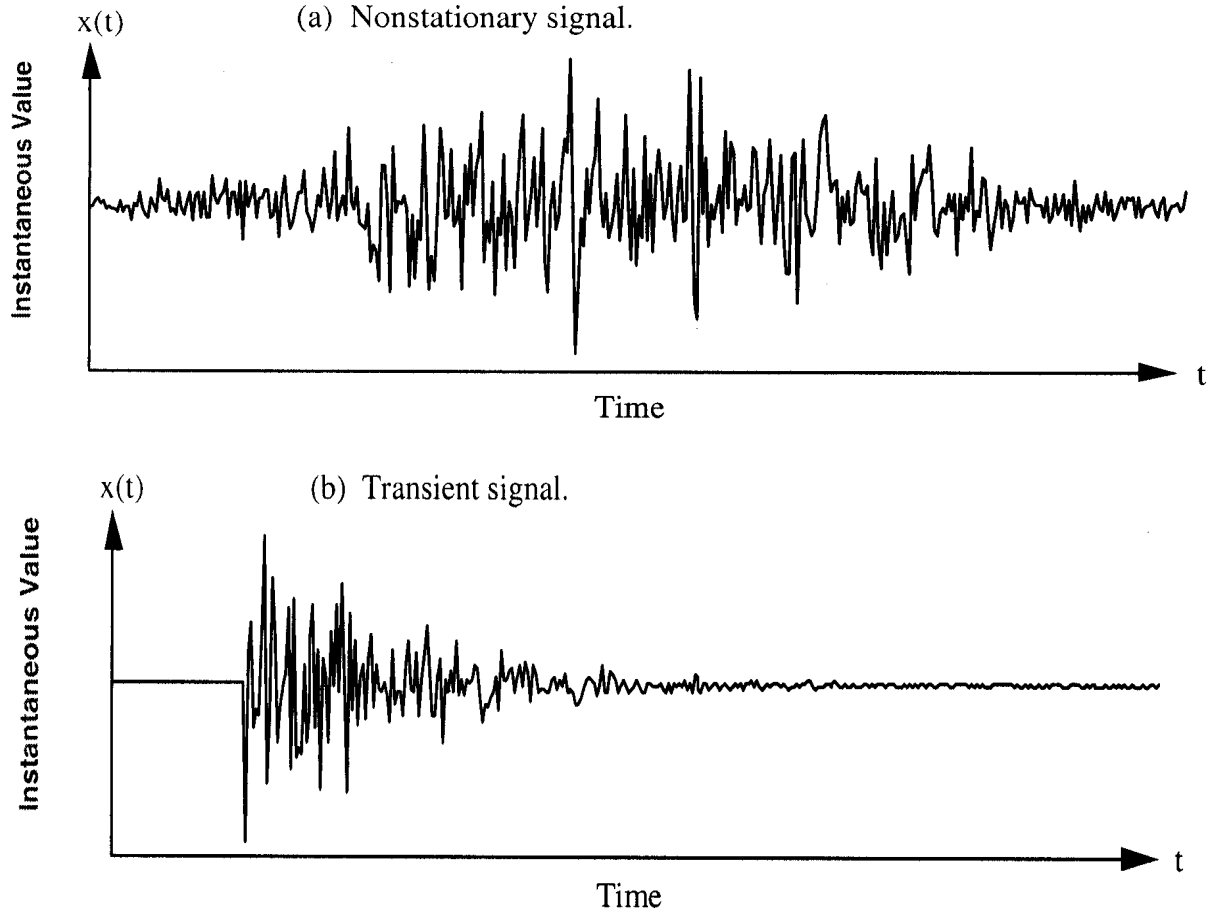

FIGURE 2.3. Illustration of Nonstationary and Transient Random Signals.

2.2 Descriptions of Dynamic Environments. There are many different ways to describe a signal x(t) representing a dynamic environment. The descriptors used in this document are: (a) representative time histories, (b) average values, (c) line spectra, autospectra, wave-number spectra, and 1/3 octave band spectra for stationary environments, (d) maximax spectra for nonstationary environments, and (e) Fourier spectra, energy spectra, and shock response spectra for transient environments. In addition, for two signals x(t) and y(t) representing two different environments or simultaneous measurements of the same environment at different locations, cross-spectra and their derivative functions (coherence, frequency response, and impulse response functions) are used to determine linear relationships. Except for time histories, 1/3 octave band spectra, and shock response spectra, all of these descriptors involve finite Fourier transforms of the signals x(t) and y(t), defined as

$$X(f,T) = \int_0^T x(t)\, e^{-j2\pi ft}\, dt \;;\; Y(f,T) = \int_0^T y(t)\, e^{-j2\pi ft}\, dt \qquad (2.1)$$

If the units of x(t) and y(t) are magnitudes in u and v (e.g., g, m, Pa, etc.) versus time in seconds (s), the units of X(f, T) and Y(f, T) are u-s and v-s versus Hz.

For clarity, all formulas in this handbook are presented in terms of continuous time and frequency domain functions. However, virtually all data analysis today is performed on discrete time and frequency domain functions using digital computers. Given a time history x(t); $0 \leq t \leq T$, which is converted to a discrete time series with a sampling interval of Δt and a total number of data values N, all equations apply with the time variable converted to $t = (n\,\Delta t)$; $n = 0, 1, 2, ..., (N - 1)$, and the frequency variable converted to $f = (k\,\Delta f)$; $k = 0, 1, 2, ..., (N - 1)$, where $\Delta f = 1/(N\,\Delta t)$. See [2.1] for details.

2.2.1 Time Histories. For low frequency (below 50 Hz) transient environments that are deterministic in character, sample time histories of the environment (such as shown in Figure 2.1) often provide an adequate description of the environment for the purposes of structural response predictions, design criteria, and/or test level determinations. However, sample time histories usually are not adequate to properly describe random environments and higher frequency deterministic environments for engineering applications.

2.2.2 Average Values. For steady-state or stationary dynamic environments represented by the signal x(t), the simplest descriptions of the magnitude of the environment are given by the mean value μ_x, which describes the central tendency of x(t), the standard deviation σ_x, which describes the dispersion of x(t), or the root-mean-square (rms) value ψ_x, which describes a combination of the central tendency and dispersion. Estimates of the mean, standard deviation, and rms value of a signal x(t); $0 \leq t \leq T$, are given by

(a) Mean value

$$\mu_x = \frac{1}{T}\int_0^T x(t)\,dt \tag{2.2a}$$

(b) Standard deviation

$$\sigma_x = \sqrt{\frac{1}{T}\int_0^T [x(t) - \mu_x]^2\,dt} \tag{2.2b}$$

(c) RMS value:

$$\psi_x = \sqrt{\frac{1}{T}\int_0^T x^2(t)\,dt} \tag{2.2c}$$

where T is the linear averaging time. It should be mentioned that high frequency dynamic environments are often measured using piezoelectric transducers that do not sense the mean value of the signal, i.e., the measured signal has no DC component. In such cases, the rms value computed in Equation (2.2c) yields the standard deviation, i.e., $\sigma_x = \psi_x$ if $\mu_x = 0$.

Time-varying average values of signals representing nonstationary environments are often computed over short, contiguous segments of the signal to obtain running averages, $\mu_x(t)$, $\sigma_x(t)$, and/or $\psi_x(t)$. For random environments, the computation of running averages requires a compromise between a random error that can be suppressed only by increasing the averaging time T, and a time-interval bias error that can be suppressed only by reducing the averaging time T. The selection of an optimum averaging time for various types of running averages is detailed in [2.1, 2.2].

2.2.3 Line Spectra. A steady-state deterministic (periodic) environment represented by the signal x(t) is described in the frequency domain by a line spectrum (sometimes called a linear spectrum), which is simply a plot of the Fourier series coefficients of x(t) given by

$$P_x(f_k) = \frac{2}{T} X(f,T) \tag{2.3}$$

where X(f,T) is defined in Equation (2.1), the factor of 2 is needed to obtain a one-sided spectrum with values at positive frequencies only, and

$$f_k = \frac{k}{T} \; ; \; k = 1, 2, 3, \ldots \tag{2.4}$$

Ideally, $T = nT_p$ where n is an integer and T_p is the period of x(t), producing a spectrum $P_x(f_k)$ that has components at the exact harmonic frequencies of the periodic function x(t), given by

$$f_p = \frac{p}{T_p} \; ; \; p = 1, 2, 3, \ldots \tag{2.5}$$

In practice, it is often inconvenient to compute a line spectrum with $T = nT_p$; n = 1, 2, 3, ... In such cases, Equation (2.3) yields spectral components at frequencies other than f_p defined in Equation (2.5). However, the computed components with the largest magnitudes will be those closest to f_p. In general, $P_x(f_k)$ in Equation (2.3) is a complex valued function that includes both magnitude and phase information, but it is common to present only the magnitude information $|P_x(f_k)|$. From Equation (2.1), the units of $|P_x(f_k)|$ are u versus Hz. See [2.3] for details and algorithms for determining accurate line spectra from computations with averaging times of $T \neq nT_p$, n = 1, 2, 3, ...

2.2.4 Autospectra. A stationary random environment represented by the signal x(t) is described in the frequency domain by an autospectral density function (also called an autospectrum, power spectrum, or PSD), which is given by

$$G_{xx}(f) = \frac{2}{T} E\left[|X(f,T)|^2\right] \tag{2.6}$$

where X(f,T) is defined in Equation (2.1), E[ ] denotes expected value of [ ], and the factor of 2 is needed to obtain a one-sided spectrum with values at positive frequencies only. Ideally, $T \rightarrow \infty$, producing a spectrum that is continuous over the frequency range of x(t). In practice, it is impossible to compute X(f,T) over an infinite time interval, so autospectra are actually estimated as a series of discrete spectral components at the frequencies given in Equation (2.4), meaning the spectral estimates have a frequency resolution of $\Delta f = 1/T$. This leads to a possible frequency resolution bias error in autospectra estimates [2.1 - 2.3]. Also, the expected value operation in Equation (2.6) implies an average over an infinite series of squared Fourier transform computations, which is impossible. However, an acceptable estimate of the autospectrum can be obtained by averaging over a finite number of squared Fourier transform computations. In practice, the averaging is usually accomplished over an ensemble of autospectra estimates computed from n_d contiguous segments of x(t). This leads to a statistical sampling (random) error in autospectra estimates.

The autospectrum $G_{xx}(f)$ in Equation (2.6) is always a real-valued function that has the units of u^2/Hz.versus Hz. See [2.1, 2.3] for details and algorithms for determining accurate autospectra from computations with a finite averaging time T and a finite number of averages n_d.

2.2.5 Wave-Number Spectra. Some environments that produce dynamic loads are more conveniently described as a function of distance rather than time, e.g., atmospheric turbulence. If such spatial dynamic environments have average properties that are invariant with distance, the environments are said to be homogeneous, which is analogous to being stationary in time. Spectra for the signals representing spatial dynamic environments are defined using the Fourier transforms in Equation (2.1) with distance, rather than time, as the independent variable, i.e., given the spatial signals $x(\delta)$ and $y(\delta)$, where δ is distance in meters (m), the spatial Fourier transforms over a total distance D are

$$X(k_n,D) = \int_0^D x(\delta)\, e^{-j2\pi k_n \delta}\, d\delta \;;\; Y(k_n,D) = \int_0^D y(\delta)\, e^{-j2\pi k_n \delta}\, d\delta \tag{2.7}$$

where k_n is called wave-number, which has the units of cycles/m. The reciprocal of wave number is wavelength ($\lambda = 1/k_n$), which has the units of m. If the units of $x(\delta)$ and $y(\delta)$ are magnitudes in u and v , respectively, (m, m/s, Pa, etc.) versus m, then the units of $X(k_n, D)$ and $Y(k_n, D)$ are u-m and v-m, respectively, versus cycles/m.

Analogous to the autospectrum defined in Equation (2.6), a wave-number spectral density function (usually called a wave-number spectrum) is defined as

$$G_{xx}(k_n) = \frac{2}{D} E\left[\left|X(k_n,D)\right|^2\right] \tag{2.8}$$

where all the approximations and errors discussed for autospectra in Section 2.2.4 apply with time replaced by distance. The wave-number spectrum $G_{xx}(k_n)$ in Equation (2.8) is always a real-valued function that has the units of u^2/(cycle/m) versus cycles/m. If a spatial dynamic environment with a wave-number spectrum of $G_{xx}(k_n)$ is transversed by a vehicle moving with a constant velocity of V in m/s, the temporal dynamic environment seen by the vehicle can be described by an autospectrum $G_{xx}(f)$ where

$$f = k_n V \quad ; \quad G_{xx}(f) = G_{xx}(k_n)/V \tag{2.9}$$

See [2.1, 2.3] for details and algorithms for determining accurate wave-number spectra from computations with a finite averaging distance D and a finite number of averages n_d.

2.2.6 1/3 Octave Band Spectra. A stationary dynamic environment, either deterministic or random, represented by the signal x(t), is often described in the frequency domain by a 1/3 octave band spectrum, which is given in dB by

$$L_x(f_i) = 10 \log_{10} \left(\frac{\Psi_x(f_i)}{\Psi_{ref}} \right)^2 \tag{2.10}$$

where $\psi_x(f_i)$ is the rms value of x(t) filtered through a 1/3 octave bandpass filter centered on frequency f_i, and ψ_{ref} is a reference rms value. The bandwidth of a 1/3 octave band filter is approximately $B_i \approx 0.23\, f_i$.

The level $L_x(f_i)$ defined in Equation (2.10) was originally developed to describe acoustic noise in terms of 1/3 octave band sound pressure levels with a reference rms pressure of ψ_{ref} = 20μPa, but the same equation with the same reference is commonly used to describe the aerodynamic-induced fluctuating pressures on the surface of a structure (aerodynamic noise). Also, it is sometimes used to describe the spectra for force and/or vibration signals with specified references. The units of the 1/3 octave band spectrum are dB (ref: 20μPa) in 1/3 octave bands versus 1/3 octave band center frequency in Hz. See [2.4] for further discussions of 1/3 octave band spectra.

2.2.7 Maximax Spectra. A nonstationary environment, either deterministic or random, is sometimes represented by a collection of signals $x_i(t)$, i = 1, 2, ..., q, which might represent, for example, measurements of the excitation at a point on a spacecraft during q different launches or at q different locations on the same launch. Each of the q measurements is often analyzed as a sequence of contiguous spectral estimates computed using Equation (2.3), (2.6), or (2.10) with a short averaging time T to obtain a time-varying spectrum, as discussed in Section 2.2.2. A single spectrum describing the environment is then determined by selecting the largest value of the time-varying spectrum computed at each frequency, independent of the time when the largest value occurs, and plotting these largest spectral values versus frequency. This is called a maximax spectrum, denoted by $P_x(f_k)_{max}$, $G_{xx}(f)_{max}$, or $L_x(f_i)_{max}$. The units of the maximax spectrum are the same as for the spectral estimates used to determine it. See [2.3] for further discussions of maximax spectra.

2.2.8 Fourier Spectra. A transient deterministic environment represented by the signal x(t) is usually described in the frequency domain by a Fourier spectrum, which is simply the Fourier transform of x(t) given by

$$F_x(f) = 2\,X(f,T) \;;\; f > 0 \qquad (2.11)$$

where X(f,T) is defined in Equation (2.1), and the factor of 2 is needed to obtain a one-sided spectrum with values at positive frequencies only. Ideally, $T \rightarrow \infty$, but this requirement is essentially met if the integration interval in Equation (2.1) includes the full duration of the transient, i.e., x(t) = 0 for t < 0 and t > T. Hence, although the Fourier spectrum is computed only at the discrete frequencies given by Equation (2.4), the exact Fourier spectrum can be interpolated from these discrete values. In general, $F_x(f)$ in Equation (2.11) is a complex valued function that includes both magnitude and phase information, but it is common to present only the magnitude information $|F_x(f)|$. From Equation (2.1), the units of $|F_x(f)|$ are u-s versus Hz. See [2.1, 2.3] for further discussions of Fourier spectra.

2.2.9 Energy Spectra. A transient random environment represented by the signal x(t) is sometimes described in the frequency domain by an energy spectral density function (usually called an energy spectrum where the term “energy” evolves from an electrical analogy), which is given by

$$E_{xx}(f) = 2\,E\left[|X(f,T)|^2\right] \;;\; f > 0 \qquad (2.12)$$

where X(f,T) is defined in Equation (2.1), E[ ] denotes expected value of [ ], and the factor of 2 is needed to obtain a one-sided spectrum with values at positive frequencies only. Ideally, $T \rightarrow \infty$, but as for Fourier spectra in Section 2.2.8, this requirement is essentially met if the integration interval in Equation (2.1) includes the full duration of the transient. Hence, although the energy spectrum is computed only at the discrete frequencies given by Equation (2.4), the exact energy spectrum can be interpolated from these discrete values.

The expected value operation in Equation (2.12) implies an average over an infinite series of squared Fourier transform computations, which is impossible. However, an acceptable estimate of the energy spectrum can be obtained by averaging over a finite number of squared Fourier transform computations. In practice, this may be accomplished by repeating the event that produces the transient n_d times, and averaging the energy spectra for the ensemble of n_d transients. In some cases, the same result can be obtained from the energy spectrum computed for a single transient event by averaging over n_d adjacent frequency components in a sequence of contiguous frequency bands, each with a bandwidth of $B = (n_d / T)$, but this approach degrades the spectral resolution of the resulting estimate. In any case, the finite number of averages n_d leads to a statistical sampling (random) error in energy spectra estimates.

From Equation (2.1), the units of $E_{xx}(f)$ are $(u\text{-}s)^2$ versus Hz, or $(u^2\text{-}s)/Hz$ versus Hz. See [2.1, 2.3] for details and algorithms for determining accurate energy spectra from computations with a finite averaging time T and a finite number of averages n_d.

2.2.10 Shock Response Spectra. The shock response spectrum (also called a shock spectrum, response spectrum, or SRS) has been traditionally used as a measure of the damaging potential of a given transient environment, either deterministic or random. For deterministic environments, the shock response spectrum concept has also been extended to calculate bound loads for design purposes (see Section 5.1).

The concept of the SRS involves a hypothetical single degree-of-freedom system (oscillator) consisting of a mass supported by a spring and a dashpot, both attached to a rigid base. The SRS, denoted by $S_x(f_n,\zeta)$, for a transient acceleration signal a(t) is commonly defined as the largest peak acceleration response of the mass of the oscillator with undamped natural frequency f_n and damping ratio ζ when the transient acceleration a(t) is applied at the base of the oscillator [2.5]. A mechanical algorithm for the SRS is shown in Figure 2.4. Although defined above in terms of acceleration for both the input and the oscillator response, the SRS is applicable to any combination of input and response parameters, including displacement, velocity, or acceleration. An implicit assumption is made in the SRS definition that the mass of the oscillator is so small compared to the mass of the base that its presence has no effect on the base input, i.e., the impedance between the oscillator mass and its base is zero. When used to estimate design loads of a multi-degree-of- freedom system in response to deterministic environments, the same definition is used with two modifications, (a) each elastic mode of the system is viewed as a single degree-of-freedom system (oscillator) with a mass represented by the so called " effective modal mass," leading to a modal SRS, and (b) the zero impedance assumption between the modal mass and the base is removed. See [2.6] for details.

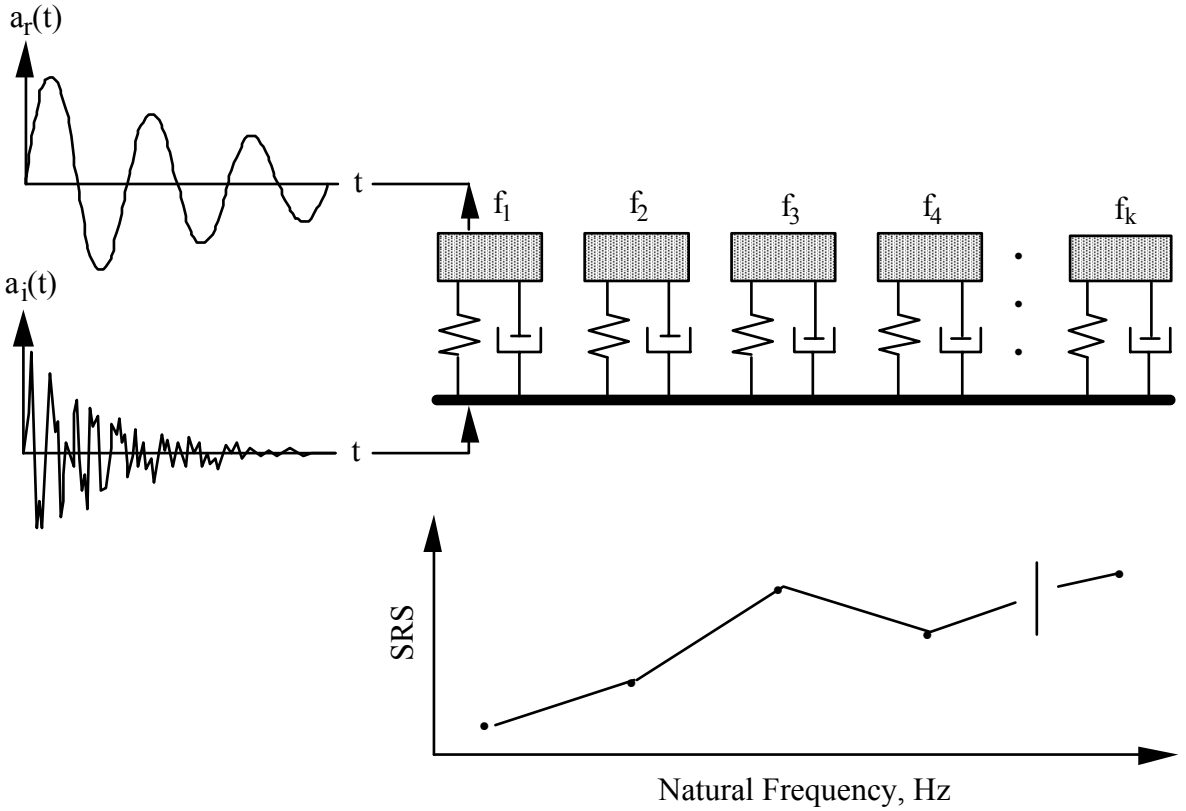

FIGURE 2.4. Mechanical Algorithm for Shock Response Spectrum Computation.

2.2.11 Cross-Spectra and Coherence Functions. The basic linear relationship between two stationary random environments, represented by the signals x(t) and y(t), is described in the frequency domain by a cross-spectrum, which is given by

$$G_{xy}(f) = \frac{2}{T} E\left[X^*(f,T)\, Y(f,T)\right] \tag{2.13}$$

where X(f,T) and Y(f,T) are defined in Equation (2.1), the asterisk (*) denotes complex conjugate, E[ ] denotes expected value of [ ], and the factor of 2 is needed to obtain a one-sided spectrum with values at positive frequencies only. Ideally, $T \rightarrow \infty$, producing a spectrum that is continuous over the frequency range of x(t). As for autospectra discussed in Section 2.2.4, it is impossible to compute X(f,T) and Y(f,T) over an infinite time interval, so cross-spectra are actually estimated as a series of discrete spectral components at the frequencies given by Equation (2.4). This leads to a possible frequency resolution bias error in cross-spectra estimates. Also, the expected value operation in Equation (2.13) implies an average over an infinite series of products of Fourier transform computations, which is impossible. In practice, the averaging is usually accomplished over n_d contiguous segments of x(t) and y(t). This leads to a statistical sampling (random) error in cross-spectra estimates. The cross-spectrum $G_{xy}(f)$ in Equation (2.13) is generally a complex valued function that has the units of uv/Hz versus Hz.

To obtain a more convenient measure of the linear dependence between two signals x(t) and y(t), the square of the cross-spectrum magnitude may be normalized by the product of the autospectra of the two signals to obtain the coherence function (sometimes called squared coherence) given by

$$\gamma^2_{xy}(f) = \frac{|G_{xy}(f)|^2}{G_{xx}(f)\, G_{yy}(f)} \tag{2.14}$$

where $G_{xy}(f)$ is the cross-spectrum between x(t) and y(t) defined in Equation (2.13), and $G_{xx}(f)$ and $G_{yy}(f)$ are the autospectra for x(t) and y(t), respectively, defined in Equation (2.6). The coherence function in Equation (2.14) is a dimensionless real number bounded by zero and unity, i.e., $0 \le \gamma^2_{xy}(f) \le 1$. See [2.1 - 2.3] for details and algorithms for determining accurate cross-spectra and coherence function estimates from computations with a finite averaging time T and a finite number of averages n_d.

2.2.12 Frequency Response and Impulse Response Functions. It is often desirable to model the linear relationship between two signals x(t) and y(t). This can be accomplished using a frequency response function (sometimes called a transfer function), which is defined as

$$H_{xy}(f) = \frac{G_{xy}(f)}{G_{xx}(f)} \tag{2.15}$$

where $G_{xy}(f)$ is the cross-spectrum between x(t) and y(t) defined in Equation (2.13), and $G_{xx}(f)$ is the autospectrum of x(t) defined in Equation (2.6). The frequency response function is generally a complex valued function that has the units of v/u versus frequency in Hz. It is often presented in terms of a magnitude function $|H_{xy}(f)|$, commonly called the gain factor of the system between x(t) and y(t), and an associated phase angle. The gain factor relates the autospectrum of a response y(t) to an excitation x(t) by

$$G_{yy}(f) = |H_{xy}(f)|^2\, G_{xx}(f) \tag{2.16}$$

The time domain equivalent of the frequency response function defined in Equation (2.16) is the impulse response function (also called the unit impulse response or weighting function), which is given by the inverse Fourier transform of the frequency response function, i.e.,

$$h_{xy}(\tau) = \int_0^\infty H_{xy}(f)\, e^{j2\pi f\tau}\, df \tag{2.17}$$

The impulse response function is more directly defined as the response of a linear system to a unit impulse (delta function) excitation. It is a real-valued function with the units of v/(u-s) versus time delay. See [2.1, 2.3] for details and algorithms for determining accurate frequency response and impulse response function estimates from computations with a finite averaging time T and a finite number of averages n_d.

2.3 Hardware Level of Assembly. The prediction of dynamic environments, as well as the formulation of design criteria and test specifications, is often accomplished for hardware at various levels of assembly. Following the definitions in [2.7], these various levels of assembly are defined as follows:

Part - A single piece, or two or more joined pieces, which are not subject to disassembly without destruction or impairment of the design use, e.g., an integrated circuit or a roller bearing.

Subassembly - A unit containing two or more parts that is capable of disassembly or part replacement, e.g., a printed circuit board or a gear train.

Unit (also called Assembly, Component, or Equipment) - A functional unit that is viewed as an entity for the purposes of manufacturing, maintenance, and/or record keeping, e.g., an electronic box or a hydraulic actuator.

Subsystem - An assembly of two or more functionally related units that may include interconnecting items, such as cables or tubing and the supporting structure to which they are attached, e.g., an instrumentation system or a propulsion system.

Vehicle - Any flight system that carries out some phase of a space mission, e.g., a launch vehicle, a satellite, or a payload.

2.4 References:

2.1 Bendat, J. S., and Piersol, A. G., *Random Data: Analysis and Measurement Procedures*, 3rd ed., Wiley, NY, 2000.

2.2 Bendat, J. S., and Piersol, A. G., *Engineering Applications of Correlation and Spectral Analysis*, 2nd ed., pp. 328 - 324, Wiley, NY, 1993.

2.3 Himelblau, H., Piersol, A. G., Wise, J. H., and Grundvig, M. R., "Handbook for Dynamic Data Acquisition and Analysis," *IES-RP-DTE012.1*, Inst. Envir. Sc.Tech., Mt Prospect, IL, Mar. 1994.

2.4 Anon, "American National Standard, Specification for Octave-Band and Fractional-Octave-Band Analog and Digital Filters," *ANSI Std S1.11-1986*, Acoust. Soc. Amer., NY, 1986.

2.5 Rubin, S., "Concepts in Shock Data Analysis", Ch. 23, *Shock and Vibration Handbook*, 4th ed., (Ed: C. M. Harris), McGraw-Hill, NY, 1996.

2.6 Trubert, M., and Salama, M. A., "Generalized Modal Shock Spectra Method for Spacecraft Loads Analysis," *AIAA J.*, Vol. 18, No 8, pp. 988-994, Aug. 1980.

2.7 Anon, "Test Requirements for Booster, Upper-Stage, and Space Vehicles," *MIL-STD-1540C*, DOD, Washington, DC, Sept. 15, 1994.

3. DYNAMIC ENVIRONMENTS AND MISSION EVENTS

The dynamic environments covered by this document are those that typically occur, or might occur, before and during the launch of a space vehicle, as well as during in-space operations and, in some cases, during landing. Twenty specific dynamic environments are considered. Since the procedures for predicting the various dynamic environments and the loads they produce often vary from one environment to another, it is necessary to clearly define each environment to be considered, and summarize its origin and basic dynamic characteristics using terms defined in Section 2.

3.1 Transportation. Space vehicles and all of their constituent elements must be transported from their points of manufacture to other points of storage and/or higher level assembly, and ultimately to a final launch site. This transportation can be by truck, train, aircraft, and/or seagoing vessel. In any case, the transportation activity will produce dynamic loads that may cause damage, particularly to the assembled space vehicle or its major subsystems. A substantial engineering effort is generally made to package space vehicle hardware for transportation in a manner that will minimize the transportation-induced dynamic loads and their resulting damage. To design appropriate packaging systems and assess the potential damage to hardware during transportation, some description of the transportation-induced dynamic loads is required. Unfortunately, these dynamic loads vary widely in character and magnitude with the mode of transportation (e.g., truck versus airplane) and the transit details (e.g., the speed of the transportation vehicle). Handling loads and the possibility of accidents (e.g., dropping a hardware item during handling) must also be considered. Some standards and specifications are currently available that define transportation-induced dynamic loads [3.1 - 3.5] and further standardization activity is in progress [3.6], but generally these loads must be measured and/or predicted on a case-by-case basis for each specific piece of hardware and its specific transportation requirements.

3.2 Seismic Loads During Pre-Launch. An important facility for the launch of space vehicles in the United States is located at Vandenberg Air Force Base (AFB) in California, which is relatively close to several earthquake faults. Although the probability is very small that an earthquake with a potentially damaging magnitude will occur during the relatively short time interval between the installation of a space vehicle on the launch pad and its launch, the possibility of such an occurrence must be considered. Of primary concern are the lateral loads that would be introduced at the base of the space vehicle by seismic induced horizontal motions of the launch pad, as well as those loads applied to a variety of ground support equipment (GSE) and flight elements prior to launch, e.g., solid rocket motors in nearby storage.

If the launch pad is supported by a hard rock site, a conventional dynamic analysis of the vehicle on its pad may be performed to determine vehicle loads and deflections during an earthquake. However, if a softer site is utilized, soil-structure interaction must be considered. Soft soil supporting the pad can be expected to permit an excess of translational and especially rotational motion at the pad/vehicle interface, causing a reduction of the system natural frequencies, an increase in the relative displacements between vehicle and GSE elements, and sometimes an increase in the vehicle loads [3.7, 3.8]. On the other hand, system damping is greatly increased due to the response-induced generation of seismic waves back into the soil.

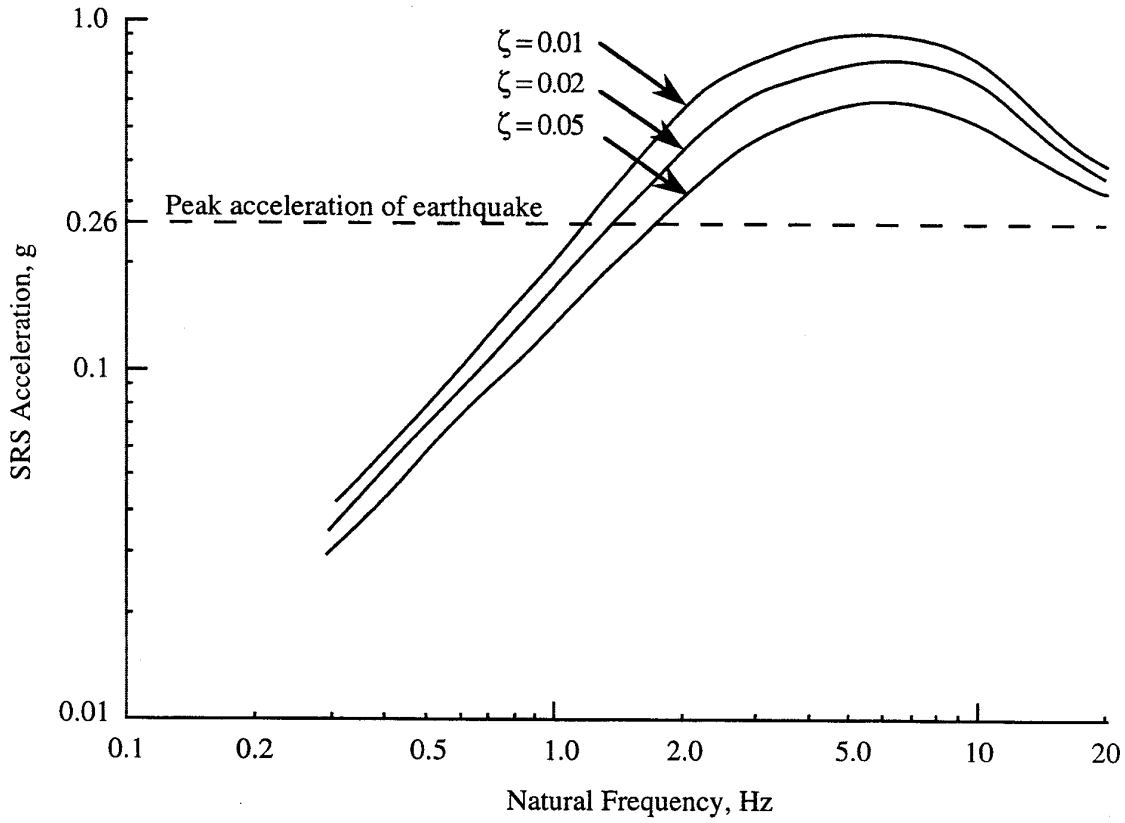

FIGURE 3.1. Shock Response Spectrum for Typical Central California Earthquake.

Earthquakes in the region near Vandenberg AFB in central California typically have durations of less than 30 seconds (although longer durations are possible) [3.9], and produce ground accelerations concentrated in the frequency range below 20 Hz [3.9, 3.10]. Using the principles of seismic risk assessment, the shock response spectrum for the earthquake design criteria developed for Space Shuttle, when it was planned to have Shuttle launches from SLC-6 at Vandenberg AFB after long on-pad exposures, is shown for three damping values in Figure 3.1 [3.9].

3.3 Wind and Turbulence. Launch vehicles and their payloads must endure loads induced by wind gusts while on the launch pad prior to liftoff and atmospheric turbulence during ascent after liftoff, as well as during the entry of reusable vehicles. Although the mechanisms that produce wind gusts [3.11] and atmospheric turbulence [3.12 - 3.14] are varied, the resulting gust velocities are random in character and generally can be described by a wave-number spectrum with a shape that is dependent on a single parameter called the integral scale, which is defined as the net area under the autocorrelation function for the turbulence signal. The wave-number spectra (normalized for an rms velocity of 1 m/s) for typical clear air turbulence with integral scales of about 120 and 300 m are shown in Figure 3.2. From Equation (2.9), even for relatively high vehicle velocities in the atmosphere, the turbulence excitation is very low frequency in character, e.g., for a vehicle speed of V = 1000 m/s, the top limit on the wave number scale in Figure 3.2 corresponds to 20 Hz. In severe atmospheric turbulence, peak gust velocities can reach 10 m/s.

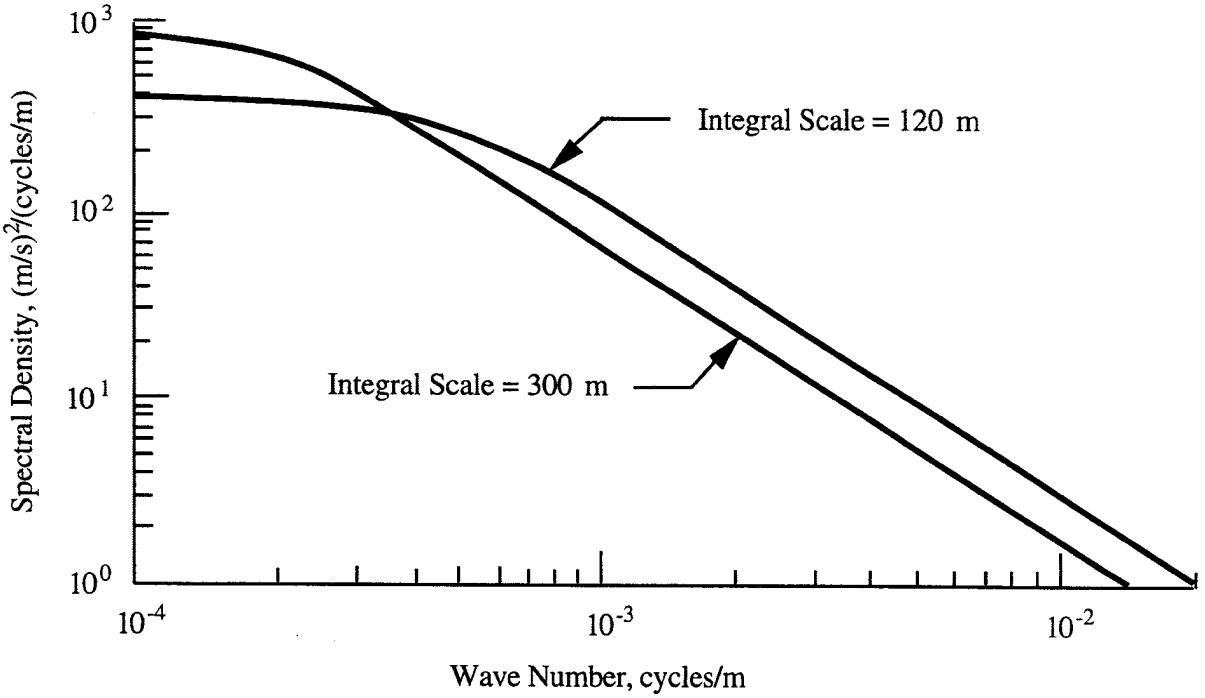

FIGURE 3.2. Wave Number Spectrum for Typical Clear Air Turbulence.

3.4 Rocket Motor Ignition Overpressure. The ignition of a solid propellant rocket motor commonly produces a shock wave that appears as a short duration overpressure transient on nearby structures, in particular, the exterior of the launch vehicle above the rocket motor nozzle. The specific characteristics of rocket motor ignition overpressures are heavily dependent on the details of the motor and the ignition procedure. Also, ignition overpressures can be suppressed by water injection on the launch pad during the motor ignition. An envelope of energy spectra computed from measured overpressures on the aft fuselage of the Space Shuttle due to the ignition of the Solid Rocket Boosters (SRBs) during an early launch is shown in Figure 3.3. Note in this figure that the dynamic load is concentrated below 20 Hz, but ignition overpressure spectra for other solid propellant rocket motors might extend up to 40 Hz. See [3.15 - 3.17] for further details on rocket motor ignition overpressures with and without water injection.

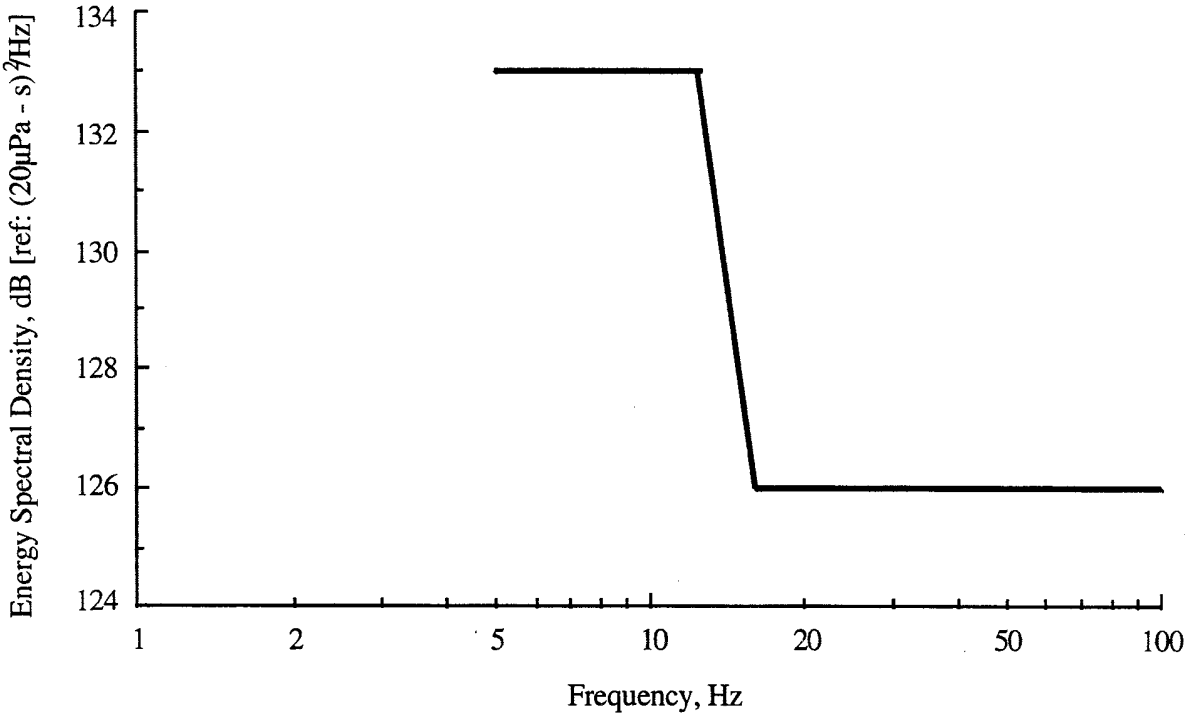

FIGURE 3.3. Energy Spectrum for Overpressure on Space Shuttle Due to SRB Ignition.

3.5 Liftoff Release Loads. Launch vehicles that use liquid propellant rocket engines for liftoff are usually held on the launch pad during thrust buildup and mechanically released after full thrust is achieved. When solid propellant rocket booster (SRB) motors are used, it is more common to allow the vehicle to freely liftoff under the SRB thrust. In either case, the rapid velocity change at liftoff produces a mechanical transient excitation along the longitudinal axis of the vehicle. This liftoff transient is a function of the engine thrust and release mechanism, or the size and ignition characteristics of the SRB motors, but it typically appears as a transient load concentrated below 50 Hz. An envelope of energy spectra computed from measured axial accelerations of Space Shuttle due to the liftoff transient is shown in Figure 3.4 [3.17]. Note in this figure that the liftoff transient energy for Space Shuttle is concentrated below 10 Hz. See [3.17] for further details and illustrations using computer models.

3.6 Engine/Motor Generated Acoustic Loads. The dominant dynamic environment at frequencies above 50 Hz for most space vehicles is the intense acoustic excitation generated by the turbulent mixing of the exhaust gases from the rocket engines/motors with the ambient atmosphere during liftoff. This acoustic excitation is random in character, and spectra for the resulting acoustic power generally collapse to a common shape when plotted against a dimensionless frequency parameter called the "Strouhal number", as shown in Figure 3.5 [3.18 - 3.21]. The sound pressure levels at various locations around the rocket engines/motors, including locations on the exterior of the space vehicle structure, are determined by (a) the number of rocket engines/motors, (b) the distance from the exhaust nozzle(s), (c) a directivity factor that is a function of frequency, and (d) the details of the launch pad, e.g., the plume deflector design and whether water injection is used [3.21]. In any case, the sound pressure levels have a wide bandwidth similar to the acoustic power spectrum in Figure 3.5, i.e., for a typical rocket motor with an exhaust gas velocity of V_e = 3,000 m/s and a nozzle diameter of D = 2 m, the upper limit on the dimensionless frequency scale in Figure 3.5 corresponds to 15 kHz.

The measurement and prediction of rocket-generated sound pressure levels is usually limited to frequencies below 10 kHz. For a large launch vehicle, the overall sound pressures on the exterior of the structure during liftoff can exceed 160 dB (ref: 20μPa). Of course, these levels diminish rapidly as the vehicle gains speed, and disappear when the vehicle goes supersonic.

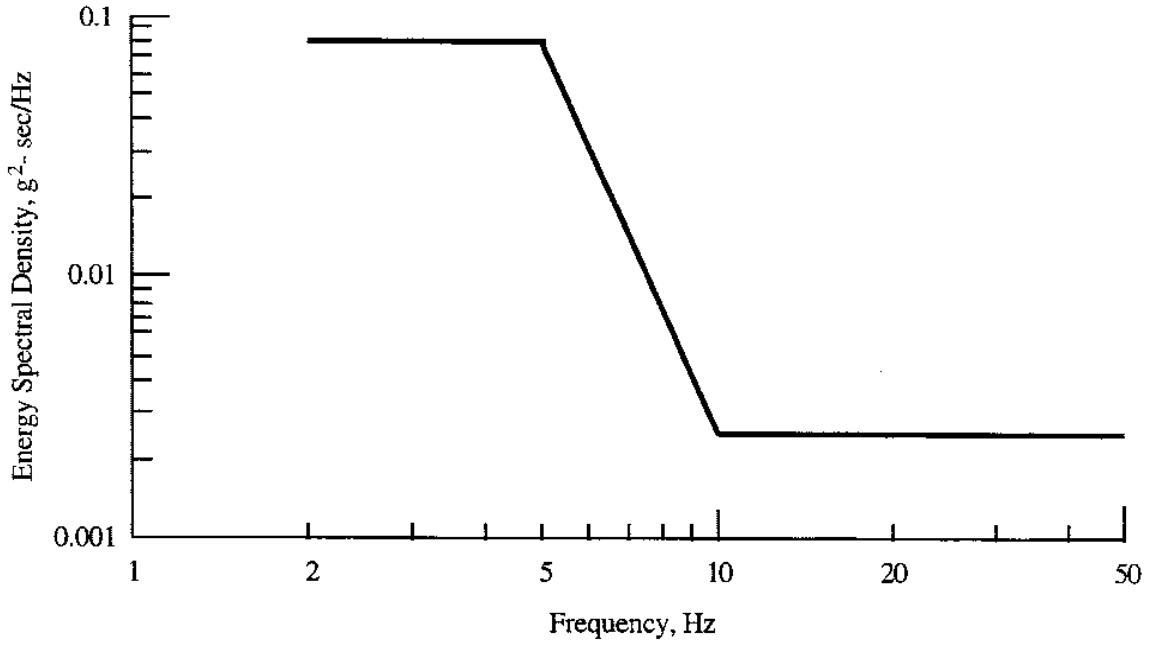

FIGURE 3.4. Energy Spectrum for Axial Acceleration of Space Shuttle Due to Liftoff Transient.

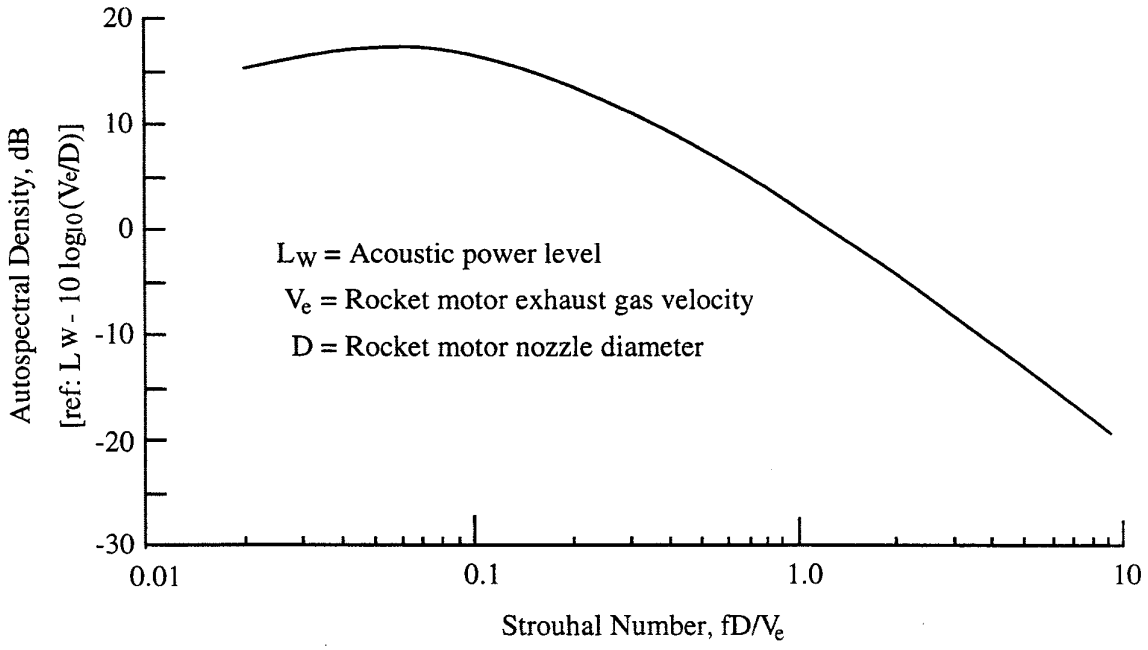

FIGURE 3.5. Normalized Autospectrum for Acoustic Power Generated by Rocket Engines/Motors.

3.7 Engine/Motor Generated Structureborne Vibration Loads. In addition to the airborne acoustic noise generated by the rocket engines/motors during liftoff, there is also some direct mechanical excitation produced by the combustion process inside the engines/motors that may transmit directly to the launch vehicle structure through the engine/motor mounts. Like the airborne acoustic noise, the structureborne noise is random in character, except for the periodic excitations discussed in Section 3.12. On the other hand, unlike the airborne acoustic noise that diminishes with increasing vehicle speed, the structureborne noise continues as long as the rocket engines/motors are operating. The resulting vibration levels at payload locations inside the vehicle are generally small compared to the vibration levels created by the airborne acoustic noise during liftoff. Nevertheless, there may be launch vehicle structure near the engine/motor attachment points where the structureborne noise-induced vibration is significant and warrants attention, particularly if the vibration is periodic (see Section 3.12). Structureborne noise due to direct mechanical excitation from rocket engines/motors usually covers a wide frequency range (about 20 Hz to 2 kHz), but its overall value and spectrum are heavily dependent on the details of the rocket engines/motors and the structure near the engine/motor attachment points, and must be evaluated on a case-by-case basis. See [3.22] for further details and illustrations.

3.8 Aerodynamic Sources During Ascent and Entry. As a space vehicle accelerates through the atmosphere, the relative velocity between the vehicle and the ambient atmosphere generates fluctuating pressures in a turbulent boundary layer (TBL) between the exterior surface of the vehicle structure and the atmosphere (often referred to as aerodynamic noise). These TBL pressures are random in character. For a flat structure parallel to the direction of the air flow, the magnitude and the spectrum for the TBL pressures generally reduce to the plot shown in Figure 3.6 [3.23 - 3.26]. The overall value of the TBL pressures is a function of the flight dynamic pressure ($q = 0.5\ \rho\ V^2$, where ρ = air density and V = velocity) and vehicle Mach number (M), while the cutoff frequency of the spectrum (f_0) is a function of the vehicle velocity (V) and the boundary layer displacement thickness parameter ($\delta*$), which increases with distance from the leading edge of the structure. Nonuniform structural geometries, such as conical skirts between stages, substantially modify both the magnitude and the spectrum of the TBL pressure [3.27, 3.28]. Also, at speeds above about Mach 0.85, shock waves are commonly created that interact with the TBL to further exaggerate the pressure levels [3.18, 3.28] and sometimes produce buffet loads. Finally, aerodynamic instabilities in payload fairing or bay vents may produce tonal pressure fluctuations on payloads, particularly during ascent [3.29].

The spectrum for TBL pressures generally covers a wide frequency range, e.g., for a vehicle traveling at a speed of V = 500 m/s and a relatively large boundary layer displacement thickness of $\delta^* = 0.01$ m, the cutoff frequency in Figure 3.6 is $f_0 = 5$ kHz. The measurement and prediction of TBL pressure levels are usually limited to frequencies below 10 kHz. In general, the TBL excitation at a given location first increases and then decreases as the vehicle accelerates through the atmosphere during launch, reaching a maximum when the flight dynamic pressure reaches a maximum (referred to as q_{max}). However, at some locations, particularly those near the forward end of the launch vehicle, shock wave-boundary layer interactions during transonic flight often produce pressure levels that exceed those that occur at q_{max}. A similar situation occurs during the entry of reusable vehicles into the Earth's atmosphere, although the entry q_{max} is usually lower than the launch q_{max}.

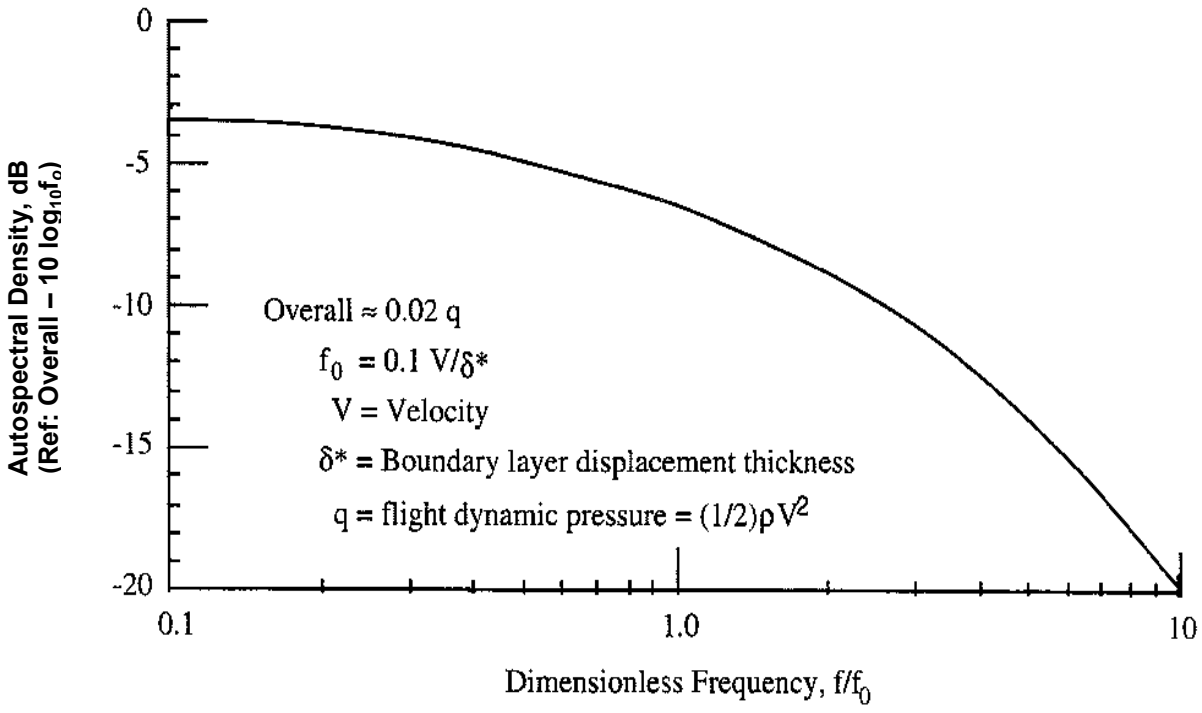

FIGURE 3.6. Normalized Autospectrum for Fluctuating Pressures in a Turbulent Boundary Layer.

3.9 Engine/Motor Thrust Transients. Beyond the liftoff transients discussed in Sections 3.4 and 3.5, the start and shutdown of liquid propellant engines and solid motors during flight produce thrust transients that are important dynamic load events for the flight vehicle. Even though a thrust axis is close to alignment with the longitudinal axis of the vehicle, due to unsymmetric nozzle flow and slight timing differences among several simultaneously acting engines or motors, lateral and moment loads are also induced at the end of the vehicle. The most significant dynamic load events tend to be liquid engine shutdowns that result from propellant depletion. This is so because of the relatively rapid thrust decay and, sometimes, sharp thrust transients due to erratic combustion or periodic thrust oscillations due to "chugging" instability resulting from limit cycling of injected flows and combustion (typically between 100 and 1000 Hz). Burnout of solid motors and commanded shutdowns of liquid engines (generated by either the guidance system or by a propellant level sensor) tend to be relatively mild dynamic events because the thrust decay is fairly slow and smooth. Of course, thrust rise at vehicle liftoff is an essential part of the complex set of processes taking place to cause low-frequency transient and random loads within the launch vehicle and spacecraft. Most often the significant vehicle structural dynamic responses resulting from thrust transients are in the frequency range below 50 Hz. See [3.30] for details and an illustration.

3.10 Maneuvering Loads. During powered ascent of both the launch vehicle and upper stages, the flight path of the vehicle is controlled by moving the thrust axis (" thrust vectoring"), usually with engine/motor gimbals or, in some cases, by varying the thrust of individual engines in a cluster. Beyond the local loads generated by the operation of the thrust vectoring devices, there are also dynamic loads on the entire vehicle due to the variations in the thrust components along the longitudinal and lateral axes of the vehicle. These maneuvering loads are composed of low frequency aerodynamic forces and the control-generated thrust-vectoring forces that steer the vehicle into the wind. These loads are generally significant only in the frequency

range below 5 to 10 Hz. For the Titan IV vehicle, maneuvering loads are a significant contributor to the total loads experienced during the period of maximum airloading, including gust, autopilot, and buffet loads. See [3.31] for details.

3.11 Pogo. Pogo is the name given to a dynamic instability phenomenon that can occur during ascent of space vehicles propelled by liquid rocket engines [3.32]. The instability is due to the interaction between structural vibration of the vehicle in one of its normal modes and thrust oscillation of the engines. The structural vibration causes propellent flow into the combustion chambers to be perturbed and thus produces thrust perturbation in synchronism with the structural vibration. This is a classical closed-loop interaction that can lead to instability if the amplitude and phasing of the thrust relative to gimbal acceleration along the thrust direction tends to do sufficient positive work on the system to overcome structural damping and hydraulic losses. Pogo occurs most often in the first longitudinal vehicle mode (like a pogo stick motion). During first liquid stage burn of medium and heavy lift vehicles, severe pogo has occurred between 5 and 20 Hz, and during second stage burn, between 17 and 125 Hz. The instability exhibits a limit-cycle with slowly varying amplitude, first building to a maximum and then decaying over a period of from a few seconds to 30 seconds.

Pogo has caused engine shutdowns on two occasions (a Titan Stage I and a Saturn V S-II stage) and has caused intolerable vibration of launch vehicle structure and of payloads. Fortunately, while pogo has occurred in several manned missions, no astronaut endangerment has resulted. Specific requirements have been levied to avoid pogo instability on all U. S. Air Force and NASA vehicles; see [3.32, 3.33] for guidance on pogo stability modeling, analysis, and stability margins. The means that has proven successful in eliminating prior pogo occurrences and preventing pogo during the design stage has been to incorporate gas-charged accumulators at engine inlets and, in the case of the Shuttle main engines, within the engine itself. See [3.32] for schematics of the configuration of accumulator devices for expendable vehicles and [3.34] for discussions of the Space Shuttle accumulator.

3.12 Solid Motor Pressure Oscillations. Solid motors characteristically experience sustained self-excited oscillations at the frequency of the first longitudinal acoustic mode of the chamber. The frequency of this half-wave mode is determined by the length of the combustion chamber and the acoustic speed in the hot gas of approximately 1100 m/s (3500 ft/s). The oscillation is often referred to as "resonant burn" or as "vortex-driven oscillation." Large motors have multiple segments with cavities or restrictors at segment interfaces. These flow discontinuities lead to the shedding of vortices, which are convected downstream and can result in a positive feedback coupling process with the cavity acoustic mode to generate sustained oscillation [3.35 - 3.37]. A sequence of oscillation occurrences takes place during a motor firing, each initiating at just above and uniformly progressing to just below the acoustic mode frequency. The salient parameter for the change in frequency about the acoustic frequency is the change in the shedding frequency which is proportional to the gradually decreasing mean flow velocity with burn time [3.37]. For smaller motors having a single segment, vortex shedding originates near fins at the aft end of the motor. The oscillation amplitudes, as measured at the top end of the motor, typically do not exceed a few tenths of a psi, and sometimes are sufficiently complex to include a significant harmonic at twice the fundamental frequency. The oscillations might produce structural loads and vibration levels of concern in some cases.

3.13 Liquid Sloshing in Tanks. During the launch of a vehicle powered by liquid propellant rocket engines, the propellant fluid in the fuel and/or oxidizer tanks may slosh in response to turbulence or thrust vector induced loads (see Sections 3.3 and 3.10). The resulting slosh loads have mixed transient and random characteristics, and they generally occur at very low frequencies (less than 5 Hz) [3.38]. The importance of slosh loads is underlined by the fact that

the propellant mass can constitute as much as half of the total vehicle mass during launch. Slosh loads are of concern to the structure of the tanks, their attachment to the vehicle, and the tank supporting structure. The magnitude of the slosh loads is strongly dependent on the details of the rocket engine fuel system design and the turbulence or thrust vector induced loads. Slosh loads may also arise during in-space operations. For example, if the space vehicle is spin-stabilized on-orbit, the possibility of slosh loads must be considered because the tank center of mass is almost always offset from the spin axis. In addition, possible adverse interactions between propellant sloshing, the attitude control system, and the vibration modes of appendages such as booms and solar panels should also be considered, since these modes tend to be closely distributed near and below 5 Hz. See [3.38 - 3.42] for details.

3.14 Stage and Fairing Separation Loads. Stage and fairing separations (including booster package, nose cone, and insulation panel jettisons) are often accomplished with the assistance of pyrotechnic devices that produce high frequency transient loads in local regions, which are discussed separately in Section 3.15. Beyond the local pyrotechnic loads, however, there are also more general low frequency transient loads due to the rapid velocity changes that accompany the rapid separation and/or jettison of structural elements of the vehicle. The specific characteristics of these more general transient loads depend on the details of the separation and/or jettison procedure, but the energy spectrum for the transient load is usually concentrated below 50 Hz, similar to the liftoff transient shown in Figure 3.4. Such loads must be evaluated on a case-by-case basis. See [3.43] for further details and an illustration.

3.15 Pyrotechnic Induced Loads. The primary sources of high frequency transient environments for space vehicles are the functioning of pyrotechnic (explosive) devices, which produce high acceleration, short duration structural responses commonly called "pyroshocks". The devices producing pyroshocks include the following [3.44, 3.45]:

a. Point Sources - explosive bolts, separation nuts, pin pullers and pushers, bolt and cable cutters, and pyro-activated operational hardware, e.g., pyrovalves. The release of point fasteners (nuts, bolts) also releases stored strain energy in the fastener.

b. Line Sources - flexible linear shaped charges (FLSC), mild detonating fuses (MDF), explosive transfer lines, Super Zip™, and Sure-Sep™. These devices contain high explosives, which produce very high pressures in less than a microsecond.

c. Combined Point and Line Sources - V-band (Marmon) clamps that use point pyrotechnic sources that may then allow the rapid release of stored strain energy from a structural preload acting along a line of contact between two structures being separated.

Some pyrotechnic devices are designed to contain virtually all the pyrotechnically generated gases required to accomplish the intended function and, hence, produce only a direct mechanical (structure borne) load. Examples of contained devices are piston/cylinder-activated mechanisms such as pyrovalves, pin pullers and pushers, and some types of nuts and bolts. Other pyrotechnic devices use secondary explosives to accomplish their intended function, which generate several million psi on activation. Thus, beyond structure borne loads, they also produce airborne loads when activated in the atmosphere. Examples of non-contained devices are FLSC and MDF, as well as some types of nuts and bolts.

The pyroshocks produced by all pyrotechnic devices can be broadly divided into three categories, (a) near-field pyroshocks, (b) mid-field pyroshocks, and (c) far-field pyroshocks, which are defined as follows:

a. Near-field is a location on the structure that is sufficiently close to the pyrotechnic source for the response to be dominated by the direct compressive wave propagation from the source, causing peak accelerations in excess of 5,000 g and substantial spectral content to frequencies above 100 kHz [3.46]. For intense pyrotechnic sources, such as most line sources, the near-field usually includes locations within approximately 15 cm (6 in.) of the source, unless there are intervening structural discontinuities, such as joints. For less intense sources, such as most point sources, the near field usually includes locations within approximately 3 cm (1 in.) of the source. It should be mentioned that the accurate measurement of near-field pyroshocks with accelerometers is difficult if not imposible for the reasons detailed in [3.46]. As an alternative, laser vibrometers or strain gages should be considered for near-field measurements.

b. Mid-field is a location on the structure that is sufficiently distant from the pyrotechnic source for the structural response to be caused by a combination of direct compressive wave propagation from the source and structural resonances induced by the transfer of structureborne energy into lower frequency bending waves in the structure, causing peak accelerations between 1,000 and 5,000 g and substantial spectral content above 10 kHz. For intense pyrotechnic sources, such as most line sources, the mid-field usually includes locations that are between approximately 15 and 60 cm (2 ft) from the source. For less intense pyrotechnic sources, such as most point sources, the mid-field may extend between 3 and 15 cm from the source. It should be mentioned that some basic references (e.g., [3.46 - 3.48]) consider the mid-field to be part of the far-field, defined next.

c. Far-field is a location on the structure that is sufficiently distant from the pyrotechnic source for the structural response to be dominated by resonances induced by the transfer of structureborne energy from the source into lower frequency bending waves in the structure, with peak accelerations below 1,000 g and most of the spectral content below 10 kHz. The far field includes all locations beyond the mid-field.

The time history and shock response spectrum for the structural response due to a typical mid-field pyroshock are shown in Figures 3.7 and 3.8. See [3.46 - 3.50] for further details and illustrations.

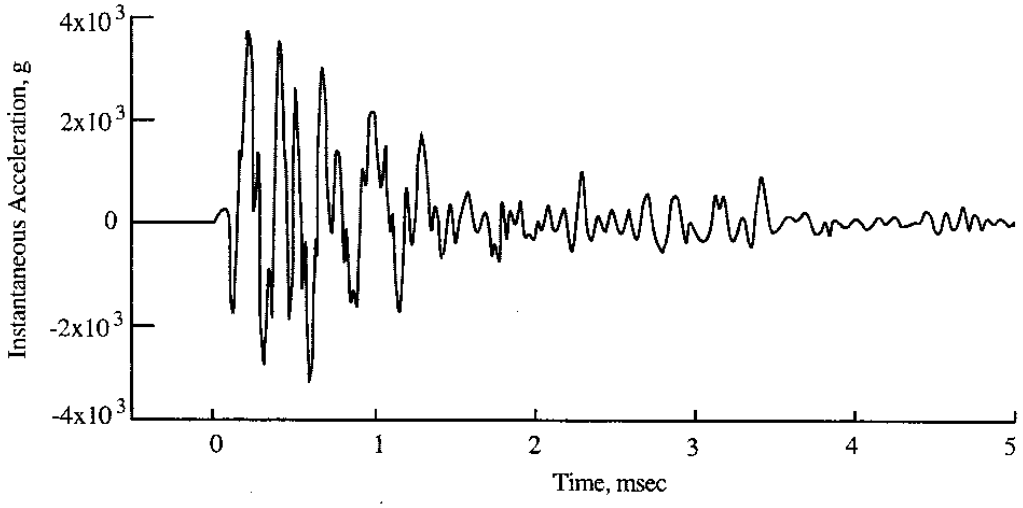

FIGURE 3.7. Typical Mid-Field Pyroshock Acceleration Time History.

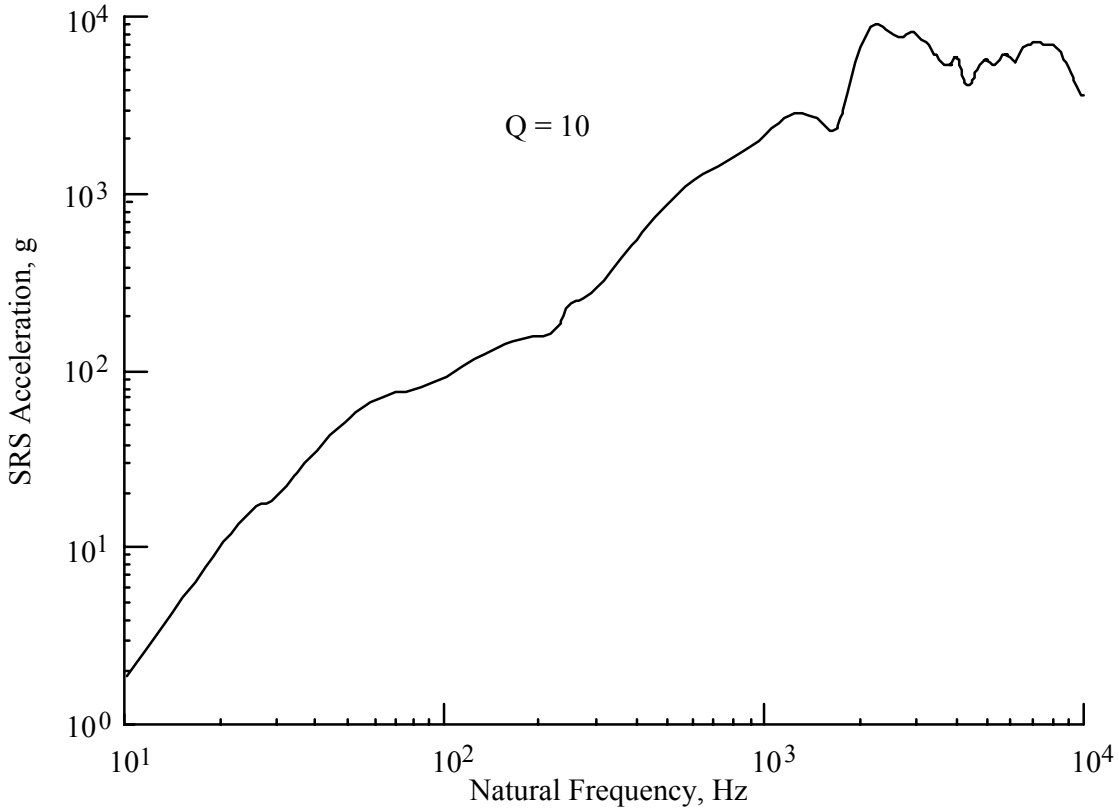

FIGURE 3.8. Maximax Shock Response Spectrum (SRS) for Pyroshock in Figure 3.7.

3.16 Flight Operations. There may be certain operations of a vehicle or its payload during space flight that will induce transient loads. Examples include (a) the deployment of antenna, solar arrays, or other appendages, (b) the firing of position jets for orbit or attitude correction maneuvers, and (c) the start-up/stop of onboard rotating sensors with scanning functions. The loads produced by these operations are generally concentrated at frequencies below 10 Hz and are relatively small in magnitude. Nevertheless, the following considerations must be addressed, as follows:

a. Because the loads may produce very lightly damped dynamic responses, their magnitude could influence the design of the deployment hinges or the bearings of the rotating elements.

b. Since these operations occur in space, operational tests must be performed in a near-vacuum to eliminate the effects of air damping on the dynamic responses.

c. The possible dynamic interactions between multiple sources should be examined to insure that the operations of sensitive onboard sensors are within their prescribed stability and accuracy margins.

Potential problems due to space operations must be evaluated on a case-by-case basis.

3.17 Onboard Equipment Operations. Beyond the operations induced loads discussed in Section 3.16, there may also be equipment items on the spacecraft that produce vibration during operation of sensitive instruments. These sources are usually characterized by the forces measured at their base over their operating speed range. Examples of such vibration sources are reaction wheels used to provide spacecraft stability [3.51, 3.52] and pumps used to provide hydraulic pressure for the operation or cooling of a space vehicle component or onboard experiment [3.53]. Even though the resulting vibration levels are often many orders of magnitude lower than the levels associated with other excitations, especially during launch, the consequences may be significant. For sensitive instruments, such as interferometry based imagers and basic physics experiments, the milli- or micro-g vibration environment may be a limiting design factor. Indeed, methodologies have been developed to understand and control the micro-vibration environment for Space Shuttle (STS), the International Space Station (ISS), and free-flying spacecraft [3.54 - 3.57]. Such excitations may be stationary random, periodic, or transient, and may occur in any frequency range from 10 Hz to 10 kHz. For further information, contact the Microgravity Analytical Team at the NASA/Marshall Space Flight Center [3.58].

3.18 Planetary Descent, Entry, and Landing. Not only reusable, earth-orbiting vehicles like Space Shuttle, but deep-space vehicles intended for close encounter and landing on other planets must be designed to survive entry into the planet's atmosphere and landing on its surface. Of course, the environmental conditions and design requirements are planet-specific. For example, in case of entry into the Martian atmosphere and depending on the trajectory, an entry velocity of the order of 10 km/s is not unusual. Such high entry velocities produce rapidly varying pressures and closely correlated heat flux pulses. An illustration of the pressure versus time for entry into the Martian atmosphere is shown in Figure 3.9. The peak pressure load in Figure 3.9 constitutes a quasi-static load to which the spacecraft protective aeroshell must be designed [3.59, 3.60]. Beyond this quasi-static load, there is a fluctuating pressure load generated by the fluid dynamic boundary layer over the exterior of the vehicle structure (see Section 3.8) as well as the potential for wind loads (see Section 3.3), which must be considered in the vehicle design. Even when planetary landing is not contemplated, entry followed by exit from a plant's atmosphere has been used as a means of aerobraking or aerocapture. In these cases too, the resulting loads must be considered in the design of the vehicle.

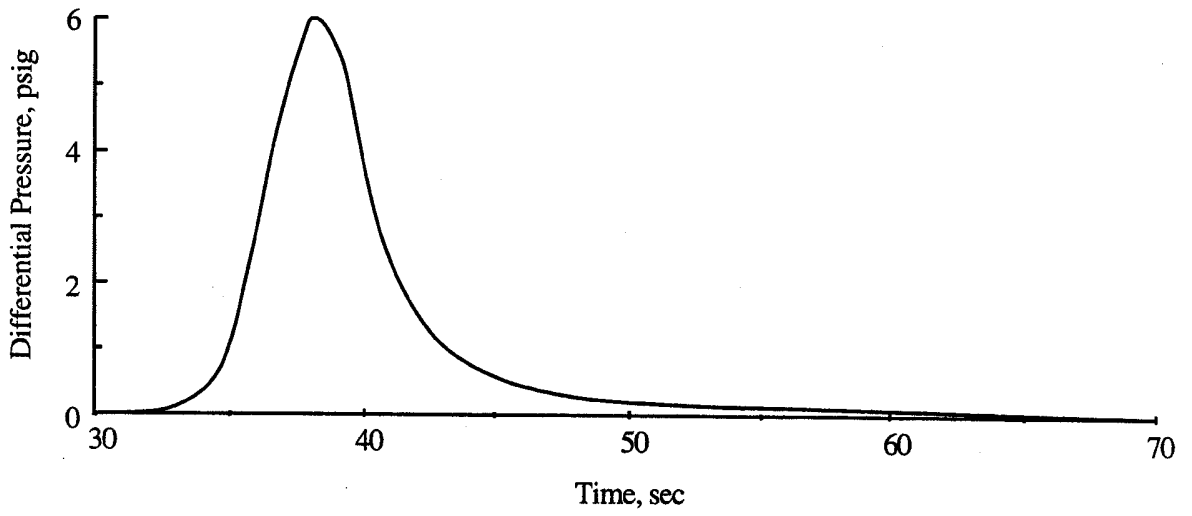

FIGURE 3.9. Example of Mars Entry Pressure Pulse Time History [3.60].

During landing, the spacecraft's primary structure and onboard instruments will experience transient impact loads which could be critical for their design. The frequency content and magnitude of the loads strongly depend on such parameters as (a) the velocity vector at touch down, (b) the dynamic characteristics of the spacecraft and its impact attenuation system, if any, and (c) the nature and properties of the planet's surface at the landing site [3.60, 3.61]. Many of these parameters could be random variables, but their interaction is usually understood well enough to permit a deterministic dynamic analysis in the low frequency regime.

3.19 Surface Penetration. As part of planet or comet subsurface exploration, penetrators are extended to reach depths below the surface on the order of one to a few meters. A penetrator can be a part of a landing system when entering a planet's atmosphere, or it may be entering the atmosphere on its own. In the latter case, the penetrator must be equipped with an entry loads and thermal protection system, as discussed in Section 3.18. A capsule tethered to the penetrator is required to remain at the surface to relay back the measurements. The required penetration depth is closely related to such factors as (a) the penetrator's mass and shape, (b) the properties of planet surface material, and (c) the incidence angle and velocity as it enters the surface [3.62]. Because parameters under (b) and (c) above are often not well characterized, the environmental loads are usually deduced from a mixture of experimental and empirical approaches, [3.63, 3.64]. An initial penetration velocity of the order of few hundred meters per second is often assumed for a penetration to about one meter beneath the Martian soil. Figure 3.10 shows the predicted acceleration magnitude versus time of penetration loads through nonhomogeneous soil [3.65]. The low frequency fluctuations in the acceleration data in Figure 3.10 are attributed to variations in the soil properties with depth.

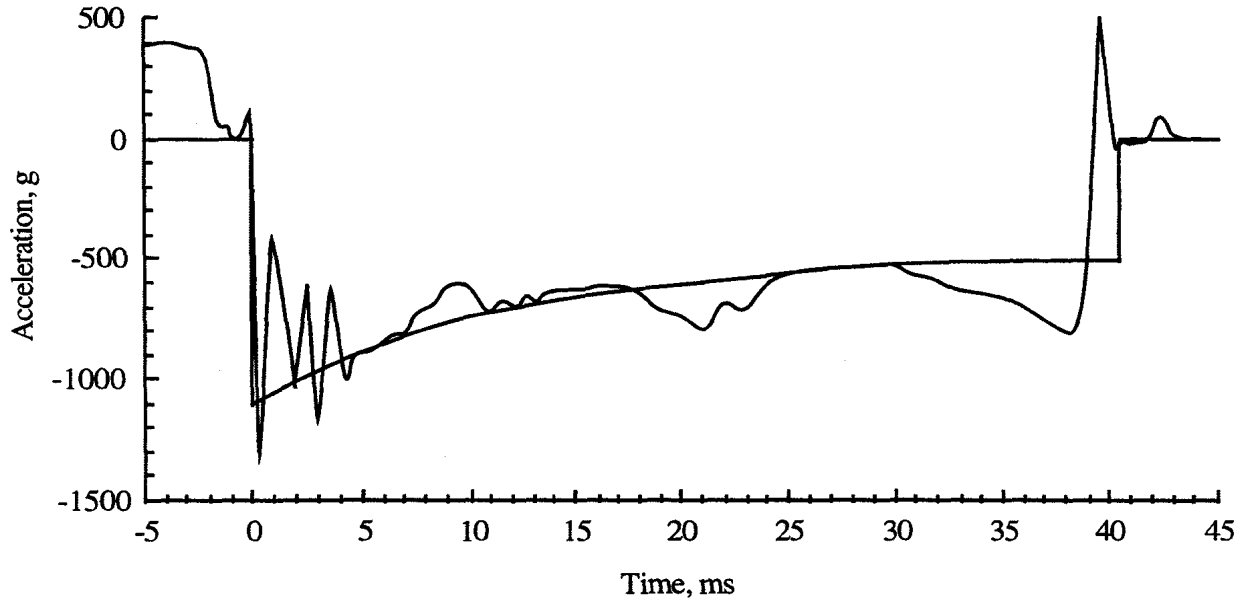

FIGURE 3.10. Penetration Deceleration Test and Prediction Data [3.64].

It is clear from Figure 3.10 that the penetration involves a very large velocity change over a duration of about 40 ms, which means the resulting load has a substantial low frequency content (below 50 Hz) that is potentially very damaging to the basic structure of the penetrator. However, there are also high frequency loads due to the initial rapid deceleration that might damage small parts. The shock response spectrum (SRS) defined in Section 2.2.10 and illustrated in Section 3.15 is commonly used as a design tool for this type of intense, low frequency transient load.

3.20 Meteoroid Impacts. The term meteoroid is used here to refer to all space-borne solid objects, including earth orbiting debris as well as particles of comet and asteroidal origin. Whether the spacecraft is intended for Earth orbit or for a long journey into deep space, a certain level of meteoroid protection is required and is usually stated in the form of “a minimum probability of spacecraft survival under a prescribed meteoroid environment”. For previous earth orbiting and interplanetary missions, a 95% minimum probability has been used. Note, however, that the total probability of spacecraft survival must, in addition, take into account the conditional probability of a mission failure, given the failure of one of its subsystems.

The meteoroid environment depends on several factors [3.66] such as the spacecraft trajectory, velocity, and mission duration, and is characterized by a nominal “meteoroid fluence”. Meteoroid fluence is defined as the number of particles with mass equal to or greater than a given value to be encountered per unit area. In addition to the specification of a mass value, the fluence also defines the mass density and weighted mean velocity. Mean velocities of meteoroid particles are in the 5 to 20 km/s range, producing a very high frequency but highly localized transient load. In the practical range of mass (10^{-6} to 10^{-2} grams) corresponding to a reasonable level of meteoroid protection, the fluence versus mass relationship is represented as a straight line on a log-log plot [3.67]. The particle size against which a spacecraft subsystem must be protected depends on the required probability of mission success.

3.21 Summary of Environments. A summary of the dynamic loads environments for space vehicles, as detailed in Sections 3.1 through 3.20, is shown in Table 3.1. The environments in Table 3.1 are categorized in two ways, (a) whether the environment is measured and described as a mechanical motion load or a pressure load, and (b) whether the environment is characterized by a stationary random, periodic, or transient load. The terms "stationary random" and "periodic" are used loosely here to include loads with average properties that are time-varying (nonstationary), but where the variations with time are sufficiently slow to allow the loads to be considered piece-wise stationary (see Section 2.1).

TABLE 3.1. Summary of Dynamic Environments for Space Vehicles.

Environment (Section Number)	Mechanical Motion (M), or Pressure (P)	Sta. Random (R), Periodic (P), or Transient (T)	Upper Frequency Limit, Hz
Transportation (3.1)	M	R, P, and/or T	50
Seismic loads (3.2)	M	T	20
Wind and turbulence (3.3)	P	R	20
Rocket motor ignition overpressure (3.4)	P	T	40
Liftoff release (3.5)	M	T	20
Engine/motor generated acoustic noise(3.6)	P	R	10,000
Engine/motor generated vibration (3.7)	M	R and P	2,000
Aerodynamic sources (3.8)	P	R	10,000
Engine/motor thrust transients (3.9)	M	T	100
Maneuvers during ascent (3.10)	M	T	10
Pogo (3.11)	M and P	P	125
Solid motor pressure oscillations (3.12)	P	P	1,000
Liquid sloshing in tanks (3.13)	M and P	R	5
Stage and fairing separations (3.14)	M	T	50
Pyrotechnic events (3.15)	M and P	T	100,000
Flight operations (3.16)	M	T	10
Onboard equipment operations (3.17)	M	R, P, and/or T	10,000
Planetary descent, entry, and landing loads (3.18)	M and P	R and/or T	10,000
Surface penetration (3.19)	M	T	3,000
Meteoroid impacts (3.20)	M	T	-

3.22 References

3.1 Anon., "DOD Test Method Standard for Environmental Engineering Considerations and Laboratory Test", *MIL~STD-810F,* Apr. 2000.

3.2 Anon., "Transportation and Handling Loads", *NASA SP-8077,* Sept.1977.

3.3 Foley, J. T., "Transportation Dynamic Events Survey", *Report EDB-A1354* (DOE/DOD Environmental Data Bank), Sandia Corporation, Albuquerque, NM, 1973.

3.4 Anon., "Military Standard - Mechanical Vibration of Shipboard Equipment", *MIL-STD-167-1 (SHIPS),* 1974.

3.5 Anon., "tVibration of Ships", *Std ISO-6954,,* Intern. Stds Orgn, 1984.

3.6 Ziegahn, K. F., and Braunmiller, U., "Transportation Stress and Packaging - Recent Developments in Germany and Europe with Special Respect to Standardization", *Proc. 39th ATM, Inst. Envir. Sc.,* Vol.2, pp 347-363, May 1993.

3.7 Hart, G. C., et al., "Seismic Study - Launch Complex 6 Vandenberg AFB", Englekirk and Hart/Woodward-Clyde report submitted to Rockwell STS Division, Downey, CA, 1985.

3.8 Hall, W. J., "Vibration of Structures Induced by Ground Motions", Ch. 24 in *Shock and Vibration Handbook,* 4th ed. (Ed. C. M. Harris), McGraw-Hill, NY, 1996.

3.9 Wolf, J. P., *Dynamic Soil-Structure Interaction,* Prentice-Hall, Englewood Cliffs, NJ, 1985.

3.10 Wolf, J. P., *Soil-Structure-Interaction Analysis in Time Domain,* Prentice-Hall, Englewood Cliffs, NJ, 1988.

3.11 Davenport, A. G., "Vibration of Structures Induced by Winds", Ch. 29, Pt II in *Shock and Vibration Handbook,* 4th ed. (Ed. C. M. Harris), McGraw-Hill, NY, 1996.

3.12 Dryden, H. L., "A Review of the Statistical Theory of Turbulence", *Turbulence* (Friedlander, S. K., and Topper, L., Ed.), pp 115-150*,* Wiley, NY, 1961.

3.13 Houbolt, J. C., "Atmospheric Turbulence" (Dryden Research Lecture), *AIAA J.*, Vol. 11, No. 4, pp 421-427, Apr. 1973.

3.14 Lumley, J. L., *Stochastic Tools in Turbulence,* Academic Press, NY, 1970.

3.15 Dougherty, N. S., Nesman, T. E., and Guest, S. H., "Shuttle SRB Ignition Overpressure: Model Suppression Test Program and Flight Results", Proc. 13th *JANNAF Plume Technology Mtg,* Apr. 1982.

3.16 Jones, J. H., et al., "Acoustic, Overpressure and Unsteady Flow Phenomena Associated with the Saturn Space Shuttle Systems: A Review of Selected Issues", *Symp. Acoustics and Dynamic Environment of Space Transportation Systems,* CNES/ONERA, Chatillon, France, Feb. 1994.

3.17 Wilby, J. F., and Piersol, A. G., "An Evaluation of the Space Shuttle Vibration at the Payload Attachments During Liftoff", *Astron Rep.* 7072-01, Aug. 1986.

3.18 Lyon, R. H., *Random Noise and Vibration in Space Vehicles,* SVM-1, Shock and Vibration Info. Anal. Ctr, Arlington, VA, 1967.

3.19 Richards, E. J., and Clarkson, B. L., "Jet and Rocket Noise", Ch. 7*, Noise and Acoustic Fatigue in Aeronautics* (Richards, E. J., and Mead, D. J., Ed.), Wiley, NY, 1968.

3.20 McInerny, S. A., "Characteristics and Predictions of Far-Field Rocket Noise", *Noise Control Engineering,* Vol. 38, No. 1, pp 5 - 16, Jan/Feb. 1992.

3.21 Potter, R. C., and Crocker, M. J., "Acoustic Prediction Methods for Rocket Engines, including the Effects of Clustered Engines and Deflected Exhaust Flow", *NASA CR-566,* 1966.

3.22 Riley, G. F., "Saturn V Flight Data - Zonal Statistical Analyses", *Boeing Doc. DS-17032-2,* 1969.

3.23 Schlichting, H., *Boundary Layer Theory* (English translation by J. Kestin), McGraw-Hill, NY, 1960.

3.24 Bies, D. A., "A Review of Flight and Wind Tunnel Measurements of Boundary Layer Pressure Fluctuations and Induced Structural Response", *NASA CR-626,* May 1966.

3.25 Bull, M. K., "Boundary Layer Pressure Fluctuations", Ch. 8, *Noise and Acoustic Fatigue in Aeronautics* (Richards, E. J., and Mead, D. J., Ed.), Wiley, NY, 1968.

3.26 Lowson, M. V., "Prediction of Boundary Layer Pressure Fluctuations", *AFFDL-TR-67-167,* Apr. 1968.

3.27 Speaker, W.V., and Ailman, C. M., "Spectra and Space-Time Correlations of the Fluctuating Pressures at a Wall Beneath a Supersonic Turbulent Boundary Layer Perturbed by Steps and Shock Waves", *NASA CR-486,* 1966.

3.28 Robertson, 3. E., "Prediction of In-Flight Fluctuating Pressure Environments Including Protuberance Induced Flow", *NASA CR-119947,* 1971.

3.29 Tanner, C. S., "Shuttle Cargo Bay Vent Noise and its Effect on the Generic Payload Specifications and Testing Methods", *Proc., Shuttle Payload Dynamic Environments and Loads Prediction Workshop,* Vol.1, pp.303 - 332, Jet Propulsion Laboratory, Jan. 1984.

3.30 Goldman, R. L., "Transient Loads from Thrust Excitations", *NASA SP-8030*, 1969.

3.31 Dotson, K. W., and Tiwari, S. B., "Formulation and Analysis of Launch Vehicle Maneuvering Loads", *J. Spacecraft and Rockets*, Vol.33, No.6, pp.813-821, 1996.

3.32 Rubin, S., "Prevention of Coupled Structure-Propulsion Instability (Pogo)", *NASA SP 8055,* Oct. 1970.

3.33 Oppenheim, B. W., and Rubin, S., "Advanced Pogo Stability Analysis for Liquid Rockets", *J. Spacecraft and Rockets,* Vol.3, No.8, pp 360-374, May/June 1993.

3.34 Fenwick, J. R., Jones, J. H., and Jewell, R. E., "Space Shuttle Main Engine (SSME) Pogo Testing and Results", *Shock and Vibration Bulletin,* No.52, Pt. 2, pp.1 - 20, 1982.

3.35 Culick, F. E. C., "Combustion Instabilities in Propulsion Systems", in *Unsteady Combustion,* Proceedings of the NATO Advanced Study Institute, NATO ASI Series, Vol. E306, pp.173-241, 1996 (available from AIAA Technical Library).

3.36 Anon., "Combustion Instability in SRMs - A Bibliography", Prop. Info. Agency, Feb. 1997.

3.37 Dotson, K. W., Womack, J.M., and Grosserode, P.J., “Structural Dynamic Analysis of Solid Rocket Motor Resonant Burn,” *AIAA 99-1201*, 40 th AIAA/ASME/ASCE/ASC Structures, Structural Dynamics, and Materials Conference, St. Louis, MO April 1999.

3.38 Abramson, H. N., Ed., "The Dynamic Behavior of Liquids in Moving Containers", *NASA SP-106,* 1966.

3.39 Koelle, H. H., *Handbook of Astronautical Engineering,* McGraw-Hill, NY, 1961.

3.40 El-Raheb, M., and Wagner, P., "Vibration of a Liquid with Free Surface in a Spinning Spherical Tank", *J. Sound and Vibration,* Vol 76, No.1, pp 83-93, Jan.1981.

3.41 Balendra, T., Ang, K. K., Paranasivan, P., and Lee, S. L., "Free Vibration Analysis of Cylindrical Liquid Storage Tanks", *Int. J. Mech. Sci.,* Vol.24, No.1, pp.47 - 59, 1982.

3.42 Agrawal, B. N., "Interaction Between Liquid Propellant Slosh Modes and Attitude Control in a Dual-Spin Spacecraft", *Proc. AIAA 28th SDM Conf,* pp 774-780, Apr.1987.

3.43 Steinmeyer, J. F., Hofeditz, J. T., and Brierley, J. M., "Separation Testing on the Titan IV 86-ft Payload Fairing", *Proc., 13th Aerospace Testing Sem.,* pp.241 - 250, 1971.

3.44 Kalbfleisch, K. C., "Review of Pyro-Shock Generating Devices and Source Levels", *IES Pyrotechnic Shock Tutorial Program, 31st ATM,* Inst. Envir. Sc., Apr.-May 1985.

3.45 Bement, L. J., and Schimmel, M. L., "A Manual for Pyrotechnic Design, Development and Qualification", *NASA TM 110172,* June 1995.

3.46 Himelblau, H., Piersol, A. G., Wise, J. H., and Grundvig, M. R., "Handbook for Dynamic Data Acquisition and Analysis", *IES-RP-DTEO12.1,* Inst. Envir. Sc. Tech., Mount Prospect, IL, Mar. 1994.

3.47 Anon., “Pyroshock Testing Techniques,” *IEST-RP-DTE032.1,* Inst. Envir. Sc. Tech., Mount Prospect, IL, 2000.

3.48 Davie, N. T., and Bateman, V.I., "Pyroshock Testing", Chapter 26, Part II in *Shock and Vibration Handbook,* 4th ed. (Ed. C. M. Harris), McGraw-Hill, NY, 1996.

3.49 Evans, M. J., Neubert, V. H., and Bement, L. J., "Measurement, Data Analysis, and Prediction of Pyrotechnic Shock from Pin Pullers and Separation Nuts", *Proc., 57th Shock and Vibration Symp.,* New Orleans, LA, 1986.

3.50 Anon., "Pyroshock Test Criteria", *NASA Technical Standard NASA-STD 7003,* May 18, 1999.

3.51 Bialke, B., "A Compilation of Reaction Wheel Induced Spacecraft Disturbance", Paper ASS 97-038, *20th Annual ASS Guidance and Control Conf.,* American Aeronautical Society, 1997.

3.52 Hasha, M.D., "Reaction Wheel Mechanical Noise Variations", *LMSC EM SSS 218,* June 1986.

3.53 Ross, R. G., Ed., *Cryocoolers 8,* Plenum Press, NY, *1995.*

3.54 DeLombard, R., "Compendium of Information for Interpreting the Microgravity Environment of the Orbiter Spacecraft", *NASA TM 107032,* Aug. 1996.

3.55 Curtis, D., and Bogert, P., "Methods for Evaluation of the Microgravity Environment Aboard the Space Station Freedom", *First SHACS,* Nice France, 1992.

3.56 Anon., "Microgravity Control Plan, International Space Station Program", *NASA SSP 500368, Revision B Draft,* JSC Contract No.15-1000 (DRIVE-16), February 1999.

3.57 Monteil, D., Guillaud, V., and Laurens, P., "Mastering the Effect of Microvibrations on the Performances of Reconnaissance Satellites", *Matra Marcone Space France Paper No. N96-13900,* 1996.

3.58 Anon., "Microgravity Environment Description Handbook", http://www. msfc.nasa.gov/WWW/MMAP/PMISHTMLS/Micro-descpt.html.

3.59 Heer, E., and Garba, J. A, "Aeroshell Structural Development for Martian Entry", *AIAA Paper 68-1159,* Apr.1968.

3.60 Sperling, F., and Garba, J. A., "A Treatise on the Surveyer Lunar Landing Dynamics, and an Evaluation of Pertinent Telemetry Data Returned by Surveyer I", *JPL TR 2-1035,* Jet Propulsion Lab, Pasadena, CA, 1967.

3.61 Salama, M.A., Kuo, C. P., Davis, G.L., Rivellini, T. P., and Sabahi, D.," Simulation of Impact Dynamics for Mars Landing", *AIAA Dynamics Specialists Conf,* Apr.1996.

3.62 Justus, C. G., "Mars Global Reference Atmospheric Model for Mission Planning and Analysis", *J. Spacecraft and Rockets,* Vol.28, No.2, pp 216-221, 1991.

3.63 Forestal, M. J., Altman, B. S., Cargile, 3. D., and Hanchak, S. J., "An Empirical Equation For Penetration Depth of Ogive-Nose Projectiles Into Concrete Targets", *Intern. J. Impact Engrg,* Vol.15, No.4, pp 395-405, 1994.

3.64 Kipp, R. J., and Bateman, V.1., "Analytical Estimation of Earth Penetrator Structural Response and Comparison with Laboratory Shock and Modal Test Data", *Proc., 59th Shock and Vibration Symp.,* Vol. IV, pp.133-144,1988.

3.65 Forestal, M. J., and Luk, V. K., "Penetration into Soil Targets", *Intern. J. Impact Engrg,* Vol.12, No.3, pp 427-444, 1992.

3.66 Anon., "Meteoroid Damage Assessment", *NASA SP - 8042,* 1970.

3.67 Rapacz, P. M., Bamford, R. M., and Lou, M. C., "Meteoroid Protection Design for Spacecraft", *JPL Rep. D-6810,* Jet Propulsion Lab, Pasadena, CA, 1989.

4. PREDICTION OF DYNAMIC EXCITATIONS

To predict the responses of spacecraft and their constituent elements to dynamic loads, the dynamic environments summarized in Section 3 must first be translated into specific excitation functions. To this end, it is convenient to map the twenty environments listed in Table 3.1 into eight categories, as summarized in Table 4.1.

TABLE 4.1. Summary of Dynamic Excitations for Space Vehicles.

Type of Excitation	Dynamic Environments (Section Number)
Low frequency transient excitations	Transportation (3.1), seismic events (3.2), rocket motor ignition overpressure (3.4), liftoff release (3.5), engine/motor thrust transients (3.9), maneuvers (3.10), stage/fairing separations (3.14), in-flight operations (3.16), and surface penetration (3.19).
Low frequency random excitations	Transportation (3.1), wind and turbulence (3.3), and fluid slosh in tanks (3.13).
Quasi-periodic excitations	Transportation (3.1), engine chugging (3.9), pogo (3.11), solid motor pressure oscillations (3.12), and onboard equipment (3.17).
Exterior acoustic noise excitations	Engine/motor generated acoustic noise (3.6).
Exterior aerodynamic noise excitations	Aerodynamic sources (3.8), and planetary descent and entry (3.18).
Interior acoustic noise excitations	Engine/motor generated acoustic noise (3.6), aerodynamic sources (3.8), and planetary descent and entry (3.18).
Structureborne vibration excitations	Engine/motor generated vibration (3.7) and onboard equipment (3.17).
High frequency transient excitations	Pyrotechnic events (3.15) and meteoroid impact (3.20).

4.1 Low Frequency Transient Excitations. Low frequency transient loads often determine the design requirements for the basic structure of space vehicles. Referring to Table 4.1, there are several potential sources of low frequency transient loads, some in the form of pressure loads (e.g., rocket motor ignition overpressure) and others in the form of motion inputs (e.g., liftoff release), as detailed in the referenced subsections of Section 3. One of the most difficult problems in designing a space vehicle is the determination of the excitations that will properly describe these loads. Typically, a large number of variables influence the form of the various excitations. Some variables may have a well understood and formulated influence on an excitation, while others may be impossible to characterize without a large degree of uncertainty. Depending on the relative degree of influence these two groups of variables have, either deterministic or statistical approaches are used to model the excitations. The basic characteristics of low frequency transient excitations are summarized in Section 3 and the applicable references in that section.

4.1.1 Analytical Models. For launch vehicles, all loads summarized in Table 3.1, excluding penetration loads, must be quantified and combined into one or more excitations. The process of predicting these excitations is one of synthesizing and describing all of the external excitations with reference to a common space and/or time/frequency scale, as discussed in the appropriate subsections in Section 3. When these excitations are applied as an input to the combination of the launch vehicle and payload, the dynamic loads at the launch vehicle/payload interface are often sought as the response quantities. On the other hand, it is these same interface responses

that constitute all or part of the low frequency transient excitation to the payload. In this regard, the method used to predict the payload interface excitation is not distinguished from predicting the response of the launch vehicle to its excitations, as detailed in Section 5.1. However, there are other excitations that may be applied to the payload only, e.g., transportation loads.

4.1.1.1 Launch Vehicle Liftoff Excitations. Those low frequency transients that occur during liftoff are very important events in the design of any space vehicle, whether it is an expendable launch vehicle such as Atlas/Centaur or a reusable one such as the Space Shuttle. Usually, extensive measurements are first made during many tests and actual firings of the vehicle engines. Information from these measurements is then synthesized to describe the dynamic excitations of liftoff. The synthesis approach used is by no means a standard one. However, as a representative approach, consider the Space Shuttle. The Space Shuttle liftoff transient excitations are synthesized [4.1] from measurements of (a) main engine thrust build-up and side loads, (b) internal pressure and overpressure during ignition of the solid rocket booster, (c) flight control forces due to closed-loop corrections of responses, (d) wind and buffet loads, and (e) reaction forces from hold-down attachments to the launch pad before release of the vehicle. These contributing phenomena are first separately modeled in detail, using several variables that describe their physics. The models may be empirically or theoretically based but are usually substantiated with experimental data. For example, the Space Shuttle main engine thrust and side loads are modeled by variables that describe the thrust build-up variations in the liquid-fueled engines, the thrust profile (based on laboratory test measurements), and the side loads resulting from the flow that alternates between being attached to and detached from the nozzle (see Section 3.8). The solid rocket booster (SRB) thrust and internal pressure buildup is modeled by two sets of variables to distinguish between the right and left boosters, thereby emulating any mismatch. The pressure time history is used to model the overpressure pulse that travels up the vehicle due to interaction between the SRB exhaust, the ambient air, and the exhaust duct during the ignition process (see Section 3.4). Structural restraint forces near the base of the launch stack are due to either inward or outward misalignment during stacking. These forces, and others simulating the cryogenic shrinkage of the external tank, are appropriately superimposed together to calculate the change in restraint forces. This change in restraint forces is applied to the free-free stack only after release (see Section 3.5). Of course, the possibility of seismic loads prior to release must also be considered if the launch site is in a region of known seismic activity.

The result of each of the separate models is a set of transient loads to be applied at specific locations on the Shuttle over specific time intervals during the liftoff sequence. For example, while the Shuttle stack is attached to the launch pad at the hold-down points, the liftoff transient excitation consists of thrust and overpressure force components. These excitations are estimated and the corresponding base restraint reactions are determined. Then the change in base restraint forces is applied simultaneously with the liftoff excitation to the free-free state. All forces described above are applied to a finite element method (FEM) model of the Space Shuttle, and a deterministic transient analysis is used to solve for the dynamic responses throughout the model, as detailed in Section 5.1.

As discussed above, the definition of the various phenomena contributing to the liftoff excitation depends on many variables, most of which are random in nature. The Space Shuttle loads criteria specifies that the design loads have a 3σ probability of occurrence. In [4.1], specification of a design liftoff excitation that is consistent with the loads criterion is determined through a Monte Carlo analysis where the values of the variable describing the phenomena are selected randomly. A statistical analysis of the results is then made to determine the statistical properties (mean, standard deviation, and 3σ values) of a single liftoff excitation.

4.1.1.2 Payload Liftoff Excitations. A direct method for predicting the liftoff transient excitation at the interface between the launch vehicle and the payload begins with a forward transient analysis of the coupled payload and launch vehicle, subject to the launch vehicle excitation discussed in Section 4.1.1.1. To accomplish this forward transient analysis within reasonable resources and time, the payload model usually is greatly simplified and reduced in detail and number of dynamic degrees-of-freedom. However, because the impedance of the simplified payload model is not identical to the impedance of the more detailed payload model, a corresponding degree of approximation will result in the predicted excitation. Once defined, the payload excitation can be used as a known applied load to predict the response of the more detailed payload model or the response of another payload to be flown on a launch vehicle of the same type. See Section 5.1 [4.2] for details.

4.1.2 Extrapolation Techniques. Extrapolation techniques have been used primarily for predicting payload excitations. Dynamics engineers usually deal with the forward problem of solving for the system response to a given disturbance or excitation. Extrapolation techniques, however, involve the inverse problem, namely, determination of the excitation that caused a given system response. This system response may be available from flight measurements as discussed in Section 4.1.3, where the responses might be a set of member forces, accelerations, or both. Several analysis approaches have been used for inferring the excitation from a given response. To do this, an accurate model is needed of the structure through which the loads are transmitted from the input to the output locations. One such approach [4.2] is as follows:

Assume a set of six accelerations $\{a(t)\} = \{a_1(t), \ldots, a_6(t)\}^T$ is measured at the interface plane between the launch vehicle and the payload. The need is to define the six components of forces and moments corresponding to the transient excitation $\{F(t)\} = \{F_1(t), \ldots, F_6(t)\}$ at the base of the launch vehicle. The solution may be presented in the frequency domain by the following relationship between the Fourier transform of the excitation {F(t)} and the Fourier transform of the response {A(f)}:

$$\{F(f)\} = [M(f)]\{A(f)\} \tag{4.1}$$

In Equation (4.1), M(f) is referred to as a dynamic mass, which is calculated from

$$[M(f)] = \left[\phi_{ir} M_{rr}^{-1} \phi_{br} + \phi_{ie} Z(f)^{-1} \phi_{be}\right]^{-1} \tag{4.2}$$

In Equation (4.2), the matrices ϕ_{br} and ϕ_{ir} represent the rigid body mode shapes at the base of the launch vehicle (where the excitation is applied), and at the interface between the payload and launch vehicle (where the response is measured), respectively; ϕ_{be} and ϕ_{ie} represent the elastic mode shapes at the base of the launch vehicle and at the launch vehicle/payload interface, respectively; M_{rr} is the 6x6 rigid body mass matrix of the entire composite system with respect to the base point; and $Z(f)^{-1}$ is a diagonal matrix with an element for each elastic mode of the form:

$$Z_n(f)^{-1} = \frac{(f/f_n)^2}{M_n[1 - (f/f_n)^2 + j\,2\zeta_n(f/f_n)]} \tag{4.3}$$

Each elastic mode (n = 1, 2, ..., N) in Equation (4.3) is characterized by its generalized mass M_n, modal damping ratio ζ_n, and natural frequency f_n.

Once the excitation {F(t)} is known, it can be used to predict the response of a new payload to be flown on the same type of launch vehicle. This becomes a very powerful tool, especially when refined by methods for modifying the properties of the interface impedance to account for differences between the old and new payload. This will be discussed further in Section 5.1. It should be noted, however, that inverse solutions are notorious for their high sensitivity to the quality of both the measured responses and the structural model used for the composite payload/launch vehicle.

4.1.3 Direct Measurements. For the launch vehicle, direct measurements of the vehicle dynamic environment are usually made during many ground tests, including (a) static firings of the solid rocket motors and/or liquid rocket engines [4.1], (b) stage and fairing separation tests, and (c) acoustic tests where acoustic noise is the primary excitation source. The purpose of these measurements is to furnish the data needed to (a) synthesize the design excitation, (b) determine the vibration specifications for expected payloads, and in some cases (c) characterize the design margins of the launch vehicle itself. Actual in-flight measurements of response quantities, such as accelerations at easily accessible locations or forces/strains on key structural members, have also been successfully made by means of telemetry [4.2 - 4.4]. Several purposes are served by these flight measurements, namely, (a) the verification of the accuracy of the analytically based design loads, (b) the verification of the flight environment itself, and (c) the verification of the entire prediction process for future flights. Detailed discussions of considerations for selecting flight instrumentation and techniques for data acquisition and reduction can be found in [4.5 - 4.7].

The primary limitation of direct in-flight measurements by telemetry is the availability of channels. Hence, a special effort is required to plan the measurements over a series of launches and to be flexible with plan changes as suggested by past measurements. Extrapolations are almost always needed to create a more complete description of the environment, as discussed in Section 4.1.2.

The area that often requires the greatest reliance on direct measurements is the determination of transportation loads (see Section 3.1) where low frequency transient excitations are common. To measure transportation environments, limitations on instrumentation and data gathering systems are minimal. The transient excitation sources are road surface defects (“pot holes”) for trailer-truck vehicles, discontinuities at rail tracks (joints, switches, etc.) for railroad vehicles, and rough landings for aircraft. For both transient and steady state excitations (see Section 4.2), it is customary to compile the response data directly as acceleration magnitudes at various locations on the transportation vehicle as a function of frequency. Techniques for synthesizing the excitation from the measured responses are discussed in Section 4.1.2.

4.1.4 Assessments. Low frequency transient excitations arise from numerous complex environmental sources that are strongly dependent upon the specific application. In most cases, both analytical and extrapolation techniques are used in an integrated manner to properly synthesize the excitations for preliminary design purposes. During initial static firings and launches, direct measurements should be made and used to upgrade the original predictions.

4.2 Low Frequency Random Excitations. Referring to Table 4.1, random loading in the low frequency regime is typically associated with transportation, fluid slosh, and wind and turbulence loads, including the buffet loads caused by a turbulent flow over the vehicle [4.8].

4.2.1 Analytical Models. Analytical models for the low frequency random excitation loads due to transportation and fluid slosh are established by the same methods used for the low frequency transient loads discussed in Section 4.1. However, the dominant low frequency stationary or quasi-stationary random excitation for space vehicles is often the wind and buffet loads that occur on the launch pad prior to and during liftoff and early ascent. The actual flow of a gaseous atmosphere (wind) around a space vehicle is never steady. Turbulence in the flow generates a randomly varying pressure field that can be quite severe when the flow separates (see Section 3.8), i.e., when buffet occurs. Hence, an appropriate description of the excitation and the response of the elastic body must account for the random character of the turbulent flow. The random nature of the atmospheric turbulence is due to the extremely complex interaction among such uncertain variables as the air viscosity, density, temperature, pressure, humidity, and velocity distribution. The model for turbulence loading is commonly expressed in terms of a power spectrum and spatial correlation of the turbulence, as detailed in Section 4.5.1. See [4.9, 4.10] for further details on analytical models for turbulence .

4.2.2 Scale Models. Because of the exceedingly complex nature of turbulence, scale models are often used in wind tunnels and other simulations [4.9 - 4.11]. From a knowledge of the relevant physical parameters which govern the dynamic similarity, dimensional analysis can be used to derive the appropriate scale factors [4.12]. At the top of the list, similarity in the geometry, mass, and stiffness distributions must be maintained. The attitude of the prototype relative to the flow field must be kept the same. Other scale factors include (a) the ratio of boundary layer thickness to the model dimensions, (b) the frequency and spectra of the turbulence, (c) the velocity of the flow, (d) the natural frequency of the model, (e) the ratio of the model mass to the mass of the displaced fluid, and (f) damping values. Satisfying the similarity relationships among all the parameters in the problem is often impossible, but simplifications in the model design can be achieved at the expense of inaccuracies in some similarity relations. See [4.11- 4.15] for examples and applications.

4.2.3 Extrapolation Techniques. As mentioned previously, the magnitude and distribution of the low frequency random loads are strongly influenced by the flexibility of the structure. Indeed, buffeting results from interaction between the turbulent flow and the flexibility of the structure. A direct characterization of the excitation can be made through measurements, either on the full scale space vehicle (see Section 4.2.4) or developmental scale models (see Section 4.2.2). Measuring the excitation on the full scale vehicle is useful for verification and possibly for creating a data base for future developments. Scale model measurements, however, are usually made to enable assessment of a proposed vehicle design. As discussed in Section 4.2.2, it is difficult to design scale models that satisfy the similarity relations for all of the parameters. Further utilization of the full scale measurements and refinement of scale model results can be made by extrapolation techniques. Such techniques may use a variety of approaches, one of which is outlined next.

The objective of the work in Ref. [4.16] was to determine the fluctuating pressure loads on proposed aircraft configurations using existing wind tunnel test data on existing designs. As an example of the methodology, the prediction of the buffeting pressures on a flexible tail is inferred from the spectra of measured wind tunnel pressure data on a geometrically identical but rigid tail.

The inference is made by a nonlinear neural network, which through a learning algorithm, combines the rigid tail data with a nonlinear model of the vortex-tail interaction. Neural networks [4.17] have the ability to learn how to solve a new problem and, hence, can adjust the values of their constant parameters by first undergoing training. Training is achieved by providing the network with the solutions of similar problems.

4.2.4 Direct Measurements. Direct measurement of the excitation can be presented in the form of an autospectral density function, as defined in Section 2.2.4. Measurements can be made simultaneously at several discrete locations on the surface of the space vehicle to map the excitation on the entire surface. Spatial correlations of buffet pressures, as given in Section 4.5.1.4, are very important for accurate response predictions. Detailed discussions of measurement transducers and techniques of data analysis can be found in [4.7].

4.2.5 Other Procedures. In some cases, a contributing excitation can only be inferred by a trial and error process to match observable responses. For example, in the case of the Titan IV launch vehicle, the aerodynamic loading on the solid motors was never measured in wind-tunnel tests, so a low frequency "equivalent" excitation at the top of the solid motors was developed to envelope certain payload interface responses.

More accurate predictions of the excitation to account for wind and aerodynamic forces, and in some cases extremely small forces, are essential for bodies with large surface areas. This would be the case, for example, when a deployed parachute is used to assist in stabilizing and decelerating a landing system [4.18, 4.19], or if solar sailing [4.20 - 4.23] is used as a propulsion system to deliver a payload to its destination. Illustrations are detailed in the cited references.

4.2.6 Assessments. Low frequency random excitations arise from complex environmental sources that are strongly dependent upon the specific application. In most cases, both analytical and extrapolation techniques are used in an integrated manner to properly synthesize the excitations for preliminary design purposes, but scale models of the vehicle on its launch pad can be effective, particularly for the formulation of wind loads. Direct measurements on the launch pad and during the first launch should be made and used to upgrade the original predictions.

4.3 Quasi-Periodic Excitations. Referring to Table 4.1, the most potentially damaging sources of quasi-periodic excitations are the two self-excited ones, namely, pogo instability (Section 3.11) and the resonant burn of a solid rocket motor (Section 3.12). The severity of these sources is not predictable analytically and is therefore only known in a statistical sense after a number of actual experiences. The severity of induced pogo vibration is only observable in flight and has been known to dramatically increase, for no apparent reason, after a number of flights. In the case of the S-II stage of the Saturn V vehicle, the level of pogo vibration rose by a factor of four over the highest level experienced during the previous twelve flights and caused a demonstrated load capability to be exceeded by a factor of two. It follows that it is dangerous to continue flying with a pogo instability, particularly since many successful suppression design implementations have been demonstrated (Section 3.11). In the case of a motor resonant burn, static firings have to be experienced to identify the severity of the resulting pressure oscillations.

Lower level quasi-periodic excitations might occur due to transportation vehicle and/or onboard equipment induced loads. Specifically, space vehicles and/or their components often see quasi-periodic forces during transportation by land, sea, or air due to reciprocating engines, rotating drive shafts, propellers, etc., in the transportation vehicle. Similarly, equipment in the space vehicle or its payload may have rotating elements that produce quasi-periodic forces. Specifications for transportation loads are available in the literature (see Section 3.1). Possible quasi-periodic loads from onboard equipment must be evaluated on a case-by-case basis.

4.4 Exterior Acoustic Noise Excitations. The dominate high frequency dynamic load for a space vehicle and/or its payload is often the intense acoustic pressure field over the exterior of the vehicle structure generated by the rocket engine/motor(s) during liftoff, as summarized in Section 3.6. The acoustic pressures at various locations on the structure, sometimes grouped into structural regions where the acoustic pressures are reasonably homogeneous within each

region, are usually predicted in terms of a 1/3 octave band spectrum of maximax values, as defined in Sections 2.2.6 and 2.2.7, respectively. Four basic procedures are used to predict the acoustic pressures on the exterior of a space vehicle structure during liftoff, namely, (a) sound power techniques, (b) scale acoustic models, (c) extrapolation techniques, and (d) direct measurements.

4.4.1 Sound Power Techniques.

4.4.1.1 Overall Sound Power Level. Conventional rocket noise theory and empirical data [4.24 - 4.26] can be used to predict the overall sound power levels produced by rocket engines/motors during liftoff. An early approximation for the overall sound power level (L_W) produced by a single rocket engine/motor with no deflection of the exhaust is given by [4.24]

$$L_W \text{ in dB (ref:} 10^{-12} \text{ watt)} = 68 + 13.5 \log_{10} (0.91\, FV_e) \qquad (4.4)$$

where

V_e = exhaust gas velocity at the nozzle exit (m/s)
F = total thrust of each rocket engine/motor (N)

However, Equation (4.4) is known to over-predict the sound power level for large rocket engines/motors (F > 500 kN). It is suggested in [4.26] that a more accurate approximation for the overall sound power level for larger rockets is given by

$$L_W \text{ in dB (ref:} 10^{-12} \text{ watt)} = 120 + 10 \log_{10} (0.005\, FV_e) \qquad (4.5)$$

where F and V_e are as defined in Equation. (4.4). For the case where two or more rocket engines/motors are mounted in a cluster, the total sound power produced by the cluster of n engines/motors is given by

$$L_{WT} \text{ in dB (ref: } 10^{-12} \text{ watt)} = 10 \log_{10} \sum_{i=1}^{n} 10^{L_{Wi}/10} \qquad (4.6)$$

For example, assume three relatively small rocket motors, each producing a thrust of F = 100 kN and having an exhaust gas velocity of V_e = 3 km/s, are clustered together to provide a total thrust of 300 kN. The sound power level produced by each motor is given by either Equation (4.4) or (4.5) as L_{Wi} = 182 dB. Thus, the total sound power for the cluster of n = 3 motors is given by Equation (4.6) as L_{WT} = 187 dB.

It should be mentioned that Equation (4.5) assumes an acoustic efficiency of 1%, which is conservative. If a more average prediction for an undeflected rocket exhaust is desired, an efficiency of 0.5% should be assumed, which corresponds to subtracting 3 dB from Equation (4.5). Exhaust deflectors generally reduce the acoustic efficiency even further, to less than 0.05% for perpendicular impingement of the exhaust on a flat plate, as summarized in [4.26]. However, deflected rocket exhausts often produce higher acoustic levels on the exterior of the vehicle than an undeflected exhaust due to the directivity pattern of the exhaust generated noise.

4.4.1.2 Sound Power Spectrum Level. It has been shown (e.g., [4.26]) that the shape of the spectra for the sound power levels produced by both liquid propellant rocket engines and solid propellant rocket motors collapse quite well when plotted against a normalized frequency called "Strouhal number", given by

$$f\, D_e/V_e \tag{4.7}$$

where D_e is the nozzle exit diameter and V_e is the exhaust gas velocity. A plot of the normalized sound power spectrum level (sound power level in 1 Hz frequency bandwidths) for rocket engines/motors with thrusts between 1.56 and 31,100 kN is shown in Figure 4.1, which is taken directly from [4.26]. For the case where two or more rocket engines/motors are mounted in a cluster, the equivalent nozzle exit diameter for the cluster of n engines/motors is approximated by

$$D_e = \sqrt{n}\, D_{ei} \tag{4.8}$$

where D_{ei} is the exit diameter for each of the individual nozzles. The sound power spectrum level in Figure 4.1 can be converted to any other desired bandwidth (usually 1/3 octave bandwidths) using the relationship

$$L_{WB}(f_B) \text{ in dB (ref: } 10^{-12} \text{ watt)} = 10 \log_{10}\left[\frac{W(f_B)}{W_{OA}}\frac{V_e}{D_e}\right] + L_W - 10 \log_{10}\left[\frac{V_e}{D_e}\right] + 10 \log B \tag{4.9}$$

where

B = bandwidth (Hz) for 1/3 octave bandwidths, $B \approx 0.23\, f_B$
f_B = center frequency of bandwidth B (Hz)
$L_{WB}(f_B)$ = sound power level [dB (ref: 10^{-12} watt)] in bandwidth B at center frequency f_B
$W(f_B)$ = sound power spectrum (in watt) at frequency f_B
W_{OA} = overall sound power (in watt)
L_W = overall sound power level [dB (ref: 10^{-12} watt)]
V_e = rocket engine/motor exhaust gas velocity (m/s)
D_e = rocket engine/motor nozzle exit diameter (m)

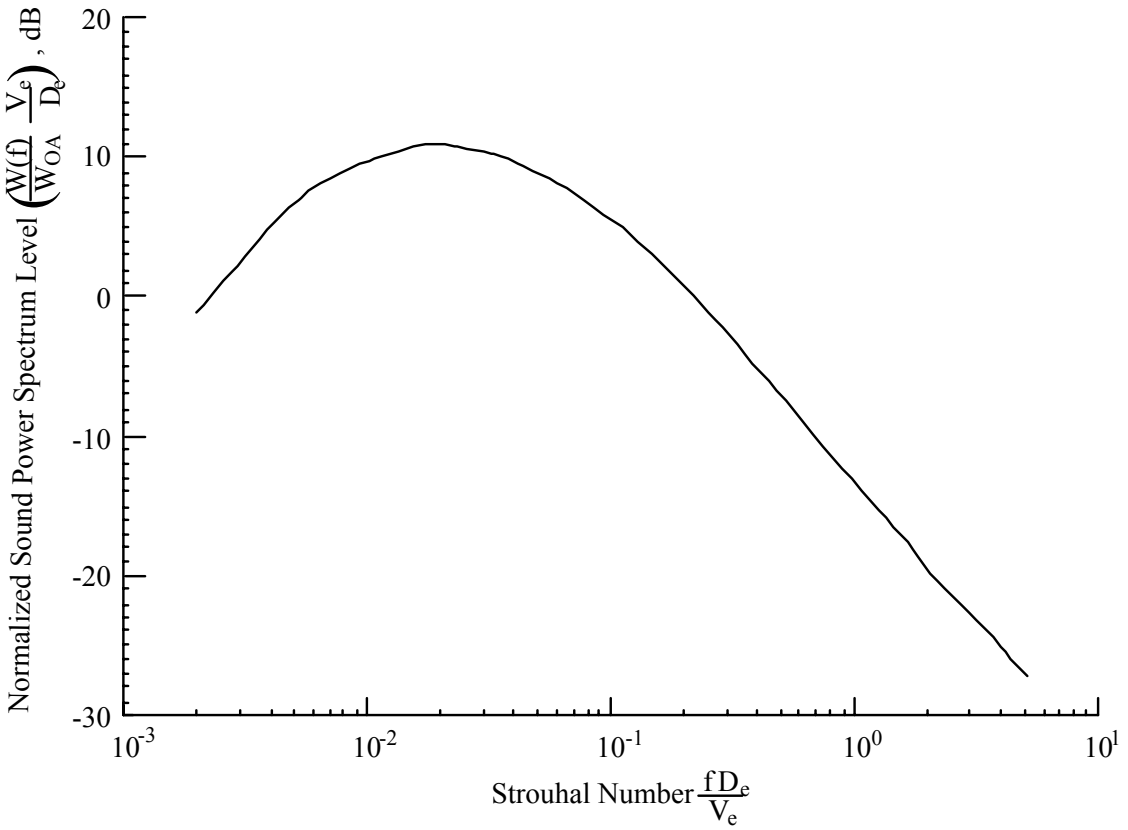

FIGURE 4.1. Normalized Sound Power Spectrum Level for Rocket Engine/Motor Acoustic Noise.

4.4.1.3 1/3 Octave Band Sound Pressure Levels. The sound power level in 1/3 octave bands determined by Equation (4.9) can be converted to a sound pressure level in 1/3 octave bands, denoted by L_{PB}, at any location on the exterior of the space vehicle structure using the relationship [4.25, 4.26]

$$L_{PB}(f_B) \text{ in dB (ref: 20 } \mu\text{Pa)} = L_{WB}(f_B) - 20 \log_{10} R + DI(\phi, f_B) - 11 \qquad (4.10)$$

where

$L_{WB}(f_B)$ = sound power level in bandwidth B computed from Equation (4.9)
R = distance from the source (m)
$DI(\phi, f_B)$ = directivity index dependent on angle ϕ from the exhaust flow axis and bandwidth center frequency f_B.

Values for the directivity index $DI(\phi, f_B)$ are given in [4.24, 4.26] for a full range of angles and 1/3 octave bandwidth center frequencies.

In practical applications, Equation (4.10) requires modifications to account for a number of factors including, (a) deflector geometry, (b) launch pad water injection, if used, and (c) reflections from the ground and nearby structures. Also, the location of the acoustic source in the rocket exhaust varies widely with frequency, which influences both the distance R and the angle ϕ in Equation (4.10). Experience plays a major role in properly accounting for such factors, but there are some documents, the most important being [4.26], that provide extensive guidelines. Although published in 1971, [4.26] is considered to still provide the best detailed procedure for computing the acoustic loads on the exterior of a space vehicle generated by the

rocket engine(s)/motor(s) during liftoff. Additional information on the determination of the directivity index in Equation (4.10) is given in [4.24], and data on the noise suppression provided by water injection are summarized in Section 4.4.1.5 to follow.

4.4.1.4 Spatial Correlation. To accurately predict the response of a structure to the acoustic pressure levels produced by a rocket engine(s)/motor(s), it is necessary to know the spatial correlation of the pressure levels from one point to another on the surface of the structure. This spatial correlation for rocket generated acoustic pressures has been empirically studied with the results summarized in numerous documents (e.g., [4.25 - 4.28]). There is a consensus from these studies that the spatial correlation for pressures on the exterior surface of a space vehicle structure during liftoff is of the form

$$\rho_x(\Delta x,f) \approx \exp[-a_x k_x \Delta x] \cos(k_x \Delta x) \quad (4.11a)$$

$$\rho_y(\Delta y,f) \approx \exp[-a_y k_y \Delta y] \cos(k_y \Delta y) \quad (4.11b)$$

where

x	= longitudinal axis of vehicle
y	= circumferential axis of vehicle
Δx, Δy	= separation distance along x axis, y axis
k_x, k_y	= trace wave number along x axis, y axis
a_x, a_y	= empirical coefficients

The values for the trace wave numbers and empirical coefficients vary somewhat among the references, but the values recommended herein are

$$k_x = \sin \beta \, (f/c_0) \; ; \; k_y = \cos \beta \, (f/c_0) \quad (4.12a)$$

$$a_x = 0.032 \; ; \; a_y = 0.31 \quad (4.12b)$$

where c_0 is the speed of sound in the local atmosphere and β is the angle of incidence of the sound waves to the longitudinal axis of the vehicle, which in turn is a function of the deflector configuration.

4.4.1.5 Water Injection. As mentioned in Section 4.4.1.3, the rocket engine/motor generated sound pressure levels, when the vehicle is on or near the launch pad during liftoff, can be suppressed by injecting water on top of the launcher, over the exhaust duct, and/or at the deflector crest. The use of water injection can also dramatically suppress the rocket motor ignition overpressure. The physical mechanisms that cause the noise suppression produced by water injection are not sufficiently well understood to allow an accurate analytical formation of the resulting noise reduction. However, considerable experimental data have been acquired that allow useful empirical estimates, as summarized in Figure 4.2 taken from [4.29]. See [4.30] for details on water suppression and launch pad configurations.

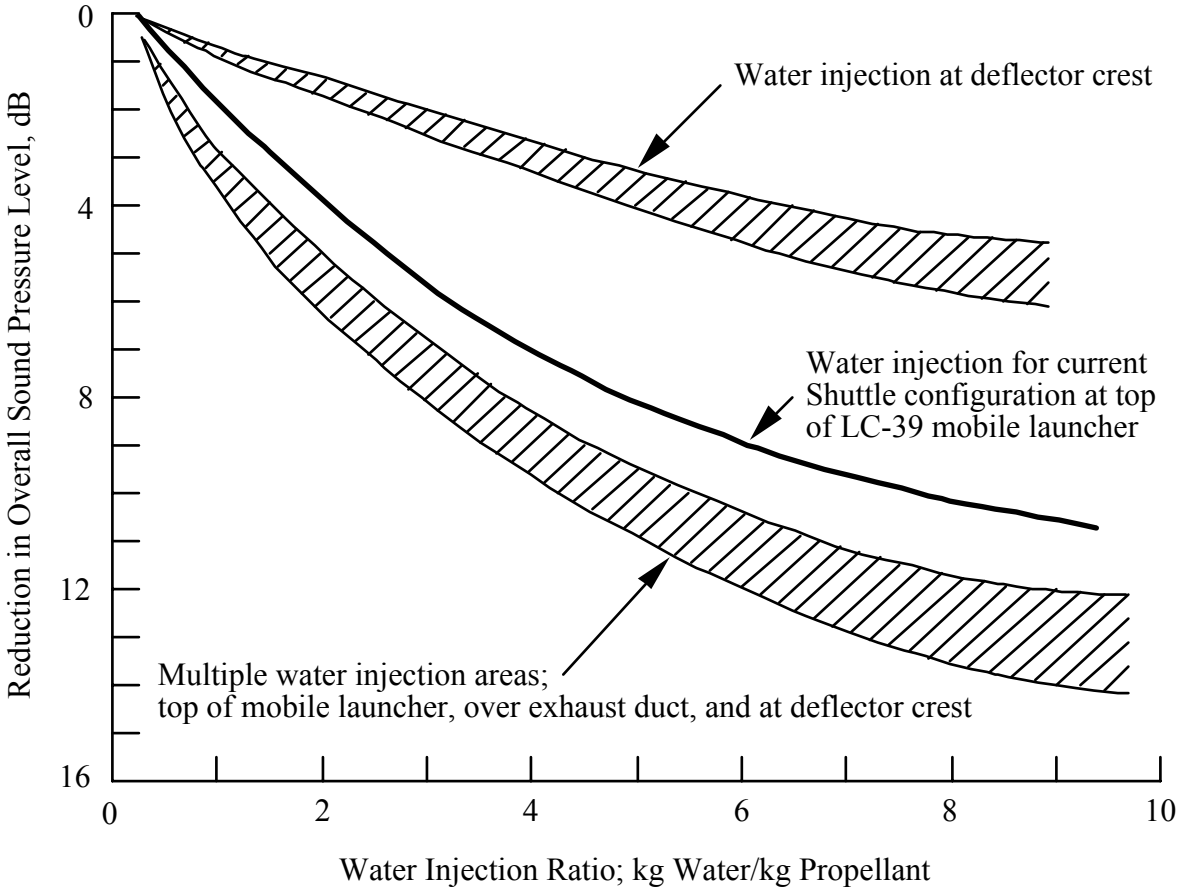

FIGURE 4.2. Reduction in Overall Sound Pressure Level Provided by Water Injection [4.29].

4.4.2 Scale Acoustic Models. Although expensive, scale acoustic models can be used to obtain reasonably accurate estimates of the acoustic loads on the exterior of a space vehicle during liftoff. In particular, scale model tests can allow a thorough evaluation of different deflector configurations, water injection systems, and other noise mitigating procedures. To achieve good results with scale models, it is necessary to accurately simulate the basic characteristics of the rocket exhaust gas flow, namely, the exhaust gas density, velocity, Mach number, and exit static pressure [4.26]. With a proper simulation of these parameters, the scaling rules for the rocket sound power level and the resulting acoustic pressures at various locations on the space vehicle reduce to those given in Equation (4.5) and (4.10) for sound power and pressure levels, and in Equation (4.7) for frequency, i.e.,

$$\begin{aligned} L_{Wf} \text{ in dB (ref: } 10^{-12} \text{ watt)} &= L_{Wm} + 10 \log_{10}(F_f / F_m) \\ L_{PBf}(f_{Bf}) \text{ in dB (ref: } 20\mu Pa) &= L_{PBm}(f_{Bm}) + 10 \log_{10}(R_f / R_m) \\ f_{Bf} &= f_{Bm}(D_{em} / D_{ef}) \end{aligned} \qquad (4.13)$$

where the subscript f denotes full scale, the subscript m denoted model scale, and all other terms are as defined in Equations. (4.9) and (4.10). Due to various practical problems, [4.26] recommends that the dimensions of a scale model be no less than 5% of full scale. See [4.29] for a detailed description of the 6.4% scale model tests used to predict the liftoff acoustic environment for Space Shuttle.

4.4.3 Extrapolation Techniques. For those cases where a new space vehicle and its proposed launch facility are broadly similar in design to a previous vehicle and launch facility for which acoustic measurements during liftoff are available, predictions for the liftoff acoustic environment over the exterior of the new vehicle can be accomplished by simply extrapolating the measurements on the previous vehicle using the scaling laws in Equation (4.13), where in this case, the subscripts f and m refer to the new and previous vehicles, respectively. Of course, this assumes the basic rocket exhaust gas characteristics (density, velocity, Mach number, and exit static pressure) and the launch facility features (deflector configuration, water injection system, and nearby reflecting structures) are the same. In most cases, such similarities between the new vehicle and a prior vehicle for which data are available will not exist. The most severe errors in extrapolated sound pressure levels usually occur because of differences between the launch pads, particularly the deflector configurations, from the previous to the new vehicle. Corrections to the extrapolated sound pressure levels for basic differences in the deflector configurations might be made using the guidelines in [4.26], but the potential for errors in the extrapolated levels is substantially increased.

4.4.4 Direct Measurements. It is obvious that the acoustic loads on the exterior of a space vehicle during liftoff must be predicted long before the vehicle is designed, fabricated, and launched. Nevertheless, direct measurements can be and often are made during the first or early launches of a space vehicle to confirm the original predictions. The best way to make direct measurements of the acoustic loads on the exterior of the vehicle is to mount microphones in the structure such that the microphone diaphragms are flush with the surface of the structure. With a flush-mounted configuration, the same microphones can be used to measure the aerodynamic loads during ascent through the transonic and maximum q regions (see Section 4.5.4). Of course, such an instrumentation system is expensive, particularly when installed on an expendable launch vehicle where the instrumentation is lost with the vehicle, but not unreasonably expensive when installed on a reusable launch vehicle. For example, three flush mounted microphones were installed on the exterior of the first launched Space Shuttle Orbiter Vehicle (OV-102, [4.31]), and acoustic and aerodynamic noise levels were measured during the first five launches.

Direct measurements of the liftoff acoustic levels can also be made using microphones mounted to the launch facility structure or other ground structures. Such ground measurements will not be at the exterior surface of the vehicle structure and will not move with the vehicle as it lifts off. However, by appropriate extrapolations using Equation (4.13), the measurements can be corrected for the microphone locations and used to describe the acoustic levels on the exterior of the structure at the start of liftoff. Unfortunately, the maximum acoustic levels on the exterior of the structure commonly occur several seconds after liftoff when the vehicle is 5 to 30 m off the launch pad. Ground measurements cannot be used to accurately predict these maximum levels.

4.4.5 Assessments. The merits of the various prediction procedures to establish the acoustic loads on the exterior of a space vehicle during liftoff are broadly summarized in Table 4.2. The accuracy of the various procedures depends heavily on when the predictions are made, e.g., the predictions produced by both the sound power and extrapolation techniques can be upgraded to a higher level of accuracy based upon acoustic measurements made during the first test firing of the rocket engine(s)/ motor(s). Also, the accuracy of some procedures is

heavily dependent on the similarity of the vehicle and its launch facility to prior vehicles launched from similar facilities, e.g., extrapolation techniques can be quite accurate under these conditions. Finally, two or more prediction techniques are often used to enhance confidence in the results, e.g., direct measurements are sometimes made at one or a few locations on the structure during the first launch to verify earlier predictions.

TABLE 4.2. Comparative Merits of Various Procedures for Predicting Liftoff Acoustic Excitations.

Merit	Sound Power Techniques	Scale Model Techniques	Extrapolation Techniques	Direct* Measurements
Relatively easy to physically accomplish	Yes	No	Yes	No
Applicable during preliminary design	Yes	No	Yes	No
Applicable before first test firing of rocket engine(s)/motor(s)	Yes	Yes	Yes	No
Applicable before first vehicle launch	Yes	Yes	Yes	No
Applicable to radical new rocket engine/motor design	Yes	Yes	No	Yes
Applicable to radically new launch pad configurations	Yes	Yes	No	Yes

*Assumes measurements are made on exterior surface of vehicle structure

4.5 Exterior Aerodynamic Excitations. A second major source of high frequency dynamic loads for a space vehicle and its payload are the fluctuating pressures generated by the turbulent boundary layer (TBL) between the exterior surface of the vehicle structure and the air during flight through the atmosphere. As for the acoustic loads during liftoff discussed in Section 4.4, the fluctuating pressures at various locations on the structure, sometimes grouped into structural regions where the fluctuating pressures are reasonably homogeneous within each region, are usually predicted in terms of a 1/3 octave band spectrum of maximax values, as defined in Sections 2.2.6 and 2.2.7. Four basic procedures are used to predict the TBL fluctuating pressures on the exterior surface of a space vehicle structure during flight through the atmosphere, namely, (a) boundary layer prediction techniques, (b) scale wind tunnel models, (c) extrapolation techniques, and (d) direct measurements.

4.5.1 Boundary Layer Prediction Techniques

4.5.1.1 Overall Fluctuating Pressure Level. There is a well developed theory formulated in [4.32] and elsewhere, backed by considerable empirical data summarized in [4.33 - 4.41], that can be used to predict the fluctuating pressures generated by a TBL. Specifically, the overall fluctuating pressure level, denoted by L_{FP}, produced by a TBL can be approximated by [4.35]

$$L_{FP} \text{ in dB (ref: } 20\mu\text{Pa)} = 20 \log_{10} \left[\frac{C_q q}{1 + 0.14 M^2} \right] \qquad (4.14)$$

where

q = flight dynamic pressure = $\frac{1}{2}\rho U_\infty^2$ (Pa)

ρ = density of air at flight altitude (kg/m^3)

U_∞ = free-stream air speed of vehicle (m/s)

M = Mach number of vehicle

C_q = constant of proportionality

The coefficient C_q depends on the geometry of the flight vehicle structure, the location on the structure, and the Mach number. For flow over flat panel structures, [4.33, 4.35] recommend a value of $C_q \approx 0.006$ for $M < 5$, but [4.34] suggests $C_q \approx 0.02$ is a more realistic value for attached flow over a space vehicle, and $0.03 \le C_q \le 0.1$ is appropriate for separated flow during subsonic and transonic flight. Even higher values of C_q may apply near structural discontinuities such as steps, struts, and cavities [4.38]. Excluding locations near structural discontinuities, it is recommended that Equation (4.14) with $C_q = 0.02$ be used to predict the fluctuating pressure level produced by the TBL over the exterior surface of space vehicles during flight through the atmosphere.

For example, assume a vehicle reaches a maximum flight dynamic pressure of q_{max} = 33,500 Pa (about 700 lb/ft^2) at a Mach number of M = 1.3 , and the TBL over a structural region of interest is attached so that $C_q \approx 0.02$. The fluctuating pressure level on the exterior of the structure is predicted by Equation (4.14) to be $L_{FP} \approx 149$ dB.

At locations near structural discontinuities where the flow separates and/or interacts with shock waves during transonic and supersonic flight, it is important to evaluate the local fluctuating pressure levels [4.38], but this is best accomplished using wind tunnel tests, as discussed in Section 4.5.2. The same is true of base pressure fluctuations at the aft end of the vehicle [4.39].

4.5.1.2 Fluctuating Pressure Spectrum Level. From [4.32], the shapes of the spectra for the fluctuating pressures produced by attached TBLs collapse quite well when plotted against a dimensionless frequency, f/f_0, where f_0, is called the "characteristic frequency" in [4.33] and is given by

$$f_0 \approx 0.1 \frac{U_\infty}{\delta^*} \qquad (4.15)$$

The term δ^* is called the boundary layer displacement thickness, broadly defined in [4.32] as the distance by which the external streamlines of the flow are shifted due to the formation of the boundary layer. The boundary layer displacement thickness is related to the boundary layer thickness denoted by δ, which is defined in [4.32] as the distance from the surface of the structure where the boundary layer velocity differs by 1% from the external velocity, and is given by

$$\delta = 0.37\, L\, R^{-0.2} \qquad (4.16)$$

where

L = distance from the leading edge

R = Reynolds number

The relationship between δ and δ^* depends on the nature of the flow (laminar versus turbulent), angle of incidence, and Mach number, but for turbulent flow over a flat plate with zero angle of incidence,

$$\delta^* = \delta/8 \tag{4.17}$$

For space vehicles, the TBL fluctuating pressure levels are of greatest interest during flight through the region of maximum dynamic pressure (q_{max}), which typically occurs during the launch phase at a Mach number in the range $1.2 < M < 1.4$. For Mach numbers in this range, [4.33] suggests that the boundary layer displacement thickness can be approximated by

$$\begin{aligned} \delta^* &\approx 0.0016\,L \quad (L \geq 3.1\,\text{m}) \\ &\approx 0.005 \quad (L < 3.1\,\text{m}) \end{aligned} \tag{4.18}$$

Various equations have been suggested in the literature for the normalized spectrum of attached TBL generated fluctuating pressure levels, e.g., [4.32 - 4.41]. However, the plot of the normalized fluctuating pressure spectrum levels in 1 Hz bands, $L_{FP}(f)$, given in [4.33] and shown in Figure 4.3 is recommended in the absence of detailed measurements. In the frequency region $f \leq f_0$, the spectrum level in Figure 4.3 is closely approximated by

$$L_{FP}(f/f_0) \text{ in dB (ref: } 20\mu\text{Pa}) = L_{FP} + 10\log_{10}\left[\frac{0.5}{1 + 0.44(f/f_0)}\right] - 10\log_{10} f_0 \tag{4.19}$$

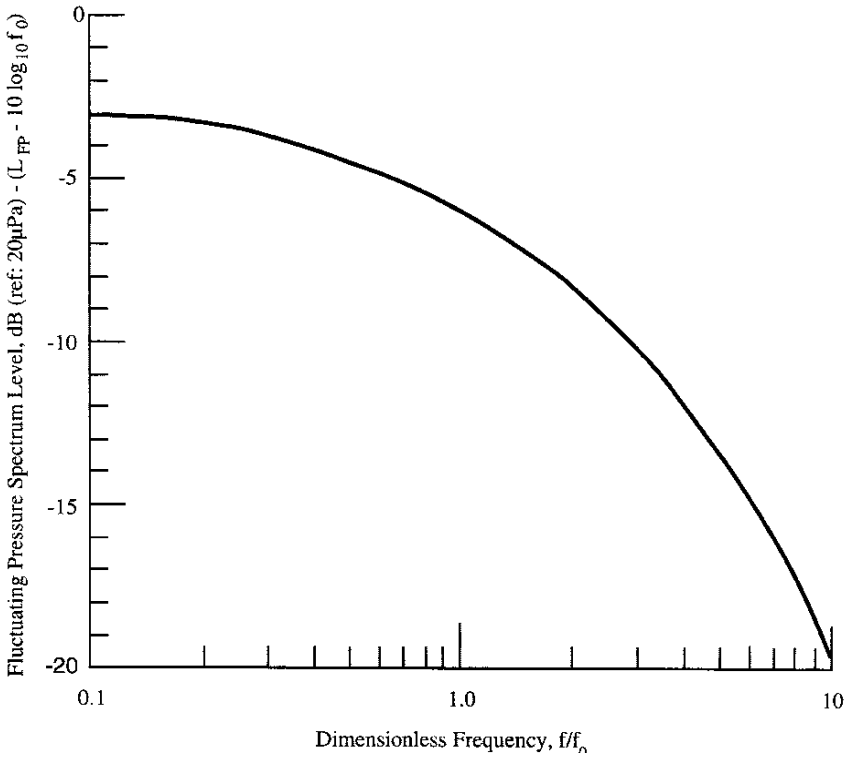

FIGURE 4.3. Normalized Spectrum Level for Attached TBL Fluctuating Pressures.

At those locations on the exterior of a space vehicle where the flow separates and interacts with shock waves, particularly during transonic and supersonic flight, the spectrum of the fluctuating TBL pressures tends to shift down towards the lower frequencies. This is illustrated in Figure 4.4, taken from [4.38], which shows both the normalized standard deviations and the spectra of the fluctuating pressures produced by a supersonic flow at several locations forward of a 45-degree ramp. The highest levels and lowest frequency content occur at that location (denoted by C) where an oscillating shock wave is positioned. Note that the influence of the oscillating shock wave is very localized, but the downstream fluctuating pressure levels are substantially higher and the spectra are more concentrated at the lower frequencies than the spectra of the oscillating shocks where the flow is attached. Various empirical prediction equations for the spectra of the fluctuating pressures produced by separated flow are given in [4.38], but wind tunnel tests provide the best way to evaluate separated flow conditions (see Section 4.5.2).

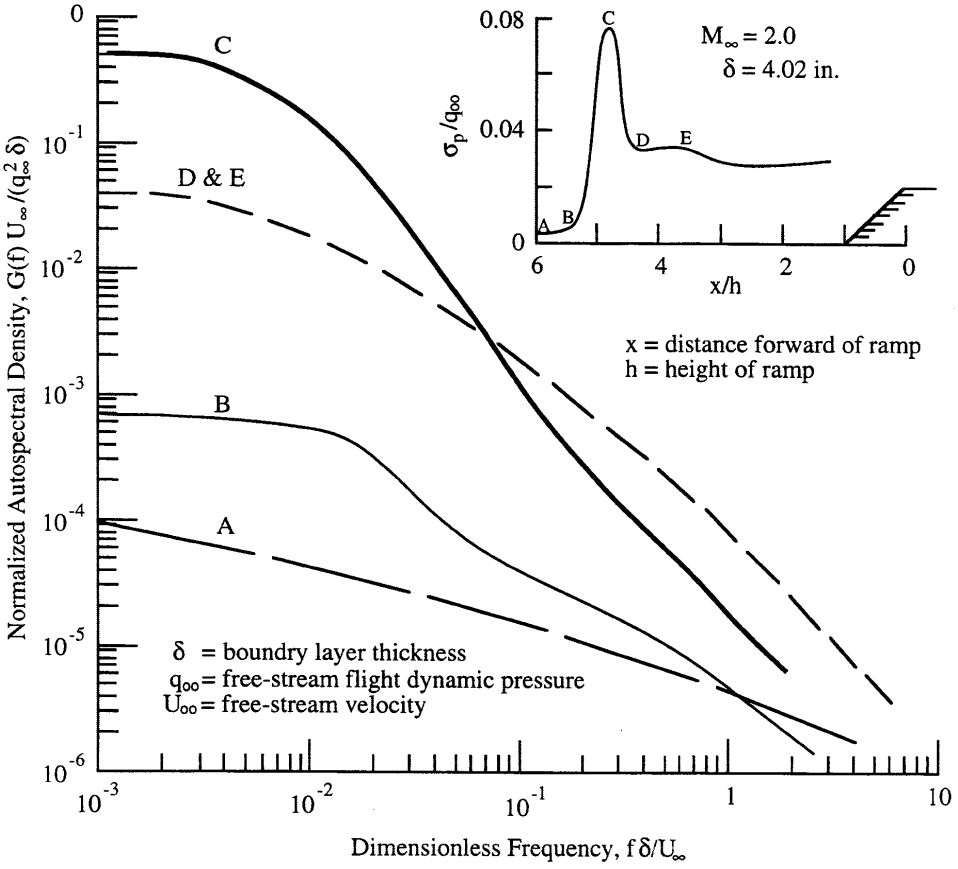

FIGURE 4.4. Normalized Spectrum Level for Separated TBL Fluctuating Pressures [4.38].

4.5.1.3 1/3 Octave Band Fluctuating Pressure Levels. The normalized fluctuating pressure spectrum levels in Figure 4.3 can be converted to spectrum levels in any other desired bandwidth (usually 1/3 octave bandwidths) by (a) computing the value of f_0, (b) converting the frequency scale to absolute frequency f in Hz, and (c) using the relationship

$$L_{FP}(B,f_B) \text{ in dB (ref: } 20\mu Pa) = L_{FP}(f_B) + 10 \log_{10} B \qquad (4.20)$$

where

B = bandwidth (Hz) - for 1/3 octave bandwidths, $B \approx 0.23\, f_B$
f_B = center frequency of bandwidth B (Hz)
$L_{FP}(B,f_B)$ = fluctuating pressure level [dB (ref: 20 μPa] in bandwidth B at center frequency f_B
$L_{FP}(f_B)$ = fluctuating pressure spectrum level (from Figure 4.3) at frequency f_B

4.5.1.4 Spatial Correlation. The spatial correlation for TBLs has been empirically studied with the results summarized in numerous documents (e.g., [4.32 - 4.41]). For most applications, it is convenient to describe the spatial correlation in terms of the real part of a cross-spectrum (see Section 2.2.11) and an associated convection velocity. It is also convenient to define all spectral quantities in terms of radial frequency $\omega = 2\pi f$ in radians/sec, rather than cyclical frequency f in Hz. With these definitions in mind, there is a consensus from the referenced studies that the real part of the cross-spectrum for the fluctuating pressures on the exterior surface of a space vehicle structure due to an attached TBL generated during flight through the atmosphere is of the form

$$G_{re:x}(\Delta x,\omega) \approx G(\omega)\, A_x(\Delta x,\omega) \cos(\omega \Delta x/U_c) \qquad (4.21a)$$

$$G_{re:y}(\Delta y,\omega) \approx G(\omega)\, A_y(\Delta y,\omega) \cos(\omega \Delta y/U_c) \qquad (4.21b)$$

where

x = longitudinal axis of vehicle (direction of motion)
y = circumferential axis of vehicle (normal to direction of motion)
Δx, Δy = separation distance along x axis, y axis (m)
U_c = convection velocity along x axis (m/s)
$A_x(\Delta x,\omega)$, $A_y(\Delta y,\omega)$ = frequency dependent coefficients along x axis, y axis

Of the various relationships for the coefficients, $A_x(\Delta x,\omega)$ and $A_y(\Delta y,\omega)$, presented in the literature, the values suggested in [4.27] are considered to have the widest application to space vehicles operating at maximum flight dynamic pressure, specifically,

$$A_x(\Delta x,\omega) = \exp\left\{-\left[(0.1\omega/U_c)^2 + (0.034/\delta^*)^2\right]^{0.5} |\Delta x|\right\} \qquad (4.22a)$$

$$A_y(\Delta y,\omega) = \exp\left\{-\left[(0.72\omega/U_c)^2 + (0.244/\delta^*)^2\right]^{0.5} |\Delta y|\right\} \qquad (4.22b)$$

where δ^* is the boundary layer displacement thickness and all other terms are as defined in Equation (4.21).

The convection velocities in Equations (4.21) and (4.24) are approximated from empirical data in various references, including [4.33] which suggests the simple expression

$$\frac{U_c}{U_\infty} \approx 0.7\left[\frac{U_\infty}{\omega \delta^*}\right]^{0.09} \qquad (4.23)$$

where U_∞ is the free-stream velocity of the vehicle. The convection velocity given by Equation (4.23) was developed from subsonic data, but is considered acceptable for the TBL generated

by space vehicles during flight at Mach numbers of M < 2. See [4.35 - 4.41] for more elaborate relationships.

The spatial correlation for separated flow TBLs is much more complicated and, under certain conditions, is near zero for even small spatial separation distances [4.38]. Wind tunnel tests provide the best means to evaluate the spatial correlation for separated flow.

4.5.2 Scale Aerodynamic Models. The various descriptions of the fluctuating pressures on the surface of a space vehicle produced by the TBL during flight, as detailed in Section 4.5.1, can be measured directly using an appropriately instrumented scale model in a wind tunnel. From Equation (4.14), for a scale model test at the full-scale flight dynamic pressure and Mach number, the overall fluctuating pressure level measured on the scale model applies to the full-scale vehicle. The scale model spectral and spatial measurements can be converted to full-scale by linearly scaling the values for Δx, Δy, δ^*, and f or ω in Equations (4.17 - 4.23).

Scale model tests provide an excellent means to determine the fluctuating pressures due to the complex boundary layer conditions in the region of structural discontinuities (e.g., near struts and skirts), as well as in the transonic and supersonic speed ranges where shock wave-boundary layer interactions may occur (see Figure 4.4). The primary problems in scale model testing are as follows:

a. Both an instrumented scale model and the actual test of a scale model in a high speed wind tunnel are relatively expensive.

b. The pressure transducers used for the scale model measurements must have diaphragms with diameters that are scaled down in size by the same amount as the geometric scaling of the vehicle. Specifically, to avoid large corrections of the spectra for the measured pressures, it is necessary to have a pressure transducer with a diaphragm diameter that is small compared to the boundary layer displacement thickness, say

$$D_{pd} < 0.2\,\delta^* \tag{4.24}$$

where D_{pd} is the diameter of the pressure transducer diaphragm. Even with a diaphragm diameter complying with Equation (4.24), corrections of the spectra for the measured pressures are required at frequencies where

$$f > \frac{U_\infty}{2\pi D_{pd}} \tag{4.25}$$

In all cases, it is critically important that the transducer not protrude above the surface of the structure, since this will cause substantial errors not accounted for by the diaphragm diameter corrections. See [4.33] for a summary of pressure transducer diaphragm diameter correction factors.

c. In some cases, surface pressures on scale models are measured using small holes in the exterior surface connected by short ducts to pressure transducers below the surface of the structure. The size of the surface hole replaces the diaphragm diameter in Equation (4.24), but the duct may introduce losses at the higher frequencies that require a careful calibration.

d. Because oscillating shock waves are localized and flow velocity dependent, closely spaced transducers are required near the anticipated location of oscillating shock waves, and a slow sweep of the flow velocity is needed to insure the capture of oscillating shock wave data.

e. Wind tunnels commonly produce acoustic noise from various internal sources that is carried in the flow during operation. Due to the acoustical modes inside the tunnel test section, substantial acoustic pressures may occur at some frequencies that can severely contaminate the desired fluctuating pressure measurements. The characteristics of the tunnel must be carefully evaluated for contaminating acoustic noise before scale model tests are performed.

4.5.3 Extrapolation Techniques. The TBL fluctuating pressure levels measured on a previous space vehicle during flight (referred to as the reference vehicle) can be easily scaled to a new vehicle, assuming similar geometries between the reference and new vehicles in the region of the measurements. Specifically, the overall fluctuating pressure level for the new vehicle can be estimated from

$$L_{FP:n} \text{ in dB (ref: } 20\mu\text{Pa)} \approx L_{FP:r} \text{ in dB (ref: } 20\mu\text{Pa)} + 20 \log_{10} \left[\frac{q_n / q_r}{(1 + 0.14M_n^2)/(1 + 0.14M_r^2)} \right] \quad (4.26)$$

where the subscripts n and r denote the new and reference vehicles, respectively, and all other terms are as defined in Equation (4.14).

Again assuming similar geometries, the measured spectrum levels from the reference vehicle can be scaled to the new vehicle by the following operations:

a. Using the ratio of the free-stream velocities for the reference and the new vehicle, compute the ratio of the characteristic frequencies defined in Equation (4.15) by

$$\frac{f_{0;\,n}}{f_{0;\,r}} = \frac{U_{\infty;\,n}}{U_{\infty;\,r}} \quad (4.27)$$

b. Scale the frequency axis for the measured spectrum levels by the ratio determined in Equation (4.27).

c. Scale the spectrum level axis so that the overall value of the frequency scaled spectrum levels agrees with the overall level given by Equation (4.26).

It is rare that sufficient measurements are available from a reference vehicle to allow the computation of the cross-spectra needed to establish spatial correlations. Hence, spatial relationships for a new vehicle are usually predicted using Equations. (4.21) through (4.23) with the appropriate parameters for the new vehicle.

4.5.4 Direct Measurements. The direct measurement of TBL fluctuating pressures on a space vehicle during flight requires the installation of pressure transducers that are flush mounted with the outside surface of the vehicle exterior structure, or at least the drilling of holes in the exterior structure that are ducted to sub-surface transducers. In either case, the vehicle structure must be violated. Such actions necessitate careful consultation with the designers of the vehicle structure, and generally are difficult and expensive to accomplish. In a few cases, usually involving a dramatically new vehicle design, such transducer installations may be authorized, e.g., three flush mounted external pressure transducers were installed in an early Space Shuttle Orbiter [4.31]. In general, however, direct measurements of TBL fluctuating pressure levels are not made on new vehicles.

4.5.5 Assessments. The merits of the various prediction procedures to establish the TBL fluctuating pressures on the exterior of a space vehicle during flight are broadly summarized in Table 4.3. Like the acoustic noise predictions covered in Section 4.4, the original prediction of TBL fluctuating pressures can sometimes be upgraded based upon flight data, but this requires expensive flight measurement instrumentation. Also, the accuracy of extrapolation techniques is heavily dependent on the similarity of the new vehicle to a prior vehicle with a similar design and flight profile.

TABLE 4.3. Comparative Merits of Various Procedures for Predicting TBL Pressure Excitations.

Merit	Boundary Layer Prediction Techniques	Scale Model Techniques	Extrapolation Techniques	Direct Measurements
Relatively easy to physically accomplish	Yes	No	Yes	No
Applicable to preliminary design	Yes	No	Yes	No
Applicable before first vehicle launch	Yes	Yes	Yes	No
Applicable to radically new vehicle designs	Yes	Yes	No	Yes

4.6 Interior Acoustic Noise Excitations. Space vehicle payloads and many launch vehicle components located within a fairing or payload bay during launch are exposed to high levels of acoustic noise. Peak interior acoustic levels are observed during three periods of vehicle ascent: liftoff, the period of time shortly after rocket motor ignition; transonic, the period at which vehicle speed is at or just below the speed of sound (Mach-one); and max-q, the period of time at which the dynamic pressure reaches a maximum. A short duration acoustic event may also be observed after ignition of solid rocket motors. Estimated interior acoustic levels for different vehicles are discussed in Section 4.6.5.

Sensitive electronic components and lightweight components with large surface areas, such as solar panels and antennas, are particularly at risk from high acoustic levels. Detailed predictions and acoustic tests are generally recommended for these components to ensure that they will survive the launch environment, see Sections 8.2 and 10.5.

The acoustic levels inside the fairing or payload bay are generally lower than the exterior levels associated with the rocket motor acoustic waves or the aerodynamic pressure fluctuations. The difference between the exterior acoustic level (or aerodynamic fluctuating pressure levels) and the interior acoustic level is defined as the noise reduction of the fairing or payload bay. This noise reduction must be computed using one of the analysis procedures described below in order to translate the exterior acoustic and /or aerodynamic loads determined in Sections 4.4 and 4.5 into the acoustic loads on the payload and other interior equipment and components.

The procedures used to compute or estimate the noise reduction of space vehicle fairings and payload bays include (a) modal analysis procedures, (b) statistical energy analysis procedures, (c) use of scale models, (d) extrapolation techniques, and (e) direct measurements. Other important considerations include (f) fill factors, (g) vent noise, and (h) mechanical vibration radiation.

4.6.1 Modal Analysis Procedures. Modal analysis procedures are often used to study the dynamic response of structures. These procedures can be extended to predict the interior acoustic environment by identifying the structural modes of the fairing and acoustical modes of the interior space. Techniques for computing the excitation of the structural modes by the exterior acoustic field and the coupling between the structural modes and the interior acoustical modes are well established [4.42]. These techniques were used to develop the "Payload Acoustic Environment for Shuttle" (PACES) computer software program [4.43]. This program predicts the acoustic levels in the Space Shuttle orbiter payload bay with any desired payload configuration over the frequency range from 12.5 Hz to 4,000 Hz. However, the formulation is quite cumbersome due to the large number of modes that must be considered. As a result, PACES and other modal analysis procedures are not commonly used to predict payload environments, although the methodology used in the program continues to be developed.

The vibroacoustic environment during the launch of a space vehicle extends over a broad range of frequencies. To encompass the entire frequency range of interest, a modal analysis must take into account the large number of acoustic and structural modes contributing to the dynamic response. Commercially available finite element method (FEM) modeling software programs make it possible to compute the structural and acoustical modes of complex dynamic systems over a broad range of frequencies. In theory, it should be possible to predict the acoustic environment using this type of prediction procedure. In practice, the large density of modes makes modal analysis too cumbersome to be of general use. In addition, the predictions obtained using this technique are generally quite sensitive to small changes in design and payload geometry, thereby requiring the analyses to be repeated several times as design changes and modifications are made. Thus, although modal analysis and FEM models hold out the promise of great accuracy and precision, this promise is often not delivered.

Boundary element method (BEM) analysis procedures have been proposed to alleviate some of the difficulties associated with the modal analysis of structural-acoustical systems [4.44]. To make a prediction of the interior acoustic field, a BEM model of the exterior and interior acoustic fields must be combined with a FEM model of the fairing. The accuracy of the BEM prediction is dependent on the accuracy of the underlying FEM model. Thus, BEM procedures may also be too cumbersome to be used over the entire frequency range of interest. They may, however, provide useful predictions of the acoustic environment at low frequencies.

4.6.2 Statistical Energy Analysis Procedures. Statistical energy analysis (SEA) and other related vibratory energy-flow techniques provide prediction procedures that are suitable for high frequencies [4.45 - 4.47]. By using a statistical description of the system and by using vibratory energy and power to formulate the dynamic equations, these procedures provide great simplifications to the analysis. SEA is much easier to apply than the classical modal analysis procedure and often yields more accurate predictions. However, in using this statistical procedure, it is not possible to predict the acoustic environment at individual points and single frequencies. The statistical prediction gives averages over spatial locations and bands of frequency. Advanced analyses may also provide higher order statistics such as the variance or standard deviation. A prediction of the mean acoustic level plus two times the standard deviation can then be used to set environmental requirements, as discussed in Section 6.

SEA draws on many of the fundamental concepts from statistical mechanics, room acoustics, wave propagation, and modal analysis [4.45 - 4.46]. At first, SEA appears to be a very simple method of analysis. However, because of the diversity of concepts used in formulating the basic SEA equations, the method quickly becomes very complex. For this reason, analysts have recommended caution in using SEA. However, when used properly, SEA is a powerful method for predicting both the acoustic and vibration environments in launch vehicles and payloads.

The application of SEA requires that the system be divided into a set of coupled subsystems. Each subsystem represents a group of modes with similar characteristics. The selection of subsystems involves several factors, including differences in geometry, differences in material properties, the ability of the subsystem to support resonant modes in the frequency bands of interest, and the expectation of a fairly uniform response within each subsystem.

The SEA subsystems can be considered to be “control volumes” for vibratory or acoustic energy flow. Under steady-state conditions, the time-average power input to a subsystem from external sources and from other connected subsystems must equal the sum of the power dissipated within the subsystem by damping and the power transmitted to the connected subsystems.

Consider, for example, a spacecraft located within a fairing enclosure as shown in Figure 4.5. The goal is to predict the acoustic levels within the fairing. A simplified SEA energy flow model is commonly used within the aerospace industry to predict interior acoustic levels [4.48]. Using this simplified model, the payload fairing and the interior acoustic space are divided axially into a number of zones [4.49]. The acoustical modes of each zone form a single SEA subsystem. The number of zones used for the analysis depends on the overall length of the fairing, the uniformity of the exterior acoustic field, and the regions of interest within the fairing. Typically, the zones are approximately 6 ft (2 m) long.

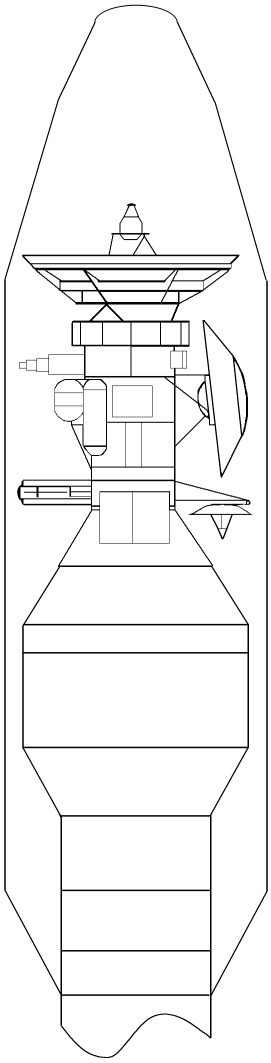

FIGURE 4.5. Illustration of Payload in Fairing Enclosure.

To carry out the analysis, an acoustic power balance is performed for each zone. The time-average power input to a zone is balanced with the sum of the power dissipated within the zone due to acoustic absorption and the net power transmitted to connected zones,

$$W_i^{in} = W_i^{absorbed} + \sum_j W_{i;j}^{transmitted} \tag{4.28}$$

where i refers to the ith zone.

The net power input to each zone from the fairing sidewall can be expressed in terms of the sound transmission coefficient of the fairing, τ, and the difference between the exterior and interior acoustic pressures,

$$W_i^{in} = \tau_i A_i \left(\frac{p_{i;ext}^2}{4\rho c_{ext}} - \frac{p_{i;int}^2}{4\rho c_{int}} \right) \tag{4.29}$$

where A_i is area of the fairing for zone i, ρc_{ext} is the characteristic impedance of the gas external to the fairing, and ρc_{int} is the characteristic impedance of the gas within the fairing. The characteristic impedances are generally the same. However, by preserving the dependence of the power input on the gas properties, Equation (4.29) can be used to predict the effect of using other gases within the fairing, such as helium, or the effects of altitude, where the static pressure and the gas density may be higher within the fairing than in the exterior space due to a lag in the venting.

The sound transmission coefficient is more commonly expressed in dB as the Transmission Loss, TL, where

$$TL = 10 \log_{10} \frac{1}{\tau} \tag{4.30}$$

The derivation of Equation (4.29) is based on the assumption that the acoustic fields are diffuse, with acoustic waves incident on the fairing from all angles of incidence. This assumption is valid when the fairing is placed in a reverberant test chamber for acoustic tests. However, adjustments may need to be made for vehicle liftoff, since acoustic waves are incident from the turbulent rocket motor exhaust flow below the vehicle. These adjustments are in the form of test chamber efficiency factors, which account for differences between the noise reduction obtained from flight data and that obtained from test chamber data [4.49]. Adjustments are also needed to account for the differences between excitation by acoustic waves during liftoff and excitation by aerodynamic fluctuating pressure fields in turbulent boundary layers, oscillating shocks, and separated flow during transonic and max-q periods of flight. These adjustments are made by applying efficiency factors to the noise reduction calculated for acoustic excitation.

The power dissipated within each zone due to acoustic absorption can be expressed in terms of a fairing absorption coefficient and the acoustic pressure in the subsystem,

$$W_i^{absorbed} = \alpha_i A_i \left(\frac{p_{i;int}^2}{4\rho c_{int}} \right) \tag{4.31}$$

When acoustic blankets are used, an average absorption factor must be calculated by averaging over the blanketed and unblanketed areas of each zone,

$$\alpha_i = \frac{1}{A_i} \sum_n \alpha_n A_n \tag{4.32}$$

where the summation is over all surface areas within the zone, A_n is the surface area for the nth area, and α_n is the absorption coefficient for the nth area. The average absorption coefficient is usually controlled by the absorption in the blanketed areas of the zone, since α_n for an unblanketed area is quite small.

Acoustic blankets may also affect the transmission coefficient. In this case, an average transmission coefficient must be calculated by averaging over the blanketed and unblanketed areas of each zone,

$$\tau_i = \frac{1}{A_i} \sum_n \tau_n A_n \tag{4.33}$$

The average transmission coefficient may be controlled by the transmission coefficient of the unblanketed areas of each zone. Finally, the net power transmitted between connected acoustic subsystems can be expressed in terms of the acoustic pressure in the two subsystems and the connection area. For example, the net power transmitted between subsystem i and j is given by,

$$W_{i;j}^{transmitted} = A_{i;j} \left(\frac{p_{i;int}^2}{4\rho c_{int}} - \frac{p_{j;int}^2}{4\rho c_{int}} \right) \tag{4.34}$$

where $A_{i;j}$ is the area of the connection between these two zones.

The power balance equations form a set of linear algebraic equations that can be solved for the average acoustic pressure in each zone of the fairing. For example, if we consider a single zone and ignore the transmitted power between zones ($W_{i;j}^{transmitted} = 0$), the power balance equation for the zone can be solved for the ratio of the acoustic pressures,

$$\frac{p_{i;int}^2}{p_{i;ext}^2} = \frac{\tau_i}{\alpha_i + \tau_i} \tag{4.35}$$

The noise reduction in dB for the ith zone is predicted to be

$$NR_i = 10 \log_{10} \left[\frac{p^2_{i;ext}}{p^2_{i;int}} \right] = 10 \log_{10} \left[1 + \frac{\alpha_i}{\tau_i} \right] \tag{4.36}$$

High values of noise reduction provide a low interior acoustic pressure environment. These are obtained by using acoustic blankets to increase the average absorption coefficient and by designing the fairing to achieve low values for the transmission coefficient.

The transmission coefficient for a particular fairing can be estimated by direct measurement, by scaling measured data for other fairings, or by analysis using a more detailed SEA model. Following the general SEA procedure presented in Section 5.2.2, an SEA model to predict the fairing transmission coefficient can be developed using three subsystems: (a) external acoustical modes, (b) fairing bending modes, and (c) internal acoustical modes. The mass-law modes of the fairing are not placed in a separate SEA subsystem since they are non-resonant. However, these nonresonant modes do contribute to the transmission coefficient of the fairing.

Three coupling paths are defined: (a) coupling between exterior acoustical modes and resonant modes of the fairing, (b) coupling between resonant modes of the fairing and interior acoustical modes, and (c) coupling between exterior and interior acoustical modes through mass-law response of the fairing. The subsystems and energy flow paths are shown in Figure 4.6. The third path is often the most dominant path of energy transmission for light-weight fairings and must not be neglected.

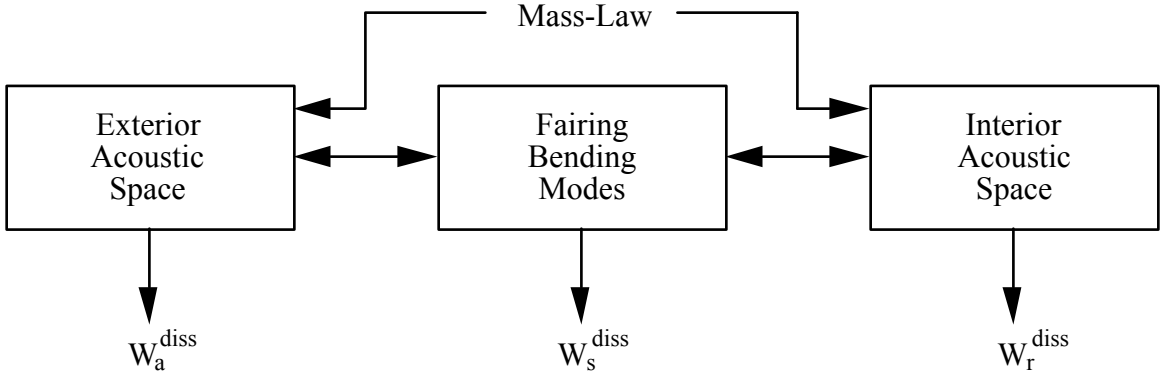

FIGURE 4.6. Simple Three Subsystem SEA Model of a Launch Vehicle Fairing.

If the energy in the external space is known, SEA power balance equations for the fairing and internal acoustic subsystems lead to the following equations,

$$\begin{bmatrix} \eta_{plf;d} + \eta_{plf;ext} + \eta_{plf;int} & -\eta_{int;plf} \\ -\eta_{plf;int} & \eta_{int;d} + \eta_{int;plf} + \eta_{int;ext} \end{bmatrix} \begin{bmatrix} E_{plf}/E_{ext} \\ E_{int}/E_{ext} \end{bmatrix} = \begin{bmatrix} \eta_{ext;plf} \\ \eta_{ext;int} \end{bmatrix} \tag{4.37}$$

where the subscript d denotes the damping loss factor and the other subscripts refer to modes of the external acoustic space, the payload fairing, and the internal acoustic space. These equations can be solved to obtain the ratio of the energies in the internal and external acoustic spaces,

$$\frac{E_{int}}{E_{ext}} = \frac{\eta_{ext;int}\left(\eta_{plf;d} + \eta_{plf;ext} + \eta_{plf;int}\right) + \eta_{plf;int}\,\eta_{ext;plf}}{\left(\eta_{plf;d} + \eta_{plf;ext} + \eta_{plf;int}\right)\left(\eta_{int;d} + \eta_{int;plf} + \eta_{int;ext}\right) - \eta_{plf;int}\,\eta_{int;plf}} \tag{4.38}$$

This equation can be further simplified if we assume the damping loss factors to be greater than the coupling loss factors.

$$\frac{E_{int}/n_{int}}{E_{ext}/n_{ext}} = \frac{1}{\eta_{int;d}}\left[\eta_{int;ext} + \frac{\eta_{plf;int}\,\eta_{plf;ext}}{\eta_{plf;d}}\right] \tag{4.39}$$

where the SEA reciprocity factor relating coupling loss factors and modal densities has been used,

$$n_{plf}\,\eta_{plf;int} = n_{int}\,\eta_{int;plf} \tag{4.40}$$

The term in the brackets represents the effective coupling loss factor between the internal and external acoustic space including both nonresonant mass law sound transmission and transmission by resonant fairing modes. This coupling loss factor is directly related to the sound transmission coefficient used in Equation (4.36) to obtain the fairing noise reduction,

$$\tau_i = \frac{8\pi f V_i}{c_i S_i}\left[\eta_{int;ext} + \frac{\eta_{plf;int}\,\eta_{plf;ext}}{\eta_{plf;d}}\right] \tag{4.41}$$

where f is the frequency of vibration, c_i is the speed of sound for the gas in zone i, V_i is the interior volume of the ith zone, and S_i is the fairing surface area for the zone.

The absorption coefficient can also be directly related to the damping loss factor of the interior acoustic space,

$$\alpha_i = \frac{8\pi f V_i}{c_i S_i}\eta_{int;d} \tag{4.42}$$

The coupling loss factor between resonant modes of the fairing and the internal acoustic space, $\eta_{plf;ext}$, is often expressed in terms of other quantities such as a radiation resistance, R_{rad}, or a radiation efficiency, σ_{rad}. These relationships are summarized below,

$$\eta_{plf;int} = \frac{R_{rad}}{\rho c_{int} A_{plf}} = \frac{\rho c_{int}}{2\pi f m_{plf}}\sigma_{rad} \tag{4.43}$$

where A_{plf} is the surface area of the fairing and m_{plf} is the mass per unit area of the fairing sidewall. These results can also be used for the coupling loss factor between the resonant modes of the fairing and an external reverberant test chamber.

A theoretical SEA model to calculate the interior acoustic levels during flight may require a more detailed representation of the external acoustic field. The assumption that the external field is a diffuse field, with acoustic waves incident from all directions, is not valid and may lead to an over prediction of the acoustic levels, particularly at the lower frequencies. One approach is to use the joint acceptance, (see Section 5.2), to compute the vibratory power input to the resonance modes of the fairing. The power input in a band of frequencies is given by

$$W_{plf}^{in} = \langle p^2 \rangle_{\Delta f} \frac{A_{plf}}{4 m_{plf}} \frac{1}{\Delta f} \sum_{\substack{n \\ \text{modes} \\ \text{in } \Delta f}} j_n^2 \tag{4.44}$$

where $\langle p^2 \rangle$ is the mean-square fluctuating pressure in the band, Δf, j_n^2 is the joint acceptance for the nth mode, and the summation is over all modes with resonance frequencies in the band, Δf. The joint acceptance is given by

$$j_n^2 = \frac{1}{A_{plf}^2} \int\int d\underline{x}_1 \int\int d\underline{x}_2 \frac{G_p(\underline{x}_1, \underline{x}_2, f)}{G_p(f)} \Psi_n(\underline{x}_1) \Psi_n(\underline{x}_2) \tag{4.45}$$

where $G_p(x_1,x_2,f)$ is the cross-spectrum of the fluctuating pressure at the surface of the fairing between vector locations x_1 and x_2, $G_p(f)$ is the average power spectrum of the fluctuating pressure, and $\Psi_n(x)$ is the nth mode shape for the fairing. Use of the joint acceptance requires an accurate determination of the cross-spectrum of the pressure field and the mode shapes. Further discussion is presented in Section 5.2.

The SEA formulation provides a procedure to calculate the interior acoustic environment. Using energy balance equations, simple predictions are obtained which can be used to carry out design studies or to develop scaling laws based on measured test or flight data. SEA formulations can also be used to provide theoretical predictions that account analytically for differences between acoustic and aerodynamic excitation.

In using SEA to predict the fairing noise reduction, fairing damping is found to affect only the second term in Equation (4.40), which accounts for sound transmission by resonant fairing modes. Since the first term, accounting for non-resonant mass-law sound transmission, may be the dominant term over most of the frequency range of interest, increased fairing damping may not provide significant reduction in the interior acoustic environment. Absorption provided by acoustic blankets is found to reduce the interior acoustic environment regardless of the mechanism of sound transmission.

4.6.3 Scale Dynamic Models. Unlike the estimation of acoustic or aerodynamic excitations using scale models (see Sections 4.4.2 and 4.5.2), the estimation of the noise reduction of a payload fairing or bay using a scale model requires a dynamically, as well as a geometrically, accurate model. Such models have been constructed and used to predict the noise reduction provided by various types of structures [4.42], including space vehicle payload fairings and bays, e.g., the Space Shuttle payload bay using full-scale [4.50] and one-quarter

scale [4.51] models. The principal advantage of scale models is that the noise reduction of a fairing or payload bay can be measured at any location inside the fairing or bay with a payload present. Theoretically, this offers the possibility of highly accurate predictions of the acoustical loading on payloads during launch, assuming the loading functions are properly scaled (see Sections 4.4.2 and 4.5.2). On the negative side, there are three major problems associated with dynamically-similar scale model experiments, as follows:

a. For dynamically similar scale models, it is often difficult to properly scale certain details of the vehicle fairing or bay construction (e.g., riveted joints) that can have a significant impact on the damping of the scale model relative to the full scale structure.

b. The construction of high fidelity, dynamically similar scale models, such as the one-quarter scale model of the Space Shuttle orbiter [4.51], can be very expensive.

c. It may be difficult and/or expensive to properly simulate the spatial correlation characteristics of the excitation for the scale model experiments, particularly the fluctuating pressure excitations over the fairing or payload bay during flight where a high-speed wind tunnel experiment is usually required (see Section 4.5.2).

4.6.4 Extrapolation Techniques. The estimation of the noise reduction for a payload fairing or bay with or without a payload present can sometimes be accomplished using extrapolation techniques, particularly when acoustical measurements on prior vehicles of similar design are available. For example, if data are available for a fairing with the same structure and dimensions as the fairing of interest, but with a different acoustical blanket configuration, the noise reduction for the fairing with the new blanket configuration can be scaled using Equation (4.29) with appropriate estimates for the previous and new absorption coefficients, as well as the transmission loss and area terms for the fairing. On the other hand, extrapolating an accurate noise reduction estimate from a previous payload fairing or bay of a highly dissimilar geometry and structural design is generally not feasible because of the complicated relationships between noise reduction and the geometry of the fairing or bay, particularly at the lower frequencies where the acoustical wave length is comparable to or greater than the dimensions of the fairing or bay.

4.6.5 Direct Measurements. The direct measurement of the acoustical levels inside a payload fairing or bay during liftoff and flight through the atmosphere is much easier to accomplish than the measurement of the external excitations discussed in Sections 4.4.4 and 4.5.4 because the installation of pressure measurement transducers does not require a violation of the vehicle-fairing structure. Also, such measurements eliminate the need for a payload fairing or bay noise reduction estimate to arrive at the acoustical excitation for payloads inside the fairing or bay (a fill-factor correction may still be required, as discussed in Section 4.6.6).

Numerous acoustical measurements were made inside the Space Shuttle orbiter payload bay during the first five missions (STS-1 through STS-5) of OV-102 (Columbia), as well as on a few later Space Shuttle flights, as documented in the DATE reports issued by the NASA Goddard Space Flight Center, e.g., [4.31]. These payload bay measurements were made with relatively small payloads in the bay and, hence, essentially represent empty bay conditions. Similar measurements have been made inside the payload fairings of many expendable launch vehicles and have been utilized to specify acoustical test levels for payloads inside their fairings [4.52]. A summary of the recommended payload acceptance test levels for a few of the launch vehicles covered in [4.52] is presented in Figure 4.7. For new vehicle-fairing configurations, direct measurements inside the payload bay on early launches are highly recommended to verify and groom preliminary predictions for the payload acoustical loads.

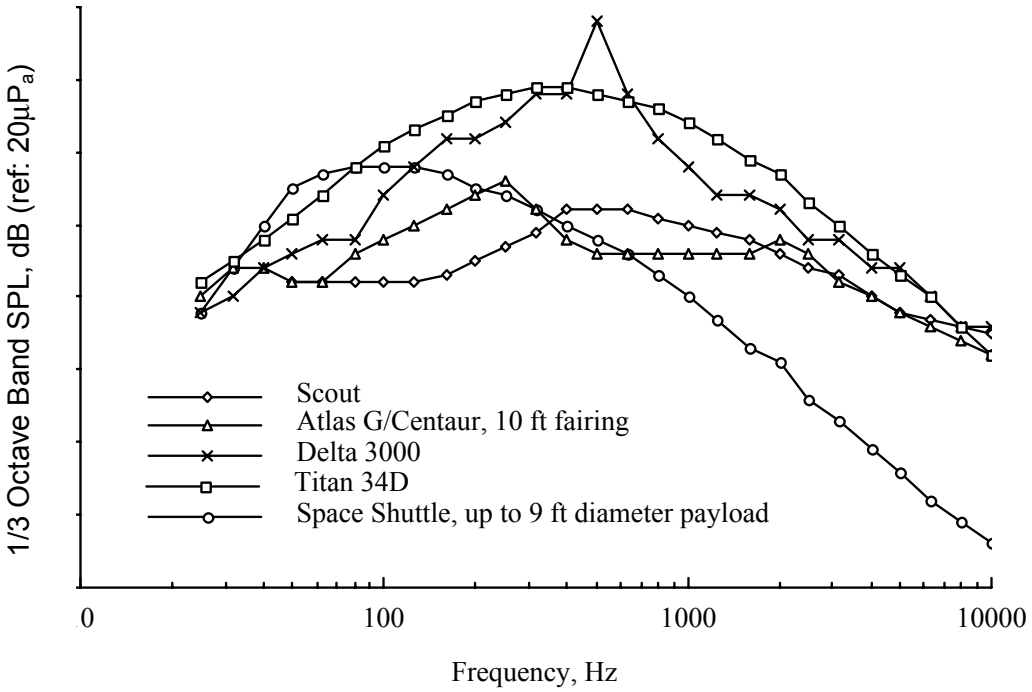

FIGURE 4.7. Estimated Acoustic Levels Inside Various Payload Fairings and Bays [4.52].

4.6.6 Fill Factors. Some of the interior acoustic noise prediction procedures discussed in Sections 4.6.1 through 4.6.5 might yield the sound pressure levels at various locations inside a payload fairing or bay with the payload of interest present, e.g., predictions using an analytical model [4.43] or direct measurements on a scale model [4.51]. In many cases, however, the interior acoustic noise prediction is for an empty fairing or bay. When a payload is introduced into the fairing or bay, the interior sound pressure levels over the exterior of the payload structure will generally be different from the empty fairing or bay levels due primarily to the change in the geometry of the acoustical space inside the fairing or bay. The sound pressure levels (in dB) on the exterior of a payload minus the predicted sound pressure level inside the empty fairing or bay is called the "fill factor." Fill factors typically are positive (the levels seen by the payload are higher than the levels in the empty fairing or bay), and are heavily dependent on (a) the clearance between the payload and the fairing or bay sidewall (the fill factor increases with decreasing clearance) and (b) frequency (the fill factor increases with decreasing frequency).

A number of fill factor correction formulas have been suggested over the years, but the procedure developed in [4.53] and evaluated in [4.54], which evolves from the SEA techniques detailed in Section 4.6.2, is considered the most accurate and has been incorporated into the NASA Standard for "Payload Vibroacoustic Test Criteria" [4.54]. The equation for the acoustic fill factor (FF) given in [4.53, 4.54] is

$$FF = 10 \log_{10} \left[\frac{1 + \frac{c_0}{2fH}}{1 + \left\{ \frac{c_0}{2fH} \left(1 - V_r\right) \right\}} \right] \qquad (4.46)$$

where

V_r = ratio of acoustic volume inside fairing or bay with and without the payload present
H = clearance between the exterior surface of the payload and the wall of the fairing or bay
c_0 = speed of sound in the acoustical volume

The fill factor in Equation (4.46) is plotted versus dimensionless frequency for various different volume ratios in Figure 4.8. To illustrate the use of Figure 4.8, assume a payload fills 80% of the volume inside its fairing, and the clearance between the side of the payload and the fairing wall is 0.1 m. The fill factor (the increase in the sound pressure levels on the side of the payload over the empty fairing levels) is (a) 6.5 dB at 50 Hz, (b) 5.1 dB at 250 Hz, or (c) 2.0 dB at 2000 Hz.

Experimental evaluations detailed in [4.53] for various payload configurations inside a 14 ft diameter Atlas/Centaur payload fairing confirm Equation (4.46) provides reasonably accurate results for the fill factor effect at frequencies above 100 Hz. Below 100 Hz where the density of the acoustical modes in the fairing is low, substantial discrepancies between predicted and measured data sometimes occur, but this is not surprising since Equation (4.46) was developed using statistical energy analysis (SEA) procedures that assume a high modal density. In any case, the fill factor predictions below 100 Hz are probably as accurate, on the average, as can be achieved by any procedure other than detailed analytical model computations (see Section 4.6.1), scale model measurements (see Section 4.6.3), or direct flight measurements (see Section 4.6.5) with the actual payload present or properly modeled.

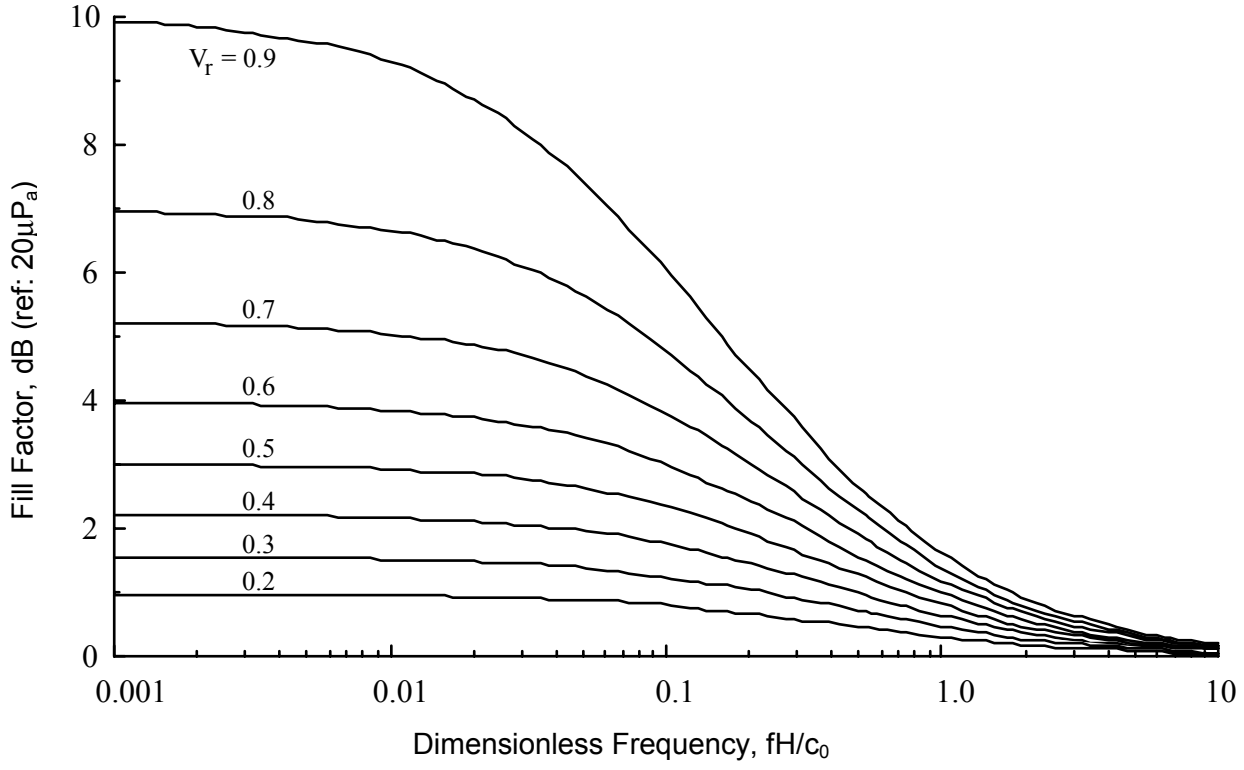

FIGURE 4.8. Fill Factor Design Chart [4.53, 4.54].

4.6.7 Vent Noise. All payload fairings and bays are vented to relieve the atmospheric pressure inside the fairing or bay as the space vehicle gains altitude during launch. In many cases, the vents are covered during liftoff to suppress leakage through the vent openings of the intense liftoff acoustical environment into the fairing or bay. For those cases where the vents are not covered during liftoff, the acoustical hole produced by the open vents must be accounted for in the prediction of the sound pressure levels inside the fairing or bay during liftoff, as accomplished by any one of the procedures discussed in Sections 4.6.1 through 4.6.5.

Since the maximum acoustical levels inside the payload fairing or bay usually occur during liftoff, the open vents after liftoff are usually not a major problem, i.e., the fluctuating pressures produced by the turbulent boundary layer (TBL) excitation on the exterior of the fairing or bay during flight through the atmosphere do not directly radiate significant acoustic noise through the vents into the interior of the fairing or bay. However, the aerodynamic flow over the vents can cause an acoustical resonance or aerodynamic instability in the vent openings. The result can be an intense, near-periodic pressure excitation inside the fairing or bay; such aerodynamic-generated vent noise occurred on the Space Shuttle orbiter [4.55]. The potential for problems of this type must be considered early in the design of payload fairings or bays, and corrective actions must be considered on a case-by-case basis. See [4.55 - 4.59] for illustrations of how to evaluate aerodynamic-generated vent noise and design a noise reduction measure.

4.6.8 Mechanical Vibration Radiation. In most cases, the acoustical levels inside a payload fairing or bay during launch are due primarily to the exterior acoustic noise environment during liftoff and the aerodynamic-generated fluctuating pressure field during flight through the atmosphere. In special cases, there may be noise sources that originate within the fairing or bay, or perhaps within the payload itself. This usually occurs because of mechanical equipment items mounted on the interior walls of the fairing or bay structure, or within the payload, that produce mechanical vibrations of structure that then radiates acoustic noise inside the interior space. The potential for problems of this type must be considered early in the design of payload fairings or bays, and corrective actions must be considered on a case-by-case basis. Such corrective actions usually involve the mounting of interior mechanical equipment on vibration isolators.

4.6.9 Assessments. The merits of the various prediction procedures to establish the acoustic loads on payloads inside a space vehicle fairing or bay are broadly summarized in Table 4.4. At least at frequencies above 100 Hz, SEA procedures are considered the best approach to the prediction of the acoustical loads on payloads inside a fairing or bay based upon the predicted exterior acoustical- or aerodynamic- generated fluctuating pressure loads on the exterior of the fairing or bay. The SEA procedures can be used to (a) directly predict the interior acoustic levels with the payload of interest present (see Section 4.6.2), or (b) first predict the interior acoustic levels in the empty fairing or bay (see Section 4.6.2), and then apply an SEA-derived fill factor correction (see Section 4.6.6). At frequencies below 100 Hz, more accurate predictions usually can be achieved using either analytical model computations or scale model measurements. For payloads that will be repeatedly launched, predictions for the sound pressure levels inside a payload fairing or bay should be upgraded by direct measurements during the first few launches, if feasible.

TABLE 4.4. Comparative Merits of Procedures for Predicting Payload Acoustic Excitations.

Merit	Analytical Models	SEA Procedures	Scale Models	Extrapolation Procedures	Direct Measurements
Relatively easy to physically accomplish	No	Yes	No	Yes	No
Applicable during preliminary design	Yes	Yes	No	Yes	No
Applicable before first vehicle launch	Yes	Yes	Yes	Yes	No
Applicable to radically new vehicle designs	Yes	Yes	Yes	No	Yes
Fill factor corrections required	No	Sometimes*	Sometimes**	Yes	Sometimes*

*No if payload is modeled for SEA predictions or present during measurements; otherwise yes.
**No if payload model is enclosed in its fairing during the test; otherwise yes.

4.7 Structureborne Vibration Excitations. Referring to Table 4.1, there is always some high frequency (above 100 Hz) vibration in the launch vehicle structure due to a direct structural transmission of vibratory energy from the operating rocket engines and/or motors of the launch vehicle, or perhaps from onboard equipment. At the typical locations of payloads, rocket engine/motor-generated structureborne vibration is generally small compared to the high frequency vibration environment generated by aeroacoustic loads (see Sections 4.4 through 4.6). This is demonstrated by numerous vibration measurements made on space vehicles during launch, where the vibration levels are seen to fall dramatically after the vehicle leaves the atmosphere, even though the rocket/motors are still operating, e.g., [4.31]. However, for equipment located on or near the rocket engines/motors, these vibrations might constitute a significant dynamic load. There is also the possibility that operating equipment items in the space vehicle might produce significant structureborne vibration levels, at least at structural locations near the equipment.

The prediction of high frequency structureborne vibration loads involves two steps. The first is the prediction of the dynamic energy produced by the source of the structureborne vibration. The second is the prediction of the transmission of the vibratory energy from the source through the structural path to a receiver location of interest. The prediction of the dynamic energy source is directly related to the specific source mechanisms and must be addressed on a case-by-case basis using conventional vibration prediction techniques [4.60, 4.61]. The prediction of structureborne vibration loads is analytically similar to the prediction of the vibration response at one location on a structure due to an excitation (either motion or pressure) at another location. Hence, the techniques to predict structureborne vibrations due to a defined excitation are the same as the prediction procedures for structural vibrations detailed in Section 5.

4.8 High Frequency Transient Excitations. The most common sources of high frequency (above 100 Hz) transient dynamic loads for a space vehicle and/or its payload are those caused by the activation of pyrotechnic devices containing high explosives (see Section 3.15). In addition to thermal loads, the detonation of explosive materials results in a near-instantaneous pressure wave with intense dynamic energy at frequencies up to at least 1 MHz. This pressure wave produces a rapid velocity change of the immediate structure, as illustrated in Figure 4.9, which is taken from [4.62] and shows the velocity response on one side of a 1.3 cm (1/2 inch) thick steel plate when 5.3 g/m (25 grains/ft) of primachord is detonated on the opposite side of the plate. The velocity is measured by a laser Doppler vibrometer with a sampling rate of 1 Msps. Note that

the velocity of the plate rises to 5.6 m/s in about 3 μsec, which corresponds to an acceleration of almost 200,000 g.

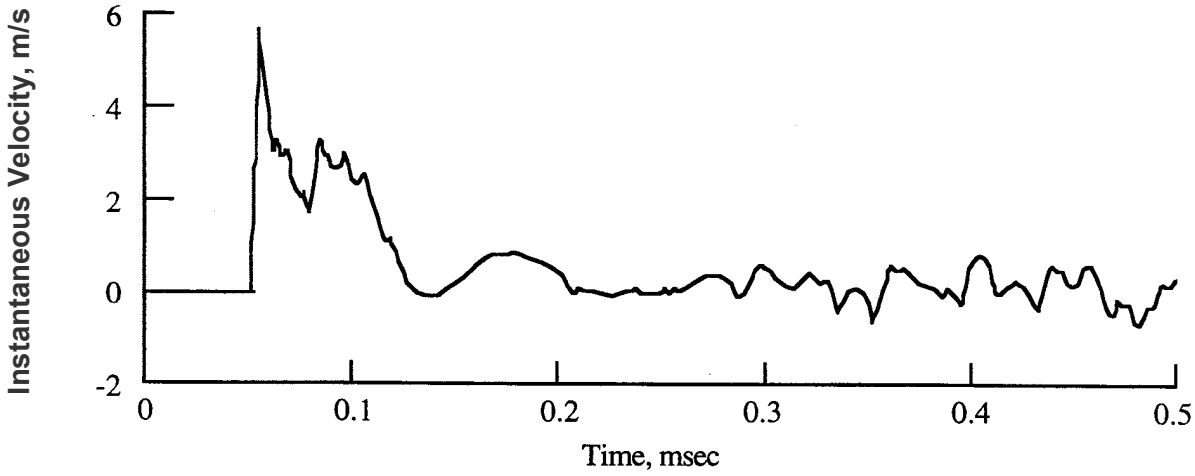

FIGURE 4.9. High Explosive-Induced Velocity Response of a Steel Plate [4.62].

The details of the structure that is directly impacted by the high-explosive-induced pressure vary widely depending on the type of explosive device, but the impacted structure is always loaded either to produce a fracture of the structure or to move an important structural element. Hence, not only the details of the excitation produced by the explosive device, but also the mechanics by which the excitation energy transfers into the impacted structure and propagates through neighboring structures are quite complex. Hydrocodes can be used to model, in the time domain, the details of the explosive detonation, as well as the nonlinear structural deformation and separation using Lagrangian and/or Eulerian meshes (see Section 5.3.1), but the implementation of hydrocode analysis usually necessitates high labor and computer costs. Rather than attempting to define the high-explosive excitation, it is more common to concentrate on the direct prediction of the structural responses induced by high-explosive devices using empirical procedures, as detailed in Section 5.3.

As discussed in Section 3.20, meteoroid impacts during space flight constitute a second potential source of high frequency transient energy. However, the techniques for designing space vehicles to withstand meteoroid loads are highly specialized [3.67, 3.68] and are normally dealt with separately from other dynamic loads.

4.9 References

4.1 Ray, G. A., and Kaminsky, J. A., "A Correlation of Analysis and Flight- Measured Space Shuttle Responses to the STS-2 Lift-Off Environment," *Proc. Shuttle Payload Dynamic Environments and Loads Prediction Workshop*, pp 173-181, Jet Propulsion Laboratory, Pasadena, CA, Jan. 1984.

4.2 Trubert, M. R., "A Practical Approach to Spacecraft Structural Dynamics Problems," *J. Spacecraft and Rockets*, Vol. 9, No. 11, pp 818-824, 1972.

4.3 Day, F. D., and Wada, B. K., "Unique Flight Instrumentation / Data Reduction Techniques Employed on the Viking Dynamic Simulator," *Shock and Vibration Bull.*, No. 46, pp 25- 35, June 1975.

4.4 Trubert, M. R., "Mariners 6 and 7 Low Frequency Flight Acceleration Measurement," *JPL Rep. PD 605-236,* Jet Propulsion Lab, Pasadena, CA, Feb. 1970.

4.5 Brodeur, S. J., "Comparison of Flight Data Versus Predictions for Low Frequency Acceleration Loads on STS-3 / OSS-1 Instruments," *Proc. Shuttle Payload Dynamic Environments and Loads Prediction Workshop*, pp 183-203, Jet Propulsion Lab, Pasadena, CA, Jan. 1984.

4.6 Day, F. D., and Wada, B. K., "Strain Gaged Struts and Data Reduction Techniques to Maximize Quality of Data from Spacecraft Flight Measurements," *Proc. AIAA 16th SDM Conf.* Denver, CO, May 1975.

4.7 Himelblau, H., Piersol, A. G., Wise, J. H., and Grudvig, M. R., "Handbook for Dynamic Data Acquisition and Analysis," *IES-RP-DTE012.1,* Inst. Envir. Sc. Tech., Mount Prospect, IL, Mar. 1994.

4.8 Liepmann, H. W., "On the Application of Statistical Concepts to the Buffeting Problem," *J. Aeronautical Sc.*, Vol. 19, pp 793-800, 1952.

4.9 Fung, Y. C., *An Introduction to the Theory of Aeroelasticity*, Dover, Mineola, NY, 1969.

4.10 Blevins, R. D., *Flow - Induced Vibration*, Kreiger, Melbourne, FL, 2nd ed., 1992.

4.11 Cho, A. C., Dougherty, N. S., and Guest, S. H., "Scale Model Acoustic Test of SSV for VAFB," *Proc. Shuttle Payload Dynamic Environments and Loads Prediction Workshop*, pp 153-172, Jet Propulsion Lab, Pasadena, CA, Jan. 1984.

4.12 Langhaar, H. L., *Dimensional Analysis and Theory of Models*, Wiley, NY, 1951.

4.13 Davenport, A. G., and Isyumov, N., "The Application of Boundary Layer Wind Tunnel Data to the Prediction of Wind Loading," *Proc. Sem. on Wind Effects on Structures*, pp 201-230, National Research Council of Canada, Ottawa, Sep. 1967.

4.14 Cermac, J.E., "Determination of Wind Loading on Structural Models in Wind Tunnel Simulated Winds," *Proc. Chicago Design Symp.on Wind Effects on High Rise Buildings*, pp 61-88, Evanston, IL , Mar. 1970.

4.15 Lee, B. H. K., and Tang, F. C., “Buffet Load Measurements on an F/A-18 Vertical Fin at High Angle of Attack,” *AIAA Dynamics Specialist Conf.*, pp 455-466, Dallas, TX, Apr. 1992.

4.16 Jacobs, J. H., Hedgecock, C. E., Lichtenwalner, P. F., Pado, L. E., and Washburn, A.E., “The Use of Artificial Intelligence for Buffet Environments,” *Proc. AIAA 34th SDM Conf.*, pp 1952-1960, Apr.1993.

4.17 Lippmann, R. P., “An Introduction to Neural Computing with Neural Nets,” *IEEE ASSP Mag.,* pp 4-22, Apr. 1987.

4.18 Smith, K. S., Peng, C.-Y., and Behboud, A., “Multibody Dynamic Simulation of Mars Pathfinder Entry, Descent, and Landing,” *JPL Doc. D-13298*, Jet Propulsion Lab, Pasadena, CA, Apr. 1995.

4.19 Cockrell, D.J., et. al., “Aerodynamic and Inertial Forces On Model Parachute Canopies,” *AIAA Paper 75-1371*, 1975.

4.20 Friedman, L., et. al., “Solar Sailing - The Concept Made Realistic,” *AIAA 16th Aerospace Sc. Mtg,* Huntsville, AL, Jan. 1978.

4.21 MacNeal, R.H., “Structural Dynamics of the Heliogyro,” *NASA CR-1745,* May 1971.

4.22 Salama, M. A., and Trubert, M. R., “Nonlinear Deformations and Loads in the Truss Cable Structure of the Square Solar Sail,” *JPL Rep. 662-39,* Jet Propulsion Lab, Pasadena, CA, Aug. 1977.

4.23 Salama, M. A., Trubert, M.R., Essawi, M., and Utku, S., “Second Order Nonlinear Equations of Motion for Spinning Highly Flexible Line Elements,” *J. Sound and Vibration*, Vol. 80, No. 4, pp 461-472, 1982.

4.24 Potter, R. C., and Crocker, M. J., "Acoustic Prediction Methods for Rocket Engines, Including the Effects of Clustered Engines and Deflected Exhaust Flow,” *NASA CR-566,* Oct. 1966.

4.25 Richards, E. J., and Clarkson, B. L., "Jet and Rocket Noise,” Ch. 7, pp. 156-158, *Noise and Acoustic Fatigue in Aeronautics* (Richards, E. J., and Mead, D. J., Ed.), Wiley, NY, 1968.

4.26 Eldred, K. M., “Acoustic Loads Generated by the Propulsion System,” *NASA SP-8072,* June 1971.

4.27 Cockburn, J. A., and Jolly, A. C., "Structural-Acoustic Response, Noise Transmission Losses and Interior Noise Levels of an Aircraft Fuselage Excited by Random Pressure Fields,” *AFFDL-TR-68-2,* 1968.

4.28 Ungar, E. E., et al., "A Guide to Estimation of Aeroacoustic Loads on Flight Vehicle Surfaces,” *AFFDL-TR-76-91,* Feb.1977.

4.29 Ryan, R. S., “The Role of Failure/Problems in Engineering: A Commentary on Failures Experienced-Lessons Learned,” *NASA TP 3213,* pp 107-108, Mar. l992.

4.30 Pratt, H.K., et al, “Space Shuttle System Acoustics and Shock Data Book,” *Rockwell Intern. Rep. SD 74-SH-0082B*, Change Notice 3, 1995.

4.31 Keegan, W. B., et al, "Payload Bay Acoustic and Vibration Data From STS-1 Flight,” *NASA GSFC DATE Rep. 002,* June 1981.

4.32 Schlichting, H., *Boundary Layer Theory* (English translation by J. Kestin), McGraw-Hill, NY, 1960.

4.33 Bies, D. A., "A Review of Flight and Wind Tunnel Measurements of Boundary Layer Pressure Fluctuations and Induced Structural Response,” *NASA CR-626,* May 1966.

4.34 Lyon, R. H., “Random Noise and Vibration in Space Vehicles,“ *Monograph SVM-1,* Shock and Vibration Info. Anal. Ctr, 1967.

4.35 Lowson, M. V., "Prediction of Boundary Layer Pressure Fluctuations,” *AFFDL-TR-67-167,* Apr. 1968.

4.36 Bull, M. K., "Boundary Layer Pressure Fluctuations,” Ch. 8, *Noise and Acoustic Fatigue in Aeronautics* (Eds: Richards, E. J., and Mead, D. J.), Wiley, NY, 1968.

4.37 Coe, C. F., "Surface-Pressure Fluctuations Associated with Aerodynamic Noise,” *Basic Aerodynamic Noise Research* (Schwartz, I. R., Ed.), *NASA SP-207,* pp 409-424, 1969.

4.38 Robertson, J. E., “Prediction of In-Flight Fluctuating Pressure Environments Including Protuberance Induced Flow,” *NASA CR-119947*, 1971.

4.39 Heller, H. H., and Clemente, A. R., “Unsteady Aerodynamic Loads on Slender Cones at Free-Stream Mach Numbers from 0 to 22,” Paper No. 73-998, *AIAA Aero-Acoustics Conf.*, Seattle, WA, 1997.

4.40 Laganelli, A. L., and Howe, J. R., "Prediction of Pressure Fluctuations Associated with Maneuvering Re-Entry Weapons,” *AFFDL-TR-77-59,* 1977.

4.41 Laganelli, A. L, Martellucci, A., and Shaw, L. L., "Wall Pressure Fluctuations in Attached Boundary-Layer Flow,” *AIAA J.*, Vol. 21, No. 4, pp 495-502, Apr. 1983.

4.42 Beranek, L. L., and Ver, I. L., Ed., *Noise and Vibration Control Engineering*, Wiley, NY, 1992.

4.43 Pope, L. D., Wilby, J. F., et al, "Space Shuttle Payload Bay Acoustic Prediction Model,” NASA CR-159956, Vol. I-V, Mar. 1980.

4.44 Seybert, A. F., Cheng, C. Y. R., and Wu, T. W., "The Solution of Coupled Interior/Exterior Acoustic Problems Using the Boundary Element Method,” *J. Acoust. Soc. Am*., pp. 1612-1618, Vol. 88, 1990.

4.45 Lyon, R. H., and DeJong, R. G., *Theory and Application of Statistical Energy Analysis*, 2nd Ed., Butterworth-Heinemann, Newton, MA, 1995.

4.46 Manning, J. E., "Statistical Modeling of Vibrating Systems," Ch. 78, *Encyclopedia of Acoustics*, ed: M. J. Crocker, John Wiley & Sons, Inc. 1997.

4.47 Burroughs, C. B., Fischer, R. W., and Kern, F. R., "An Introduction to Statistical Energy Analysis," *J. Acoust. Soc. Am.*, Vol. 101, No. 4, April 1997.

4.48 Lee, Y. A., Henricks, W., et al, "Vibroacoustic Payload Environment Prediction System (VAPEPS)," Vol. 1 to 5, NASA CR-166823, June 1984.

4.49 Bradford, L., and Manning, J. E., "Acoustic Blanket Effect on Payload Acoustic Environment," pp. 244-253, *Proc., 42 ATM, Inst. Envir. Sc. Tech.,* Mount Prospect, IL, 1996.

4.50 Wilby, J. F., and Pope, L. D., "The Development of a Method for Predicting the Noise Exposure of Payloads in the Space Shuttle Orbiter Vehicle," *Shock and Vibration Bull.*, No. 49, Part 1, pp 1-29, Sep. 1979.

4.51 Piersol, A. G. and Rentz, P.E., "Experimental Studies of the Space Shuttle Payload Acoustic Environment," *SAE Paper 770973,* Nov. 1977.

4.52 Milne, J. S., "General Environmental Verification for STS & ELV Payloads, Subsystems, and Components," *NASA GSFC Doc. GEVS-SE,* Rev. A, 1996.

4.53 Hughes, W. O., McNelis, M. E., and Manning, J. E., "NASA LeRC's Acoustic Fill Effect Test Program and Results Analysis and Evaluation of the Fill Factor," *Proc. 15th Aerospace Testing Sem.,* Inst. Envir. Sc., pp 205-221, Oct. l994. (Also *Proc. 65th Shock and Vibration Symp.*, Vol. 1, pp 459-474, Nov. 1994, and NASA TM-106688, 1994.)

4.54 Anon., "Payload Vibroacoustic Test Criteria," *NASA Engrg Standard NASA-STD-7001,* June 21, 1996.

4.55 Tanner, C. S., "Shuttle Cargo Bay Vent Noise and its Effect on the Generic Payload Specifications and Testing Methods," *Proc., Shuttle Payload Dynamic Environments and Loads Prediction Workshop*, Vol. I, pp. 303 - 332, Jet Propulsion Lab, Jan. 1984.

4.56 Rossiter, J. E., "Wind Tunnel Experiments in Flow Over Rectangular Cavities at Subsonic and Transonic Speeds," *Reports and Memoranda No. 3438*, Communicated by Deputy Controller Aircraft (Research and Development), Ministry of Aviation, England, 1964.

4.57 Heller, H. H., Holmes, D. G., and Covert, E. E., "Flow-Induced Pressure Oscillations in Shallow Cavities," *J. Sound and Vibration*, Vol. 18, pp. 545 - 553, 1971.

4.58 Heller, H. H., and Bliss, D. B., "Aerodynamically Induced Pressure Oscillations in Cavities - Physical Mechanisms and Suppression Concepts," *AFFDL-TR-74-133*, Wright-Patterson AFB, OH, 1975.

4.59 Johnston, J. D., "Payload Bay Atmospheric Vent Airflow Testing at the Vibration and Acoustic Test Facility," *NASA TM 100460*, Feb. 1988.

4.60 Harris, C. M., Ed., *Shock and Vibration Handbook*, 4th ed., McGraw-Hill, NY, 1996.

4.61 Heckl, M., Cremer, L., and Ungar, E. E., *Structure-Borne Sound*, Springer-Verlag, NY, 1973.

4.62 Valentekovich, V. M., and Goding, A. C., "Characterizing Near Field Pyroshock with a Laser Doppler Vibrometer," *Proc. 61st Shock and Vibration Symp.*, Vol. II, pp 205-221, Oct. 1990.

5. PREDICTION OF STRUCTURAL RESPONSES

Having defined the dynamic excitations for space vehicles in Section 4, the next step is to predict the structural responses to these excitations. From the viewpoint of basic prediction methodologies, it is convenient to divide the structural response prediction procedures into three categories, as summarized in Table 5.1. Beyond the basic categories of structural response predictions in Table 5.1, there are three additional actions that are sometimes required to arrive at the final response predictions, namely, (a) the computation of multimodal responses, (b) the verification of analytical models, and (c) the computation of responses under combined loads.

TABLE 5.1. Summary of Structural Response Predictions.

Type of Structural Response	Dynamic Excitations (Section Number)
Low frequency vibration and transients responses	Low frequency transient (4.1), low frequency random (4.2), and low frequency, quasi-periodic (4.3).
High frequency vibration responses	High frequency, quasi-periodic (4.3), exterior acoustic noise (4.4), exterior aerodynamic noise (4.5), interior acoustic noise (4.6), and structureborne vibration (4.7).
High frequency transient responses	High frequency transient (4.8).

5.1 Low Frequency Vibration and Transient Responses. Low frequency vibration and transient responses of payloads and spacecraft result in loads and motions that must be determined analytically to evaluate structural integrity and functionality. From the Sections referenced in Table 5.1, the primary sources of these low frequency loads are pre-launch events (ground winds and possible seismic loads), liftoff (engine/motor thrust buildup, ignition overpressure, and pad release), airloads (buffet, gust, and static-elastic), and liquid engine ignitions and shutdowns. These events have an upper frequency limit that is dependent on the launch vehicle and the stage of its operation, e.g., 35 Hz for Shuttle, 50-60 Hz in most cases for expendables. Major load events due to spacecraft operation are deployments and transients peculiar to the mission, such as docking and landing. Most cases involve linear system response, but nonlinear responses occur in certain cases. Examples are the account of trunnion sliding for Shuttle payloads, the liftoff release mechanism for Atlas, and the response of spacecraft deployment and docking mechanisms.

The process of predicting the dynamic responses typically involves a series of analytical steps as follows (illustrated in Figure 5.1 taken from [5.1]):

a. A finite element method (FEM) model is created to describe the stiffness and distributed mass properties.

b. The degrees of freedom (DOF) in the FEM model are reduced to create the dynamic model to be valid within the frequency range of concern. Discrete elements are incorporated when a lumped-parameter representation is appropriate. Examples are rigid elements to represent hardware which have no modes in the frequency range of interest and discrete flexible elements such as vibration isolators.

c. Modal analysis, including “component-mode synthesis” if portions of the spacecraft are modeled separately, is performed to develop a “component-mode representation” of the spacecraft as the basis for dynamic coupling with the launch vehicle. Effects to be represented nonlinearly in subsequent loads analyses have been removed. The boundary conditions at the

interface with the launch vehicle are matched to those which are used for the experimental modal test to facilitate test planning (particularly, sensor and forcing locations), and evaluation of analysis/test correlation. Critical damping ratios are assigned to the modes based on the modal test data.

d. Component mode synthesis is performed to couple the spacecraft to the remainder of the flight vehicle to determine the normal modes of the complete system for each of the load events to be analyzed. Employed in a final verification analysis is the test-verified analytical model assuming acceptable correlation has been achieved with the experimental modes or, if that is not possible, the test-derived modes themselves. The off-diagonal elements of the system damping matrix resulting from the coupling process are retained unless experience has shown that the off-diagonal terms are insignificant [5.1].

e. Forcing functions are developed to serve as excitations for the various load events. Analytical predictions, ground test data, and flight data may be involved.

f. After coupling all nonlinear effects into the equations of motion, responses are calculated for the generalized coordinates of the total system. These system generalized responses are then transformed to the generalized coordinate responses for the component modes of the spacecraft. This is followed by a transformation to the DOF in the physical dynamic model.

g. The physical acceleration and displacements responses are then transformed into physical member loads (for example, shear forces and bending moments) and relative deflections (for example between a spacecraft appendage and the fairing) by means of a load transformation matrix (LTM). Stresses that involve multiple load contributions are determined conservatively by worst case combination of extreme values, by statistical combination for random aspects, or by time-domain superposition. The last step is the assessment of safety margins.

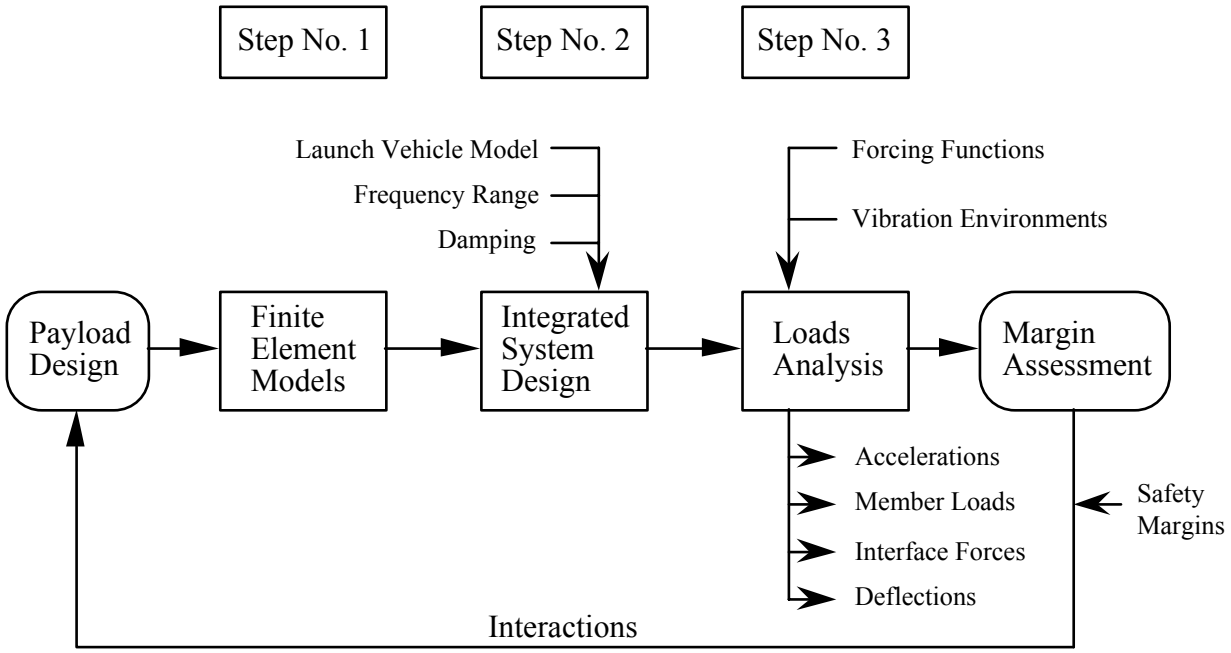

FIGURE 5.1. The Loads Analysis Process

Since many design loads are dynamic in nature, the loads not only strongly influence the spacecraft configuration, but the configuration has a major influence on the loads as well. This interaction leads to an iterative design process as indicated in Figure 5.1, usually referred to as the "load cycle process" illustrated in Figure 5.2 taken from [5.2]. In the Preliminary Design Load Cycle, preliminary design load factors are applied, usually in the form of static accelerations, to a preliminary design spacecraft model. The results are used to make necessary design changes, and along with changes due to ongoing design maturity, yield a Final Design Model used for the second or Final Design Loads Cycle. These results are used to make necessary design changes and are subjected to a Critical Design Review. After the critical design review, a commitment is made to fabricate structural hardware, which is eventually subjected to qualification static tests based on the loads predicted in the Final Design Loads Cycle. The truly final load cycle, called the Verification Loads Cycle, takes place after the spacecraft has been built and mode survey tested. The verified dynamic model, either an adjustment of the Final Design Model or a modal model derived directly from the measured modes, is used. The resulting loads are considered in a final assessment of structural qualification, including an assessment of the adequacy of the static qualification tests. A positive outcome is necessary to make the commitment to flight.

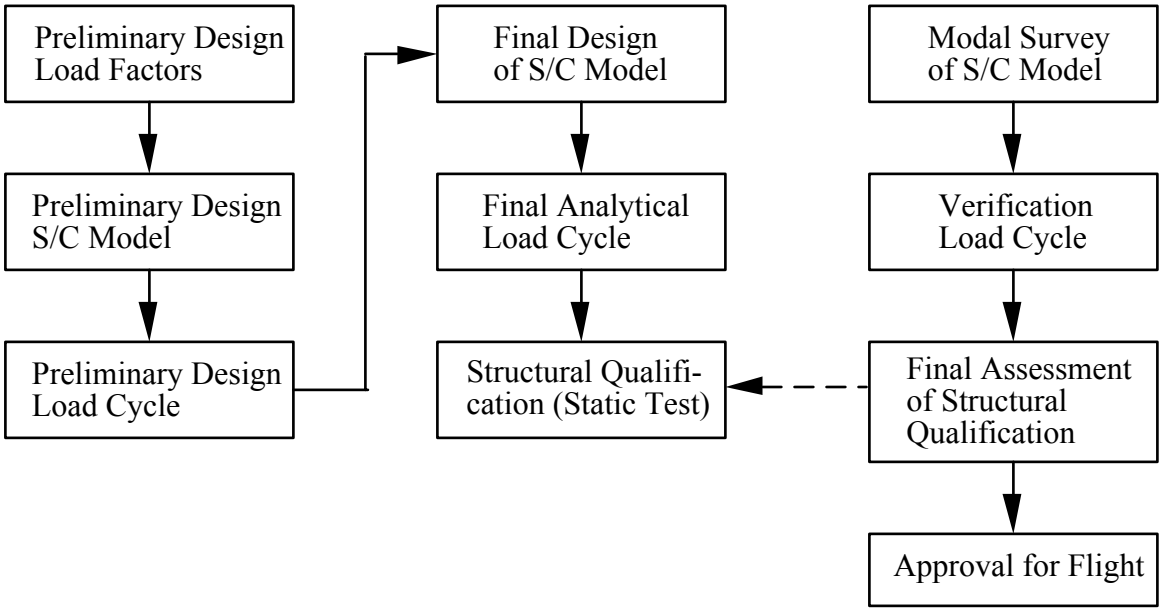

FIGURE 5.2. The Load Cycle Process.

5.1.1 Structural Dynamic Models. Dynamic models are classified broadly based upon whether they involve physical or generalized coordinates. Physical models are in the form of mass and stiffness matrices, usually constructed from FEM models. They may also contain some non-physical degrees of freedom, such as used to represent motion of liquids in tanks. The generalized coordinate models involve physical deflection shapes (Ritz vectors) into which responses in the frequency range of interest can be decomposed. These shapes include normal mode shapes of the component, either for the interface points fixed, free, or loaded (i.e., constrained in some intermediate manner such as with imposed mass or stiffness elements). For the fixed and free interface cases, additional shapes are generated as a basis for the consequences of interface motions and forces in the coupled system.

The equations of motion for a component in physical coordinates, when damping is neglected, can be written in the standard form

$$M\ddot{x} + Kx = F \tag{5.1}$$

where M is the component mass matrix, K is its stiffness matrix, x is a vector of physical displacement coordinates, and F is a vector of forces acting. To insure symmetry of the mass and stiffness matrices, the forces must be compatible with the displacements, meaning that the product of each force and its associated displacement coordinate must be the external work done (in consistent units) at that coordinate. For example, in addition to the usual pairing of force with displacement, other appropriate pairings are pressure with area-displacement and moment with angular displacement.

The physical coordinates are separated into a set of interface coordinates x_I and a set of non-interface (interior) coordinates x_N. Equation (5.1) can then be partitioned to yield

$$\begin{bmatrix} M_{NN} & M_{NI} \\ M_{NI}^T & M_{II} \end{bmatrix} \begin{Bmatrix} \ddot{x}_N \\ \ddot{x}_I \end{Bmatrix} + \begin{bmatrix} K_{NN} & K_{NI} \\ K_{NI}^T & K_{II} \end{bmatrix} \begin{Bmatrix} x_N \\ x_I \end{Bmatrix} = \begin{Bmatrix} F_N \\ F_I \end{Bmatrix} \tag{5.2}$$

For a spacecraft responding to liftoff and ascent excitations, the non-interface forces $F_N = 0$ unless direct acoustic impingement on large surface area elements is being considered.

5.1.2 Classical Normal Mode Analysis Procedures. The type of normal modes obtained depends on whether the interface degrees of freedom are fully constrained (fixed) or unconstrained (free) or intermediately constrained. In any case, the normal modes are the eigensolutions for Equation (5.1)

$$\left(K - \Omega_n^2 M\right)\Phi_n = 0 \tag{5.3}$$

where Φ_n is the matrix of mode shapes and Ω_n^2 the diagonal matrix containing the square of the corresponding circular natural frequencies. It is customary to orthonormalize the mode shapes, namely

$$\Phi_n^T M \Phi_n = I \tag{5.4}$$

where **I** is the identity matrix. This then yields

$$\Phi_n^T K \Phi_n = \Omega_n^2 \tag{5.5}$$

The physical coordinates x are related to the generalized coordinates q by the transformation

$$x = \Phi_n q \tag{5.6}$$

Assuming that the eigenvalue problem has been solved completely, the modal matrix Φ_n contains as many eigenvectors as there are degrees of freedom in the physical dynamic model. One of the advantages of the modal method is that a model for the frequency range of interest can be established using a small subset of the modes. In further discussion, Φ and Φ_d denote the retained mode set and the deleted mode set, respectively:

$$\Phi_n = [\Phi \mid \Phi_d] \tag{5.7}$$

5.1.2.1 Fixed-Interface Model (Hurty/Craig-Bampton). Fixed-interface modeling is the most commonly employed technique for spacecraft. It is commonly viewed as capable of producing lower modes similar to those occurring in the coupled system because the spacecraft interface points are attached to relatively stiff structure. Furthermore, the well established base-fixed modal test approach is applicable for model verification purposes.

The analytical method of fixed-interface modeling was originated by Hurty [5.3] and then simplified, with respect to rigid body modes by Craig and Bampton [5.4]. Involved are fixed-interface normal modes and "constraint modes" to serve as a set of vectors with which to create the coupled system behavior within the component. These mode shapes are discussed below.

Fixed-interface normal modes are obtained by constraining the interface degrees of freedom (DOF) in Equation (5.2) and then solving the eigenproblem for the modes to be retained Φ_N:

$$\left(K_{NN} - \Omega_n^2 M_{NN}\right)\Phi_N = 0 \tag{5.8}$$

The fixed-interface normal modes are augmented with constraint modes, one for each interface DOF. The ith constraint mode shape is defined to be the static displacements of the non-interface DOF x_{Ni} due to a unit displacement of the ith interface DOF x_{Ii}, obtained from the static solution of Equation (5.2). An application of successive unit static displacements at interface DOF yields the columns of the constraint mode matrix Φ_{cN} for the non-interface DOF. Since the constraint modes are derived from the unconstrained stiffness matrix, the rigid body modes are contained implicitly.

The physical coordinates are then related to the generalized coordinates as follows:

$$\begin{Bmatrix} x_N \\ x_I \end{Bmatrix} = \begin{bmatrix} \Phi_{nN} & \Phi_{cN} \\ 0 & I \end{bmatrix} \begin{Bmatrix} q_n \\ x_I \end{Bmatrix} \text{ or } x = \tilde{\Phi} q \text{ where } \Phi_{cN} = -K_{NN}^{-1} K_{NI} \tag{5.9}$$

The transformation in Equation (5.9) is applied to the physical equations of motion (5.1) yielding

$$\tilde{M} = \tilde{\Phi}^T M \tilde{\Phi} = \begin{bmatrix} I & \tilde{M}_{NI} \\ \tilde{M}_{NI}^T & \tilde{M}_{II} \end{bmatrix} \text{ and } \tilde{K} = \tilde{\Phi}^T K \tilde{\Phi} = \begin{bmatrix} \Omega_N^2 & 0 \\ 0 & K_{II} \end{bmatrix} \tag{5.10}$$

Thus the fixed-interface component-mode approach results in component equations of motion which have only inertial coupling between the fixed-interface normal modes and the constraint modes. If a six DOF statically indeterminate interface is present in the model, the constraint modes are rigid body displacements and $K_{II} = 0$. Also, it should be mentioned that Equation (5.10) assumes the mode shapes have been mass normalized according to Equation (5.4).

While this is common practice, it is not required. For example, NASTRAN includes other procedures that might be chosen to normalize the eigenvectors.

5.1.2.2 Loaded-Interface Model (Benfield/Hruda). While fixed-interface modeling is most common, there are cases where this may not be appropriate. An example is a very large spacecraft for which rigid supports in a modal test may be impractical, or when the spacecraft interface points are supported by bearings or flexible couplings intended to reduce load transfer. Especially if these devices are nonlinear, they would not be appropriate to be included in a modal survey which is intended to identify linear behavior. Yet another consideration for not using the constraint-interface approach is that it leads to either full reliance on the analytical model for stiffness properties associated with the interface points, or it requires structural stiffness testing in addition to the modal test.

On the other hand, total dependence on free-interface modes for system synthesis is undesirable because the local flexibility properties at the interface points are not represented. This leads to poor convergence resulting in the need to include an excessively large number of modes to yield accurate system modes. The method in [5.5] aimed to circumvent this problem by including stiffness and/or mass loading of the interface points to approximate the degree of constraint produced in the coupled system. This implies that the model is tied to a specific launch vehicle, which is contrary to having the freedom to deal with other vehicles. Of course, another possibility is to include arbitrary stiffnesses or masses to the interface points, simply to "work" the points, in a manner that can readily be implemented in a modal test. In either case, such an approach leads to the need to include these interface constraints in a modal test and to analytically remove these interface constraints as part of the coupling process to develop system modes.

For example, a launch vehicle is sometimes loaded with a rigid body representation of the payload for its component-mode representation. That rigid body is subsequently removed as part of the coupled system modal analysis.

5.1.2.3 Free-Interface Model (Rubin/MacNeal). Another approach is to use free-interface modes and to append attachment modes, which can also be called interface residual modes. The attachment modes are static elastic deflection shapes due to unit forces at the interface DOF that are only the result of the high frequency modes not retained for the dynamic model. Since the structure is free to undergo rigid body motion, these deflection shapes are derived with inertia relief to avoid any rigid body contribution. The total static elastic deflection for a unit force at each interface DOF is determined first. Then, the contributions to these shapes of the retained modes are removed. The number of attachment modes is the same as the number of interface DOF, and is the same as the number of constraint modes needed to augment fixed-interface modes.

This approach stemmed from the concept of "residual flexibility", first introduced by MacNeal [5.6] to account for the static contribution of neglected higher modes. Rubin [5.7] added a first-order residual mass and showed a substantially improved benefit for convergence beyond that afforded by residual flexibility alone. This work was reframed by Coppolino [5.8] into the use of residual flexibility shapes to become Ritz vectors now referred to as *attachment modes* (also [5.9]).

The displacement vector x is expressed as a sum over the free-interface normal mode shapes Φ_n and the attachment mode shapes Φ_a, weighted by their corresponding generalized coordinates q_n and q_a, respectively:

$$\begin{Bmatrix} x_N \\ x_I \end{Bmatrix} = \begin{bmatrix} \Phi_{nN} & \Phi_{aN} \\ \Phi_{nI} & \Phi_{aN} \end{bmatrix} \begin{Bmatrix} q_n \\ q_a \end{Bmatrix} \text{ or } x = \Phi_n q_n + \Phi_a q_a \tag{5.11}$$

Each attachment mode Φ_a is the static deflection shape over all DOF for a unit force at one interface DOF. Let G_c be the elastic flexibility matrix when the component is constrained non-redundantly to prevent rigid body motion, G_e be the elastic flexibility matrix for the unrestrained component having imposed inertia relief, and G_N be the flexibility matrix due to the retained elastic modes. Then the flexibility matrix G_d contributed by the deleted modes is given by

$$G_d = G_e - G_N \text{ where } G_e = A^T G_c A,\ A = I - M\Phi_r \Phi_r^T,\ G_N = \Phi_N \Omega_N^{-2} \Phi_N^T \tag{5.12}$$

In the above equation, Φ_r is the matrix of rigid body mode shapes and Ω_N is the diagonal matrix of the reciprocal of squared natural frequencies corresponding to G_N. The attachment mode matrix Φ_a in Equation (5.11) is the subset of G_d containing the columns associated with forces at the attachment DOF.

For use in component mode synthesis, it is necessary to replace the attachment generalized coordinates q_a in the transformation Equation (5.11) by the physical interface DOF x_I. This is accomplished by manipulating Equation (5.11) to produce the desired transformation, namely,

$$\begin{Bmatrix} x_N \\ x_I \end{Bmatrix} = \begin{bmatrix} \overline{\Phi}_N & \overline{\Phi}_{aN} \\ 0 & I \end{bmatrix} \begin{Bmatrix} q_n \\ x_I \end{Bmatrix} \text{ or } x = \overline{\Phi} q \tag{5.13a}$$

where $\overline{\Phi}$ is the set of modified free-interface normal modes and $\overline{\Phi}_{aN}$ is the set of modified attachment modes, both pertaining to the non-interface DOF given by

$$\begin{aligned} \overline{\Phi}_{nN} &= \Phi_{nN} - \Phi_{aN} \Phi_{aI}^{-1} \Phi_{nI} \\ \overline{\Phi}_{aN} &= \Phi_{aN} \Phi_{aI}^{-1} \end{aligned} \tag{5.13b}$$

The transformation in Equation (5.13a) is used to transform the physical equations of motion (5.1):

$$\overline{M}\,\ddot{q}' + \overline{K}\,q' = \overline{\Phi}\,F \text{ where } \overline{M} = \overline{\Phi}^T M \overline{\Phi},\ \overline{K} = \overline{\Phi}^T K \overline{\Phi} \tag{5.14}$$

In this case, the matrices $\overline{M}$ and $\overline{K}$ are fully populated.

5.1.3 Finite Element Method (FEM) Model Procedures. The stiffness model created by the structural analysts who are responsible for structural strength provides the usual starting point for the analytical dynamic model of the spacecraft. This is a recommended practice since the major objective of the dynamic analysis is a set of loads which can be used to determine safety margins, and a common basis for the strength and loads analyses greatly facilitates this objective. The basic analysis tool used for the stiffness modeling is a FEM modeling program, as exemplified by NASTRAN. The use of such programs as a basis for the dynamic model is very much an art to assure adequacy for the frequency range of interest in terms of both modes

and loads. The structural stiffness viewpoint must be expanded to assure that sufficient DOF and mass properties are included to reflect the translational and rotational kinetic energies of all parts on the spacecraft, including auxiliary bodies (such as tanks). In general, three translational and three rotational DOF are included for each node in the model.

A special case of FEM modeling occurs when a liquid containing tank is to be modeled. When slosh effects are to be modeled, and the elasticity of the tank is not significant, a spring-mass or pendulum modeling is appropriate [5.10]. A special form of FEM analysis, used for hydroelastic modeling, represents an incompressible liquid and the coupling between liquid pressure and tank wall elastic deflection. Such modeling capability is available, for example, using NASTRAN [5.11, 5.12]. In this case hydroelastic vibration modes are determined using the vibration analysis capability of the FEM program itself and then used for a component-mode representation of the tank.

Since static stress analysis generally requires more spatial detail (often tens of thousands of DOF) than required for dynamic analysis (a few hundred at most), a transformation method is used for reduction to the dynamic set. The principal techniques are static condensation (commonly known as Guyan reduction) and generalized dynamic reduction (also called subspace iteration). These are discussed below. The criterion for the acceptability of a dynamic DOF set should be based on the degree of orthogonality between the dynamic mode set and modes derived from as refined a model as possible in the frequency range of interest.

5.1.3.1 Static Condensation (Guyan Reduction). The homogeneous equations of motion, prior to condensation (reduction of DOF) to the dynamic equations, is written in terms of the retained DOF x_a (the "a-set") and the eliminated DOF x_0 as

$$\begin{bmatrix} M_{aa} & M_{ao} \\ M_{ao}^T & M_{oo} \end{bmatrix} \begin{Bmatrix} \ddot{x}_a \\ \ddot{x}_o \end{Bmatrix} + \begin{bmatrix} K_{aa} & K_{ao} \\ K_{ao}^T & K_{oo} \end{bmatrix} \begin{Bmatrix} \ddot{x}_a \\ \ddot{x}_o \end{Bmatrix} = \begin{Bmatrix} 0 \\ 0 \end{Bmatrix} \tag{5.15}$$

Guyan reduction [5.13] uses the static displacement relationship to define the following transformation between the two DOF sets obtained from the lower half of Equation (5.15):

$$x_o = G_{oa} x_a \quad \text{where} \quad G_{oa} = -K_{oo}^{-1} K_{ao}^T \tag{5.16}$$

The result of the condensation, indicated by the addition of the subscript c, is

$$M_{aa,c}\, \ddot{x}_a + K_{aa,c}\, x_a = 0 \tag{5.17}$$

where

$$M_{aa,c} = M_{aa} + M_{ao} G_{oa} = G_{oa}^T M_{ao}^T + G_{oa}^T M_{oo} G_{oa}$$
$$K_{aa,c} = K_{aa} + K_{ao} G_{oa}$$

Note that the mass properties associated with the eliminated DOF x_0 are distributed to the mass coefficients for the retained DOF x_a.

The application of Guyan reduction requires significant user experience since no connection is provided to the frequency range of interest. It is vital to retain the DOF required to characterize the complete kinetic energy (translational and rotational) of major mass items and then to distribute other DOF over the structure using judgment to include the DOF necessary to characterize deflected shapes for dynamic behavior in the frequency range of interest.

Experience has shown that for a more accurate representation of plate dynamics, it is better to include all translational and rotational DOF at fewer grid points than it is to include only translational DOF at a larger number of grid points. As a rule of thumb, a reasonably good selection of the dynamic DOF (the "a-set") will produce modal frequencies within 5% for the lowest one third of the complete set of modes from the dynamic model. Said another way, the number of dynamic DOF should be at least three times the number of modes within the frequency range of interest.

5.1.3.2 Generalized Dynamic Reduction. The goal of generalized dynamic reduction, also called subspace iteration [5.14], is to generate a set of Ritz vectors that are rich in the modes within the frequency range of interest. These vectors are obtained by inverse iteration on the unreduced model to determine an approximation to the lowest orthonormalized mode shapes, extending beyond the frequency range of interest for the dynamic model [5.15]. In addition to these generalized coordinates, some physical DOF may be useful as a convenience for representing nonlinear effects and for economy in the recovery of displacements. Also, for improved accuracy in response calculations, physical DOF corresponding to applied loads should be included. The generalized and selected physical coordinates comprise the vector u_a, which replaces x_a in Equation (5.15), and the remaining steps in the condensation proceed as for static condensation.

5.1.3.3 Load Transformation Matrix. The internal dynamic loads L of a payload or spacecraft are derived from the displacements x using a load transformation matrix LTM where

$$L = (LTM)x = [LTM_N \; LTM_I] \begin{Bmatrix} x_N \\ x_I \end{Bmatrix} \tag{5.18}$$

The LTM is derived from the FEM stiffness model. Each row of the LTM yields an internal load resulting from displacements of the non-interface displacements x_N and interface displacements x_I. The term "load" is a general one, referring to any form of load (for example, bending moment or shear force), any form of stress, and relative displacements where there is concern about collision. Due to the truncation of the system modes, much better convergence to accurate dynamic loads is achieved by reformulating the transformation to involve inertial forces rather than displacements. This is possible for the non-interface DOF by solving the upper half of Equation (5.12) for the displacements x_N in terms of the accelerations $\ddot{x}_N$ and applied interface forces F_N, and inserting the result into Equation (5.17). The result is

$$L = LTM_N k_{NN}^{-1}(-M_{NN}\ddot{x}_N - M_{NI}\ddot{x}_I + F_N) + (LTM_N \Phi_{cN} + LTM_I)x_I \tag{5.19}$$

where F_{cN} is the constraint mode matrix for the non-interface degrees of freedom, defined in Equation (5.9), and applicable equally to the case of free-interface modeling of the spacecraft.

5.1.4 Other Modeling Procedures.

5.1.4.1 Payload Reanalysis. The results of a previous analysis can be used as a basis for the calculation of loads for a new or modified payload design when the launch vehicle and forcing functions are unchanged. This approach has been called reanalysis. Payload loads are calculated throughout its design cycle without need for a model of the launch vehicle nor definition of the forcing functions. The method is not necessarily limited to small changes in the design. Reanalysis explicitly takes into account the changes in the payload interface motions that result from design changes. The only approximation made is that the modified set of system modes can be represented as a linear combination of the original system modes and the new payload component modes. If there were no truncation of the system, this requirement is met exactly. In practice, modes are truncated above a frequency limit and thus some degree of inaccuracy is incurred dependent on the degree of payload change and the degree of truncation.

One reanalysis method combines frequency and time-domain calculations [5.16]. Accelerations at the payload interface DOF in the time domain from a previous analysis are FFT converted to the frequency domain. Modifications to these motions are then made in the frequency domain. Finally a conversion is made back to the time domain. Care must be taken to avoid significant corruption due to the forward and inverse FFT processes. A similar method that performs solely in the time domain, thereby avoiding the possibility of corruption due to time/frequency transformations, is also available [5.17]. This time-domain method also specifically addresses the case of statically determinate interfaces as well as nonzero initial conditions.

5.1.4.2 Generalized Modal Shock Spectrum Procedure. This method seeks to estimate a bound on individual responses via a generalized modal shock spectrum approach [5.18]. The objective is to reduce the analysis effort and degree of dependence between the spacecraft and launch vehicle design processes. The dynamic interaction affecting the motions at the spacecraft interface is taken into account and an indeterminate interface is allowed. An important aspect is the easy consideration of the sensitivity of the design loads to variations in the modal properties of the spacecraft and launch vehicle. For example, artificial tuning between spacecraft and launch vehicle modal frequencies can be imposed.

System equations of motion in component modal coordinates are developed for the launch vehicle represented by its free-interface normal modes, including rigid body modes, and for the spacecraft represented by its fixed-interface normal modes. Bounds on responses are developed for each spacecraft mode with each launch vehicle mode, and bounds on overall responses are obtained by the SRSS technique (square root of the sum of squares).

Application to the Galileo spacecraft resulted in conservatism relative to a full transient analysis with up to a factor of 1.5 for the larger response values, and up to a factor of 5 for smaller response values for a particular transient event. The conservatism was reduced to an overall factor of no greater than 1.5 for design values that envelope the requirements from multiple events.

5.1.5 Model Verification.

5.1.5.1 Static Tests. Static tests can be used to determine stiffness parameters when analysis is uncertain or simply more difficult than test, or when nonlinear effects are involved such as differences in stiffness for tension versus compression loading. Joints are particularly troublesome and are typically not modeled in a finite-element fashion unless major significance is attached to accurate modeling from a structural standpoint. In the case of a viscoelastic

material, such as a solid propellant or a vibration isolator, both static and dynamic tests are required to address strength, deflection, and dynamic behavior.

5.1.5.2 Modal Tests. When analytical predictions of spacecraft modes are compared to experimentally determined modes, it is invariably found that a number of modes were either poorly predicted or not predicted at all. Stiffnesses of spacecraft joints and of fittings that connect substructures to each other are often poorly modeled. As a result, high-order modes and modes dominated by motion of local components are error prone. Even low-order modes can be troublesome when they are dominated by appendages such as solar arrays. A comprehensive comparison of analysis and test results was published for the Viking spacecraft in [5.19].

It is therefore required that spacecraft be mode survey tested [5.1, 5.2]. Mode survey testing has benefitted greatly from the many advances in measurement systems (digital acquisition and processing), transducers, testing rigor, and mode extraction algorithms [5.20, 5.21]. The Galileo Spacecraft modal survey was performed using a variety of test methods, including multiple-input sine dwell, incremental sine sweep, single- and multiple-input random, and chirp excitation, and involved various investigators [5.22]. Mode survey testing has continued to evolve to a point where multi-shaker random vibration and multi-shaker sine sweep test techniques are at the pinnacle of the technology [5.23 - 5.26]. Base-driven modal testing, which can be conducted in conjuction with environmental and qualification vibration tests, is an attractive approach for smaller spacecraft with low budgets and short development cycles [5.27].

5.1.5.3 Mathematical Checks. There are a number of mathematical checks that can be made to determine that all is well with the formulation of an unconstrained dynamic model. Some of these checks are identified below.

a. Stiffness Matrix Checks

1. Symmetric (Maxwell's reciprocity relationship).
2. Positive diagonal elements.
3. Positive semi-definite (no negative eigenvalues of **K**).
4. Number of zero eigenvalues of **K** equal to the number of rigid body DOF (usually six) plus the number of mechanism DOF.
5. Internal forces vanish under rigid body motion (or strain energy vanishes).

b. Mass Matrix Checks

1. Symmetric.
2. Positive diagonal elements.
3. Positive semi-definite (no negative eigenvalues of **M**).
4. Symmetric rigid body mass matrix containing only diagonal elements for translational DOF.
5. Overall principal axes and inertias match that of the mass properties model.

c. Normal Modes Checks

1. Unconstrained models:
   (a) Orthonormal with respect to **M**, namely, Φ_T **M** Φ is the unit matrix. If mode shapes are experimentally derived and orthonormalized, as a goal the off-diagonal elements should be less than 0.1.
   (b) Orthogonal with respect to **K**, namely, Φ_T **K** Φ is diagonal.

(c) Number of zero frequency modes equal to the number of rigid body DOF (usually six) plus the number of mechanism DOF.

2. Models with fixed-interface DOF:
   (a) Same as (a) and (b) for unconstrained models.
   (b) No rigid body modes should be present for the fixed-interface model, other than for mechanism DOF.

d. Load Transformation Matrix Checks

1. Loads (internal forces, stresses, relative displacements) resulting from a steady translational or rotational physical acceleration should match those predicted by the finite-element model using the corresponding inertia forces.

2. Zero loads should result from rigid body displacement of the set of fixed-interface DOF.

5.1.5.4 Analysis/Test Correlation. The mode survey test (or modal survey) is conducted to provide the basis for the test-verified dynamic model to be used in the Verification Load Cycle (VLC). Even for fairly simple spacecraft configurations, the analytical model almost assuredly requires some adjustments to achieve acceptable correlation with the experimental modes. For most complex spacecraft configurations, acceptable correlation is not achievable and the experimental modes themselves are then used to take the place of the analytically produced modes. The practice of using the experimental modes as the most reliable basis for dynamic loads prediction was initiated for Air Force programs in the early 1960s. In order to directly correlate analysis and test modes, the interface boundary conditions for the component-mode representation must be the same in the analysis as they are in the test. Some reliance on the mathematical dynamic model is required since its mass matrix is needed to perform orthogonality checks. Moreover, when fixed-interface component modes are used, analytically derived constraint modes are required, recognizing that static test definition of constraint modes is usually impractical.

In some cases, there are serious problems associated with fixed-interface modal testing. The problems are (a) contamination of data due to coupling between the fixture and the test article, (b) difficulty in accurately simulating flight boundary conditions, such as trunnion bearings for Shuttle payloads, and (c) the cost of construction and checkouts of the fixture. Correspondingly, when free-interface component modes are used, analytically derived attachment modes would be required; in this case, however, there is a practical possibility of experimentally deriving attachment modes at least for translational interface DOF by direct forcing during the modal test at those DOF [5.7]. Free-interface modal testing has been studied at the Marshall Space Flight Center, including the experimental determination of residual flexibility functions for the payload interfaces [5.28]. In a first phase, the technique was applied and was reported to work well for a space station module (SSM) prototype, a complex shell structure, and for the Material Science Laboratory [5.29]. The approach taken was to analytically convert the test results to determine the fixed-interface representation for use in system synthesis, instead of using the free-interface model for this purpose. Convergence studies for the SSM showed a superiority of the Rubin method relative to the methods of MacNeal (neglecting residual mass) and Benfield-Hruda (mass-addition). Unpublished follow-on studies have involved a planar-grid Shuttle simulator with simulated trunnions and a Space Station Pathfinder simulator; with the latter a good correlation was achieved between the free-interface experimental representation converted analytically to a fixed-interface representation and modes obtained experimentally with a fixed-interface configuration.

Damped normal modes, as opposed to "complex modes" are determined in modal testing. This means that deviations from real mode shapes (that is, all motions either in or out of phase) are not translated into cross coupling terms in the damping matrix representing the spacecraft. Also, the modal test article is invariably somewhat different from the flight configuration. For example, the actual liquid propellant is typically replaced by a benign liquid (such as water or alcohol) and a tank for liquid hydrogen is usually left empty for the test. Also, some components are unavailable for the test so they are either not included or are replaced by a crude mass simulator. Furthermore, in order to facilitate the experimental measurement of primary structural modes, some parts of the spacecraft may be removed for the modal test. Examples are light, relatively flexible, components such as antennas and solar arrays. To avoid dealing with nonlinearities in the modal test, when possible, nonlinear elements are removed or modified to cause linear behavior (such as shimming of gaps). Removed components are separately tested to be subsequently analytically coupled into the spacecraft model. This approach is usually combined with some treatment of the attachment points for a missing component. This treatment can be to install a rigid simulator or one or more arbitrary rigid masses to assure that the interface flexibility properties are contributing to the modes in the frequency range of interest during the modal test. In effect, the Benfield/Hruda approach discussed in Sec. 5.1.2.2 is applied. All differences between the modal test article and the flight configuration must be analytically dealt with to upgrade the test-based dynamic model to the flight configuration to produce the test-verified dynamic model for use in the Verification Load Cycle.

5.1.6 Low Frequency Response Analysis.

5.1.6.1 Low Frequency Transient Response Analysis. In general low frequency transient forcing functions are expressed as deterministic functions of time. Responses of the flight vehicle are computed by integration of the equations of motion for the vehicle modes. A form convenient for numerical integration is

$$\ddot{q} + \mathbf{B}_{diag}\,\dot{q} + \Omega^2\, q = \mathbf{\Phi}_F^{\,T}\,\mathbf{F}(t) + \mathbf{\Phi}_{NL}^{\,T}\,\mathbf{F}_{NL}(\dot{q}, q) - \mathbf{B}_{odiag}\,\dot{q} \qquad (5.20)$$

The system modes result from a modal synthesis process, as described in Section 5.1.2. The system generalized coordinates are contained in the vector q; natural frequencies are the diagonal elements Ω; mode shapes are the columns Φ. The matrix B is a full damping matrix resulting from the transformation to system modes of modally damped component modes. Note that **B** has been split into a diagonal part $\mathbf{B}_{diag}$ and an off-diagonal part $\mathbf{B}_{odiag}$; the common practice of ignoring $\mathbf{B}_{odiag}$ can lead to significant error [5.30]. Thus the left side of the Equation (5.20) involves only uncoupled real modes. The right side of the equation contains the generalized forces split into three parts: Φ_F^T F(t) is the generalized force vector for prescribed external forces, $\Phi_{NL}^T F_{NL}$ ($\dot{q}$ q) is the vector of generalized nonlinear forces which arise from response motions (for example, launch stand release mechanisms or from nonlinear elements within the vehicle), and $\mathbf{B}_{odiag}\,\dot{q}$ is the vector of modal coupling forces due to damping interaction. These last two sets of forces give rise to an iterative process in each time step if required to achieve acceptable compatibility with the motions occurring during the time step. A sudden jump in a force (for example, release from a stand support or closure of a clearance or reversal of a friction or hydraulic force) may also require an iterative process. A formulation and analysis that specifically addresses launch vehicle loads induced by maneuvering through winds is presented in [5.31].

Computational procedures have been published that are well suited to handling the damping and nonlinear terms in Equation (5.20) [5.30, 5.32]. Initial conditions $\dot{q}(0)$, $q(0)$ are required in order to initiate the integration process. For example, a liftoff transient computation will involve wind induced initial motions.

Output choices can be put into three categories:

a. Response time histories. The specific response variables (for example, accelerations and loads) are selected by a response recovery transformation matrix acting on the generalized responses.

b. Maximum and minimum values of the selected responses.

c. Statistics for the selected responses. For example: mean μ, standard deviation σ, $\mu \pm k\sigma$ for a selected value of k.

Often a family of forcing cases is involved and only the overall max-min values for each individual case within the family may be of interest. Statistical measures may be applied to these max-min values.

5.1.6.2 Response Analysis to Low Frequency Acoustic Impingement. Certain payload items respond significantly to the acoustic field inside the fairing during liftoff and maximum airload periods of ascent [5.34]. This tends to be especially true for large area, lightweight items such as solar arrays and dish antennas. If structural evaluation of such items requires that structure-borne and direct acoustic impingement be combined, then analytical prediction of responses to the acoustic excitation is required. Flight measurements on Shuttle and Titan launch vehicles suggest that significant payload acoustic environments exist in the range of about 30 to 200 Hz. To cover this frequency range, it is implied that only the individual substructure directly involved is modally analyzed and not the entire spacecraft. For example, although a solar array might be evaluated structurally solely by an acoustic test, it will have to be modeled if its boom and attachment hardware require combined load analysis.

Response to acoustic excitation is predicted in the frequency domain using spectrally described pressures over surface regions on the response item and frequency response functions. Corresponding to Equation (5.20), the matrix equation of motion for modal coordinates q subjected to discretized surface forces is

$$\ddot{q} + \mathbf{B}\dot{q} + \mathbf{\Omega^2 q} = \mathbf{Q(t)} = \mathbf{\Phi_F}^T \mathbf{F(t)} \qquad (5.21)$$

where the elements of the force vector $\mathbf{F(t)} = \{\mathbf{A_{eff}}\ \mathbf{p(t)}\}$ are forces acting on a surface patch with effective areas $\mathbf{A_{eff}}$ in association with the external pressure p(t). The pressures are usually based on a frequency-dependent correction of free-field pressures (from 1 to 3 dB higher as frequency increases from 20 to 315 Hz and above [5.34]). Premultiplication by the transpose of the mode shape matrix applicable to the forcing positions, $\mathbf{\Phi_F}^T$, converts these forces to modal (generalized) forces **Q(t).** **B** is a diagonal damping matrix with elements of the form $2\zeta_n\omega_n$, assuming uncoupled damping since synthesis of component modes is not involved to obtain modes of an element of the payload such as an antenna dish.

The effective areas, denoted by $\mathbf{A_{eff}}$, account for the consequence of the degree of correlation of pressure on opposing sides of a surface patch. The ratio of local $\mathbf{A_{eff}}$ to true area is actually frequency dependent and can range from near zero for acoustic wavelengths large relative to

the acoustic path length from one side to the other, to $\sqrt{2}$ for uncorrelated but equal levels on the two sides. Of course the ratio is one if only one side is exposed. One simplified approach to the forcing distribution is to set up different area patches, which are uncorrelated, for each of several frequency bands, with the size of the patches decreasing with increase in the frequency of the band.

In the frequency domain, the spectral matrix (autospectral densities in diagonal elements and cross-spectral densities in off-diagonal elements) of modal displacement responses $G_q(f)$ is expressed as

$$\mathbf{G_q(f) = H_q^*(f)\, G_Q(f)\, H_q(f)} \tag{5.22}$$

where $H_q(f)$ is a diagonal matrix of the modal-displacement frequency response functions and H_q^* is its complex conjugate. For the n*th* orthonormalized mode

$$H_{q,n}(f) = [\, f_n^2 - f^2 + j2\zeta_n f_n f \,]^{-1} \tag{5.23}$$

and

$$\mathbf{G_Q = \Phi_F^T\, G_F\, \Phi_F} \tag{5.24}$$

where $\mathbf{G_Q(f)}$ and $\mathbf{G_F(f)}$ are the spectral matrices of **Q(t)** and **F(t)**, respectively, appearing in Equation (5.21). Note that $\mathbf{G_Q(f)}$ is a nondiagonal matrix even if each area patch has a pressure uncorrelated with that of the other patches since each modal force is made up of a weighted sum of the same pressures, the weighting factors involve modal displacements and effective areas.

The spectral matrix of physical displacements x and of accelerations $\ddot{x}$ are then given by

$$\mathbf{G_x}(f) = \Phi\, G_q(f)\, \Phi^T \text{ and } G_{\ddot{x}}(f) = (2\pi f)^4\, G_x(f) \tag{5.25}$$

The overall result of the operations in Equations (5.22), (5.24) and (5.25) to transform spectral forces into spectral displacements is

$$\mathbf{G_x = \Phi\, H_q^*\, \Phi_F^T\, G_F\, \Phi_F\, H_q\, \Phi^T} \tag{5.26}$$

where the frequency dependence of $\mathbf{G_x}$, $\mathbf{G_F}$, $\mathbf{H_q}$ is not explicitly shown. It is usually sufficient for structural evaluation to determine only the diagonal elements of $\mathbf{G}_x$ and $\mathbf{G}_{\ddot{x}}$, which are autospectral densities of physical displacements and accelerations, respectively. Next these autospectra are integrated over the frequency range of the excitation to yield mean-square responses, followed by a square root operation to obtain rms values, which are actually standard deviations of the responses, σ_x, since the responses have a zero mean value.

A FORTRAN implementation in matrix form is presented in [5.35] along with a user's guide. In particular, it is stated that the frequency incrementing in the frequency neighborhood of a mode must be no greater than one-fourth of the half-power bandwidth of that mode. Refer also to Sections 5.2.1 and 5.2.3 which contain information for frequency domain analysis not presented in matrix form. It should also be pointed out that if the pressure data are available in the time domain, direct integration of Equation (5.21) can be performed to obtain modal responses q(t),

which are then transformed to obtain physical responses x(t), and finally rms values are determined.

Taking the most general view, the pressure field acting on the fairing exterior excites the elastic-acoustic coupled system consisting of the fairing and payload structures, and the intervening acoustic volume. In recent years, such coupled systems have been analyzed using a finite element method (FEM) to obtain modes of a structure that is uncoupled from the fluid, and a boundary element method (BEM) for the fluid [5.36]. Using BEM, the fluid is modeled with pressure degrees-of-freedom at the structural bounding surface areas and their corresponding normal fluid motion. Most applications have been to automotive problems, but an application to a solar array is described in [5.37]. Two state-of-the-art computational tools for the fluid modeling and coupling to supplied structural modes are I-DEAS Vibro-Acoustics™ by the Structural Dynamics Research Corporation (SDRC) and SYSNOISE by Leuven Measurement Systems (LMS).

5.1.6.3 Stationary Equivalent to Nonstationary Random Excitation Based on the Shock Response Spectrum. A random excitation measured in flight is invariably nonstationary. When resulting structural loads are to be calculated or random vibration test specifications are to be developed, the common practice is to provide a power spectral density (PSD) characterization which is then imposed as a stationary random forcing function for the analysis or test. The conversion of the data to the PSD is usually a maximax process on the PSD's from a sequence of short time intervals covering the event. Assessments of a best combination of averaging time and bandwidth have focused on minimizing the result of bias and random errors for the individual spectra [5.38].

The maximax PSD process does not address the nonstationarity of the data in terms that directly relate to structural response. A direct approach can be taken when the calculation of the peak response of structural modes is the desired use for the PSD developed from the nonstationary data. Specifically, a single degree-of-freedom (DOF) response spectrum (RS) is calculated (often called a shock response spectrum or SRS, see Section 2.2.10), then adjusted to be a limit response spectrum (LRS), followed by a calculation of the PSD of the stationary random white excitation which would produce the same maximum response for each natural frequency analyzed.

The mean-square response σ^2 of a single DOF system (natural frequency f_n and resonant magnification Q) to white zero-mean stationary excitation with a PSD G_0 is given by

$$\sigma^2 = (\pi/2)\, G_0 f_n Q \qquad (5.27)$$

This equation is often referred to as the Miles' equation and is generally a good approximation if G_0 is taken to be the value at the natural frequency f_n when the random input is nonwhite. A factor r times the rms response σ can be equated with the limit response spectrum, $LRS(f_n,Q)$, namely

$$r\sigma = LRS(f_n,Q) \qquad (5.28)$$

Using Equation (5.27) to solve for the corresponding $G_0(f_n,Q,r)$ yields

$$G_0(f_n,Q,r) = (2/\pi f_n Q)\, [LRS(f_n,Q)/r]^2 \qquad (5.29)$$

Gaussian input $G_0(f_n,Q,r)$ is analytically input to an individual structural mode characterized by f_n,Q, and the peak modal response is taken to be r times the rms stationary modal response σ, the peak response will be exactly equal to the corresponding limit response spectrum value. If, after developing the equivalent spectrum, it is desired to change the multiplier to r_1, an adjusted equivalent PSD, denoted by $G_1(f_n,Q,r_1)$, is required where

$$G_1(f_n,Q,r_1) = (r/r_1)^2 \, G_0(f_n,Q,r) \qquad (5.30)$$

It is emphasized that, as long as the same r factor is used for calculating both the equivalent PSD and the resulting peak modal response, that response will be the same as the original limit response spectrum value. It is clearly essential that a presentation of an equivalent PSD be accompanied by the Q and r values used for its derivation.

The resolution in natural frequency should be high enough so as not to miss any narrowband peaking. This will be an increasingly demanding requirement the greater the Q. A Fourier transform of the time data can be used to identify frequencies at which peaks occur. In a case for liftoff pressure internal to the fairing on a Titan IVB vehicle, using Q=50 (1% critical damping), the spectrum was satisfactorily resolved with frequency spacing of 1/12th octave.

If a fatigue basis for equivalence of the derived stationary PSD is desired, a counting process of single DOF response cycle amplitudes is necessary, as well as a specification of a duration for its application [5.39]. See Sections 7.1.2 and 7.1.3 for further discussions of fatigue.

5.1.7 Combining Low Frequency Responses.

5.1.7.1 Combining Responses in Individual Modes. Bounds on the responses in individual modes of a spacecraft are sometimes determined and then combined to establish overall peak loads. For example, see 5.1.4.2 and also see 5.1.6.3 for a method of dealing with nonstationary data that is pertinent to computing peak modal response. A common approach for the combination is to SRSS (square root of the sum of squares) the peak modal responses. This is based on the assumption that the modal responses can be treated as if they were each zero-mean stationary random and uncorrelated from each other. The correlation between modal responses can be highly significant, however, for modes with closely spaced frequencies. A method has been developed that accounts for such correlation [5.40]. A numerical study involving earthquake input to a three-dimensional building model having several pairs of very closely spaced modes showed that the SRSS method gave results both well below and well above correct responses. Retaining the sign of local responses in such mode pairs is clearly necessary to allow reinforcement or cancellation to be accounted for in the combination process for their modal responses.

The method is called the Complete Quadratic Combination (CQC) method. It is applicable when the duration of the excitation is long compared to the periods of the structural modes and the excitation spectrum is smooth over the range of frequencies. The method requires that a peak combined load L_c (equally applicable to any response quantity) be calculated using the quadratic form:

$$L_c = \left(\sum_i \sum_j L_i \, \rho_{ij} \, L_j \right)^{1/2} \qquad (5.31)$$

where L_i and L_j denote peak loads in the i*th* and j*th* modes, including their sign associated with their modal (generalized) forcing function and mode shape. The cross-modal coefficients ρ_{ij} are given by

$$\rho_{ij} = \rho_{ji} = \frac{8\zeta^2 r^{3/2}}{(r+1)[(r-1)^2 + 4\zeta^2 r]} \tag{5.32}$$

where $r = \omega_j/\omega_i$, the ratio of modal natural frequencies. This is a simplified form applicable when all modes have the same viscous damping ratio ζ (see [5.40]) if different damping values are involved). A ρ_{ij} approaches unity as the frequencies of the two modes involved become very close and approaches zero as the frequencies become well separated. If all the frequencies are well separated, the CQC method approaches the SRSS method.

In matrix form, Equation (5.31) becomes

$$\mathbf{L_c = L^T \rho L} \tag{5.33}$$

where $\mathbf{L_c}$ is a vector of combined loads, **L** is the matrix of the corresponding loads in the individual modes (each column contains the modal components to a particular load), and **ρ** is the matrix of corresponding cross-modal coefficients.

5.1.7.2 Combining Loads from Deterministic and Random Excitations. Random load components (generally, vibroacoustic in nature) occurring simultaneously with deterministic load components (generally, transient in nature) can be a significant part of the total loads [5.33]. When deterministic and random loads are to be combined, the simplest practice is to SRSS the maximum loads from each source. Namely,

$$L = (LD_{max}^2 + LR_{max}^2)^{1/2} \tag{5.34}$$

where LD and LR denote the deterministically and randomly induced loads, respectively. In effect both load time histories, LD(t) and LR(t), are treated as if they were zero-mean uncorrelated stationary random variables. An issue is the proper factor to place on the rms random load to determine the maximum load. One study that considered Shuttle and Titan vehicles recommended 3.5 for liftoff and 4.0 for maximum airloads [5.34].

Another approach is to treat the two load sources in terms of the statistics of the peak value reached during their individual fluctuations, considering positive load and negative load directions separately. From this viewpoint, for each direction of load the average of peak values and the greatest of the dispersed values in a direction that increases the load (that is, the difference of maximum and average peak values) are established for each source. For each direction, these are combined by adding the averages and the SRSS of the dispersed values. In effect the value of oscillation peaks relative to the average of the peaks for the two load sources are taken to be zero-mean uncorrelated stationary random variables. In equation form, for each direction.

$$L = LD_{av} + LR_{av} + (LD_{disp}^2 + LR_{disp}^2)^{1/2} \tag{5.35}$$

An example for which a statistical superposition of loads can be significant is the combination of mechanically induced spacecraft loads (LM) due to liftoff and loads due to direct impingement of the interior fairing acoustic field. One approach to such a combination is expressed by the following equation:

$$L = LM_{av} + 1.25\,\sigma_A + [\,(LM_{max} - LM_{av})^2 + (2.19\,\sigma_A)^2\,]^{1/2} \qquad (5.36)$$

where it has been assumed that the acoustically induced response peaks are Rayleigh distributed, so that the mean of the peak values is 1.25 times the rms value σ_A and the three-sigma peak value is 3.44 σ_A (note that 2.19 = 3.44 - 1.25).

A procedure for determining the probability of exceeding a specific load level, based upon a first passage statistic (see Section 7.1.4), is recommended in [5.40]. A stationary zero-mean Gaussian random load is represented by its standard deviation and the standard deviation of its first derivative. The uncorrelated deterministic transient load and its first time derivative are involved in the expression for the probability of not exceeding a specified peak load. It is stated that application can be made to the piece-wise stationary random intervals and summing the probabilities of not exceeding in each interval.

The validity of any prediction method should be determined from a comparison of the predictions to flight occurrences. Unfortunately, response data from payloads is rarely available, so assessments of a particular prediction process for a component of a payload (such as combined acoustic and transient excitation of an antenna during liftoff) has been based on computer simulations to gain insight into the degree of conservatism in the predictions.

A shock response spectrum basis for deriving an equivalent acoustic forcing spectrum is discussed in 5.1.6.3. Note that if 3 σ_A is the basis for defining an equivalent load, then the 2.19 in Equation (5.36) would be replaced by 1.75 (from 3 - 1.25).

5.1.8 Assessments.

5.1.8.1 Assessment of Boundary Condition Alternatives for Modal Analysis. The decision on the boundary conditions to be used for the interface points (fixed, free, intermediately constrained) should be made so as to match those to be used for the modal test. Each of the approaches has merits and limitations. At this point a distinction must be made between two types of interface points. There are the launch vehicle interface points and there are the component interface points, the latter resulting from the absence of a component in the modal test.

Fixed interface modeling is the method of choice for launch vehicle interface points [5.1] largely because the other two methods have a relatively small experience base. It should be remembered that fixed interface modeling does not lead to verification of the dynamics associated with motion of these interface points, total reliance having been placed in the analytical stiffness model. The justification given that the experimental modes will approximate those in the coupled vehicle system because of a relatively stiff launch vehicle interface is seldom valid. Also, especially for large spacecraft, the ability to simulate fixed conditions may be poor because of a lack of an adequate fixity in the test facility. A factory floor generally provides inadequate fixity. Instead, a large, massive, seismically supported block should be used. Another limitation can be that the dimensions of the mounting surface of the block may not accommodate a very large test item.

For component interface points, access restrictions typically rule out fixity. The typical approach is to replace the missing item by a mass simulator. The component may be missing because it is unavailable for the test, or it may behave nonlinearly and is to be tested separately, or it may be a complex multimode item such as a large antenna that is deemed better to test separately. It is vital that all six DOF of the simulator be instrumented. Also, if the item is not actually rigid, the simulator should not constrain relative motion among the points so as to require reliance on the analytical stiffness model. In this case, several local rigid simulators may be preferable. Unless a missing component has been tested to show that a rigid simulator is acceptable for dynamic modeling, it is necessary to analytically remove and replace the simulator with a dynamic model determined by modal test of that component. Another approach is to leave the interface points free and drive those points during the modal test. This, however, requires access for the exciter, which may not be available.

Free interface conditions for launch vehicle interface points is an option that can be adopted, although great care must be taken to drive the points during the modal test to obtain accurate frequency response functions for the interface DOF (discussed in 5.1.5.4). This has been implemented in only a few situations, so the procedures are not well established. Driving the rotational DOF, in addition to the translational DOF, requires a special forcing block at the drive point to allow transformation of a sequence of applied forces into translational and rotational components.

A mix of the three types of interface conditions may be adopted to deal with the peculiarities of a given situation. For example, fixity can be adopted for some of the launch vehicle interface points to accommodate larger spacecraft in the test facility (perhaps only three are fixed to provide a nonredundant support). The other interface points can then be mass loaded to "work" them, or they can be attached to a support whose impedance has been measured in all its DOF. Alternatively, the other interface points can be left free to be driven during the modal test.

5.1.8.2 Assessment of Model Verification Procedures. A key matter for model verification is what precisely is meant by the model to be verified. Is it a model that accurately describes all modes in the frequency range of interest or is it only expected to describe significant modes, as stated in [5.1], "based on an effective mass calculation augmented by modes which are critical for specific load or deflection definition"? If prior loads analyses are used to judge which modes are insignificant, there is a danger that an erroneous model has been misleading. If all modes are involved in the verification, a higher burden is imposed on the modal survey test complexity and on the extent of correlation sought between test and analytical modes.

The analytical model adjustment problem has been exhaustively treated in the literature and is still very much unsettled. See [5.2] for a detailed review and an extensive list of references. As stated in [5.2]: "Present day capability for modifying large analytical models, in a realistic way, to obtain agreement with measured modal data is problematic at best. All of the schemes developed to date must be viewed merely as guides to accompany engineering judgement in a trial and error approach to developing the verified analytical model." In view of this, Air Force programs long ago decided that, except for the simplest of spacecraft, adjusting the analytical model is fruitless and the experimental modes themselves are the analytical model to be used in the Verification Load Cycle. Experience has shown that when troublesome appendages (such as solar arrays, large sensors and antennas, and nonlinear items) are removed from the spacecraft for its modal survey, modes of the remaining structure can usually be measured with considerable precision. These appendages are then subjected to individual modal surveys and component mode synthesis is used to generate the overall spacecraft model. Acceptability of the experimental modes implies those meeting stringent orthogonality checks (off diagonals less than 0.1) and "completeness," namely no missing modes as determined by careful inspection of

the frequency response functions. If orthogonality goals cannot be met after expending a reasonable effort to achieve them, model uncertainty factors (MUF) are usually invoked as a compensation.

5.1.8.3 Assessment of Alternatives to All-Up Vehicle Modal Analysis. As discussed in 5.1.4.1, reanalysis has been used to conservatively predict changes in interface response due to changes in the spacecraft with no changes to the launch vehicle or forcing functions. This facilitates the spacecraft design process by allowing independent analyses by the spacecraft contractor to obtain consequences in ascent loads during the design process. The generalized shock spectra (5.1.4.2) approach also has this objective and also facilitates sensitivity studies such as by tolerancing natural frequencies. The advantage of these approaches is counteracted by their tendency to yield more conservative loads than those resulting from a full vehicle analysis. As long as this is tolerable, it can make sense from a programmatic standpoint to employ such a method even after the design is fixed. A hierarchy of prediction methods for payload loads is summarized in Table 5.2.

TABLE 5.2. Summary of Prediction Methods for Payload Loads

Method	Frequency Range	Requirements	Application	Comments
Modal Mass Acceleration Curve (see Section 8.1.2.1)	Up to 150 Hz	Curve of acceleration versus modal effective mass (based upon past experience)	Curve values yield peak acceleration in individual modes. Physical loads by SRSS* of modal loads.	Inexpensive to apply. Requires only payload modes. Generally yields upper-bound loads. Verified or refined by CLA.
Generalized Modal Shock Spectrum (see Section 5.1.4.2)	Below 50 Hz	Modal acceleration bounds obtained by frequency tuning in a prior CLA	Same as MMAC except use prior analysis for bounding modal accelerations. Account for difference in interface impedance from prior analysis. Physical loads by SRSS* of the modal loads.	Mid-frequency modal loads from MMAC.
Reanalysis (see Section 5.1.4.1)	Below 50 Hz	Interface x(t) from prior CLA with same launch vehicle. Fixed-interface modes of prior and new spacecrafts. System modes with prior spacecraft.	Base-driven transient response analysis with account for change in payload modes. Series of modal frequency variations introduced to obtain highest loads from worst-case coupling interactions.	Require determinate interface (not usually a significant drawback). Spacecraft contractor, acting alone, derives loads using previous CLA results.
Coupled Loads Anal. (see Section 5.1.6.1)	Below 50 Hz	Modes of vehicle system and vehicle forcing function.	Transient response analysis (see Section 5.1.6.1). Mid-frequency loads from MMAC combined with CLA loads by SRSS.	Tends to be least conservative prediction method.

* CQC method (see Section 5.1.7.1) tends to improve accuracy for combined loads from close-frequency modes.

5.2 High Frequency Vibration Responses. The high frequency vibration response of space vehicles (i.e., the vibration response at frequencies above 50 Hz) may be due to one or more of five types of excitations, as summarized in Table 5.1. In almost all cases, the engine/ motor acoustic noise during liftoff and/or the aerodynamic noise during ascent through the transonic and qmax speed regions are the dominate sources of the high frequency structural vibrations of space vehicles. The forcing functions produced by these events, as detailed in Sections 4.4 through 4.6, result in pressure loads on the space vehicle/payload structure that are random in character. Hence, the emphasis in this section is on the prediction of structural responses to random pressure loads. However, most of the prediction procedures outlined in this section are also applicable to the other two sources of high frequency structural vibration in Table 5.1 (i.e., high-frequency quasi-periodic and structureborne vibration loads), which involve a motion input to the structure that may or may not be random in character.

Five basic procedures are used to predict the high frequency vibration responses of space vehicle structures, namely, (a) classical normal mode analysis (b) statistical energy analysis (SEA), (c) finite element method (FEM) models, (d) extrapolation techniques, and (e) direct measurements. Brief summaries of these procedures are now presented.

5.2.1 Classical Normal Mode Analysis Procedures. Given an arbitrary structure subjected to a random pressure field over an area A, the autospectrum for the response of the structure at any vector location $\underline{x}$ in the area is given by [5.41].

$$G_r(\underline{x},f) = A^2 G_p(f) \sum_i \sum_k \phi_i(\underline{x}) \phi_k(\underline{x}) H_i^*(f) H_k(f) j_{ik}^2(f) \tag{5.37}$$

where

$$j_{ik}^2(f) = \frac{1}{A^2 G_p(f)} \int_{\underline{v}} \int_{\underline{u}} G(\underline{u},\underline{v},f) \phi_i(\underline{u}) \phi_k(\underline{v}) d\underline{u}\, d\underline{v} \tag{5.38}$$

and

$\underline{u}, \underline{v}$ = vector locations on the structural surface exposed to these pressure fields

$\phi_i(\underline{u})$ = mode shape of ith normal mode of the structure

$\phi_k(\underline{v})$ = mode shape of kth normal mode of the structure

$H_i(f)$ = modal frequency response for the ith normal mode of the structure

$G_p(f)$ = reference autospectrum of the pressure field (usually at point of maximum pressure)

$G_p(\underline{u},\underline{v},f)$ = cross – spectrum of the pressure field between vector locations $\underline{u}$ and $\underline{v}$

* = complex conjugate

The function $j_{ik}^2(f)$ in Equation (5.38) is called the "cross-acceptance function", and can be viewed as a "Green's function". The modal response functions in Equation (5.37) are given by

$$H(f) = \frac{1/K}{\left[1 - (f/f_n)^2 + j2\varsigma f/f_n\right]} \tag{5.39}$$

where

$$f_n = \frac{1}{2\pi}\sqrt{\frac{K}{M}}$$

$$\varsigma = \frac{C}{2\sqrt{KM}}$$

K = modal stiffness = $4\pi^2 f_n^2 M$

M = modal mass = $\int_{\underline{x}} m(\underline{x})\phi^2(\underline{x})\,d\underline{x}$

C = modal damping = $\int_{\underline{x}} c(\underline{x})\phi^2(\underline{x})\,d\underline{x}$

$m(\underline{x})$ = mass density of structure at vector location $\underline{x}$

$c(\underline{x})$ = damping density of structure at vector location $\underline{x}$

For aerospace applications, Equation (5.37) is commonly simplified by assuming the cross terms (where $i \neq k$) are negligible. This assumption, which is generally valid in air but not in water, allows Equation (5.37) to be replaced by

$$G_r(\underline{x},f) = A^2 G_p(f) \sum_i \phi_i^2(f) |H_i(f)|^2 j_i^2(f) \tag{5.40}$$

where $j_{ik}^2(f)$ is called the "joint acceptance function".

The advantage of using the classical normal mode analysis approach to predict structural responses to pressure fields, as detailed in Equations. (5.37) - (5.40), is that the technique provides highly accurate results as a function of both frequency and spatial location, assuming the necessary pressure field and structural data are available. The primary disadvantages of the technique are as follows:

a. The procedure requires an accurate knowledge of the spatial cross-spectrum of the vibration-producing pressure field over the structural surface. Such cross-spectrum information often can be only crudely approximated (see Sections 4.4 through 4.6).

b. The procedure requires an accurate knowledge of the normal modes of the structure (i.e., both mode shapes and frequencies) to the highest frequency of interest in the vibration prediction. The determination of normal modes for complex structures by either experimental or analytical (FEM) procedures becomes increasing inaccurate at frequencies above about the 50th normal mode, which may correspond to less than 100 Hz for a large space vehicle. Hence, the technique is generally limited to the lower end of the frequency range for high frequency vibration predictions in relatively small assemblies, e.g., payloads.

The latter problem (i.e., errors in the definition of the mode shapes and frequencies) leads directly to errors in the autospectra computed at specific locations and frequencies. These errors can be suppressed by computing results that are averaged over both an area A and over frequency intervals of width Δf. With both frequency and space averaging, Equation (5.40) reduces to [5.42]

$$\left\langle G_r(\underline{x}, f) \right\rangle \approx \frac{f^4 A^2}{16 \Delta f} G_p(f) \sum_{i \in \Delta f} \frac{j_i^2(f)}{f_i^3 M_i^2 \eta_i} \tag{5.41}$$

where η_i is the loss factor of the ith normal mode (i.e.,$\eta_i = 2\zeta_i$). The loss factor is assumed to be the sum of three contributions, namely, (a) structural damping, (b) radiation damping, and (c) aerodynamic damping, i.e.,

$$\eta_i = \eta_{i,struc} + \eta_{i,rad} + \eta_{i,aero} \tag{5.42}$$

The radiation damping is essentially the air damping associated with the zero mean flow environment, and the aerodynamic damping is the incremental change associated with the presence of a nonzero mean flow. See [5.43] for the details of classical normal mode analysis procedures and an illustration of their application to Space Shuttle vibration and acoustic predictions.

5.2.2 Statistical Energy Analysis Procedures. Statistical energy analysis, or SEA as it is commonly called, has gained acceptance as a method of high-frequency vibration analysis for aerospace systems. [5.44, 5.45]. The advent of computer codes such as VAPEPS, SEAM, and AutoSEA [5.46] makes it possible to develop the large SEA models needed to obtain accurate predictions for realistic flight systems. SEA draws on many of the fundamental concepts from statistical mechanics, room acoustics, wave propagation, and modal analysis [5.47-5.52]. At first, the procedure appears to be a very simple method of analysis. However, because of the diversity of concepts used in formulating the basic SEA equations, the method quickly becomes very complex. For this reason, analysts have recommended caution in using SEA. However, when used properly, SEA is a powerful method of analysis.

SEA can be used to estimate high-frequency random vibration in two ways. First, SEA can be used to predict vibration transfer functions relating the excitation at one location to the response at another location. The high frequency vibration transmitted through a structure is referred to as structure-borne noise and vibration (see, for example, Section 4.7). SEA can also be used to predict the vibration response to excitation by an acoustic or fluctuating aerodynamic pressure field. Typically, both the structural excitation by exterior acoustic and aerodynamic fields and the transmission of the resulting vibration to interior equipment locations must be considered.

In SEA, the system being analyzed is divided into a set of coupled subsystems. Each subsystem represents a group of modes with similar characteristics. The SEA subsystems can be considered to be “control volumes” for vibratory or acoustic energy flow. Under steady-state conditions, the time-average power input to a subsystem from external sources and from other connected subsystems must equal the sum of the power dissipated within the subsystem by damping and the power transmitted to the connected subsystems.

SEA models of large, complex aerospace structures have been developed using 400 to 500 subsystems. However, much smaller models can be used with less than 10 subsystems to study the vibration response of directly excited structures or to study structure-borne vibration transmission over short distances.

Consider, as an example, an electronic component mounted on an equipment platform within a launch vehicle fairing, as shown in Figure 5.3. The high-frequency random vibration environment for the component is of concern since typical components have internal resonance frequencies in the range of 200 to 400 Hz. A simple SEA model for this problem is shown in Figure 5.4. In this model three subsystems are used: one for the modes of the fairing; one for the modes of a ring frame connected to the fairing, and one for the modes of the equipment platform. To simplify the problem, only bending modes are considered. For more complex problems, subsystems would be added for inplane compression and shear modes of these structures and additional substructures and acoustic spaces could be added to model complete spacecraft assemblies.

The vibratory power input from the exterior acoustic field during vehicle lift-off is specified as the excitation of the fairing modes, W_f^{in}. This parameter can be calculated using joint acceptance functions if the fairing mode shapes are known, as described in Section 5.2.1, or it can be calculated using statistical techniques. In many cases the SEA model can be expanded to include a subsystem for the exterior acoustic field. The pressure level is specified for this subsystem and SEA is used to calculate the coupling between the exterior acoustic subsystem and the fairing.

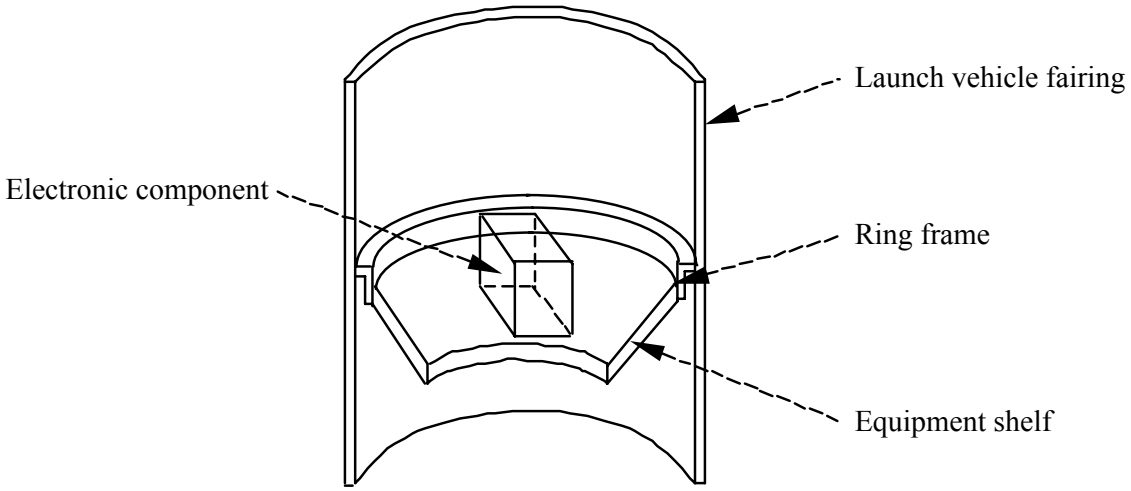

FIGURE 5.3 Electronic Component Vibration Problem

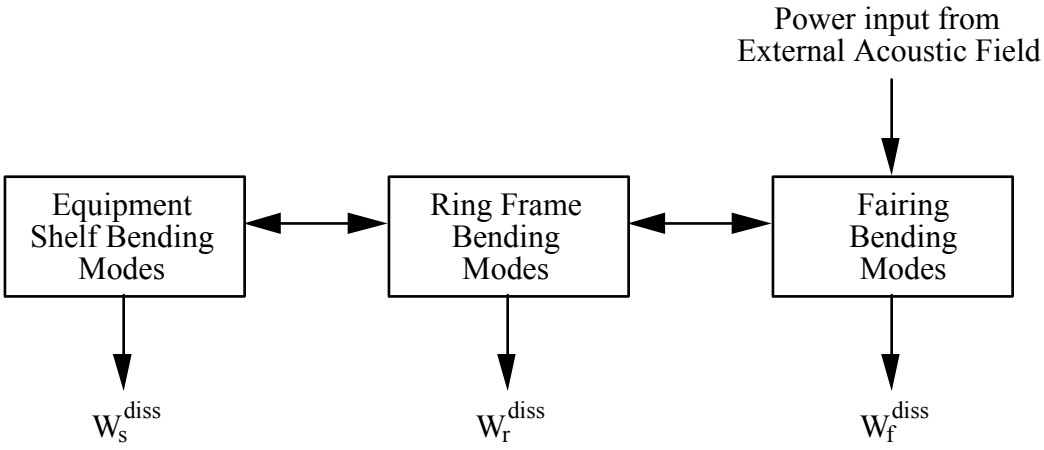

FIGURE 5.4 SEA Model of Structureborne Vibration Transmission

Caution must be used, however, since SEA assumes the exterior acoustic field to be diffuse. "Efficiency" factors are needed to relate the power input from a directional lift-off acoustic field or from a turbulent boundary layer field or separated flow field.

The time-average power dissipated within each subsystem is indicated by the terms: W_f^{diss}, W_r^{diss}, and W_s^{diss}. Following the usual definition of the damping loss factor, the time-average power dissipated within the subsystem can be written in terms of the time-average energy of the system and the radian frequency of vibration,

$$W_s^{diss} = \omega \eta_{s,diss} E_s \tag{5.43}$$

where ω is the radian frequency (typically, a one-third-octave band center frequency), $\eta_{s;diss}$ is the damping loss factor for subsystem s, and E_s is the time-average energy for subsystem s. A similar equation applies for subsystems r and f.

The energy transmitted between the connected subsystems can also be assumed to be proportional to the energy in each system. By analogy to the dissipated power, the factor of proportionality for transmitted power is called the coupling loss factor. However, since energy flow between the two systems can be in either direction, two coupling loss factors must be identified, so that the net energy flow between two connected subsystems is given by

$$W_{f,r}^{trans} = \omega \eta_{f,r} E_f - \omega \eta_{r,f} E_r \tag{5.44}$$

where $\eta_{f;r}$ and $\eta_{r;f}$ are the coupling loss factors between subsystem f and r and between r and f.

These two coupling loss factors are not equal. A power balance can now be performed on each subsystem to form a set of linear equations relating the energies of the subsystems to the power inputs,

$$\omega\begin{bmatrix} \eta_{f;d}+\eta_{f;r}+\eta_{f;s} & -\eta_{r;f} & -\eta_{s;r} \\ -\eta_{f;r} & \eta_{r;d}+\eta_{r;f}+\eta_{r;s} & -\eta_{s;r} \\ -\eta_{f;s} & -\eta_{r;s} & \eta_{s;d}+\eta_{s;f}+\eta_{s;r} \end{bmatrix}\begin{bmatrix} E_f \\ E_r \\ E_s \end{bmatrix}=\begin{bmatrix} W_f^{in} \\ W_r^{in} \\ W_s^{in} \end{bmatrix} \qquad (5.45)$$

Note that the subscript notation typically used in SEA is not conventional matrix notation. Also note that the loss factor matrix is not symmetric.

SEA Reciprocity The coupling loss factors used in SEA are generally not reciprocal, that is $\eta_{s;r} \neq \eta_{r;s}$. If it is assumed, however, that the energies of the modes in a given subsystem are equal, at least within the concept of an ensemble average, and that the responses of the different modes are uncorrelated, a reciprocity relationship can be developed. The assumptions for this relationship are more restrictive than required for a general statement of reciprocity, so that the term SEA reciprocity should be used.

SEA reciprocity requires that the coupling loss factors between two subsystems be related by the modal densities,

$$n(\omega)_s\,\eta_{s;r} = n(\omega)_r\,\eta_{r;s} \qquad (5.46)$$

Using this relationship, a new coupling factor, β, can be introduced which allows the energy balance equations to be written in a symmetric form,

$$\begin{bmatrix} \beta_{f;d}+\beta_{f;r}+\beta_{f;s} & -\beta_{r;f} & -\beta_{s;f} \\ -\beta_{f;r} & \beta_{r;d}+\beta_{r;f}+\beta_{r;s} & -\beta_{s;r} \\ -\beta_{f;s} & -\beta_{r;s} & \beta_{s;d}+\beta_{s;r}+\beta_{s;f} \end{bmatrix}\begin{bmatrix} E_f/n(\omega)_f \\ E_r/n(\omega)_r \\ E_s/n(\omega)_s \end{bmatrix}=\begin{bmatrix} W_f^{in} \\ W_r^{in} \\ W_s^{in} \end{bmatrix} \qquad (5.47)$$

where

$$\beta_{s;r} = \omega\,\eta_{s;r}\,n(\omega)_s = \omega\,\eta_{r;s}\,n(\omega)_r = \beta_{r;s} \qquad (5.48)$$

The ratio of total energy to modal density has the units of power and can be called “modal power”.

Coupling Loss Factor Measurement The coupling loss factors or coupling factors cannot be measured directly. However, a power injection technique can be used to infer the coupling factor from measured values of power input and response energy. Using this technique each subsystem is excited in turn with a unit power input and the response energy of the subsystems is measured to form a matrix of measured energies. Each column in the matrix corresponds to the measured response energies when one subsystem is excited. For example, the second column contains the measured energies when the 2nd subsystem is excited. The coupling loss factor matrix is determined by inverting the matrix of measured subsystem energies,

$$[\eta] = [E]^{-1} \qquad (5.49)$$

The off-diagonal terms are the negative values of the coupling loss factors, while the sum of terms for each row give the damping loss factors. This measurement technique has been successfully used to "measure" in-situ coupling and damping loss factors. However, errors in the energy measurement can result in large errors in the measured loss factors. Systems containing highly coupled subsystems will result in energy matrices that are poorly conditioned, since two or more columns will be nearly equal. Thus, the success of the measurement technique requires careful identification of the subsystems. The best results are obtained for light coupling, when the coupling loss factors are small compared to the damping loss factors, so that the loss factor matrix is diagonally dominant.

The measurement of subsystem energy is particularly difficult for subsystems with inplane compression and shear modes. Because of the high stiffness of the inplane modes, a small amount of motion results in a large amount of energy. The measurement of subsystem energy is also difficult for subsystems in which the mass is nonuniformly distributed. For these subsystems, an effective or dynamic mass must be determined at each measurement point.

Coupling Loss Factor Theory Coupling loss factors can be predicted analytically using wave and mode descriptions of the subsystem vibrations. Waves are used when the number of dimensions of the subsystem is greater than the number of dimensions of the connection: e.g., a beam connected at a point, a plate connected at a point or along a line, and an acoustic space connected at a point, line, or area. Modes are used when the number of dimensions of the subsystem is equal to the number of dimensions of the connection: e.g., a beam connected along a line and a plate connected over an area.

When a wave description can be used for all subsystems at the connection, the coupling loss factor between subsystems can be written in terms of a power transmission coefficient. For a point connection between beams, the coupling factor between subsystem s and subsystem r can be written

$$\beta_{s;r} = \omega \eta_{s;r} n_s(\omega) = \frac{1}{2\pi} \tau_{s;r} \tag{5.50}$$

where $\tau_{s;r}$ is the power transmission coefficient. The power transmission coefficient must take into account energy transmitted by all degrees of freedom at the connection: three translational degrees of freedom and three rotational degrees of freedom. For a point connection with a single degree of freedom (all other degrees of freedom are constrained), the transmission coefficient is given by

$$\tau_{s;r} = \frac{4 R_s R_r}{\left| Z_j \right|^2} \tag{5.51}$$

where R is the subsystem resistance (real part of the impedance) for the unconstrained degree of freedom and Z_j is the junction impedance - the sum of the impedances of all subsystems connected at the point. The coupling factor given by Equations. (5.50) and (5.51) can also be used for two and three-dimensional subsystems connected at a point with a single degree of freedom, as long as the correct impedances are used. For point connections with multiple degrees of freedom, an estimate of the coupling factor can be obtained by summing the power transmission coefficients for each degree of freedom.

The coupling factor between two-dimensional subsystems connected along a line of length L can also be written in terms of a power transmission coefficient. However, for this case an integration must be performed over all angles of incidence. The coupling factor is given in terms of the angle-averaged transmission coefficient as

$$\beta_{s;r} = \omega \eta_{s;r} n_s(\omega) = \frac{1}{2\pi} \frac{k_s L}{\pi} \overline{\tau_{s;r}} \tag{5.52}$$

where k_s is the wavenumber of the source subsystem and $\tau_{s;r}$ is given

$$\overline{\tau_{s,r}} = \frac{1}{2} \int_{-\pi/2}^{\pi/2} \tau_{s;r}(\theta_s) \cos(\theta_s) \, d\theta_{s_s} \tag{5.53}$$

and θ_s is the angle of incidence for a wave in the source subsystem. The parameter, $k_s L/\pi$, is the effective number of points for the line connection. For a line connection, the power transmission coefficient must take into account the energy transmitted by four degrees of freedom: three translational and one rotational. For a single degree of freedom, the transmission coefficient for an incident angle, θ_s, can be expressed in terms of the line impedances of the source and receiver subsystems as

$$\tau_{s;r}(\theta_s) = \frac{4 R_s(k_t) R_r(k_t)}{\left| Z_j(k_t) \right|^2} \tag{5.54}$$

where k_t is the trace wavenumber given by $k_s \cos(\theta_s)$, and $R(k_t)$ is the real part of the line impedance for the unconstrained degree of freedom.

The formulation above can also be used to predict the coupling loss factor between three-dimensional subsystems coupled along a line, if the integration is performed over all solid angles of incidence. For this case, the angle-averaged transmission coefficient is written as

$$\overline{\tau_{s;r}} = \int_{-\pi/2}^{\pi/2} \tau_{s;r}(\theta_s) \sin(\theta_s) \cos(\theta_s) \, d\theta_s \tag{5.55}$$

For an area connection between three-dimensional subsystems, the coupling factor is given in terms of the angle-averaged transmission coefficient as

$$\beta_{s;r} = \omega \eta_{s;r} n_s(\omega) = \frac{1}{2\pi} \frac{k_s^2 S}{4\pi} \overline{\tau_{s;r}} \tag{5.56}$$

where S is the area of the connection. The effective number of points for the area connection is given by the parameter, $k_s^2 S/4\pi$.

When the number of dimensions of a subsystem is equal to the number of dimensions of the coupling, modes are used to calculate the coupling loss factor. For example, the coupling loss factor between a two-dimensional system such as a plate or shell and a three-dimensional system such as an acoustic space is obtained by calculating the radiation efficiency for each mode of the plate, and averaging over all modes with resonance frequencies in the analysis bandwidth,

$$\eta_{s;r} = \frac{\rho_r c_r S}{\omega M_s} \frac{1}{N_s} \sum_i \sigma_i^{rad} \tag{5.57}$$

where $\rho_r c_r$ is the characteristic impedance of the acoustic space, M_s is the mass of the plate, N_s is the mode count for the plate, and σ_i^{rad} is the radiation efficiency for mode i of the plate. Approximations to the summation can be made by grouping the modes into "edge" and "corner" modes [5.53].

The power transmission coefficients and radiation efficiencies can be calculated with great accuracy. However, the relationship between these parameters and the SEA coupling loss factors requires that some assumptions be made regarding the vibration fields in the connected subsystems. First, the vibrations of the two subsystems are assumed to be uncorrelated. Second, the vibrations of the two subsystems are assumed to be "diffuse" - waves are incident on a point within the subsystem from all angles with equal intensity. Although these assumptions are difficult to prove, even for idealized structures and acoustic spaces, they are generally valid for lightly coupled systems at high frequencies, where many modes participate in the vibration response. The validity of the assumptions for highly coupled subsystems is open to question.

Fortunately, the errors incurred using the above equations for highly coupled subsystems are generally small. The assumptions are also open to question at low frequencies, where only a few modes participate in the response. At these frequencies, the equations above may predict coupling loss factors that are too large. However, it is difficult to quantify the error. In spite of the limited validity of the assumptions, the equations above provide useful estimates of the coupling loss factors, even for highly coupled subsystems at low frequencies.

Damping Loss Factor Theory The damping loss factors can be predicted analytically for free-layer and constrained layer treatments. The damping for an acoustic space is often specified by the average absorption coefficient for the space rather than a damping loss factor. The power dissipated within the acoustic space can be written in terms of the time-average energy and the absorption coefficient as,

$$W_a^{diss} = \omega \frac{S_a}{4 k_a V_a} \alpha_{a;diss} E_a = \omega \eta_{a;diss} E_a \tag{5.58}$$

where S_a is the area of the absorbing surface, V_a is the volume of the acoustic space, and k_a is the acoustic wavenumber. It follows that the damping loss factor for an acoustic space can be obtained from the average absorption coefficient by the relation,

$$\eta_{a,diss} = \frac{S_a}{4 k_a V_a} \alpha_{a;diss} \tag{5.59}$$

where the constant 4V/S is commonly referred to as the mean-free-path.

Energy and Response The SEA power balance equations can be solved to obtain the modal energy or modal power of each subsystem. The final step in the analysis is to relate these variables to the subsystem response. For structural subsystems, the spatial-average mean-square velocity is calculated from the kinetic energy. For resonant vibrations, the time-average kinetic energy is equal to the time-average potential energy. Thus, the average mean-square velocity in a band of frequencies is given by

$$\left\langle v^2 \right\rangle_{x;t} = \frac{E}{M} \tag{5.60}$$

where E is the total energy of all modes in the band and M is the mass of the subsystem. For acoustic subsystems, the spatial-average mean-square acoustic pressure is calculated from the potential energy,

$$\left\langle p^2 \right\rangle_{x;t} = \frac{E}{C_a} \tag{5.61}$$

where C_a is the compliance of the subsystem, $V/\rho c^2$, for an acoustic space with rigid walls.

Variance SEA provides a statistical description of the subsystem response. However, in many cases, SEA is used only to obtain an estimate of the mean. Although the mean provides the "best estimate" of the response, this estimate may differ significantly from the response measured for a single member of the ensemble of dynamic systems. The variance or standard deviation of the response provides a method to quantify the expected confidence intervals for the SEA prediction. When the variance is high, the confidence intervals will be large, and the mean does not provide an accurate estimate of the response.

Using SEA in design requires that a confidence interval be established for the response prediction, so that an upper bound or "worst case" estimate can be compared with design requirements. If the mean response is used for design, half the products produced will fail to meet the design requirements. Use of the mean plus two times the standard deviation (square-root of the variance) provides a reasonable upper bound for the response prediction. Methods to predict the variance of the SEA prediction are not well established. Often an empirical estimate of the variance or confidence interval is used. In other cases, an estimate based on the modal overlap parameter and the frequency bandwidth of the analysis is used. The modal overlap parameter, $M_{overlap}$, is the ratio of the average damping bandwidth for an individual mode to the average spacing between resonance frequencies. This parameter can be written in terms of the damping loss factor and the modal density as

$$M_{overlap} = \frac{\pi}{2} \omega \eta_d n(\omega) \tag{5.62}$$

where η_d is the effective total damping loss factor for the subsystem. Large values of the product of the modal overlap parameter and the analysis bandwidth result in low variance and a narrow confidence interval. In this case, the mean is a good estimate of the response. Small values of the product result in high variance and wide confidence intervals. In this case, the mean does not give a good estimate of the response, and the variance should be determined so that an upper bound to the prediction can be obtained.

Failure to include an estimate of the variance in the SEA analysis leads to some misunderstandings regarding the capabilities of SEA. First, SEA is not limited to high frequencies and high modal densities. However, at low frequencies and for low modal densities, the confidence interval for the SEA predictions will be large, so that an estimate of the variance must be made. Second, SEA is not limited to broadband noise analysis. However, for a single-frequency or narrow band analysis, the confidence interval for the SEA predictions will be larger than for a one-third octave or octave band analysis.

5.2.3 Finite Element Method Procedures. Finite element method (FEM) models are most widely used to predict the response of structures to low frequency dynamic loads (generally less than 50 Hz), as detailed in Section 5.1. However, FEM models can also be used to predict the acoustic or fluctuating pressure-induced vibration response of structures up to the frequency of about the 50th normal mode, or even higher frequencies if the model has a sufficient number of degrees-of-freedom. Like SEA procedures, FEM procedures can be used to predict the vibration response of a structure at one location due to the application of a motion load at another location (structureborne vibration), or to predict the response of a structure due to a pressure load on that structure. For a random pressure field excitation, the autospectrum of the vibration response of an FEM modelled structure at any vector location $\underline{x}$ is computed by applying discrete inputs to the model at q number of node points, as follows [5.54]:

$$G_r(\underline{x},f) = \sum_{i=1}^{q}\sum_{k=1}^{q} H^*_{i\,\underline{x}}(f)\frac{A_x}{A_i} H_{k\,\underline{x}}(f)\frac{A_x}{A_k} G_{ik}(f) \qquad (5.63)$$

where

$H_{i\,x}(f)$ = frequency response function between the ith input and response location

$H_{k\,\underline{x}}(f)$ = frequency response function between the kth input and response location

$G_{ik}(f)$ = cross-spectrum between the ith and kth input locations

A_x = nodal area at the response location

A_i = nodal area at the ith input location

A_k = nodal area at the kth input location

* = complex conjugate

The cross-spectrum term in Equation (5.63) represents a discrete version of the spatial cross-spectrum of the pressure field that is applied to the surface of the structure, as detailed in Sections 4.4 through 4.6. See [5.55] for an illustration of vibration predictions made for a large aerospace vehicle up to about 150 Hz using a FEM model.

The advantage of using the FEM analysis approach to predict structural responses to pressure fields, as detailed in Equation (5.63), is that the technique provides reasonably accurate results as a function of both frequency and spatial location, assuming the necessary pressure field and structural data are available, and the FEM has a sufficient number of degrees-of-freedom (see Section 5.1). The primary disadvantages of the technique are as follows:

a. The procedure requires an accurate knowledge of the spatial cross-spectrum of the vibration-producing pressure field over the structural surface. Such cross-spectrum information often can be only crudely approximated (see Sections 4.4 through 4.6).

b. FEM models become increasing inaccurate at frequencies above about the 50th normal mode of the structure being modeled. For large spacecraft, this may correspond to less than 100 Hz. However, as for the classical normal mode analysis procedures discussed in Section 5.2.1, the errors due to inaccuracies in the definition of individual mode shapes and frequencies can be suppressed by spatial and frequency averaging of the vibration predictions at various locations over the structure.

5.2.4 Extrapolation Procedures. A vast amount of high frequency vibration data have been acquired and analyzed over the years for many space vehicle programs, both in the laboratory and in flight. Even though the data may have been acquired for totally different vehicle designs and flight conditions, at least crude estimates for the vibration levels to be expected on a new space vehicle design can be determined by extrapolations from measurements on a previous vehicle with a different design, commonly referred to as the reference vehicle. Of course, the closer the design details of the new and reference vehicles, the more accurate the extrapolations. Also, the most accurate extrapolations are provided when vibrations on the new and reference vehicles are caused by the same launch or flight event, e.g., the acoustic noise-induced vibration during liftoff.

Extrapolation procedures for high frequency vibration responses generally involve two primary scaling operations, namely, (a) scaling for the vibration source level, and (b) scaling for the surface weight density of the structure [5.56, 5.57]. For cylindrical vehicles, scaling for the diameter of the vehicle may also be accomplished in some cases [5.58]. Based upon these prior studies and more recent experience, the following scaling rules for source level and structural weight density are recommended:

a. Letting $G_r(f)$ and $G_n(f)$ denote the autospectra of the high frequency vibration responses on the reference and new space vehicle, respectively, the autospectrum at all frequencies is scaled for source level from the reference to the new vehicle by

$$G_n(f) = \frac{G_{pn}(f)}{G_{pr}(f)} G_r(f) \tag{5.64}$$

where $G_{pr}(f)$ and $G_{pn}(f)$ are the autospectra of the pressure excitations on the exterior of the structure for the reference and new vehicle, respectively.

b. Again, letting $G_r(f)$ and $G_n(f)$ denote the autospectra of the high frequency vibration responses on the reference and new space vehicle, respectively, the autospectrum at all frequencies is scaled for structural surface weight density from the reference to the new vehicle by

$$G_n(f) = \frac{w_r^2}{w_n^2} G_r(f) \tag{5.65}$$

where w_r and w_n are the surface weight densities of the structure for the reference and new vehicle, respectively. Surface weight density is computed by determining the total weight in kg, including mounted equipment, for a structural area of interest, and dividing this total weight by the surface area in m^2.

c. For predictions on cylindrical space vehicle structures, letting f_r and f_n denote the values along the frequency axes for the autospectra of the high frequency vibration responses on the reference and new vehicle, respectively, the frequency axis of the autospectrum is scaled for diameter from the reference to the new vehicle by

$$f_n = \frac{D_r}{D_n} f_r \tag{5.66}$$

where D_r and D_n are the diameters for the reference and new vehicle, respectively.

For example, assume vibration data are measured or computed at a location of interest during the liftoff of a reference space vehicle, as follows:

a. the autospectrum of the vibration response of the structure is $G_r(f) = 0.04\ g^2/Hz$ at a frequency of $f_r = 100$ Hz,

b. the sound pressure level on the exterior of the structure in the region of the vibration response is $G_{pr}(f) = 100\ Pa^2/Hz$ at a frequency of $f_r = 100$ Hz,

c. the average surface weight density of the structure in the region of the vibration response is $w_r = 16\ kg/m^2$, and

d. the vehicle structure has a cylindrical shape with a diameter of $D_r = 10$ m.

Further assume these data are used to predict the vibration response of a new space vehicle at a similar structural location during liftoff, where the following predictions or computations apply:

a. the sound pressure level on the exterior of the structure in the region of the vibration response is $G_{pn}(f) = 200\ Pa^2/Hz$ at a frequency of $f_n = 125$ Hz,

b. the average surface weight density of the structure in the region of the vibration response is $w_n = 20\ kg/m^2$, and

c. the vehicle structure has a cylindrical shape with a diameter of $D_n = 8$ m.

From Equation (5.64), the difference in the exterior sound pressures scales the autospectrum of the vibration response measured on the reference vehicle to $G_n(f)_1 = (200/100)(0.040) = 0.080\ g^2/Hz$. From Equation (5.65), the difference in surface weight densities further scales the autospectrum of the vibration response measured on the reference vehicle to $G_n(f) = (16/20)^2(0.080) = 0.051\ g^2/Hz$. Finally, from Equation (5.66), the difference in diameters scales the frequency of the autospectrum of the vibration response measured on the reference vehicle at $f_r = 100$ Hz to $f_n = (10/8)(100) = 125$ Hz. Hence, the predicted vibration response of the new vehicle at the selected location during liftoff is $G_n(f) = 0.051\ g^2/Hz$ at $f_n = 125$ Hz.

The advantage of using the extrapolation approach to predict structural responses to pressure fields, as detailed in Equations. (5.64) through (5.66), is that the technique is easy to apply at all frequencies, including frequencies above about 100 Hz where classical normal mode analysis and FEM procedures are not effective, i.e., it does not require a detailed description of the excitation or the structure. The primary disadvantages of the procedure are as follows:

a. The procedure produces acceptably accurate results only if the vibration predictions are made at locations where the structural designs of the new vehicle and the reference vehicle are similar, e.g., the vibration response normal to the surface of a cylindrical structure.

b. The procedure produces acceptably accurate results only if the excitation pressure fields for the new vehicle and the reference vehicle represent the same flight event, e.g., both represent the acoustic noise excitation during liftoff, or the boundary layer pressure fluctuations during q_{max} flight.

It should be mentioned that general extrapolation curves have been developed by a number of investigators over the years [5.56 - 5.58] by collapsing large amounts of space vehicle vibration data from many different references vehicles into a single normalized curve using the scaling rules in Equations (5.64) through (5.66). One of the earliest of these general extrapolation curves developed for cylindrical vehicles exposed to acoustic noise is shown in Figure 5.5, which is taken from [5.58] with appropriate conversions to metric units. Note that the predicted values in Figure 5.5 are for the acceleration response in dB (ref: 1 g rms) in the radial direction (normal to the structural surface) with a frequency bandwidth equal to the bandwidth used to describe the acoustic excitation (often 1/3 octave bands). Further note that a 6 dB range of predicted values is shown to emphasize the crude nature of the predictions. Various other general extrapolation curves developed for aerospace vehicles are detailed in [5.56, 5.57]. General extrapolation curves are easy to use, but in most cases, they do not produce the accuracy of extrapolations from a specific, properly selected, reference vehicle.

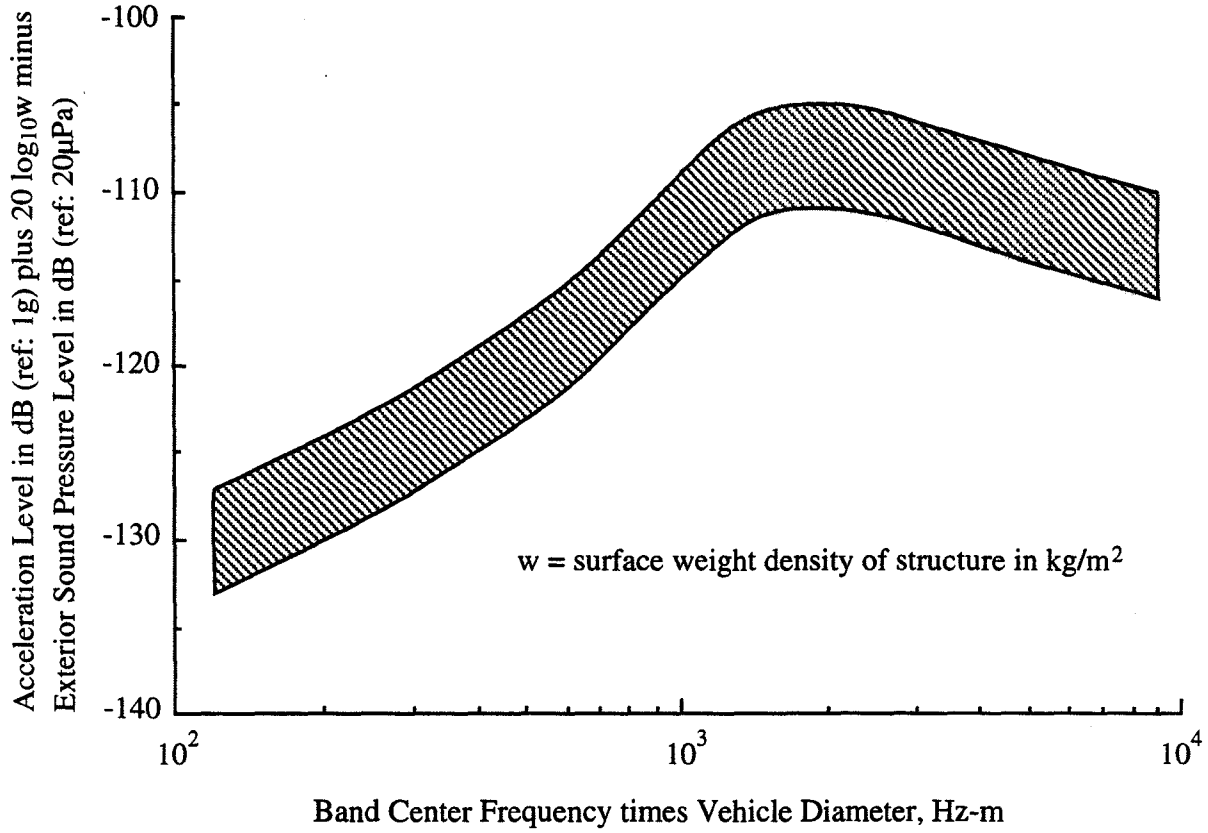

FIGURE 5.5. Radial Vibration Response of Cylindrical Vehicles to Liftoff Acoustic Noise.

To illustrate the use of Figure 5.5, assume the same data for a new vehicle detailed in the previous illustration. For a prediction at f_n = 125 Hz on a vehicle with a diameter of D_n = 8 m, the desired value along the abscissa in Figure 5.5 is (125)(8) = 1,000 Hz-m. The ordinate value in Figure 5.5 ranges between -109 and -115 dB. Assuming a sound pressure level of 135 dB in the 1/3 octave band centered at 125 Hz, the acceleration level = [135 - 20 $\log_{10}$(20) - (109 to 115)] = (0 to -6) dB, so the vibration environment in the 1/3 octave band centered at 125 Hz is 0.5 to 1.0 g rms.

5.2.5 Direct Measurements. The direct measurement of high frequency vibration responses at selected locations on a space vehicle is commonly accomplished during at least the first flight of the vehicle and/or a laboratory acoustic test of the fully assembled vehicle prior to the first flight (see Section 10.5).

5.2.5.1 Vibration Measurements During Flight. Unlike the external pressure measurements discussed in Sections 4.4 and 4.5, vibration transducers are relatively easy to install on a flight vehicle without violating the vehicle structure. For expendable vehicles, the primary restriction on the acquisition of directly measured flight vibration data is the availability of the RF channels needed to telemeter the data to a ground station. Flight vibration measurements are useful to verify and update pre-flight vibration predictions, but obviously come too late for the formulation of the original design and test criteria for the vehicle.

5.2.5.2 Vibration Measurements During Laboratory Acoustic Tests. Many space vehicles are subjected to a laboratory acoustic test prior to the first flight (see Section 10.5), either on the fully assembled vehicle or the vehicle structure with mass-simulating mockup components. Direct vibration measurements during a laboratory acoustic test will reflect the mass-loading effects of the components on the vehicle structure (see Section 6.5.1), although stiffness and damping differences between mass-simulating mockup components and the flight components can affect the accuracy of the measurements. In addition, the accuracy of the measurements will be limited due to errors in the spectrum and spatial correlation characteristics of the acoustic test levels, as compared to the actual acoustic levels during lift-off (see Section 4.4) and/or the fluctuating pressure levels produced by the aerodynamic flow over the exterior surface of the vehicle structure during flight (see Section 4.5). As for direct flight measurements, vibration measurements during laboratory acoustic tests can be useful to verify and update pre-flight vibration predictions, but generally come too late for the formulation of the original design and test criteria for the vehicle.

5.2.6 Assessments. The merits of the various high frequency vibration prediction procedures are summarized in Table 5.3. Extrapolation procedures and/or statistical energy analysis (SEA) procedures offer the best approach for preliminary design purposes, but the other prediction techniques will usually produce more accurate results, at least at frequencies below the 50th normal mode frequency of the vehicle structure.

TABLE 5.3. Summary of Merits of Various High Frequency Vibration Prediction Procedures.

Merit	Classical Procedures	SEA Procedures	FEM Procedures	Extrap. Procedures	Flight Measure.	Acoustic Test Measure.
Relatively easy to accomplish	No	No	No	Yes	No	Yes
Applicable at frequencies up to 2 kHz	No	Yes	Sometimes	Yes	Yes	Yes
Applicable during preliminary design	No	Yes	No	Yes	No	No
Applicable before first vehicle launch	Yes	Yes	Yes	Yes	No	Yes
Applicable to radically new vehicle designs	Yes	Yes	Yes	No	Yes	Yes

5.3 High Frequency Transient Responses. Referring to Section 3.15, the high frequency transient response of space vehicle structures (i.e., the transient response at frequencies above 100 Hz) is due primarily to the activation of pyrotechnic (explosive) devices that produce structural responses at frequencies up to 1 MHz. As discussed in Section 4.8, the prediction of pyrotechnic source loads is a complex problem. Furthermore, because of the very high frequency character of pyrotechnic loads, classical normal mode analysis and finite element method (FEM) models are not effective for predicting structural responses to pyrotechnic loads. Hence, the prediction of structural responses produced by pyrotechnic devices (commonly referred to as pyroshocks) is usually accomplished using (a) analytical (hydrocode) models, (b) empirical models, (c) statistical energy analysis (SEA) procedures, (d) extrapolation techniques, and/or (e) direct measurements. In all cases, predictions are usually made in terms of a shock response spectrum (SRS), as defined in Section 2.2.10. It should be noted that there is an NASA Standard for Pyroshock Testing [5.59] that includes additional discussions and references that support the material in this section.

5.3.1 Analytical Models. Various analytical models have been developed over the years that are designed to predict, at least crudely, the response of space vehicle structures to the loads produced by certain types of transient excitations. The most recent of these analytical modeling procedures involves Hydrocodes, which model in the time domain the details of the explosive or propellent ignition and burning process, the nonlinear structural deformation and separation using Lagrangian and/or Eulerian meshes, and the generation and propagation of structural waves. Unfortunately, the implementation of Hydrocode analysis is generally expensive. Also, the accuracy of such predictions is often poor. See [5.60 - 5.62] for details on the application of Hydrocode analysis to pyroshock predictions.

5.3.2 Empirical Models. Empirical models involve the use of shock response spectra determined from prior data for various pyrotechnic sources, and attenuation versus distance data. From [5.63], the prediction procedure is as follows:

a. Identify each pyrotechnic source and its relationship to the location of each component.

b. Establish the shock response spectrum for each pyrotechnic source.

c. Calculate the distance attenuation for each pyrotechnic source and component.

d. Calculate the excess attenuation of each joint in the path between each pyrotechnic source and component.

e. Using the data from Steps b. through d., compute the attenuated shock response spectrum for each pyrotechnic source at the location of each component.

f. For all component locations in a defined structural zone, determine the maximum expected flight environment by the procedures detailed in Section 6.

g. Apply the appropriate margin from Section 8.3.2 to the maximum expected flight environment to arrive at the test shock response spectrum.

Shock response spectra for various point sources, as recommended in [5.63], are summarized in Figure 5.6. These data represent measurements at distances of 0.10 to 0.13 m (4 to 5 in.) from the source. Also from [5.63], summary data for the attenuation of shock response spectra values with distance from point sources are presented in Figure 5.7. Additional distance attenuation data are given in Section 5.3.4. The estimated excess attenuation of shock response spectra due to joints is recommended in [5.63] to be (a) 40% per joint up to a maximum of three joints for the peak SRS value and (b) no attenuation for the up-ramp portion of the SRS.

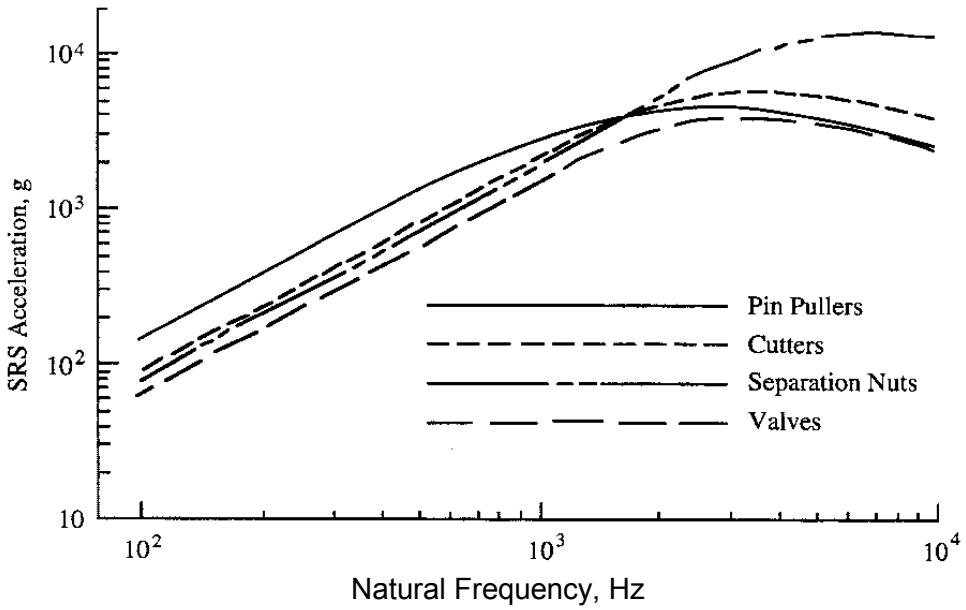

FIGURE 5.6. Shock Response Spectra for Various Point Source Pyrotechnic Devices.

The primary advantage of the empirical model approach to the prediction of high frequency transient responses is that the technique is relatively easy to apply without the need for a detailed description of the structural elements involved, assuming appropriate source data are available. The primary disadvantages of the technique are as follows:

a. The procedure requires near- or mid-field shock response spectra for the various potential pyrotechnic sources. Reliable source data have been published only for certain point sources, as summarized in Figure 5.6.

b. The procedure provides predictions with very limited accuracy, i.e., the predictions may be in error by an order of magnitude at some frequencies. Any predictions made by empirical procedures should be updated by direct measurements when such measurements become available (see Section 5.3.5).

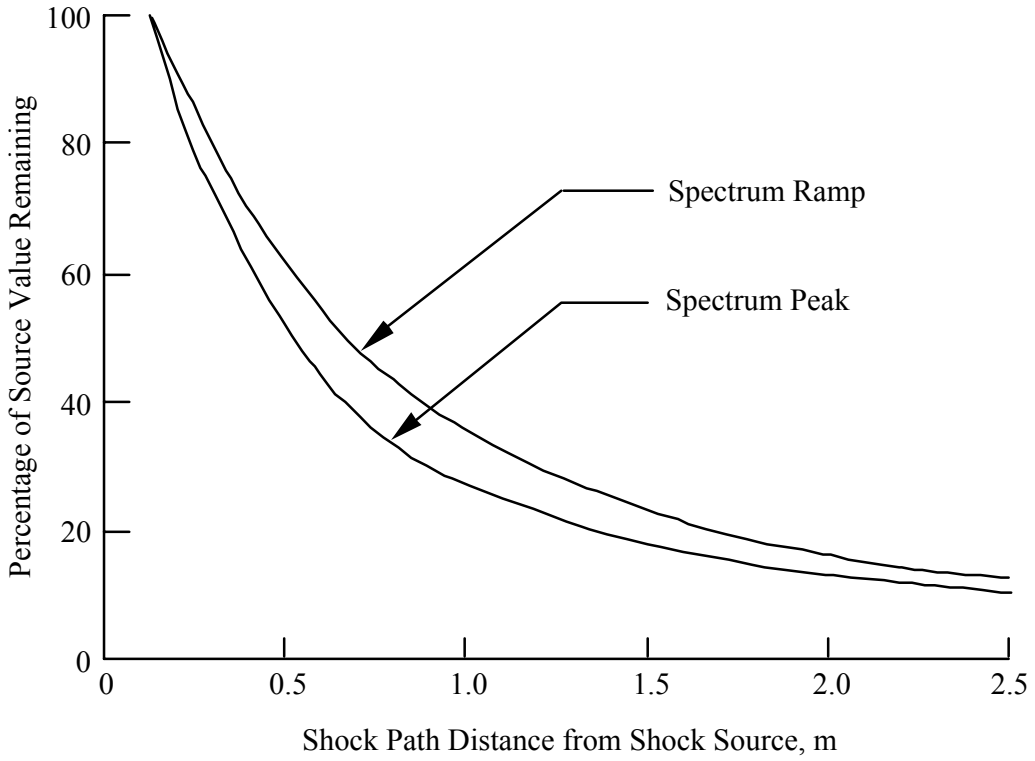

FIGURE 5.7. Shock Response Spectrum Versus Distance from Pyroshock Source.

5.3.3 Statistical Energy Analysis Procedures

5.3.3.1 Transient SEA Analysis. Although statistical energy analysis (SEA) methods are usually applied to the prediction of steady-state vibration responses (see Section 5.2.2), similar methods can also be used to predict transient responses [5.64 - 5.72]. In transient SEA, the general steady-state power balance equation

$$\Pi_{in}(t) = \Pi_{dissipate}(t) + \Pi_{out}(t) \qquad (5.67)$$

is replaced by the corresponding transient equation

$$\Pi_{in}(t) = \Pi_{dissipate}(t) + \Pi_{out}(t) + \frac{dE(t)}{dt} \tag{5.68}$$

where power and subsystem energy are now assumed to be time dependent functions, and E(t) represents the dynamic energy of the modes. Under steady-state conditions, dE(t)/dt = 0.

The steady-state SEA matrix equation, as given in Equation (4.37) in Section 4.6.2, is now replaced by the corresponding transient SEA matrix equation

$$\begin{bmatrix} \eta_1 + \sum_{i\neq 1}^{k} \eta_{1i} & -\eta_{21} & \cdots & -\eta_{k1} \\ -\eta_{12} & \eta_2 + \sum_{i\neq 2}^{k} \eta_{2i} & \cdots & -\eta_{k2} \\ \cdots & \cdots & \cdots & \cdots \\ -\eta_{1k} & -\eta_{2k} & \cdots & \eta_k + \sum_{i\neq k}^{k} \eta_{ki} \end{bmatrix} \begin{bmatrix} E_1(t) \\ E_2(t) \\ \cdots \\ E_k(t) \end{bmatrix} (2\pi f) + \begin{bmatrix} \frac{dE_1(t)}{dt} \\ \frac{dE_2(t)}{dt} \\ \cdots \\ \frac{dE_k(t)}{dt} \end{bmatrix} = \begin{bmatrix} \Pi_1(t) \\ \Pi_2(t) \\ \cdots \\ \Pi_k(t) \end{bmatrix} \tag{5.69}$$

where the symbols are defined in Equation (4.37). It is assumed in Equation (5.69) that the coefficients, which are functions of the damping and coupling loss factors, retain their steady-state values (see Sections 4.6.2 and 5.2.2).

SEA, whether steady-state or transient, is a linear analysis. Consequently, when the input power involves a nonlinear process, which is the usual case for local responses to pyrotechnic excitations, other methods have to be used to estimate the input power and structural response close to the power source. It follows that transient SEA is most useful for the estimation of high frequency structural responses some distance from the location of the pyrotechnic excitation where the structural response is linear. There is a second reason for restricting the application of transient SEA to regions away from the pyrotechnic source, namely, SEA assumes that the response is at least quasi-stationary. This means, for example, that the decay time of the response should be longer than the period of the oscillations at the frequency of interest. Such conditions may not exist near the pyrotechnic excitation (i.e., in the near field as defined in Section 3.15), but do exist at more distant locations where the response is controlled more by the reverberant conditions in the structure than by the time history of the initial compressive wave produced by the excitation, (i.e., in the far field as defined in Section 3.15).

The solution of the transient SEA equations is more complicated than for steady-state equations because of the presence of the time-derivative terms. However, TRANSTAR (Transient Analysis, Storage and Retrieval) software [5.73 - 5.77] has been developed to perform such analyses. Upper bounds on the response time history envelopes and shock response spectra are included in TRANSTAR.

The primary advantage of the transient SEA analysis approach to the prediction of high frequency transient responses is that the technique, if applied with skill, will provide reasonably accurate results without the need for a detailed description of the structural elements involved. The primary disadvantages of the technique are as follows:

a. The procedure applies only to the prediction of far-field transient responses (see Section 3.15).

b. The procedure requires estimates for various structural and coupling loss factors, which often can be only crudely approximated.

c. The procedure provides predictions only for space-averaged transient responses within specified frequency bandwidths, usually 1/3 octave bands.

d. The procedure is not applicable at the lower frequencies where there are less than two or three resonant modes in the specified bandwidths, usually 1/3 octave bands.

5.3.3.2 Virtual Mode Synthesis and Simulation. Another method for high frequency transient response analysis is Virtual Mode Synthesis and Simulation (VMSS) [5.68 - 5.71]. Although some of the principles of SEA are used in the formulation, VMSS is not a direct SEA transient response method of the type described by Equation (5.68).

The VMSS process begins with an estimate of the steady-state frequency response magnitude envelope, i.e., the peak sinusoidal response at a selected location due to a sinusoidal force at another selected location, mapped over the range of selected frequencies. The source of this frequency response can be the result of a steady-state SEA solution per Equation (5.69), a detailed finite element solution per Equation (5.63), or a measurement made directly from a test article. At high frequencies, it is assumed that the frequency response envelope can be represented as the peak response from a collection of localized vibration modes with frequencies spaced according to the estimated modal density of the local structure. The governing equations of this virtual mode dynamical system are in the classical normal mode form given in Equation (5.37). A synthesis operation, described in the next paragraph, is performed to determine the virtual mode coefficients in the equations. To simulate the time response, the dynamical system is numerically convolved with a measurement or simulated transient excitation force. Since the governing equations are in this normal mode form, physically measured or modeled low frequency modes may be included to simulate the entire broadband of response.

The normal mode equations used by VMSS are of the form

$$[I]\left\{\ddot{\xi}\right\} + 2\zeta\omega\left\{\dot{\xi}\right\} + \omega^2\left\{\xi\right\} = [\phi]^T\{F\} \tag{5.70}$$

where

- **[ϕ]** = the virtual mode shape matrix in which each column represents the mode shape for each frequency (each row represents a physical DOF)
- **{F}** = the applied loads
- **[I]** = the identity matrix
- **{ξ}** = the modal coordinates that represent the virtual modal response

The frequency response function (FRF) for the ith response DOF and the kth loaded DOF may be approximated by

$$|H(\Omega)_{ik}| = \sum_{m=1}^{N} \frac{\phi_{im}\,\phi_{km}}{\left[(\omega_m^2 - \Omega^2)^2 + (2\zeta_m\omega_m\Omega)^2\right]^{0.5}} \tag{5.71}$$

where N is the number of vibration modes in the substructure selected for response (referred to as the mode count). For convenience, this FRF magnitude can be rewritten as the product of two vectors, namely,

$$|H(\Omega)_{ik}| = \{\Phi\}^T \{\Lambda\} \tag{5.72}$$

where

$$\{\Phi\} = \begin{Bmatrix} (\phi_{i1} \bullet \phi_{k1}) \\ (\phi_{i2} \bullet \phi_{k2}) \\ \bullet \\ (\phi_{iN} \bullet \phi_{kN}) \end{Bmatrix} ; \Lambda = \begin{Bmatrix} \left[(\omega_1^2 - \Omega^2)^2 + (2\xi_1 \omega_1 \Omega)^2 \right]^{-1/2} \\ \left[(\omega_2^2 - \Omega^2)^2 + (2\xi_2 \omega_2 \Omega)^2 \right]^{-1/2} \\ \bullet \\ \left[(\omega_N^2 - \Omega^2)^2 + (2\xi_N \omega_N \Omega)^2 \right]^{-1/2} \end{Bmatrix} \tag{5.73}$$

The synthesis operation for the virtual modes is performed by packing the FRF magnitudes available from steady-state methods into a column vector **{H}**, where each element of the vector represents the FRF magnitude at the assumed virtual mode frequencies. Equating those column vector elements to Equation (5.72) results in the matrix form

$$\{|H|\}_{ik} = [\Lambda]^T \{\Phi\}_{ik} \tag{5.74}$$

where

$$[\Lambda] = \left[\{\Lambda(\Omega_1\} \vdots \{\Lambda(\Omega_2\} \vdots \cdots \vdots \{\Lambda(\Omega_J\} \right] \tag{5.75}$$

The virtual mode coefficients are then obtained from the relationship

$$\{\Phi\}_{ik} = \left([\Lambda]^T \right)^{-1} \{|H|\}_{ik} \tag{5.76}$$

With these coefficients synthesized, the governing equations given by Equations (5.70) and (5.73) can be solved for the time response. The computer code MANTA (Method of Analysis by Thermodynamic Analogy) procedure [5.78 - 5.81] has been written to perform these VMSS operations.

The VMSS method has several advantages over transient SEA, namely,

a. there is no quasi-stationary requirement for the excitation,
b. if the structure is reasonably linear, near-field response may be estimated,
c. a time domain solution is obtained (not just peak values), and
d. a shock response spectrum may be obtained (not just envelope estimates).

5.3.4 Extrapolation Procedures. A vast amount of pyroshock data have been acquired and analyzed over the years for many space vehicle programs, both in the laboratory and in flight (see Section 5.3.2). These data have been acquired for many different space vehicle designs and different pyrotechnic devices. Hence, at least crude estimates for the pyroshock levels to be expected on a new space vehicle design usually can be determined by extrapolations from measurements on a previous space vehicle of similar design, commonly referred to as the reference vehicle. Of course, the closer the design details of the new and reference vehicle, the more accurate the extrapolations. Also, the most accurate extrapolations are provided when the pyroshocks on the new and reference vehicle are caused by the same type of pyrotechnic device.

Extrapolation procedures for pyroshock environments generally involve two primary scaling operations, namely, (a) scaling for the total energy released by the pyrotechnic device, and (b) scaling for the distance between the locations of the pyrotechnic device source and the response point of concern. Sometimes scaling for the surface weight density of the structure is also employed (see Section 5.2.4), but such extrapolations usually are not effective for the prediction of pyroshocks because the intense compressive waves generated by pyrotechnic devices are not strongly influenced by surface weight density.

5.3.4.1 Source Energy Scaling. Letting E_r and E_n denote the total explosive energy released by the pyrotechnic device on the reference and new spacecraft, respectively, the shock response spectrum at all frequencies is scaled from the reference to the new vehicle by

$$SRS_n(D_1) = SRS_r(D_1)\sqrt{\frac{E_n}{E_r}} \tag{5.77}$$

where SRS_r and SRS_n are the shock response spectra for the reference and new spacecraft, respectively, at the same distance D_1 from the pyrotechnic source. Caution should be exercised in the utilization of Equation (5.77) since, in many cases, an excess of source energy beyond that required to cause structural separation will not increase the shock transmission, but instead will generate an increased shock or blast wave that will be transmitted into the atmosphere or vacuum adjacent to the structure. This excess energy may not be as effective in generating structural response. Thus, when $E_n > E_r$, the application of Equation (5.77) may cause an over-prediction of the pyroshock environment. Similarly, an under-prediction may result when $E_n < E_r$.

5.3.4.2 Source to Response Location Distance Scaling. A number of empirically derived scaling relationships to correct the magnitude of pyroshock environments for distance from a pyrotechnic source to a response location of interest have been proposed over the years [5.82 - 5.84]. The distance attenuation curves shown in Figure 5.7 can be used to scale shock response spectra values with distance for point sources. Another set of scaling curves for typical pyroshocks propagating through various types of structure, as developed in [5.82], is summarized in Figure 5.8. Note the results in Figure 5.8 apply to the peak value of the pyroshock response, as opposed to the peak value of a shock response spectrum.

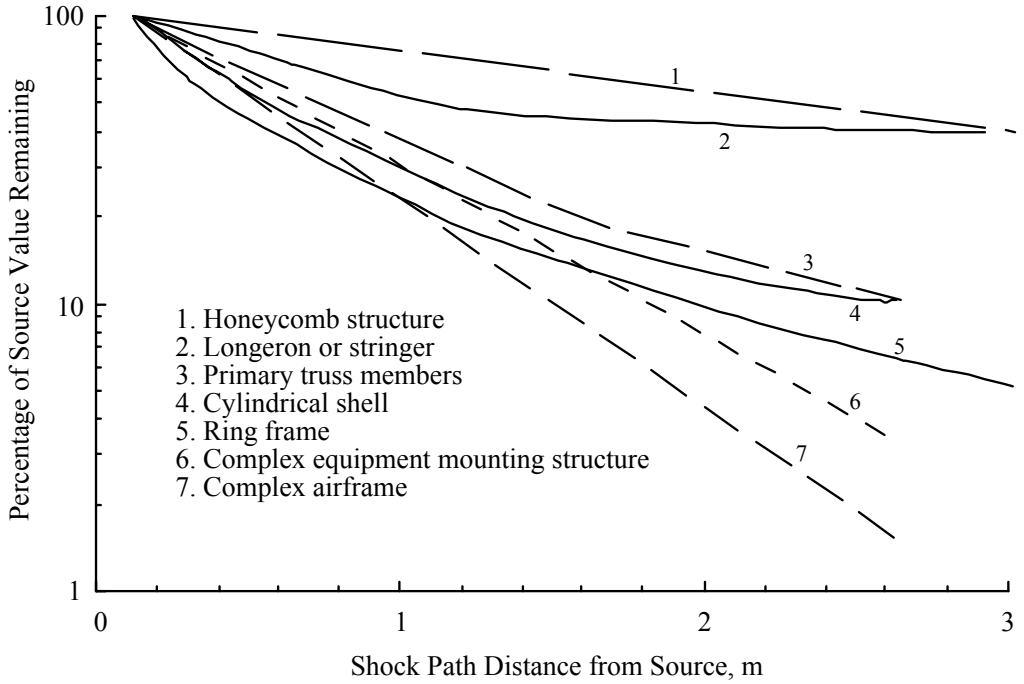

FIGURE 5.8. Peak Pyroshock Response Versus Distance from Pyrotechnic Source.

Another scaling relationship developed in [5.84] for the shock response spectrum produced by point sources on complex structures is given by

$$SRS(D_2) = SRS(D_1) \exp\left\{\left[-8x10^{-4} f_n^{(2.4 f_n^{-0.105})} \left[D_2 - D_1\right]\right]\right\} \quad (5.78)$$

where D_1 and D_2 are the distances in meters from the pyrotechnic source to the reference and new locations, respectively, on the spacecraft, and $SRS(D_1)$ and $SRS(D_2)$ are the shock response spectra for the responses at the reference and new locations, respectively. Since Equation (5.78) predicts an SRS, the results are a function of the SRS natural frequency. Plots of Equation (5.78) for various values of $\Delta D = D_2 - D_1$ are shown in Figure 5.9.

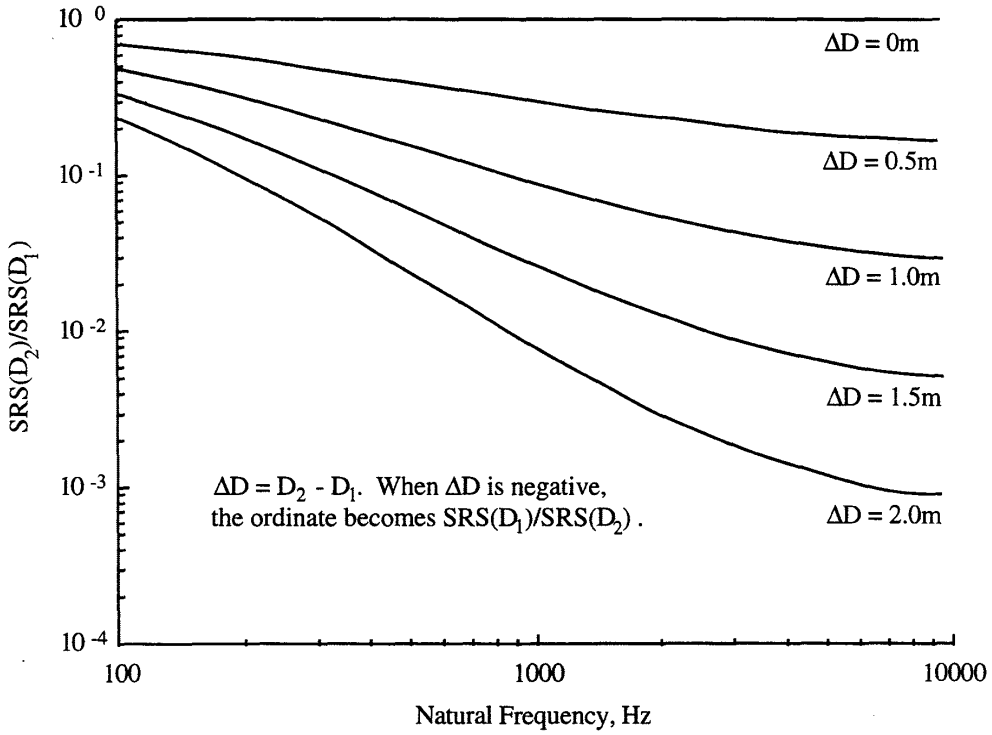

FIGURE 5.9. Correction of Shock Response Spectrum for Distance from Point Pyrotechnic Source.

It is important to note that Equation (5.78) was derived from pyroshock data produced by a point source on complex structure at sea level, and may not be representative of other sources and structures in space. Other source scaling rules may be developed from data for sources and structures more like those associated with a specific spacecraft, which may be substituted for the results in Figures 5.8 and 5.9.

As a final point concerning the attenuation of pyroshocks with distance, there is usually a substantial reduction in pyroshock magnitudes due to transmission across structural joints. Specifically, [5.82] suggests that the attenuation due to structural joints ranges from 20 to 75%, depending on the type of joint and the manner in which it changes the shock transmission path. Other data for joint attenuation that might be available from prior experience should be used, as appropriate.

To illustrate the use of Equations. (5.77) and (5.78), assume pyroshock data are measured during a pyrotechnic event on a reference space vehicle, as follows:

a. the SRS of the pyroshock is $SRS_r(f_n) = 10{,}000$ g at a natural frequency of $f_n = 1$ kHz,
b. the pyrotechnic device producing the pyroshock is activated by 0.1 gram of explosive material, and
c. the pyroshock is measured at a location that is $D_1 = 0.3$ m from the pyrotechnic device.

Further assume these data are used to predict the high frequency transient response of a new space vehicle at a structural location where equipment is mounted during the activation of a similar pyrotechnic device, and the following data apply:

a. the pyrotechnic device causing the pyroshock is activated by 0.2 gram of explosive material, and
b. the response location of interest is D_2 = 0.8 m from the pyrotechnic device.

From Equation (5.77), assuming the energy released by the pyrotechnic devices is proportional to the weight of the explosive material, the ratio of the energies scales the SRS of the high frequency transient response measured on the reference vehicle to $SRS_n(f_n)_1 = 10{,}000\ (0.2/0.1)^{1/2} \approx 14{,}000$ g. From Equation (5.78), the difference in distances from the pyrotechnic device further scales the SRS of the high frequency transient response measured on the reference vehicle to

$$SRS_n(f_n) \approx 14{,}000 \exp\left\{\left[\left(-8 \times 10^{-4}\right) 1000^{\left(2.4\,(1000)^{-0.105}\right)}\right][0.8 - 0.3]\right\}$$
$$\approx 4{,}100\ \text{g} \quad \text{at} \quad f_n = 1\ \text{kHz}$$

The advantage of using an extrapolation curve or formula to predict high frequency transient responses to pyrotechnic devices, as summarized in Figures 5.8 and 5.9, is that such techniques are easy to apply. The primary disadvantages of extrapolation procedures are as follows:

a. The procedure produces acceptably accurate results only if the pyroshock predictions are made at locations where the structural designs of the new and the reference space vehicles are similar, e.g., equipment mounting frame structures.

b. The procedure produces acceptably accurate results only if the pyrotechnic loads for the new and the reference space vehicles are produced by the same type of device, e.g., explosive bolts.

5.3.5 Direct Measurements. In many cases, direct measurements can be made of the high frequency transient responses at critical locations on the spacecraft structure induced by pyrotechnic devices, either in flight or in the laboratory. In either case, the measurements should be acquired and analyzed in accordance with the recommended practices detailed in [5.85]. As mentioned earlier, pyrotechnic devices are usually designed or selected to generate more than enough source energy to cause structural separation. The excess energy normally causes a shock or blast wave in the atmosphere or vacuum adjacent to the structure, with the wave magnitude increasing with excess energy and static pressure. However, for small amounts of excess energy, the separation process usually controls the pyroshock environment.

5.3.5.1 Measurements on the Vehicle in Flight. For some spacecraft, more than one assembly is manufactured because the same spacecraft design will be used for more than one flight. In this case, measurements may be made on the first flight of that design to establish the response of the structure at critical locations due to all flight pyrotechnic events. The advantage of this approach is that it provides the most accurate pyroshock predictions for later flights of that design. The primary disadvantages are as follows:

a. The procedure applies only to updating predictions after the first flight and, hence, cannot be used to establish initial test requirements for the spacecraft or its components.

b. Flight pyroshock measurements are expensive to acquire.

5.3.5.2 Measurements on the Vehicle in the Laboratory Prior to Flight. Certain types of pyrotechnic devices can be activated and replaced without doing permanent damage to the space vehicle structure, e.g., ordnance activated valves. In this case, measurements might be made on the vehicle in the laboratory prior to flight to establish the response of the structure at critical locations due to the activation of these particular devices. The advantage of this approach is that it provides reasonable accurate predictions for pyroshock levels on that specific vehicle during flight. The primary disadvantages are as follows:

a. The procedures allows the determination of the pyroshock levels due only to a limited number of pyrotechnic devices.

b. It may be expensive to replace the activated pyrotechnic devices and recondition the vehicle for flight.

5.3.5.3 Measurements on a Prototype Vehicle in the Laboratory. Some space vehicle programs involve the manufacture of a prototype vehicle that is used for various laboratory tests, including shock and vibration tests, prior to the launch of a flight assembly. Because the activation of pyrotechnic devices sometimes alter the vehicle structure, pyroshock measurements on prototypes are usually made after all other tests are complete. The advantages of a prototype test are as follows:

a. It provides reasonable accurate predictions for pyroshock levels prior to the flights of all space vehicles of that design.

b. The predictions are achieved without jeopardizing the structural integrity of the flight article.

c. No reconditioning of flight hardware is required.

The primary disadvantage is that the program must provide for the manufacture of a prototype vehicle that will be available for testing.

5.3.5.4 Measurements on a Dynamically Similar Structure in the Laboratory. If a space vehicle program does not involve the manufacture of a prototype, it may still allow the construction of a dynamically similar model of at least those subassemblies that incorporate pyrotechnic devices, or such a dynamically similar model might be available from a previous space vehicle program, e.g., [5.86]. The advantages of a test using a dynamically similar model are as follows:

a. It might provide acceptably accurate predictions for pyroshock levels, depending on how closely the model dynamically represents the space vehicle of interest.

b. The predictions are achieved without jeopardizing the structural integrity of the flight article.

c. No reconditioning of flight hardware is required.

The primary disadvantage is that the program must provide for the manufacture of a dynamically similar model, or an appropriate model must be available from a previous program.

5.3.6 Assessments. The merits of the various high frequency transient (pyroshock) prediction procedures are summarized in Table 5.4. Empirical models, extrapolation procedures, and/or statistical energy analysis procedures are believed to offer the best approaches for preliminary design purposes. For the final design, direct measurement techniques, perhaps supported by statistical energy analysis procedures, will usually produce more accurate results, although analytical (hydrocode) models might also be used if budgets permit.

TABLE 5.4. Summary of Merits of Various High Frequency Transient Response Prediction Procedures.

Merit	Analytical models	Empirical models	Transient SEA and VMSS analyses	Extrapo-lation procedures	Measure-ments in flight on flight vehicle	Measure-ments in lab. on prototype or flight vehicle	Measure-ments in lab. on similar structure
Relatively easy to accomplish	No	Yes	No	Yes	No	No	No
Applicable in preliminary design	No	Yes	Yes	Yes	No	No	No
Applicable before first launch	Yes	Yes	Yes	Yes	No	Yes	Yes
Applicable to radical new vehicle design	Yes	No	Yes	No	Yes	Yes	No

5.4 References

5.1 Anon., "Loads Analysis of Spacecraft and Payloads," NASA Technical Standard *NASA-STD-5002*, June 1996.

5.2 Fleming, E. R., " New and Projected Aeronautical and Space Systems, Design Concepts, and Loads", *ASME Flight-Vehicle Materials, Structures, and Dynamics - Assessment and Future Directions* (Noor, A. K. and Venneri, S. L., Ed.), Vol. 1, 1996.

5.3 Hurty, W. C. "Dynamic Analysis of Structural Systems Using Component Modes," *AIAA J*., Vol. 3, No. 4, pp 1152-1154, Apr .1965.

5.4 Craig, R. R., and Bampton, C. C., "Coupling of Substructures for Dynamic Analyses", *AIAA J*., Vol. 6, No. 7, pp 1313-1319, July 1968.

5.5 Benfield, W. A., and Hruda, R. F. "Vibration Analysis of Structures by Component Mode Substitution", *AIAA J*., Vol. 9, No. 7, pp 1255-1261, July 1971.

5.6 MacNeal, R. H., "A Hybrid Method of Component Mode Synthesis", *Computers and Structures*, Vol. 1, pp 581-601, 1971.

5.7 Rubin, S., "Improved Component Mode Representation for Structural Dynamics Analysis", *AIAA J*., Vol. 13, No. 8, pp 995-1006, Aug 1975.

5.8 Coppolino, R. N., "Employment of Residual Mode Effects in Vehicle/Payload Dynamic Loads Analysis", Government/Industry Workshop on Payload Loads Technology, *NASA GP-2075*, 1978.

5.9 Martinez, D. R., Carne, T. G., and Miller, A. K., "Combined Experimental/Analytical Modeling Using Component Mode Synthesis", *Proc. AIAA 25th SDM Conf*., pp 140-152, May 1984.

5.10 Abramson, H. N., Ed., "The Dynamic Behavior of Liquids in Moving Containers", *NASA SP-106*, 1966.

5.11 Coppolino, R. N., "A Numerically Efficient Finite Element Hydroelastic Analysis", *NASA CR-2662*, Apr. 1975.

5.12 Kim, M. C.; Williamson, D. R. "A Fluid-Structure Interaction Formulation for Fluids With Free Surface," *6th AIAA/NASA/ISSMO Symposium on Multidisciplinary Analysis and Optimization*, Sep. 4-6 1996.

5.13 Guyan, R. J., "Reduction of Mass and Stiffness Matrices," *AIAA J*., Vol. 3, No. 2, p. 380, 1965.

5.14 Bathe, K. J., *Finite Element Procedures in Engineering Analysis*, Prentice-Hall, Englewood Cliffs, NJ, 1982.

5.15 Gockel, M. A., Ed., "Handbook for Dynamic Analysis", *MSC/NASTRAN Version 63*, MacNeal Schwendler Corp., June 1983.

5.16 Trubert, M. R., and Peretti, L., "A Cost-Effective Component Modes Analysis for Shuttle Payloads Using a Combination of Frequency Domain and Time Domain Approaches", *AIAA Paper 85-0733*, Apr. 1985.

5.17 Blelloch, P. A., and Flanigan, C. C., "A Time Domain Approach for Spacecraft Reanalysis," *Proc. AIAA 33rd SDM Conf*., Pt 4, pp 2295-2306, Apr. 1992.

5.18 Salama, M. A., Trubert, M. R., Chian, C, and Peretti, L., "Generalized Modal Shock Spectra with Indeterminate Interface," *AIAA J*., Vol. 22, No. 6, pp 824-830, June 1984.

5.19 Wada, B. K., “Modal Test: Measurement and Analysis Requirements", *SAE Paper 751066*, Nov. 1975.

5.20 Ewins, D. J., *Modal Testing: Theory and Practice*, Wiley, NY, 1984.

5.21 Hunt, D. L., and Brillhart, R. D., "Lessons Learned from Modal Testing of Aerospace Structures", *Proc. 13th Aerospace Testing Sem.,* Inst. Envir. Sc., Oct .1991.

5.22 Chen, J. C., "Comparison of Results for the Galileo Modal Test Program”, *Proc., 2nd Intern. Modal Analysis Conf.,* 1984.

5.23 Hunt, R. L., and Brillhart, R. D., "Modal Testing Using Multiple Input Random Excitation", *Proc., 9th Intern. Modal Analysis Conf.*, Apr .1991.

5.24 Hunt, D. L., Vold, H., and Williams, R., "Modal Testing Using Modern Sine Excitation", *Proc., 8th Inter. Modal Analysis Conf.*, Feb. 1990.

5.25 Targoff, W. P. "Orthogonality Check and Correction of Measured Modes," *AIAA J.*, 14(2), Feb. 1976, pp 164-167.

5.26 McGrew, J. "Orthogonalization of Measured Modes and Calculation of Influence Coefficients," *AIAA J.*, 28(9), Sep. 1990, pp 1650-1654.

5.27 Fullekrug, U., “Determination of Effective Masses and Modal Masses from Base-Driven Tests”, *Proc., 14th Inter. Modal Analysis Conf.*, Dearborn, MI, Feb. 1996.

5.28 Tinker, M. L., and Bookout, P. S., "Measurement of Residual Flexibility for Substructures Having Prominent Flexible Interfaces," *NASA TM-110074*, Jan. 1994.

5.29 Admire, J. R., Tinker, M. L., and Ivey, E. W., "Residual Flexibility Test Method for Verification of Constrained Structural Models", *AIAA J*., Vol .32 , No. 1, pp 170-175, Jan. 1994.

5.30 Chapman, J. M. "Incorporating a Full Damping Matrix in the Transient Analysis of Nonlinear Structures," Proceedings of Damping '93, sponsored by Wright Laboratory, Air Force Systems Command, *WL-TR-93-3105*, Vol. 2, June 1993, pp FBB 1-17.

5.31 Dotson, K. W., and Tiwari, S. B., "Formulation and Analysis of Launch Vehicle Maneuvering Loads," *AIAA J. Spacecraft and Rockets*, Vol. 33, No. 6, Nov.-Dec. 1996, pp 815-821.

5.32 Henkel, E. E.; Mar R. "Improved Method for Calculating Booster to Launch Pad Interface Transient Forces," *AIAA J. Spacecraft and Rockets*, Vol. 25, No. 6, Nov.-Dec. 1988.

5.33 Kern, D., Salama, M., and Smith, K., “Combined Loads Methodologies for Vibroacoustic and Transient Environments”, *Proc., 61st Shock and Vibration Symp.,* Vol. II, pp. 21-32, 1990.

5.34 Gordon, D. T. "Combining Transient and Acoustic Loads, A Review of Approaches," *Report TOR-93(3530)-14,* The Aerospace Corp., July 1993.

5.35 Broussinos, P.; Kabe, A. M. "Multi-Mode Response Analysis Procedure," Report *SSD-TR-90-53*, The Aerospace Corp., Jan. 1990.

5.36 Mariem, J. B., and Hamdl, M. A., “A New Boundary Finite Element Method for Fluid-Structure Interaction Problems”, *International J. For Numerical Methods in Engineering,* Vol. 24, pp. 1251-1267, 1987.

5.37 Coyette, J. P., and Wijker, J. J., “The Combined use of MSC/NASTRAN and SYSNOISE for Evaluating the Dynamic Behavior of Solar Panels”, *Proc., MSC/NASTRAN European Users Conf.*, Vienna, Austria, pp. 20-22, 1993.

5.38 Piersol, A. G., “Optimum Resolution Bandwidth for Spectral Analysis of Stationary Random Vibration Data”, *J. Shock and Vibration*, Vol. 1, Issue 1, pp. 33-43, 1993/1994.

5.39 Miskel, J. F. "Fatigue-Based Random Vibration and Acoustic Test Specification," Master's thesis, Dept. of Mech. Eng., MIT, Mar. 1994.

5.40 Wilson, E. L.; Der Kiureghian, A.; Bayo, E. P. "A Replacement for the SRSS Method in Seismic Analysis," *Earthquake Engineering and Structural Dynamics,* Vol. 9, No. 2, pp 187-194, Mar.-Apr. 1981.

5.41 Bendat, J. S., and Piersol, A. G., *Engineering Applications of Correlation and Spectral Analysis*, 3rd ed., Wiley, NY, 2000.

5.42 Wilby, J. F., and Piersol, A. G., "Analytical Prediction of Aerospace Vibration Environments", *ASME Paper 81-DET-29,* 1981.

5.43 Pope, L. D., and Wilby, J. F., "Space Shuttle Payload Bay Acoustics Prediction Study", *NASA CR-159956*, Vol. II (Analytical Model), 1980.

5.44 Manning, J.E., “Statistical Energy Analysis - An Overview of its Development and Engineering Applications”, *Proc. 59th Shock and Vibration Symp.*, 1988.

5.45 Hsu, K. H., and Nefske, D. J., Ed., “Statistical Energy Analysis”, Amer. Soc. Mech. Eng., *Pub. NCA-Vol.3,* 1987.

5.46 VAPEPS was developed by Lockheed Martin Co. and is available from the NASA Jet Propulsion Laboratory, Pasadena, CA. SEAM® is available from Cambridge Collaborative, Inc., Cambridge, MA. AutoSEA is available from Vibro-acoustics Sciences, San Diego, CA.

5.47 Lyon, R. H., and DeJong, R. G., *Theory and Application of Statistical Energy Analysis*, 2nd ed., Butterworth-Heinemann, Newton, MA, 1995.

5.48 Norton, M. P., “Statistical Energy Analysis of Noise and Vibration”, *Fundamentals of Noise and Vibration Analysis for Engineers*, Ch. 6, Cambridge Univ. Press, 1989.

5.49 Fahy, F. J., “Statistical Energy Analysis,” *Noise and Vibration* , (White, R. G., and Walker, J. G., Ed.),Ch. 7, Ellis Horwood, 1982.

5.50 Ver, I. L., “Statistical Energy Analysis”, *Noise and Vibration Control Engineering: Principles and Applications*, (L. L. Beranek and I. L. Ver, Ed.), Sect. 9.8, Wiley, NY, 1992.

5.51 Ungar, E. E., “Statistical Energy Analysis”, Cremer, L., Heckl, M., and Ungar, E. E., *Structure-Borne Sound,* 2nd ed., Sect. V.8, Springer-Verlag, Berlin, 1988.

5.52 Price, W. G., and Keane, A. J., Ed., “Statistical Energy Analysis”, *Phil. Trans. Royal Soc*., London, Vol. 346, No. 1681, 1994.

5.53 Maidanik, G., “Response of Ribbed Panels to Reverberant Acoustic Fields”, *J. Acoust. Soc. Amer.*, Vol. 34, pp 809-826, 1962.

5.54 Hipol, P. J., and Piersol, A. G., "Efficient Implementation of Random Pressure Fields with the Finite Element Method", Paper 871740, *Trans. SAE*, Vol. 96, Sec. 6, Sept. 1988.

5.55 Chung, Y. T., and Foist, B. L., “Prediction of Payload Random Vibration Loads”, *Proc. 13th Intern. Modal Analysis Conf.*, pp 934-9940, Feb. 1995.

5.56 Barnoski, R. L., et al, "Summary of Random Vibration Prediction Procedures", *NASA CR-1302*, Apr. 1969.

5.57 Himelblau, H., Fuller, C. M., and Scharton, T. D., "Assessment of Space Vehicle Aeroacoustic-Vibration Prediction, Design, and Testing", *NASA CR-1596*, July 1970.

5.58 Franken, P. A., "Sound Induced Vibrations of Cylindrical Vehicles", *J. Acoust. Soc. Amer.*, Vol. 34, No. 4, pp 453-454, 1962.

5.59 Anon., “Pyroshock Test Criteria”, NASA Technical Standard *NASA-STD-7003*, May 18, 1999.

5.60 Hancock, S., et al, "Numerical Simulation of Atlas-Centaur Stage-Separation Shaped Charge Firing and Structural Response", *Shock and Vibration Bull.*, No. 56, Pt. 3, pp 45-57, Aug. 1986.

5.61 Goldstein, S., Lu, Y.-M., and Wong, T.E., "Importance of Enhanced Test Data for Computer Modeling of Explosive Activated Devices", *AIAA Paper 95-2852*, July 1995.

5.62 Frey, J. D., Janicot, F., Renard, V., and Movillat, P. A., "Pyrotechnic Separation of the VEB Structure, Shock Propagation", *Proc. Symp. Europeen, Ariane-5 Structures & Technologies,* May 1993.

5.63 Barrett, S., "The Development of Pyro Shock Test Requirements for Viking Lander Capsule Components", *Proc. 21st ATM, Inst. Envir. Sc*., pp 5-10, Apr. 1975.

5.64 Lyon, R. H., and DeJong, R. G., Ch. 14, "Transient SEA", *Theory and Application of Statistical Energy Analysis*, 2nd ed., Butterworth-Heinemann, Newton, MA, 1995.

5.65 Manning, J. E., and Lee, K., "Predicting Mechanical Shock Transmission", *Shock and Vibration Bull.*, No. 37, Pt. 4, pp 65-70, Jan. 1968.

5.66 Powell, R. E., and Quartararo, L. R., "Statistical Energy Analysis of Transient Vibration", *Statistical Energy Analysis* (Hsu, K. H., Nefske, D. J., and Akay, A., Ed.), ASME NCA-Vol. 3, pp 3-8, 1987.

5.67 Pinnington, R. J., and Lednick, D., "Transient Statistical Energy Analysis of an Impulsively Excited Two Oscillator System", *J. Sound Vibration*., Vol. 189, No. 2, pp 249-264, 1996.

5.68 Pinnington, R. J., and Lednick, D., "Transient Energy Flow between Two Coupled Beams", *J. Sound and Vibration*, Vol. 189, No. 2, pp 265-287, 1996.

5.69 Pinnington, R. J., Lednick, D., "A Comparison between Wave Propagation Techniques and Transient SEA for the Prediction of Shock Response in One-Dimensional Systems", *Proc. Inter-Noise 96* (Eds: Hill, F A., and Lawrence, R.), pp 1343-1348, July 1996.

5.70 Lai, M. L., and Soom, A., "Prediction of Transient Vibration Envelopes using Statistical Energy Analysis Techniques", *J. Vibration and Acoustics, Trans. ASME*, Vol. 112, No. 1, pp 127-137, 1990.

5.71 Lai, M. L., and Soom, A., "Statistical Energy Analysis for the Time-Integrated Transient Response of Vibrating Systems" *J. Vibration and Acoustics, Trans. ASME,* Vol. 112, No. 2, pp 206-213, 1990.

5.72 Honda, I., and Irie, Y., "Transient Structure Borne Energy Analysis by Using SEA", *Proc.Inter-Noise 95*, pp 1233-1238, July 1995.

5.73 Lee, Y. A., Crowe, D. R., Henricks, W., and Park, D. M., "Shock Prediction Technology: Technical Manual", *NASA CR-183479,* Apr. 1989.

5.74 Singh, A. K., "Impact Analysis by TRANSTAR Statistical Energy Method", *2nd Intern. Cong. of Air- and Structure-Borne Sound and Vibration,* Mar. 1992.

5.75 Singh, A. K., "Shock Source Characterization Methods for TRANSTAR SEA Program", *Proc. 63rd Shock and Vibration Symp.*, Vol. 1, pp 439-450, Oct. 1992.

5.76 Singh, A. K., "Multiple Impact Analysis by TRANSTAR SEA Program", *Proc. 63rd Shock and Vibration Symp*., Vol. 1, pp 451-463, Oct. 1992.

5.77 Singh, A. K., "Shock Environment Prediction of Isolated Equipment by TRANSTAR SEA Program", *Proc., 39th ATM, Inst. Envir. Sc.*, pp 267-272, 1993.

5.78 Dalton, E. C., “Ballistic Shock Response Analysis by an Extension of Statistical Energy Analysis”, *Proc., 63rd Shock and Vibration Symp.*, Vol. 1, pp 411-424, Oct. 1992.

5.79 Dalton, E. C., “High Frequency Shock Prediction in Multiply-Connected Plate Structures”, *Proc., 64th Shock and Vibration Symp.*, Vol. 2, pp 81-91, Oct. 1993.

5.80 Dalton, E. C., Chambers III, B. S., Katz, B., and White, M. D., “Analysis of Shock in a Pyrotechnically Separated Missile Structure”, *Proc., 66th Shock and Vibration Symp.,* Vol. 2, pp 195-201, Oct.-Nov. 1995.

5.81 Dalton, E. C., Chambers III, B. S., “Analysis and Validation Testing of Impulsive Load Response in Complex, Multi-Compartmented Structures”, *AIAA Paper 95-1243*, Apr. 1995.

5.82 Kacena, W. J., McGrath, M. B., Engelsgjerd, I. K.,and Rader, W. P., “Aerospace Systems Pyrotechnic Shock Data”, *NASA CR-116437*, *-116450*, *-116401*, *-116402, -116403*, *-116406*, and *-116019*, Vol. I-VII, 1970.

5.83 Spann, F. W., Hain, R. F., and Beck, C. J., “IUS Program Shock Analyses”, *Boeing Doc. D290-75303-2*, Vol. I-III, Feb. 3, 1982, June 25, 1982 and Apr. 2, 1993. (Available from DTIC as ADA 318331, 30 and 29.)

5.84 Van Ert, D. L., “Survey of Pyroshock Prediction Methodology”, IES Pyrotechnic Shock Tutorial Program, *31st ATM, Inst. Envir. Sc.*, Apr.-May 1985.

5.85 Himelblau, H., Piersol, A. G., Wise, J. H., and Grundvig, M. R., “Handbook for Dynamic Data Acquisition and Analysis”, *IES-RP-DTE012.1,* Inst. Envir. Sc. Tech., Mt Prospect, IL, Mar. 1994.

5.86 Powers, D. R., “Summary of Testing Techniques”, *Shock and Vibration Bull.*, No. 56, Pt. 3, pp 135-142, Aug. 1986.

6. COMPUTATION OF MAXIMUM EXPECTED ENVIRONMENT

The prediction procedures detailed in Section 5 generally yield the response of a structure at individual points or, at best, over relatively small areas, which do not necessarily correspond to all the points of interest in the formulation of design and/or test criteria. Furthermore, the predictions may be based upon computed, assumed, or measured dynamic loads (see Section 4) that do not reflect the potential flight-to-flight variations that will occur in service use. Hence, it is necessary to add a factor to the predicted vibration levels to arrive at a "maximum expected environment" (MEE) that will account for point-to-point (spatial) and flight-to-flight variations in service, and thus assure the predictions are conservative relative to the potential flight environment. This maximum expected environment is usually described in terms of the spectrum of a motion parameter, commonly acceleration. However, any equipment item mounted on the vehicle structure will modify the vibratory motion of the structure, particularly at the resonance frequencies of the equipment. It follows that the maximum expected environment often must be modified at the frequencies of equipment resonances to arrive at accurate design and/or vibration test criteria for aerospace flight vehicle equipment.

This section details the various procedures used to arrive at a maximum expected environment, as well as the procedures used to modify the maximum expected environment to account for equipment loading effects. Much of this material is also presented or summarized in [6.1, 6.2].

6.1 Spatial Variations - Point Predictions. The procedures commonly used to predict the response of structures to low frequency dynamic loads (see Section 5.1) generally produce motions at the specific locations and/or forces in the specific structural members of interest in the formulation of design and/or test criteria. On the other hand, some procedures used to predict the structural responses to high frequency random loads yield only spectra for motions at point locations (e.g., the extrapolation techniques and direct measurements discussed in Sections 5.2 and 5.3). In some cases, the response predictions might be made at the specific points of interest in the formulation of design and/or test criteria, e.g., the attachment points for equipment mounted on the structure. In most cases, however, the points where response predictions are made do not correspond exactly to the specific points of interest, and even when they do, the equipment items to be mounted at those points are often not modeled for the predictions or in place for direct measurements. Hence, it is necessary to pool the predicted responses at various points to obtain a single spectrum that will conservatively bound the spectra for the responses at all points in a structural region, including the specific points of interest. This approach requires that the structure be divided into a collection of regions often referred to as "zones". A conservative bound on the spectra for the responses of all points in a single zone is commonly called the zone "limit".

a. *Definition of Zones*. Assume the high frequency dynamic loads-induced responses at all points on a large structure (a vehicle or a large payload) is of interest. The responses at various points on the structure will typically vary widely from one location to another. The goal in zoning is to divide the structure into regions or zones such that the responses at all points within each zone are reasonably homogeneous, meaning the spectra for the responses at all points can be described by a single spectrum that will exceed most or all of the spectra at the individual points without severely exceeding the spectrum at any point. It is also required that the selected zones correspond to structural regions of interest in the formulation of design and/or test criteria. For example, if the ultimate goal is the definition of vibration inputs to equipment that will be mounted on the structure, as required to derive test specifications, a single zone should include all the attachment points for at least one, and preferably for several, equipment items. It is not necessary for a zone to be a single contiguous structural region. For example, all frames of a given size in a vehicle, no matter where they are located, might

constitute a single zone if the responses of those frames are similar. In any case, it is desirable to minimize the number of zones used to describe the dynamic loads-induced responses over the entire vehicle so as to minimize the number of specified spectra needed to test the equipment for that vehicle.

b. *Determination of Zones*. There are direct analytical techniques that can be used to arrive at structural zones based upon tests for the statistical equivalence of the spectra for the predicted responses at various locations on the structure [6.3]. However, the zoning operation is usually accomplished based upon engineering judgment, experience, and/or a cursory evaluation of predicted spectra. For example, engineering judgment dictates that frame structures and skin panels should represent different zones, since the response of light skin panels will generally be higher than the much heavier frames. Also, experience suggests that the aft structural regions of a vehicle usually experience higher responses during the launch phase than the forward structural regions, meaning even similar structures in the forward and aft regions of the vehicle should be represented by different zones. Furthermore, the responses normal to the surface of the structure are generally higher than those in the plane of the structure, so the responses along these two axes might be divided into separate zones. Beyond such engineering considerations, a visual inspection of the spectra for the predicted responses can be used to group locations with spectra of similar magnitudes to arrive at appropriate zones. See [6.4] for an example of the selection of the zones used to describe the high frequency dynamic response of the Space Shuttle.

c. *Unbiased Selection of Response Points*. All of the procedures to establish zone limits assume the available spectra for a given zone are predicted at locations that typify all points of interest in that zone. Ideally, this would be achieved by a random selection from all possible response points within the zone. In practice, a random selection usually is not feasible since the predictions are commonly made before the zones are selected; in fact, the spectra for the predicted responses are often used to establish the zones, as discussed above. In some cases, however, the predictions may be made at those points where equipment are mounted. If the ultimate goal is to establish test criteria for those equipment, this would constitute a good selection of response points, even though such mounting points might not typify all points within the zone. In any case, it is important to assess the locations represented by the available predicted spectra to assure that they are typical of all points of interest in the zone.

d. *Definition of Response Terms*. To simplify subsequent discussions, the following terms are defined:

x = spectrum for the high frequency dynamic loads-induced structural response at any point within the zone of interest. The spectral value may be an autospectrum in g^2/Hz, an energy spectrum in g^2-sec/Hz, a line spectrum in g, or a shock response spectrum in g, depending on the nature of the dynamic environment and the spectral analysis procedure employed (see Section 2.2).

x_i = spectrum for the predicted high frequency dynamic loads-induced structural response at the ith point (i = 1, 2, ..., n) within the zone of interest. The term prediction is used here to include direct measurements that might be available in those cases where the structure of interest is on an existing vehicle flown to obtain measured data.

x_{ij} = spectral value in the jth frequency resolution bandwidth (j = 1, 2, ..., m) for the predicted high frequency dynamic loads-induced structural response at the ith point (i = 1, 2, ..., n) within the zone of interest.

x_{hj} = largest spectral value in the jth frequency resolution bandwidth for the predicted high frequency dynamic loads-induced structural responses at the n points within the zone of interest, i.e., x_{hj} = largest value of x_{ij}; i = 1, 2, ..., n.

6.1.1 Envelope Limits. The most common way to arrive at a limit for the spectral values of the responses at all points within a zone is to superimpose the spectral values predicted at n points within a given zone, x_{ij}; i = 1, 2, ..., n, and then to select and plot the maximum spectral value x_{hj} in each of the m frequency resolution bandwidths. This yields an unsmoothed envelope that, for simplicity, is often smoothed using a series of straight line segments (usually not more than seven with slopes of 0, ± 3 dB/octave, or ± 6 dB/octave). The computation of unsmoothed and smoothed envelopes is illustrated in Figure 6.1 using the maximax autospectra for 12 vibration measurements made at different locations in a selected structural zone of a large launch vehicle during liftoff. The individual spectra were computed using a 1/6 octave band frequency resolution.

The primary advantage of the envelope approach is that it is easy to apply. The primary disadvantages are as follows:

a. It does not provide a specific probability that the envelope at a given frequency will exceed the spectrum for the response at another location of interest, i.e., the envelope, in itself, does not allow a quantitative evaluation of uncertainties. However, if the number of predicted spectra is sufficiently large, say, $n \geq 14$, this deficiency can be removed by computing the distribution-free tolerance limit detailed in Section 6.1.3.

b. It can produce somewhat different results depending on the frequency resolution of the predicted spectra, i.e., spectra predicted in narrow bandwidths will display substantially higher peak magnitudes than spectra predicted in, say, 1/3 octave bands (see Section 6.2.1).

There is a final problem with the envelope procedure that applies to all other procedures. Specifically, for the usual case where the envelope is smoothed by a series of straight lines, the procedure becomes somewhat subjective in terms of the number of straight lines used to define the envelope, and whether all spectral peaks are enveloped or some are clipped, i.e., two experienced engineers using the same data might arrive at substantially different smoothed limits.

This problem is sometimes addressed by using some systematic method for determining which spectral peaks will be either fully covered or partially clipped by the smoothed envelope. For example, a commonly used rule is that all narrowband spectral peaks should be clipped by 3 dB. Another more rigorous rule is that all spectral peaks with a bandwidth less than 5% of center frequency should be clipped to the level where the bandwidth is 5% of center frequency. Perhaps the best approach is to compute all spectra with a resolution bandwidth that is proportional to frequency (e.g., a 1/6 octave bandwidth), and then envelope all peaks without clipping. This is the procedure used in Figure 6.1. In any case, the use of enveloped spectral data for the formulation of design and/or test criteria is always subjected to the special restrictions detailed in Section 6.5.

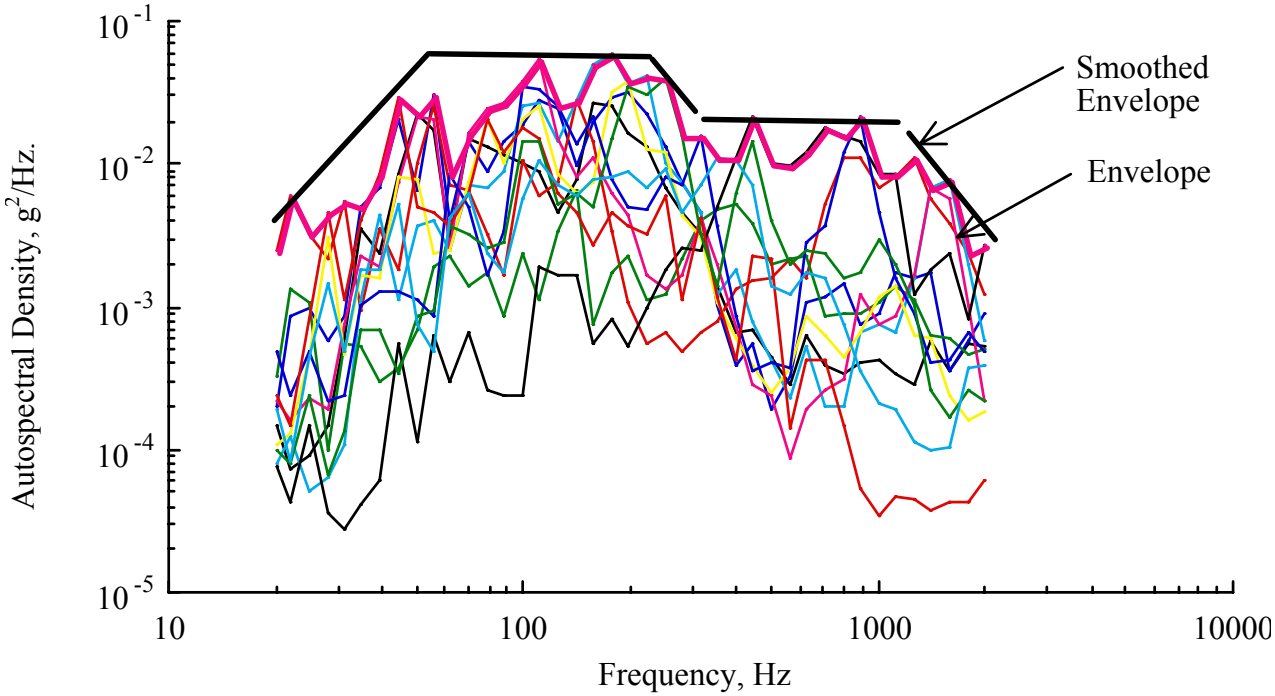

FIGURE 6.1. Envelope for Twelve Measured Vibration Response Spectra Within a Zone.

6.1.2 Normal Tolerance Limits. A more definitive way to arrive at a conservative limit for the spectral values of the structural responses in a zone is to compute a normal tolerance limit for the predicted spectra in each frequency resolution bandwidth. Normal tolerance limits apply only to normally distributed random variables. The spatial variation of structural responses to stationary, nonstationary, and transient dynamic loads is generally not normally distributed. However, there is considerable empirical evidence (e.g., [6.5 - 6.8]) that the logarithm of the spectral values for any motion parameter describing the response of aerospace vehicle structures from one point to another does have an approximately normal distribution, i.e., the spatial distribution for the structural response spectral values in a specific frequency resolution bandwidth approximately fits a lognormal distribution. Hence, by simply making the logarithmic transformation

$$y = \log_{10} x \tag{6.1}$$

a normal tolerance limit can be computed for the transformed predictions, y_{ij}; i = 1, 2, ..., n, and j = 1, 2, ..., m. Specifically, the one-sided (upper-tail) normal tolerance limit for y, denoted by $NTL_y(n,\beta,\gamma)$, is defined as that value of y that will exceed at least β portion of all possible values of y with a confidence coefficient of γ, and is given by

$$NTL_y(n,\beta,\gamma) = \bar{y} + k_{n,\beta,\gamma}\, s_y \tag{6.2}$$

where $\bar{y}$ is the sample average and s_y is the sample standard deviation of y, given by

$$\bar{y} = \frac{1}{n}\sum_{i=1}^{n} y_i \; ; \; s_y = \sqrt{\frac{1}{n-1}\sum_{i=1}^{n}(y_i - \bar{y})^2} \tag{6.3}$$

The normal tolerance limit in the original engineering units of x can be retrieved by

$$NTL_x(n,\beta,\gamma) = 10^{NTL_y(n,\beta,\gamma)} \tag{6.4}$$

In Equation (6.2), the term $k_{n,\beta,\gamma}$ is called the normal tolerance factor, and is a tabulated value; a tabulation of $k_{n,\beta,\gamma}$ for selected values of n, β, and γ is presented in Table 6.1, which is extracted from [6.9, 6.10]. Note in Table 6.1 that for $n = \infty$,

$$NTL_y(\beta) = \mu_y + z_\alpha \sigma_y \;\; ; \;\; \alpha = 1 - \beta \tag{6.5}$$

where μ_y is the true mean and σ_y is the true standard deviation of y, and z_α is the $\alpha = (1 - \beta)$ percentage point of the standardized normal distribution, which is tabulated in any statistics text book, e.g., [6.11]. The confidence coefficient associated with Equation (6.5) is essentially 100%, independent of the value of α. Also, Equation (6.5) is sometimes routinely substituted for Equation (6.2) with $\bar{y}$ and s_y replacing μ_y and σ_y, but this should never be done unless the sample size is n > 50. See [6.12] for the derivation of normal tolerance limits and [6.9] for further discussions of their general applications.

TABLE 6.1. Normal Tolerance Factors, $k_{n,\beta,\gamma}$

n	γ= 0.50			γ= 0.75			γ= 0.90		
	β=0.90	β=0.95	β=0.99	β=0.90	β=0.95	β=0.99	β=0.90	β=0.95	β=0.99
3	1.50	1.94	2.76	2.50	3.15	4.40	4.26	5.31	7.34
4	1.42	1.83	2.60	2.13	2.68	3.73	3.19	3.96	5.44
5	1.38	1.78	2.53	1.96	2.46	3.42	2.74	3.40	4.67
6	1.36	1.75	2.48	1.86	2.34	3.24	2.49	3.09	4.24
7	1.35	1.73	2.46	1.79	2.25	3.13	2.33	2.89	3.97
8	1.34	1.72	2.44	1.74	2.19	3.04	2.22	2.76	3.78
9	1.33	1.71	2.42	1.70	2.14	2.98	2.13	2.65	3.64
10	1.32	1.70	2.41	1.67	2.10	2.93	2.06	2.57	3.53
12	1.32	1.69	2.40	1.62	2.05	2.85	1.97	2.45	3.37
14	1.31	1.68	2.39	1.59	2.01	2.80	1.90	2.36	3.26
16	1.31	1.68	2.38	1.57	1.98	2.76	1.84	2.30	3.17
18	1.30	1.67	2.37	1.54	1.95	2.72	1.80	2.25	3.11
20	1.30	1.67	2.37	1.53	1.93	2.70	1.76	2.21	3.05
25	1.30	1.67	2.36	1.50	1.90	2.65	1.70	2.13	2.95
30	1.29	1.66	2.35	1.48	1.87	2.61	1.66	2.08	2.88
35	1.29	1.66	2.35	1.46	1.85	2.59	1.62	2.04	2.83
40	1.29	1.66	2.35	1.44	1.83	2.57	1.60	2.01	2.79
50	1.29	1.65	2.34	1.43	1.81	2.54	1.56	1.96	2.74
∞	1.28	1.64	2.33	1.28	1.64	2.33	1.28	1.64	2.33

As an illustration, the normal tolerance limit versus frequency for the data in Figure 6.1 computed with $\beta = 0.95$ and $\gamma = 0.50$ is shown in Figure 6.2. This limit is commonly referred to as the 95% normal tolerance limit with 50% confidence, or simply the 95/50 limit, and is interpreted as the limit that will exceed the response spectral values for at least 95% of all points within the zone with a confidence coefficient of 50%. Note the 95/50 limit in Figure 6.2 is similar to the envelope for the twelve measurements at all frequencies, but might be higher or lower than the envelope depending on the values of β and γ. Also, computed normal tolerance limits are sometimes

smoothed by enveloping with a series of straight line segments, as illustrated in Figure 6.2. Of course, this step involves subjective judgments that pose the problems discussed in Section 6.1.1 for the envelope procedure. Also, the use of the normal tolerance limit for the formulation of design and/or test criteria is always subject to the special restrictions detailed in Section 6.5.

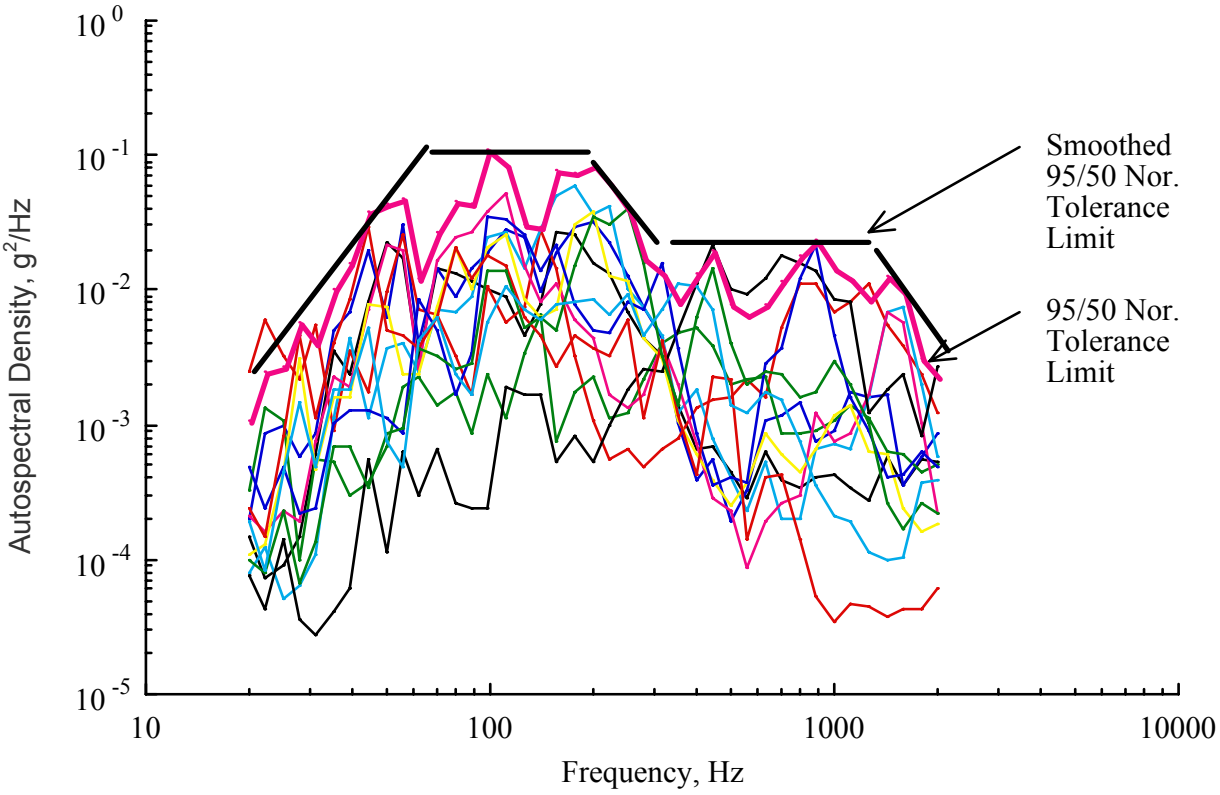

FIGURE 6.2. 95/50 Normal Tolerance Limit for Vibration Response Spectra in Figure 6.1.

The normal tolerance limit approach offers three major advantages over the envelope procedure discussed in Section 6.1.1, as follows:

a. It provides a limit that will exceed a well-defined fractional portion β of the spectra at all locations in the zone with a well-defined confidence γ, i.e., the normal tolerance limit has a rigorous statistical interpretation.

b. For any number of predictions, n, a normal tolerance limit can be computed for any independently selected values of β and γ, i.e., the normal tolerance limit is not restricted to the range of the predicted spectra used for its determination.

c. Although the frequency resolution bandwidth of the predicted spectra can have some impact on the normal tolerance limit, it is not as sensitive to the frequency resolution bandwidth as the envelope procedure.

The last advantage follows from the fact that the normal tolerance limit is computed from average values (the sample mean and standard deviation), which in turn are computed from the predicted spectral values in each frequency resolution bandwidth at all n locations. The sensitivity of the predicted spectral values to the frequency resolution bandwidth (the frequency

resolution bias error) is most pronounced at the frequencies of spectral peaks [6.13]. At most frequencies, a spectral peak may be present at some locations, but not at most locations. Hence, the impact of frequency resolution bias errors on the sample mean and standard deviation is minimal. On the other hand, the envelope of the various predicted spectra is determined at most frequencies by a spectral peak at one location, meaning the frequency resolution bias error is often large.

In spite of the above noted advantages, the use of normal tolerance limits does pose one potential problem, namely, the procedure is sensitive to the assumption that the spatial distribution of the structural response spectral values within the zone is lognormal. This assumption might come into question for the higher values of β and γ.

As a final point concerning normal tolerance limits, Figure 6.2 presents a limit computed with a confidence coefficient of $\gamma = 0.50$, which is a common value of γ used to derive aerospace vehicle vibration test levels, e.g., MIL-STD-1540C and NASA-STD-7001. However, normal tolerance limits could be computed with a higher level of confidence, e.g., $\gamma = 0.90$ or 0.95. For any value of β, the value of the confidence coefficient can have a substantial impact on the limit. This fact is illustrated in Figure 6.3, which shows the 95% tolerance limit for the twelve measurements in Figure 6.1 computed with $\gamma = 0.50$, 0.90, and 0.95. Note that the limit computed with $\gamma = 0.95$ is up to 6 times (7.8 dB) higher than the limit computed with $\gamma = 0.50$. For consistency with MIL-STD-1540C and NASA-STD-7001, it is recommended that normal tolerance limits be computed with a confidence coefficient of $\gamma = 0.50$ unless there is a reason to use a more conservative value.

6.1.3 Distribution-Free Tolerance Limits. Distribution-free tolerance limits circumvent the primary problem associated with normal tolerance limits, namely, the need to assume a lognormal distribution for the spatial variations of the structural response spectral values within the zone. The assumption is eliminated by fixing the tolerance limit to the maximum spectral value in each of the m frequency resolution bandwidths, i.e., the one-sided (upper-tail) distribution-free tolerance limit, denoted by $DFL_x(n,\beta,\gamma)$, is essentially the unsmoothed envelope determined by the procedure detailed in Section 6.1.1. The fractional portion β of all locations where the response spectral values x will be less than the maximum spectral value x_{hj} with a confidence coefficient γ can be determined using order statistics [6.14] to be

$$DFL_x(n, \beta, \gamma) = x_{hj} \;\; ; \;\; \gamma = 1 - \beta^n \qquad (6.6)$$

The interpretation of distribution-free tolerance limits is the same as for the normal tolerance limits detailed in Section 6.1.2, namely, x_{hj} is that spectral value that will exceed the response spectral values for at least β portion of all points in the zone with a confidence coefficient of γ. For example, the unsmoothed envelope for the data in Figure 6.1 represents the tolerance limit that will exceed the response spectral values for at least 95% of all points in the zone with a confidence coefficient of 46%. The unsmoothed envelope is often smoothed with a series of straight lines, as illustrated in Figure 6.1. This step involves subjective judgments that pose the problems discussed in Section 6.1.1 for the envelope procedure. Also, the use of the distribution-free tolerance limit for the formulation of design and/or test criteria is always subject to the special restrictions detailed in Section 6.5.

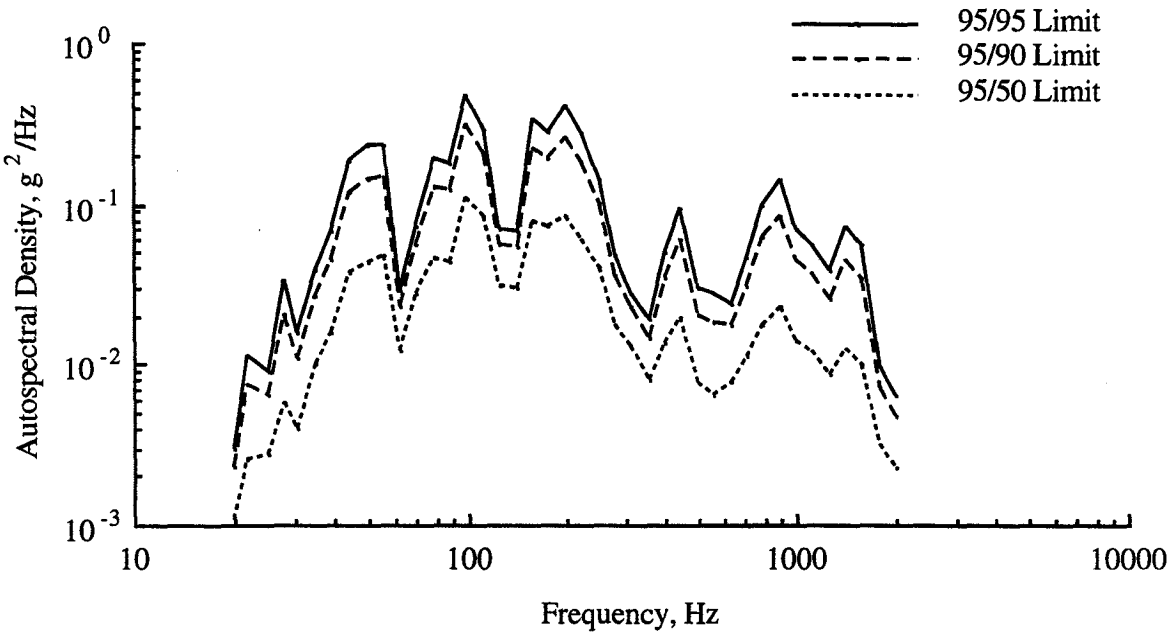

FIGURE 6.3. Normal Tolerance Limits for Data in Figure 6.1 with Various Confidence Coefficients.

The primary advantage of the distribution-free tolerance limit over the normal tolerance limit is that it is not sensitive to the spatial distribution of the spectral values for the responses within the zone, i.e., it is nonparametric. However, it does pose two problems not present in the normal tolerance limit, as follows:

a. The procedure does not permit an independent selection of the values for β and γ. The usual approach here is to select a desired value for the fractional portion β, and accept whatever value of the confidence coefficient γ that results from Equation (6.6). However, the specification writer generally wants to have a common value of β and γ for all zones, even though the number of spectra for each zone may be different. This is not possible using nonparametric tolerance limits, which simply quantify the confidence coefficient associated with the envelope approach in Section 6.1.1.

b. As for the envelope approach in Section 6.1.1, the procedure can produce somewhat different results depending on the frequency resolution of the predicted spectra.

6.1.4 Empirical Tolerance Limits. A third method of selecting a conservative limit for the spectral values of structural responses within a zone is to determine an empirical distribution function for the predicted spectral values at n locations, and then select some large percentile x_β from the distribution (that value of x which exceeds β portion of the available values) to be a conservative limit, referred to as an empirical tolerance limit. Ideally, this would be done independently for the spectral values in each frequency resolution bandwidth. In practice, however, it is rare to have predictions at enough locations to allow a determination of a large percentile for the values in each bandwidth; i.e., for $\beta = 0.95$, at least 20 values are needed to determine a limit. Hence, it is common to normalize the spectral values in each frequency resolution bandwidth to a common mean value, and then pool all the spectral values to arrive at a single distribution function for the determination of a limit that covers β portion of the values. Of course, this pooling approach assumes the spatial distribution of the spectral values is the

same in all the frequency resolution bandwidths, and further that the ratio of the limit value to the mean value, $x_\beta / \bar{x}$, is a constant over all frequency resolution bandwidths.

Given a total of n spectral values within the zone covering m frequency resolution bandwidths, x_{ij}; i = 1, 2, ..., n, and j = 1, 2, ..., m, the specific procedure to determine an empirical tolerance limit is as follows:

a. Compute the mean value of the spectral values in each frequency resolution bandwidth; i.e.,

$$\overline{x}_j = \frac{1}{n_j} \sum_{i=1}^{n_j} x_{ij} \tag{6.7}$$

b. Divide the spectral values in each frequency resolution bandwidth by the average value in that bandwidth to obtain the normalized values u_{ij}; i.e.,

$$u_{ij} = \frac{x_{ij}}{\overline{x}_j} \tag{6.8}$$

c. Pool the normalized values in all frequency resolution bandwidths to obtain a single set of values u_k; k = 1, 2, ..., nm, and rank-order the pooled normalized values from the smallest to the largest to obtain the set $u_{(k)}$, where

$$\begin{aligned} &(k) = 1 \text{ is smallest value of } u_k \\ &(k) = 2 \text{ is next smallest value of } u_k \\ &\quad \ldots . \\ &(k) = nm \text{ is largest value of } u_k \end{aligned} \tag{6.9}$$

d. Select that normalized value u_β that covers β portion of all the pooled and rank-ordered normalized values $u_{(k)}$; i.e.,

$$u_\beta = u_{(k)} \text{ where } (k) = nm\beta \tag{6.10}$$

e. Determine the limit value $x_{\beta j}$ in each frequency resolution bandwidth by multiplying the average value for each bandwidth by the normalized limit u_β to obtain the empirical tolerance limit, denoted by $ETL_x(\beta)$; i.e.,

$$ETL_x(\beta) = x_{\beta j} = u_\beta \overline{x}_j \tag{6.11}$$

As an illustration, the empirical distribution for the normalized values of the data in Figure 6.1 is detailed in Figure 6.4, and the 95% empirical tolerance limit is shown in Figure 6.5. The multiplier determined from the rank-ordered, normalized spectral values Figure 6.4 to arrive at the 95% limit in Figure 6.5 is $u_\beta = 3.37$. Of course, this value of u_β is an estimate computed from a statistical sample of 492 values, and may be larger or smaller than the true value of μ_β for all points in the zone. The statistical variability of the estimate u_β is governed by the binomial probability function [6.11] and, hence, an upper bound, $U_\beta = C\, u_\beta$; C > 1, could be determined to produce a limit in Equation (6.11) that exceeds the spectral values at β portion of the points in the zone with a high level of confidence. In practice, however, it is customary to use the value of u_β computed from Equation (6.10) without modification, meaning the confidence coefficient associated with the limit

in Equation (6.11) is essentially γ = 50%; i.e., the empirical tolerance limit derived in Equation (6.11) is the value of x that will exceed the response spectral values at 95% of all points within the zone with a confidence coefficient of 50%. As for the other procedures, computed empirical tolerance limits are sometimes smoothed by enveloping with a series of straight lines. This step involves subjective judgments that pose the problems discussed in Section 6.1.1 for the envelope procedure. Also, the use of the empirical tolerance limit for the formulation of design and/or test criteria is always subject to the special restrictions detailed in Section 6.5.

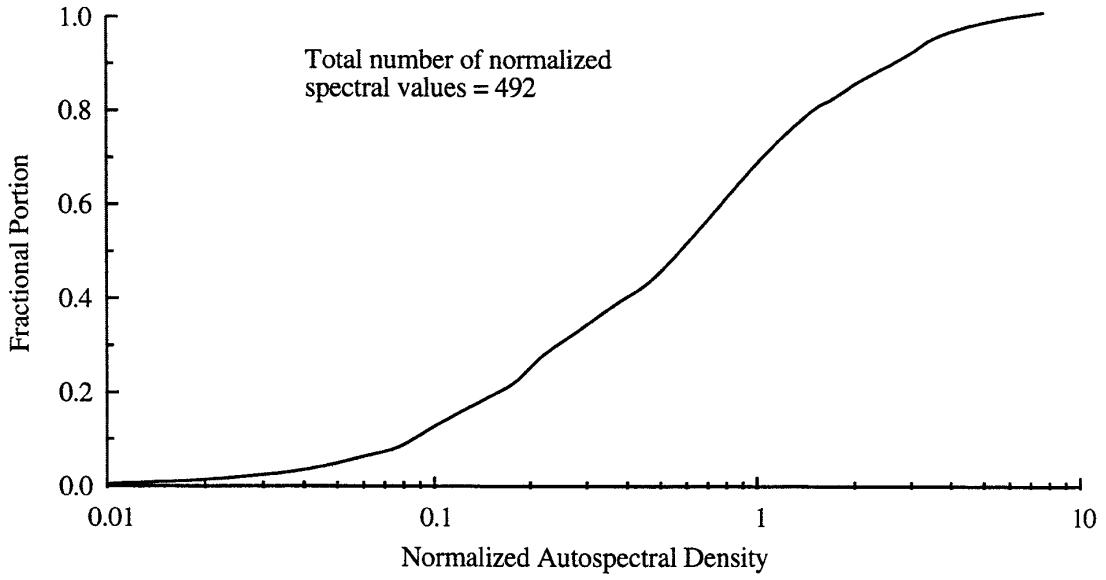

FIGURE 6.4. Empirical Distribution for Normalized Vibration Response Spectra in Figure 6.1.

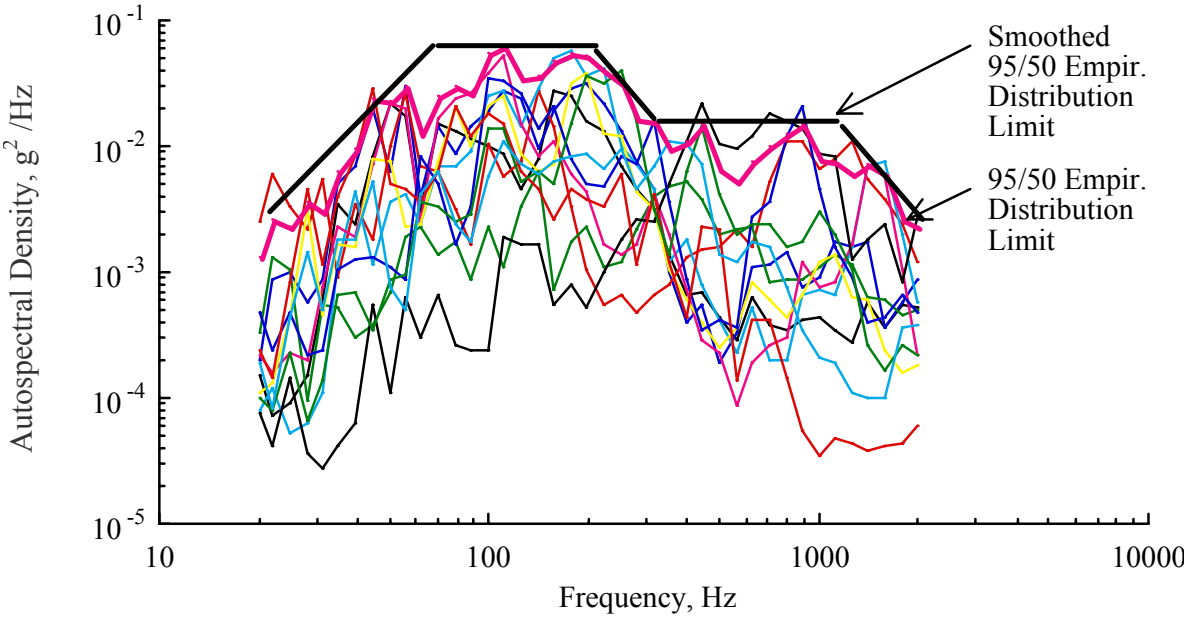

FIGURE 6.5. 95/50 Empirical Tolerance Limit for Vibration Response Spectra in Figure 6.1.

Like the distribution-free tolerance limits detailed in Section 6.3, the empirical tolerance limit approach does not assume a lognormal spatial distribution for the response spectral values within the zone. Furthermore, like normal tolerance limits, the empirical tolerance limit is not as sensitive as the envelope to the frequency resolution bandwidth of the predicted spectral values used for its determination for the reasons detailed in Section 6.1.2. However, the empirical tolerance limit does pose some potential problems, as follows:

a. If the spectral values in all frequency resolution bandwidths are pooled to arrive at the empirical distribution, it is sensitive to the assumption that the spatial distribution of the response spectral values is the same in all bandwidths.

b. It is most effective when response predictions are available at a relatively large number of locations (generally, n > 10).

c. It provides a limit with a confidence coefficient of $\gamma = 0.50$ only, unless further extensive computations are performed.

6.1.5 Normal Prediction Limits. The final way to arrive at a conservative limit for the spectral values of the structural responses in a zone is to compute a normal prediction limit for the predicted spectra in each frequency resolution bandwidth. As for normal tolerance limits, normal prediction limits apply only to normally distributed random variables. Hence, the logarithmic transformation in Equation (6.1) is again required to obtain an approximately normal distribution for the transformed predictions, $y_i = 1, 2, ..., n$. The one-sided (upper-tail) normal prediction limit for y, denoted by $NPL_y(n,\gamma)$, is defined as that value of y that will exceed the next predicted value of y with a confidence coefficient of γ, and is given by [6.1]

$$NPL_y(n,\gamma) = \bar{y} + \sqrt{1 + \frac{1}{n}}\, s_y\, t_{n-1;\,\alpha} \quad ; \quad \alpha = 1 - \gamma \tag{6.12}$$

where $\bar{y}$ is the sample mean and s_y is the sample standard deviation of y, as defined in Equation (6.3), and $t_{n-1;\,\alpha}$ is the α percentage point of the "Student" t variable with n - 1 degrees-of-freedom, which is tabulated in any statistics text book, e.g., [6.11]. The normal prediction limit in the original engineering units of x can be retrieved by

$$NPL_x(n,\gamma) = 10^{NPL_y(n,\gamma)} \tag{6.13}$$

The normal prediction limit should not to be confused with the normal tolerance limit given by Equation (6.2), which defines an upper limit that will exceed at least β portion of all possible values of x with a confidence coefficient of γ. Also, the value of γ for normal prediction limits is sometimes referred to as a probability, but after the measurements are made, it is more correctly referred to as a confidence coefficient.

As an illustration, the normal prediction limit versus frequency for the data shown in Figure 6.1 computed with $\gamma = 0.95$ is shown in Figure 6.6. This limit is commonly referred to as the 95% normal prediction limit for the spectral value of the next predicted response at a randomly selected point within the zone. As for the various tolerance limits, normal prediction limits are sometimes smoothed by enveloping with a series of straight lines, as illustrated in Figure 6.6. This step involves subjective judgments that pose the problems discussed in Section 6.1.1 for the envelope procedure. Also, the use of the normal prediction limit for the formation of design and/or test criteria is always subject to the special restrictions detailed in Section 6.5.

Equation (6.13) defines the normal prediction limit for the next value of y (i.e., y_{n+1}) based upon the sample average and standard deviation for the previous n values of y, i.e., y_i; i = 1, 2, ..., n. This equation can be used to establish the limit that will exceed the next two values of y (i.e., y_{n+1} and y_{n+2}) by simply squaring γ. For example, if the limit $NPL_y(n,\gamma)$ in Equation (6.12) is determined for the next value of y with a confidence coefficient of $\gamma = 0.95$, that same limit will apply to the next two values of y with a confidence coefficient of $\gamma = (0.95)^2 = 0.90$. Conversely, if a limit for the next two values of y with a confidence coefficient of $\gamma = 0.95$ is desired, Equation (6.12) can be solved for $NPL_y(n,\gamma)$ with a confidence coefficient of $\gamma = \sqrt{0.95} = 0.975$. The same procedure can be used to determine an upper prediction limit for any number of future values of y. It should be noted, however, that the normal prediction limit is unbounded as the number of values becomes large.

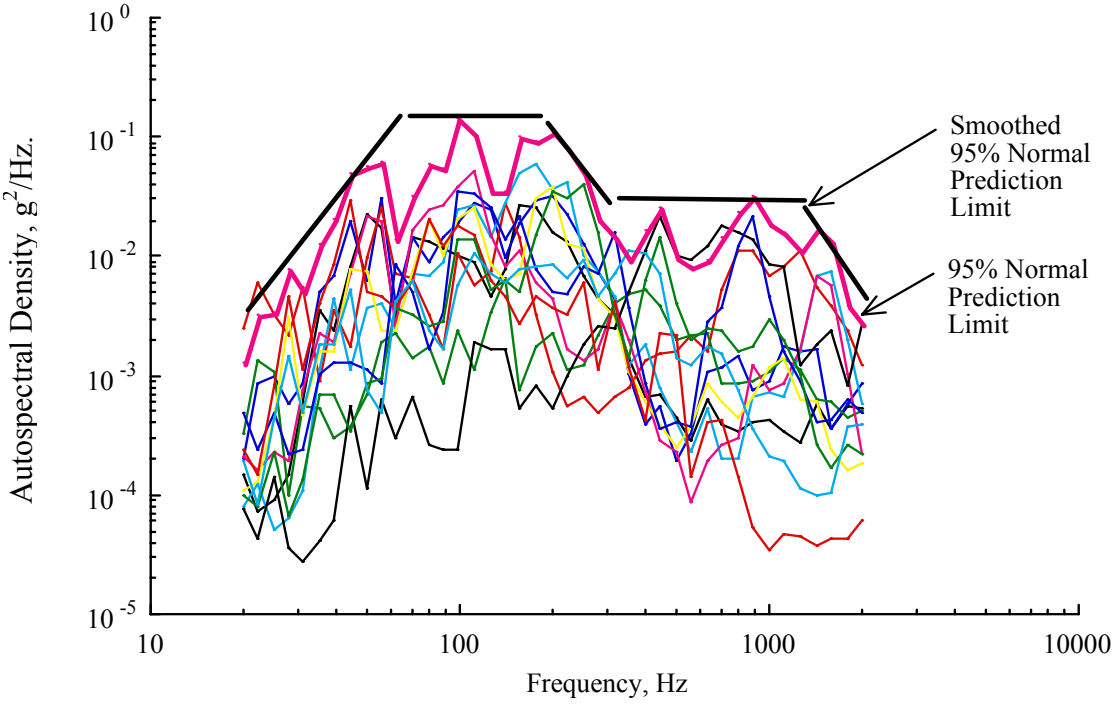

FIGURE 6.6. 95% Normal Prediction Limit for Vibration Response Spectra in Figure 6.1.

Normal prediction limits are somewhat simpler to apply than any of the tolerance limits because they involve only one probability related parameter, namely, a confidence coefficient γ. On the other hand, the normal prediction limit poses two problems, as follows:

a. It is sensitive to the assumption that the spatial distribution of the spectral values of the structural responses values within the zone is lognormal. This assumption might come into question for the higher values of γ.

b. It provides a conservative limit for only one or some other specific number of future response predictions at randomly selected points within the zone, rather than to the response at all locations within the zone.

6.1.6 Assessments. Using the twelve measured autospectra in Figure 6.1, the five different methods presented in Sections 6.1.1 through 6.1.5 for deriving a conservative limit for random dynamic loads-induced structural responses are compared in Figure 6.7. All three tolerance limits in Figure 6.7 cover the response spectra for $\beta = 0.95$ portion of all points within the zone with similar confidence coefficients, namely, $\gamma = 0.46$ to 0.50. The normal prediction limit in Figure 6.7 covers the spectrum for the response at the next selected point within the zone with a confidence coefficient (probability) of $\gamma = 0.95$. The following interesting features should be noted in Figure 6.7.

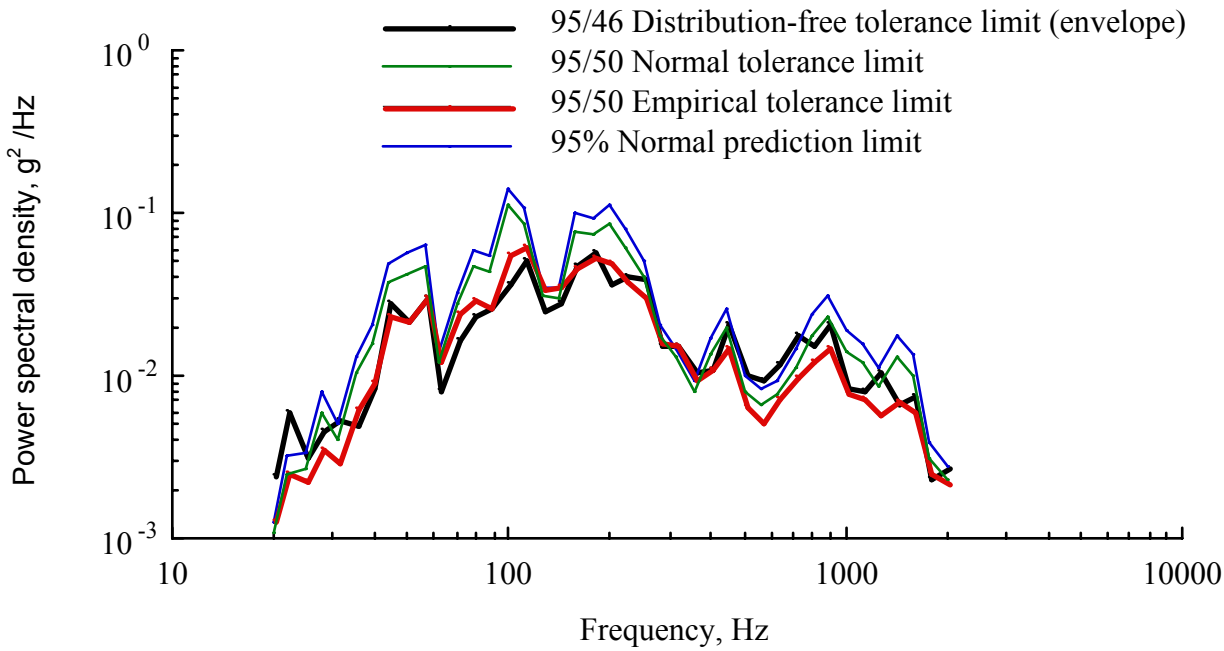

FIGURE 6.7. Comparison of Various Limits for Vibration Response Spectra in Figure 6.1.

a. The distribution-free and empirical tolerance limits are similar at most frequencies. This is consistent with the fact that these two limits do not involve a lognormal assumption for the spatial distribution of the spectral values, and further are computed with similar confidence coefficients; i.e., $\gamma = 0.46$ for the distribution-free limit and $\gamma = 0.50$ for the empirical limit.

b. The normal tolerance limit is somewhat higher at many frequencies than the distribution-free and empirical tolerance limits, even though it has a similar confidence coefficient, i.e., $\gamma = 0.50$. This discrepancy probably reflects a slight inaccuracy in the lognormal assumption associated with the normal tolerance limit.

c. The normal prediction limit is higher than all three tolerance limits at most frequencies. However, if the tolerance limits were computed with a higher confidence coefficient, they would probably exceed the normal prediction limit.

The comparative merits of the various procedures to establish limits for the dynamic loads-induced structural responses in a zone are summarized in Table 6.2. Based upon these comparisons, it is suggested that a conservative limit for the response spectra in a zone be computed from the predicted spectra at n points within the zone, as follows:

TABLE 6.2. Summary of Merits of Various Procedures for Selecting Limits.

Merit	Simple Envelope	Normal Tolerance Limit	Distr.-Free Tolerance Limit	Empirical Tolerance Limit	Normal Prediction Limit
Covers known portion, β, of spectra at all locations in zone	No	Yes	Yes	Yes	No
Associated with a known confidence coefficient γ	No	Yes	Yes	Yes	Yes
Allows independent selection of portion β and confidence coefficient γ	No	Yes	No	No*	Not Applicable
Insensitive to assumption of lognormal spatial distribution	Yes	No	Yes	Yes	No
Insensitive to different spatial distributions in bandwidths	Yes	No	Yes	No**	No
Relatively insensitive to frequency resolution bandwidth	No	Yes	No	Yes	Yes

* Unless extensive computations are performed
** Unless sufficient data are available to compute independent limits for each bandwidth

a. The normal tolerance limit given by Equation (6.2) and computed with a confidence coefficient of $\gamma = 0.5$ is recommended. This is the most common procedure used to arrive at maximum expected environments in other documents, e.g., MIL-STD-1540C and NASA-STD-7001. It should be mentioned that, for small values of n, the normal tolerance limit will become quite large compared to the average value of the predicted spectra in the zone. Nevertheless, this is a statistically correct result, assuming a lognormal distribution applies, because a limit based upon spectra at a small number of points naturally leads to a high uncertainty in what the spectral values may be at all other points.

b. If $n > 10$, the empirical tolerance limit given by Equation (6.11) can be used as a substitute for the normal tolerance limit.

Again, when any conservative limit for the dynamic responses in a structural zone is used for the derivation of design and/or test criteria, the restrictions detailed in Section 6.5 should be carefully observed.

6.2 Spatial Variations - Area Predictions. Some high frequency prediction procedures produce a spectrum for the average response over a structural area that may include the specific points of interest, but without a clearly defined degree of conservatism (e.g., SEA techniques in Sections 5.2.2 and 5.3.3). Also, these area prediction procedures usually produce a spectrum with a relatively coarse frequency resolution, commonly a 1/3 octave bandwidth. In

some cases, several area predictions may be available within a single structural zone of interest for establishing design and/or test criteria. In such cases, the area predictions can be treated as point predictions and the procedures detailed in Section 6.1 can be applied directly, although some additional factor might be needed to account for the narrow bandwidth spectral peaks that might occur within the frequency resolution bandwidth (probably a 1/3 octave bandwidth) used for the area predictions. In other cases, a single area prediction may correspond to a single structural zone of interest. In this situation, some factor is needed to allow for the variability of the spectral magnitudes for the dynamic response at all points within the zone.

6.2.1 Variations within a Frequency Resolution Bandwidth. Assuming an area prediction for the dynamic response of a structure is made in 1/3 octave bands, there will be narrow bandwidth spectral peaks representing lightly damped structural resonances that have substantially higher magnitudes than the corresponding 1/3 octave band levels. If it is further assumed that only one spectral peak occurs within a given 1/3 octave band, the ratio of the spectral peak to the 1/3 octave band magnitudes can be determined by analytical techniques [6.15]. However, empirical studies provide a more realistic measure of the ratio of the spectral peak to 1/3 octave band magnitude that can be expected in dynamic loads-induced structural response data. The results of one comprehensive empirical study based upon the random vibration response of externally carried aircraft stores [6.8] is presented in terms of an empirical distribution function in Figure 6.8. From this figure, a 3 dB increase in the spectral magnitude measured in 1/3 octave bands would envelope about 90% of all spectral peaks, an increase of 4 dB would envelope about 95% of all spectral peaks, and an increase of 5 dB would envelope about 98% of all spectral peaks. It follows that predictions for structural responses in the form of 1/3 octave band spectra can be converted to an envelope for most narrowband spectral peaks by adding an appropriate factor determined from Figure 6.8. However, this should not be done without careful consideration of the restrictions on spectral envelopes detailed in Section 6.5.

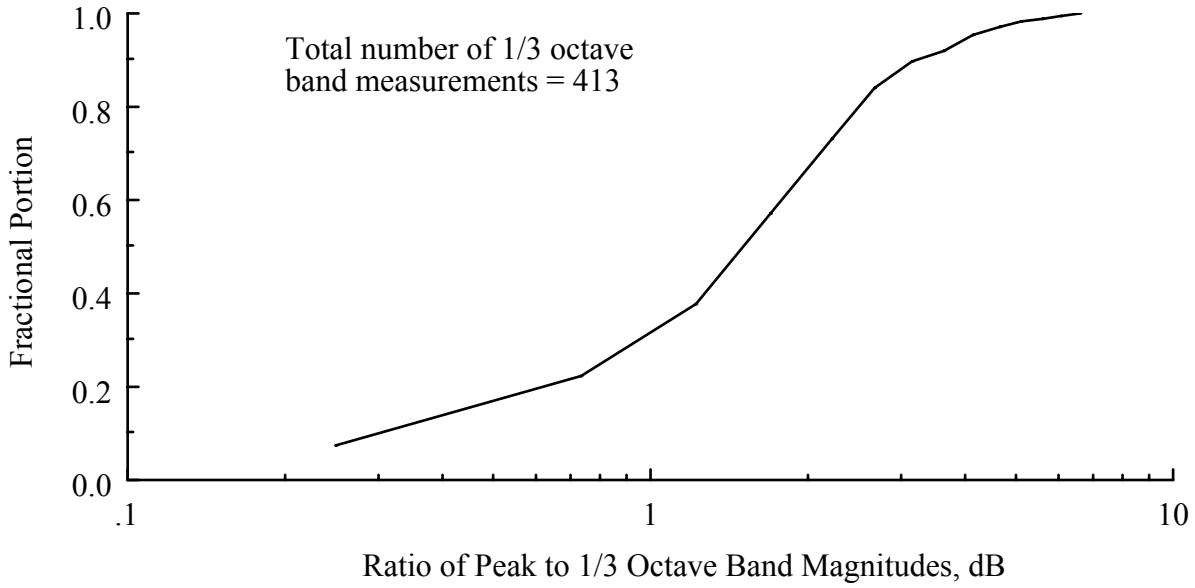

FIGURE 6.8. Empirical Distribution for Peak to 1/3 Octave Band Magnitudes for Vibration Spectra.

6.2.2 Variations within a Structural Area. Depending on the size of the structural region covered by an area prediction, there may be wide variations of the dynamic responses within that area (see Section 5.2.2). If the area prediction encompasses a structural zone of interest for the formulation of design and/or test criteria, the variations will be similar to those represented by the data in Figure 6.1. In terms of dB = 10 $\log_{10}$x where x is the spectral value in a given frequency resolution bandwidth, the standard deviation of the pooled spectra for the vibration response data in Figure 6.1 is 5.5 dB. This is consistent with the standard deviations of other published spectral data for the random vibration responses measured over relatively homogeneous structural regions of aerospace vehicles, e.g., the standard deviations of spatially distributed data in [6.5 - 6.8] range from 5 to 6 dB. The standard deviations deduced from a large data bank of vibration autospectra measured on rocket vehicle structures [6.16] generally fall below 6 dB. Hence, it is believed that a reasonable upper bound on the standard deviation of random dynamic loads-induced responses over typical structural zones is

$$\sigma_{spatial} = 6 \text{ dB} \tag{6.14}$$

where the standard deviation estimate is assumed to represent a known value σ, rather than a sample value s, because the sample size associated with the past data used to arrive at the estimate is very large.

Now assume the spatial variations of the dynamic responses within the structural region covered by an area prediction have a lognormal distribution, as discussed in Section 6.1.2. A normal tolerance limit for β portion of the responses at all points in the area can be approximated from Equation (6.5) by

$$NTL_x(\beta) = 10^{C/10} \;\; ; \;\; C = AP(dB) + 6\, z_\alpha \;\; ; \;\; \alpha = 1 - \beta \tag{6.15}$$

where AP(dB) = area prediction for the response in dB and $z_\alpha = \alpha$ percentage point [$\beta = (1 - \alpha)$ percentile] of the standardized normal distribution, which is tabulated in essentially all statistical text books, e.g., [6.11]. If it is further assumed the area prediction represents an estimate for the energy averaged response within the area, the confidence coefficient associated with the normal tolerance limit in Equation (6.15) is $\gamma = 0.50$, i.e., $NTL_x(\beta)$ is the $100\beta/50$ normal tolerance limit for point-to-point variations.

As an illustration, let the area prediction for the random vibration response be 0.02 g^2/Hz (-17.0 dB referenced to 1 g^2/Hz) over a given frequency range. The 95/50 normal tolerance limit ($\alpha = 0.05$) for the spectral densities at all points in the area is given by Equation (6.15) with AP(dB) = -17.0 and $z_{0.05} = 1.645$. Hence, C = -7.1 and $NTL_x(\beta) = 0.19$ g^2/Hz, i.e., the 95/50% normal tolerance limit is 9.7 times (9.9 dB above) the area predicted spectral density.

It should be emphasized that the standard deviation for dynamic responses over a structural region given in Equation (6.14) is based upon spectral data analyzed with relatively narrow frequency resolution bandwidths. Hence, this standard deviation essentially includes the correction from the coarse bandwidth typically used for area predictions (usually 1/3 octave bands) to a tolerance limit representing the spectral peaks produced by a more narrow frequency resolution bandwidth. It follows that the frequency resolution bandwidth correction discussed in Section 6.2.1 and summarized in Figure 6.8 should not be added to the normal tolerance interval given by Equation (6.15).

6.3 Flight-to-Flight Variations. Beyond the spatial variations of random dynamic loads-induced responses of aerospace vehicle structures, there is also some variability in the response at a given location on the structure from one flight to the next. It is rare to make vibration measurements at the same point on the structure of the same type of vehicle during many flights, particularly a space vehicle, but some such data are available. For example, [6.17] presents shock response spectra and autospectra for the shock and vibration measured at one point on the Trident I missile during 24 static firings and over 40 flights. A careful evaluation of these data leads to the conclusion that the flight-to-flight variations in both shock response spectra and vibration spectral density values have an approximately lognormal distribution with a standard deviation bounded by

$$\sigma_{\text{flt-to-flt}} = 3 \text{ dB} \tag{6.16}$$

As in Equation (6.14), the standard deviation estimate is assumed to represent a known value σ, rather than a sample value s, because the sample size associated with the past data used to arrive at the estimate is very large. Using the lognormal assumption, a normal tolerance limit for the dynamic response at a specific point on a structure for at least β portion of all flights can be approximated from Equation (6.5) by

$$NTL_x(\beta) = 10^{C/10} \;\; ; \;\; C = P(dB) + 3\, z_\alpha \;\; ; \;\; \alpha = 1 - \beta \tag{6.17}$$

where P(dB) = prediction for the response in dB and z_α = α percentage point [β = (1 - α) percentile] of the standardized normal distribution, which is tabulated in essentially all statistical text books, e.g., [6.11]. If it is further assumed the prediction represents an estimate for the energy averaged response for all flights, the confidence coefficient associated with the normal tolerance limit in Equation (6.17) is γ = 0.50, i.e., $NTL_x(\beta)$ is the 100β/50 normal tolerance limit for flight-to-flight variations.

As an illustration, let the prediction for the random vibration response at some point on an aerospace vehicle structure be 0.02 g^2/Hz (-17.0 dB referenced to 1 g^2/Hz) over a given frequency range. The 95/50 normal tolerance limit (α = 0.05) for the spectral densities on all flights of that vehicle is given by Equation (6.17) with P(dB) = -17.0 and $z_{0.05}$ = 1.645. Hence, C = -12.1 and $NTL_x(\beta)$ = 0.062 g^2/Hz, i.e., the 95/50 normal tolerance limit is 3.1 times (4.9 dB above) the predicted spectral density.

Referring to the discussions at the end of Section 6.2.2, it should be mentioned that the flight-to-flight variation given by Equation (6.16) may already be accounted for in a computed tolerance limit for point-to-point variations. For example, the twelve spectra used to compute the normal tolerance limit in Figure 6.2 were measured on three different flights and, hence, flight-to-flight variations are reflected in the resulting normal tolerance limit. On the other hand, there may be situations where a tolerance limit for the dynamic responses within a zone is computed from point-to-point predictions or measurements made on a single flight, or may be estimated using Equation (6.15). In these cases, the flight-to-flight variance should be added to the point-to-point variance before computing the tolerance limit; i.e., the standard deviation for the normal tolerance limit computation is given by

$$\sigma_{\text{total}} = \sqrt{\sigma^2_{\text{spatial}} + \sigma^2_{\text{flt-to-flt}}} \tag{6.18}$$

In no case should a tolerance limit for point-to-point variations within a zone be added directly to a tolerance limit for flight-to-flight variations.

For example, if the point-to-point standard deviation is $\sigma_{spatial}$ = 6 dB and the flight-to-flight standard deviation is accepted as $\sigma_{flt\text{-}to\text{-}flt}$ = 3 dB, the standard deviation for the normal tolerance limit computation is σ_{total} = 6.7 dB. There is a possible complication in this process in that the point-to-point standard deviation may be an estimate $s_{spatial}$ computed from a sample of n spectra, while the flight-to-flight standard deviation, $\sigma_{flt\text{-}to\text{-}flt}$ given by Equation (6.17), is assumed to be known. Since the point-to-point variation typically dominates the total standard deviation, it is recommended that the final normal tolerance limit be computed using the tolerance factor for a desired confidence coefficient in Table 6.1 appropriate for the point-to-point standard deviation computation, and that the result be associated with that confidence coefficient.

6.4 Selection of Fractional Portion for Tolerance Limits. The various tolerance limits detailed in Sections 6.1 through 6.3 all require the selection of a value for β, the fraction portion of the locations within a zone where the response spectral values will be exceeded by the tolerance limit. This selection is often made somewhat arbitrarily, with β = 0.95 being a common selection for the derivation of shock and vibration test levels, e.g., MIL-STD-1540C and NASA-STD-7001. However, for testing purposes, a number of procedures have been formulated to select an optimum value for β based upon the adverse consequences of an undertest versus an overtest. Specifically, if β is too small, the test level might be too low to detect defects that would cause a flight failure. On the other hand, if β is too large, the test level might be high enough to cause a failure that would not occur in flight.

Well-known procedures developed specifically to optimize test level selections are detailed in [6.18 - 6.22]. All the referenced procedures yield an optimum test level in terms of a percentile of the environmental distribution function, which is essentially the value of β in Sections 6.1 through 6.3, as a function of a "cost" ratio C_T/C_F, where C_T is the "cost" of a test failure and C_F is the "cost" of a flight failure. The procedure in [6.18] applies to qualification and protoflight tests, and allows for the possibility that the item being tested has already been manufactured in quantity for service use, i.e., it includes possible refurbishing costs. The result in [6.19] applies to acceptance tests and is arrived at using assessments of the uncertainties in both the severity of the environment and the strength of the item to be tested, i.e., it involves a dependence on the design safety factor for the test item. The procedure in [6.20] applies to acceptance and protoflight tests, and includes consideration of a "test factor" based upon the strength of the item being tested. The simplest of the procedures, which is first presented in [6.21] and is more thoroughly derived in [6.22], applies to acceptance and protoflight tests, and yields an optimum test level given by

$$\beta = \frac{1}{1 + (C_T/C_F)} \tag{6.19}$$

Under appropriate assumptions, primarily a large design safety factor and no refurbishing costs, it is shown in [6.21] that all of the procedures lead to essentially the same result, as given by Equation (6.19) and plotted in Figure 6.9. It should be emphasized that the result plotted in Figure 6.9 applies to the selection of test levels for acceptance and protoflight tests only, i.e., those tests performed on hardware that will be flown (see Section 9.1). The result does not rigorously apply to the selection of qualification test levels where the test is performed on one or more sample items that will not be flown. Nevertheless, Figure 6.9 is sometimes used as an approximation for optimum qualification test levels where C_T is interpreted to include the

estimated cost of redesigning the hardware as required to pass the test, and C_F is interpreted to include the estimated cost of failure of all flight hardware items.

The result in Figure 6.9 is intuitively satisfying. Specifically, consider an item where a failure during test could be corrected by a relatively simple and inexpensive design change, but a failure during flight could result in the loss of the entire space vehicle, e.g., a thrust vector control component that is essential to achieve a successful liftoff. Figure 6.9 says that the item should be tested to a very severe level relative to the anticipated flight environment so as to sharply minimize the risk of an undertest. For example, if a flight failure is assessed to be 1000 times more costly than the consequences of a test failure, $\beta = 0.999$, which could produce test levels over 10 dB higher than those associated with the customary $\beta = 0.95$. On the other hand, consider an item where a failure in test would lead to a difficult and expensive redesign, but the failure in flight would not be catastrophic, e.g., a "piggyback" space experiment that could be attempted again on a later flight. Figure 6.9 now says that the test level should be modest relative to the anticipated flight environment so as to minimize the risk of an overtest. For example, if a flight failure is assessed to be no more costly than the consequences of a test failure, $\beta = 0.50$, which could produce test levels over 10 dB lower than those associated with the customary $\beta = 0.95$. It is interesting to note that the commonly used value of $\beta = 0.95$ corresponds to a cost ratio of $C_T/C_F = 0.053$, meaning a flight failure is being assessed as 19 time more costly than the consequences of a test failure.

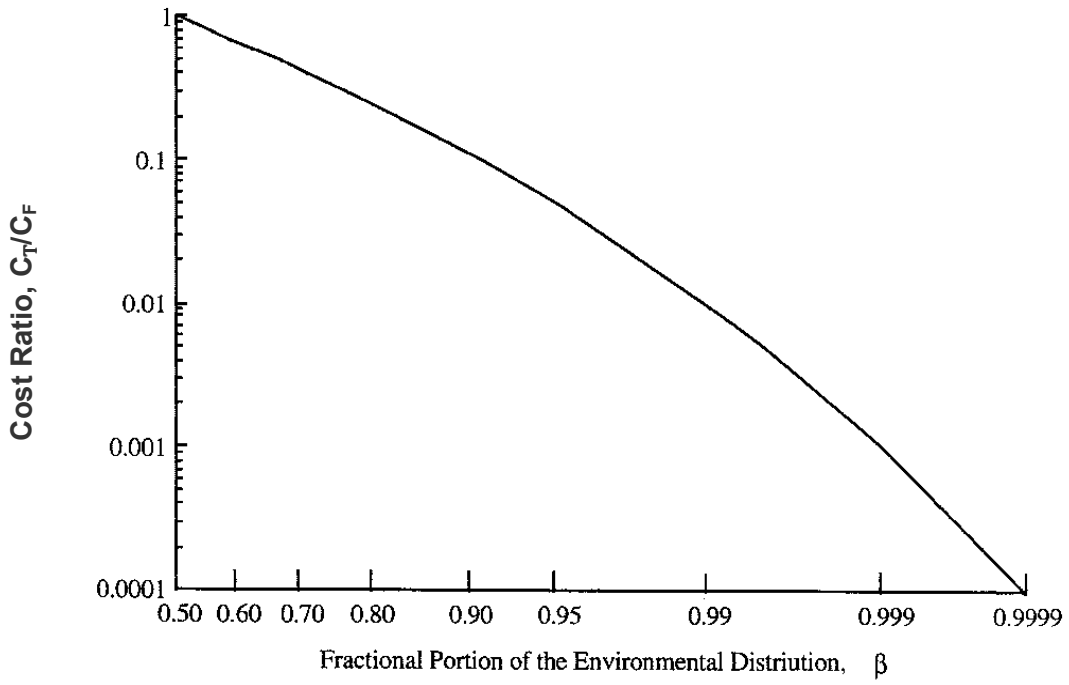

FIGURE 6.9. Optimum Selection of Fractional Portion β Versus Test to Flight Failure Cost Ratio.

In practice, an optimum procedure of the type shown in Figure 6.9 is rarely used to select the value of β for tolerance limit computations that will ultimately be used to arrive at test levels. This is probably due to two practical problems, as follows:

a. The procedure requires that someone specify a cost ratio, which produces an exposure to potential criticism, particularly if a flight failure occurs. This problem is most severe when the space vehicle is manned and human life is at risk.

b. The procedure leads to different values of β and, hence, different test levels for different components mounted on the same vehicle. This is inconsistent with the traditional desire to standardize test levels for flight vehicles and their components through general specification documents.

On the other hand, optimum test level selection procedures provide a statistically sound way to eliminate the unnecessary overtesting that often occurs when the standard test levels in a general specification are arbitrarily imposed, i.e., the procedure allows a logical method for "tailoring" tests to the requirements of specific payloads and components. Also, the selection procedure does not require the determination of quantitative "costs" in dollars, but only relative costs, which can be interpreted in qualitative terms. This allows such factors as the consequences of possible schedule delays caused by a test failure or the national embarrassment caused by a flight failure to be considered.

6.5 Restrictions on Input Motion Limits. The various limits detailed in Sections 6.1 and 6.2, as possibly modified by the considerations in Sections 6.3 and 6.4, yield the maximum expected environment (the maximum response at any point within a zone) in terms of the spectrum of a motion parameter, commonly acceleration, e.g., a maximum expected random vibration environment is usually described by an acceleration autospectral density function in g^2/Hz versus frequency in Hz (see Section 2.2.4). Such limits are applicable to the general description of the responses of flight vehicle structures to random dynamic loads, but care must be exercised when interpreting these limits as an input to equipment items that may be mounted on the vehicle structure. In particular, when the maximum expected environment in a zone is used to formulate dynamic design and/or test criteria for equipment that will be mounted in that zone, it must be remembered that a relatively heavy equipment item will load the structure and, hence, experience input motions that may be substantially less than those given by the computed maximum expected environment. This problem is particularly severe at the resonance frequencies of the equipment, where the apparent weight of the equipment becomes quite large [6.23] and the equipment essentially becomes a dynamic absorber [6.24]. If this problem is not addressed in the formulation of design and/or test criteria, severe overdesign or overtesting of the equipment may result.

6.5.1 Basic Principles. Assume a vehicle structure is subjected to a dynamic excitation that produces an acceleration response of x(t). Further assume that, when an item of equipment is attached to the structure, the acceleration response of the vehicle structure at the mounting points of the equipment becomes a(t). The autospectral density functions for the structural response accelerations with and without the equipment present are related by [6.25]

$$G_{aa}(f) = \frac{G_{xx}(f)}{\left|1 + \left[W_p(f)/W_s(f)\right]\right|^2} \qquad (6.20)$$

where

$G_{xx}(f)$ = autospectral density function of free acceleration x(t)
$G_{aa}(f)$ = autospectral density function of interface acceleration a(t)
$W_s(f)$ = source apparent weight function of vehicle structure
$W_p(f)$ = driving point apparent weight function of equipment

In Equation (6.20), the apparent weight terms are given by

$$W(f) = \frac{F(f)}{A(f)} \tag{6.21}$$

where F(t) is the Fourier transform of an applied force and A(f) is the Fourier transform of a response acceleration. For $W_s(f)$, the source apparent weight of the vehicle structure, F(f) is the Fourier transform of a force applied to the structure at the mounting point of the equipment, and A(f) is the Fourier transform of acceleration response of structure at that point due to the applied force. For $W_p(f)$, the driving point apparent weight of the equipment, F(f) is the Fourier transform of a force applied to the equipment at its mounting point, and A(f) is Fourier transform of the acceleration response of the equipment at its mounting point due to the applied force. When the acceleration response is measured in gravity units (g), W(f) has the units of N/g (lb/g). It should be mentioned that Equation (6.20) is sometimes presented in terms of mechanical impedance functions, Z(f) = F(f)/V(f), where V(f) is the Fourier transform of velocity. Mechanical impedance is related to apparent weight by $Z(f) = (2\pi f)W(f)/g$.

It is clear from Equation (6.20) that the vibration response of the vehicle structure with an equipment item present approaches the vibration response of the vehicle structure without the equipment item present as the driving point apparent weight of the equipment becomes small compared to the source apparent weight of the structure, i.e., $G_{aa}(f) \rightarrow G_{xx}(f)$ as $W_p(f)/W_s(f) \rightarrow 0$. Hence, a light weight equipment item mounted on a heavy structure will generally see about the same vibration environment as measured on the structure at the equipment mounting points without the equipment present. However, a heavy equipment item may substantially reduce the structural vibration at the equipment mounting points, particularly at the resonance frequencies of the equipment where the driving point apparent weight dramatically increases, e.g., the driving point apparent weight of a single degree-of-freedom system at its resonance frequency is $W_p(f_n) = QW$ where $Q = 1/(2\zeta)$ and $W = Mg$ (ζ is the damping ratio and M is the modal mass of the system). Unfortunately, this reduction in the vibration input to equipment items, particularly at their resonance frequencies, is not accounted for in design or test criteria based upon a computed maximum expected environment that has been smoothed over frequency, as derived in Sections 6.1 through 6.4.

Theoretically, if the driving point apparent weight of the equipment and the source apparent weight of the vehicle structure at the equipment mounting points were both known, corrected input motion levels to the equipment for design and/or test purposes could be computed using Equation (6.20). This is often done in establishing structural design criteria, but the problem is more complicated in establishing test criteria. Specifically, shock and vibration test levels for space vehicle equipment are often derived in generic terms (applicable to all equipment that might be mounted in a specific zone on the vehicle structure) using the maximum expected environment. To produce a vibratory motion input corresponding to the maximum expected environment, the vibration test machine will deliver enough force (within its capabilities) to achieve the specified input motions at the equipment mounting points even though such forces cannot occur in the flight environment, i.e., the vibration test machine behaves as if it has an infinite source apparent weight, even though the apparent weight of the flight vehicle structure where the equipment will be mounted is always finite. Hence, special procedures must be used

to limit the overtesting of equipment due to the essentially infinite source apparent weight of vibration testing machines through the use of either (a) input force limiting techniques, (b) simplified input acceleration limiting techniques, (c) response acceleration limiting techniques, or (d) acoustic tests involving the vehicle or a major subsystem thereof.

6.5.2 Input Force Limiting Procedures. Numerous approaches have been proposed to limit the force into equipment items during vibration tests so as to prevent overtesting at the resonance frequencies of the equipment. Three of the better known approaches that have been employed and/or experimentally evaluated are (a) force-acceleration product limiting [6.25], (b) interface force limiting based upon the test item driving point impedance [6.26], and (c) simplified interface force limiting based upon the test item total weight [6.27]. In all three procedures, it is necessary to measure the total force delivered to the test item during the vibration test. This is best accomplished by mounting the test item to its test fixture through force transducers at each attachment point, where the total force delivered to the test item is obtained by summing the signals from the force transducers. However, for vibration tests performed on electrodynamic shakers with wire-wound armatures, the total force can also be determined from armature voltage and current measurements with appropriate shaker table-fixture mass corrections, as discussed and illustrated in [6.28].

6.5.2.1 Force-Acceleration Product Limits. An early procedure to achieve force limiting is to use the product of the force and acceleration delivered to the test item [6.25]. The test procedure is as follows:

a. Attach the test item to an electrodynamic shaker through an appropriate test fixture with force transducers between the test item and the test fixture, and mount a control accelerometer near the attachment points of the test item to the test fixture. For vibration tests performed on electrodynamic shakers with wire-wound armatures, the shaker armature voltage and current can be used as a measurement of force [6.28].

b. Sum the signals from the force transducers (or use the shaker armature current signal) and multiply by the input acceleration signal from the control accelerometer. It is recommended in [6.25] that the average force-acceleration product be determined by taking the logarithms of the analog force and acceleration signals, and then summing and averaging the results. However, modern digital control systems can compute this average product directly in real time.

c. For sweep-sine test excitations, manually override the specified input motion signal from the control accelerometer to maintain an approximately constant average product of the force and acceleration signals through the narrow frequency range of each strong test item resonance.

d. For random test excitations, manually override the specified autospectrum for the input motion signal from the control accelerometer, as established by the shaker equalizer control system (see Section 10.1.1.3), to maintain an approximately constant average product of the force and acceleration signals through the frequency range of strong test item resonances.

Force-acceleration product limiting will automatically notch the specified motion test levels at the frequencies of strong test item resonances, as illustrated in Figure 6.10.

The advantages of the force-acceleration product limiting procedure are as follows:

a. It is relatively simple to implement, particularly for sweep-sine vibration tests where the shaker armature current is used as the force signal.

b. No source apparent weight data for the vehicle structure at the test item mounting points are required.

c. No driving point apparent weight data for the test item are required.

The primary disadvantage of the procedure is that it provides only an approximate correction for test item loading effects, although it is believed that the correction will usually produce realistic test conditions.

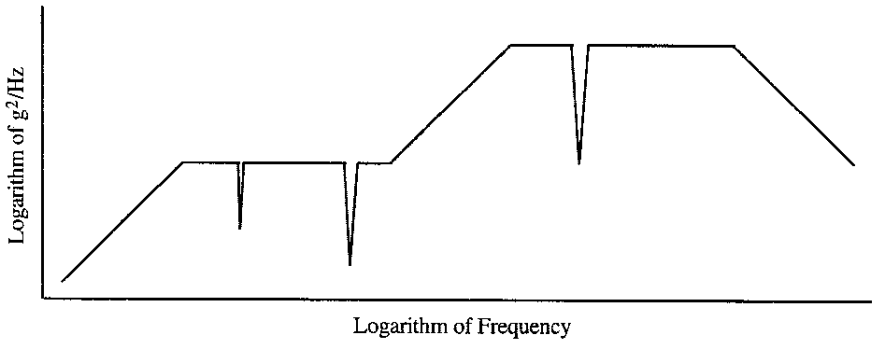

FIGURE 6.10. Illustration of Notching of Random Vibration Test Specification for Test Item.

6.5.2.2 Analytical Force Limits. The most accurate way to establish a force limit for a vibration test is to estimate the actual interface force between the test item and its mounting structure by analytical procedures. Specifically, the interface force for an equipment item mounted on a vehicle structure, to be used as the force limit for a vibration test, can be expressed by

$$G_{FF}(f) = |W_p(f)|^2 \, G_{aa}(f) \qquad (6.22)$$

where $G_{aa}(f)$ is the autospectrum of the interface acceleration given by Equation (6.20) and $W_p(f)$ is the driving point apparent weight of the test item. The driving point apparent weight of any test item can be easily measured prior to a vibration test by mounting the test item to the vibration test machine through force transducers between the test item and its test fixture, and applying a low level vibration input. The driving point apparent weight of the test item is obtained by computing the frequency response function between the force and the acceleration at the test item mounting points (see Section 6.5.1). The problem then essentially reduces to estimating the interface acceleration spectrum $G_{aa}(f)$, which in turn is dependent on the source apparent weight of the vehicle structure, $W_s(f)$. Procedures for determining a conservative estimate for the interface force spectrum in Equation (6.22) are summarized in [6.27] and its references. Assuming the necessary information is available, the test procedure is as follows:

a. Attach the test item to the vibration test machine through an appropriate test fixture with force transducers between the test item and its test fixture, and mount a control accelerometer near the attachment points of the test item to its test fixture. For vibration tests performed on electrodynamic shakers with wire-wound armatures, the shaker armature voltage and current can be used as a measurement of force [6.28].

b. Sum the signals from the force transducers and use this sum signal as the force control signal.

c. Using a dual control vibration test equalization system (see Section 10.1.1.4), apply the specified motion input test levels (either sweep-sine or random) through the main shaker equalizer control channel, and the analytically derived force limits computed using Equation (6.22) through the second shaker equalizer control channel such that the shaker will deliver the interface force limit at any frequency where the force required to achieve the specified motion exceeds the interface force.

Analytically derived force limits will automatically notch the specified motion vibration test levels as illustrated in Figure 6.10.

If properly implemented, the advantage of the analytical force limiting procedure is that it produces a test with a very low risk of either undertesting or severe overtesting. The primary disadvantages of the procedure are as follows:

a. Information concerning the source apparent weight of the vehicle structure where the test item will be mounted is required.

b. The driving point apparent weight of the test item must be measured prior to the test.

c. A dual control system for the vibration test machine is required, as detailed in Section 10.1.1.4.

6.5.2.3 Semi-Empirical Force Limits. A simplified way to derive force limits, which was originally proposed in [6.29], is outlined in [6.27] and demonstrated in [6.30]. The procedure essentially applies Equation (6.22) with the total weight of the test item replacing its driving point apparent weight, $W_P(f)$, and the specified motion input test levels replacing the interface acceleration, $G_{aa}(f)$, up to the first resonance frequency of the test item. Beyond the first resonance frequency, the total weight of the test item is reduced inversely with frequency, i.e., $W_P(f) = W_T(f_1/f)$; $f > f_1$, where f_1 is its first resonance frequency of the test item and W_T is its total weight. Specifically, for sine wave and transient tests, the Fourier transform of the force limit is given by

$$F(t) = C\, W_P(f)\, X(f) \text{ where } W_P(f) = W_T;\ f \le f_1, \text{ and } W_P(f) = W_T(f_1/f);\ f > f_1 \qquad (6.23)$$

where X(f) is the Fourier transform of the input motion test level in g, and C is an empirical correction factor. For random vibration tests, the autospectral density of the force limit is given by

$$G_{FF}(f) = C^2\, |W_P(f)|^2\, G_{xx}(f) \qquad (6.24)$$

where $G_{xx}(f)$ is the autospectral density of the input motion test level in g^2/Hz, and $W_P(f)$ is as defined in Equation (6.23).

A factor of C = 1.2 was recommended in [6.29], but a factor of C = 1 was considered adequate for the testing of several heavy components in the Cassini space vehicle in [6.30]. On the other hand, [6.27] states that $C \ge 1.4$ might be required for light weight components mounted on heavy structure. Quoting from [6.27], “Some judgement and reference test data for similar configurations must be considered to choose the value of C.. .” The test procedure is then the same as detailed in Section 6.5.2.2. See [6.30] for an illustration of the application of the procedure for the vibration testing of a large spacecraft.

The primary advantages of the simplified interface force limiting procedure are as follows:

a. No information concerning the source apparent weight of the vehicle structure where the test item will be mounted is required.

b. There is no need to measure the driving point apparent weight of the test item prior to the test.

c. If properly implemented, the procedure will produce test results with an accuracy similar to that provided by the more complex interface force limiting procedure in Section 6.5.2.2.

The primary disadvantage of the procedure is that a dual control system for the vibration test machine is required, as detailed in Section 10.1.1.4.

6.5.3 Input Acceleration Limiting Procedures. A simple procedure to restrict the possible overtesting of a test item due to the use of input motion test specifications is to modify the specified test levels at the frequency of the lowest resonance frequency (usually the strongest resonant response of the test item) using the procedure detailed in [6.31]. Specifically, the procedure is as follows:

a. Attach the test item to the vibration test machine with one accelerometer mounted near the attachment points of the test item to its test fixture (the input accelerometer), and a second accelerometer mounted at a selected location on the test item where the test item response is large at its first resonance frequency (the output accelerometer).

b. Using a low level vibration input, measure the frequency response function between the input and output accelerometers through the frequency range of the first test item resonance. For either a sine-wave or random excitation, the frequency response function H(f) can be computed as outlined in Section 2.2.12, where x(t) is the input acceleration and y(t) is the output acceleration.

c. From the computed frequency response function magnitude (gain factor) given by |H(f)|, compute a modified input motion vibration test specification as follows:

1. For sine-wave test excitations, either dwell or sweep, where the original input motion test specification is $P_x(f)$ in g (see Section 2.2.3), the modified test specification through the first resonance frequency of the test item is

$$P_x(f)_{mod} = \frac{P_x(f)}{\sqrt{|H(f)|}} \; ; \; 0 < f \leq \sqrt{2}\, f_n \qquad (6.25)$$

where f_n is the frequency of the first resonance of the test item.

2. For stationary random test excitations where the original input motion test specification is $G_{xx}(f)$ in g^2/Hz (see Section 2.2.4), the modified test specification through the first resonance frequency of the test item is

$$G_{xx}(f)_{mod} = \frac{G_{xx}(f)}{|H(f)|} \; ; \; 0 < f \leq \sqrt{2}\, f_n \qquad (6.26)$$

Input acceleration limiting produces a notch in the specified motion vibration test levels at the lowest resonance frequency of the test item. See [6.31] for details.

Three characteristics of the input acceleration limiting procedure should be mentioned, as follows:

a. Noting that $H(f_n) = Q = 1/(2\zeta)$, Equations (6.25) and (6.26) are essentially equivalent to reducing the input excitation at the first resonance frequency of the test item by $\sqrt{Q}$ for a sine-wave input $P_x(f)$ or Q for a random input $G_{xx}(f)$.

b. The input acceleration limiting procedure can be implemented by (a) applying a low level sweep sine wave excitation to the test item with constant amplitude through its first resonance frequency, (b) measuring the response of the test item through its first resonance frequency to obtain |H(f)|, and (c) reducing the specified excitation level in accordance with Equations (6.25) and (6.26).

c. It can be shown that the input acceleration limiting procedure is essentially equivalent to the force-acceleration product limiting procedure described in Section 6.5.2.1.

The advantages of the input acceleration limiting procedure are as follows:

a. It is relatively easy to implement for both sine-wave and random vibration tests.

b. No source apparent weight data for the vehicle structure where the test item will be mounted is required.

c. No force transducers between the test item and its mounting fixture on the vibration test machine are required.

The primary disadvantages of the procedure are as follows:

a. The frequency response function of the test item through its first resonance frequency must be measured prior to the test.

b. The procedure provides an approximate correction for mounting point impedance effects only at the lowest resonance frequency of the test item.

6.5.4 Response Acceleration Limiting Procedures. An alternate approach to force limiting or modification of the input acceleration test specification is to restrict the specified acceleration test levels to limit the response acceleration of one or more key parts or subassemblies in the test item. Of course, this approach requires information concerning the maximum response of those key parts or subassemblies of the test item during flight. In a few cases, such responses might have been measured on previous flights or be predicted by analytical procedures, but often the necessary information is not available. For those cases where the required response information is available, the procedure is as follows:

a. Attach the test item to the vibration test machine with one accelerometer mounted near the attachment points of the test item to its test fixture (the input accelerometer), and one or more additional accelerometers mounted at selected locations on critical elements of the test item (the output accelerometers). The critical elements are typically at locations where test item responses have been measured in flight or predicted by the procedures detailed in Section 5.

b. Beyond the input acceleration test specification for the test item, generate a maximum response spectrum for each of the response accelerometers mounted on the test item.

c. Using dual control procedures (see Section 9.1.1.4), apply the specified input acceleration test spectrum with the input acceleration levels notched so that none of the maximum response levels are exceeded at any frequency.

Response acceleration limiting will automatically notch the specified input acceleration test levels as illustrated in Figure 6.10.

The advantages of the response acceleration limiting procedure are as follows:

a. No driving point apparent weight data for the test item are required.

b. No source apparent weight data for the vehicle structure at the mounting points of the test item are required.

c. No force transducers between the test item and its test fixture are required.

The primary disadvantage of the procedure is that measurements or predictions for the response accelerations at critical locations on the test item are required.

6.5.5 Acoustic Test Procedures. A final approach to avoiding the overtesting of test items during a vibration test due to the essentially infinite apparent weight of the vibration test machine is to substitute an acoustic test for the vibration test. Specifically, if a prototype vehicle or a major subsystem thereof is available for an acoustic test, then all test items can be attached to the prototype vehicle structure exactly as they will be installed during flight, and the prototype vehicle can be subjected to an acoustic excitation that conservatively simulates the maximum aeroacoustic loads during flight. The result is a vibration test of all test items that properly accounts for the driving point apparent weight of the test item and the source apparent weight of the vehicle structure. Of course, the resulting vibration test will account only for those vibration environments that are of an aeroacoustic origin (see Section 3). However, the high frequency vibration environment for space vehicle equipment is typically dominated by the aeroacoustic loads-induced vibrations. The performance of acoustic tests is discussed in Section 10.5, and an illustration is given in [6.32].

The advantages of the acoustic test procedure are as follows:

a. No driving point apparent weight data for the test item are required.

b. No source apparent weight data for the vehicle structure at the mounting points of the test item are required.

c. No force transducers between the test item and its mounting structure are required.

d. Assuming the acoustic simulation is accurate, the risk of overtesting or undertesting is essentially eliminated at all frequencies.

The primary disadvantages of the procedure are as follows:

a. The space vehicle or a major subsystem thereof must be available for acoustic tests. Even when the vehicle is available, it usually is too late in the program for at least the qualification testing of space vehicle equipment.

b. A large, high intensity acoustic test facility is required.

6.5.6 Assessments. The comparative merits of the various procedures to limit the specified motion inputs to test items during vibration tests so as to avoid overtesting due to the essentially infinite apparent weight of the vibration test machine are summarized in Table 6.3. From Table 6.3, the acoustic test approach is the most desirable from all viewpoints, i.e., it is the easiest to control, provides the best accuracy, and requires the least apparent weight information for the equipment and its mounting structure in the vehicle. However, the acoustic test approach does require the availability of the vehicle or a major subsystem thereof, as well as a large acoustic test facility that can produce the intense acoustic pressure levels experienced by a space vehicle during its launch phase. Acoustic tests are the common choice for the final test in a flight vehicle program when the entire vehicle is available. However, vibration tests of individual equipment items are usually required before this late point in a program, i.e., at a time when the vehicle or a major subsystem thereof are not available. Among the procedures that employ a vibration test machine, the interface force limiting procedure is believed to provide the greatest degree of accuracy, although it requires the greatest amount of information to implement. The simplified interface force limiting procedure, which is much easier to implement and can provide similar accuracy, is also considered a good choice.

As a final point of evaluation, the force-acceleration product limiting, interface force limiting, and input acceleration modification procedures were compared in terms of the potential fatigue damage to a simple test item in [6.33]. That comparison ranked the force-acceleration product and the interface force limiting as the best choices, and further demonstrated the dramatic reduction in overtesting provided by both procedures.

TABLE 6.3. Summary of Merits of Various Procedures for Limiting Input Acceleration Test Levels.

Merit	Force Times Acceleration Limiting	Interface Force Limiting	Simplified Interface Force Limiting	Input Acceleration Modification	Response Acceleration Limiting	Acoustic Test
Simplicity of test requirement derivations.[1]	A	C	A	A	B	A
Accuracy of simulation in vibration test.[1]	B	A	A	B	B	A
Requires driving point apparent weight data.	No	Yes[2]	No	No[3]	No	No
Requires source apparent weight data.	No	Yes	No	No	No	No
Requires force transducers in vibration test[4].	Yes	Yes	Yes	No	No	No
Requires dual control in vibration test.	No	Yes	Yes	No	Yes	No

1. A - good; B - medium; C - poor.
2. Can be measured on a shaker using a low level vibration input prior to a full level vibration test.
3. Frequency response of equipment through its lowest resonance frequency must be measured.
4. Shaker current can sometimes be substituted for force transducer measurements.

6.6 Reconstruction of Waveforms for Transients. The maximum expected environment (MEE) for transients is commonly computed in the frequency domain using the procedures detailed in Sections 6.1 through 6.4, where the MEE represents a conservative limit for a collection of measured or predicted spectra defining the transient environment in a structural zone of concern. Either Fourier spectra, energy spectra, or shock response spectra, as defined in Sections 2.2.8 through 2.2.10, might be used to compute the MEE. On the other hand, some of the test procedures discussed in Section 10, particularly those applicable to low frequency (below 100 Hz) transient simulations on electrodynamic shakers, require a time history (waveform) for the specified test signal. When the MEE is defined in terms of a shock response spectrum (SRS), there is no direct analytical way to reconstruct a representative waveform because the SRS does not have a unique relationship to the waveform from which it is computed. For this case, test time history signals with an appropriate waveform are usually constructed using decaying sine waves [6.34 - 6.36] or wavelets [6.35, 6.36] ([6.36] includes FORTRAN programs). Also, energy spectra do not lend themselves to waveform reconstruction because they have no phase information. It follows that Fourier spectra should be used to define the MEE for transients when the reconstruction of a waveform is required for test simulation purposes.

Various ways to reconstruct waveforms from the MEE computed from Fourier spectra for transients are detailed and evaluated in [6.37, 6.38]. The procedure recommended in [6.38] is as follows:

a. Let the Fourier spectrum (see Section 2.2.8) for each measured or predicted transient used to compute the MEE be denoted by $F_i(f) = F_{i,Re}(f) + jF_{i,Im}(f)$; i = 1, 2, ..., N, where $F_{i,Re}(f)$ is the real part and $F_{i,Im}(f)$ is the imaginary part of the Fourier spectrum. It follows that the magnitude of each Fourier spectrum is given by

$$|F_i(f)| = \sqrt{F^2_{i,Re}(f) + F^2_{i,Im}(f)} \tag{6.27}$$

b. Compute the MEE of the i = 1, 2, ..., N Fourier spectrum magnitudes given by Equation (6.27) using one of the procedures detailed in Section 6.1 to obtain $|F_{MEE}(f)|$.

c. At each frequency for the computed Fourier spectra, $F_i(f)$; i = 1, 2, ..., N, determine the measured or predicted Fourier spectrum that has the largest magnitude $|F_i(f)|$ of the N measured or predicted values used for the MEE computation.

d. Again at each frequency, identify the phase angle of the Fourier spectrum with the largest magnitude determined in Step c above, and assign those phase angles to the MEE Fourier spectrum to obtain $F_{MEE}(f) = F_{MEE,Re}(f) + j\, F_{MEE,Im}(f)$.

e. Compute the inverse Fourier transform of the MEE Fourier spectrum determined in Step d above to obtain the MEE waveform.

6.7 References

6.1 Piersol, A. G., "Review of Procedures to Compute Maximum Structural Response from Predictions or Measurements at Selected Points," *J. Shock and Vibration*, Vol. 3, No. 3, pp 211-221, 1996.

6.2 Piersol, A. G., "Test Criteria and Specifications," Ch. 20, *Shock and Vibration Handbook*, 4th ed. (Ed: C. M. Harris), McGraw-Hill, NY, 1996.

6.3 Bendat, J. S., and Piersol, A. G., *Random Data: Analysis and Measurement Procedures*, 3rd ed., p. 355, Wiley, NY, 2000.

6.4 Wallace, C. C., et al, "Environmental Requirements and Test Criteria for the Orbiter Vehicle," *Spec. MF 0004-014*, Rev. E, Rockwell Intern./Space Division, Downey, CA, June 1989.

6.5 Condos, F. M., and Butler, W. L., "A Critical Analysis of Vibration Prediction Techniques," *Proc., Inst. Envir. Sc.*, pp 321-326, 1963.

6.6 Barrett, R. E., "Statistical Techniques for Describing Localized Vibration Environments of Rocket Vehicles," *NASA TN D-2158*, July 1964.

6.7 Anon., "Procedures Utilized in Developing All-Random Vibration Test Specifications for Titan III," *BBN Rep. No. 1083*, Bolt Beranek and Newman, Canoga Park, CA, 1964.

6.8 Piersol, A. G., "Vibration and Acoustic Test Criteria for Captive Flight of Externally Carried Aircraft Stores," *AFFDL-TR-71-158*, Dec. 1971.

6.9 Bowker, A. H., and Lieberman, G. J., *Engineering Statistics*, 2nd ed., pp 314-315, Prentice-Hall, Englewood Cliffs, NJ, 1972.

6.10 Owen, D. B., “Factors for One-Sided Tolerance Limits and for Variables Sampling Plans,” *Sandia Monograph SC-R-607*, Sandia Corp., Albuquerque, NM, Mar. 1963.

6.11 Ross, S. M., *Introduction to Probability and Statistics for Engineers and Scientists*, Wiley, NY, 1987.

6.12 Kendall, M. G., and Stuart, A., *The Advanced Theory of Statistics*, Vol. 2, "Inference and Relationships,” pp 128-130, Hafner, NY, 1961.

6.13 Piersol. A. G., "Optimum Resolution Bandwidth for Spectral Analysis of Stationary Random Vibration Data,” *J. Shock and Vibration*, Vol. 1, No. 1, pp 33-43, 1993.

6.14 Guttman, I., Wilks, S. S., and Hunter, J. S., *Introductory Engineering Statistics*, 3rd ed., p. 311, Wiley, NY, 1982.

6.15 Schmidt, H., "Resolution Bias Errors in the Spectral Density, Frequency Response and Coherence Function Measurements,” *J. Sound and Vibration*, Vol. 101, No. 3, pp 347-427, 1985.

6.16 Bandgren, H. J., and Smith, W. C., "Development and Application of Vibroacoustic Structural Data Banks in Predicting Vibration Design and Test Criteria for Rocket Vehicle Structures,” *NASA TN D-7159*, Feb. 1973.

6.17 Pendleton, L. R., and Henrikson, R. L., "Flight-to-Flight Variability in Shock and Vibration Levels Based on Trident I Flight Data,” *Proc., 53rd Shock and Vibration Symp.*, Classified Supplement (Unclassified paper), 1983.

6.18 Choi, S. C., and Piersol, A. G., "Selection of Test Levels for Space Vehicle Component Vibration Tests,” *ASQC J. Electronics Div.*, Vol. 4, No. 3, pp 3-9, July 1966.

6.19 Shinozuka, M., and Yang, J. N., "Optimum Structural Design Based on Reliability and Proof-Load Testing,” *JPL TR 32-1402*, Jet Propulsion Lab., Pasadena, CA, June 1969.

6.20 Young, J. P., "Spacecraft Vibration Test Level Cost Optimization Study,” *Proc., 44th Shock and Vibration Symp.*, pp 99-105, 1974.

6.21 Piersol, A. G., "Criteria for the Optimum Selection of Aerospace Component Vibration Test Levels,” *Proc., Inst. Envir. Sc.*, pp 88-94, Apr. 1974.

6.22 Piersol, A. G., "Optimum Levels for Shock and Vibration Acceptance Tests,” *Proc., 66th Shock and Vibration Symp.,* pp 221-230, 1995.

6.23 Smallwood, D. O., "The Application of Unloaded (Free) Motion Measurements and Mechanical Impedance to Vibration Testing,” *Proc., Inst. Envir. Sc.*, pp 71-82, 1976.

6.24 Reed, F. E., "Dynamic Vibration Absorbers and Auxiliary Mass Dampers,” Ch. 6, *Shock and Vibration Handbook* (Ed: C. M. Harris), 4th ed., McGraw-Hill, NY, 1996.

6.25 Witte, A. F., “Realistic Vibration Tests,” *Instrumentation Technology*, Vol. XX, pp 45-48, Feb. 1970.

6.26 Scharton, T. D., “Vibration-Test Force Limits Derived from Frequency-Shift Method,” *J. Spacecraft and Rockets*, Vol. 32, No. 2, pp 312-316, 1995.

6.27 Scharton, T. D., “Force Limited Vibration Testing Monograph,” *NASA RP-1403*, 1997.

6.28 Smallwood, D. O., “Shaker Force Measurements Using Voltage and Current,” *Proc., 67th Shock and Vibration Symp.*, Vol. I, pp 31-37, 1996.

6.29 Salter, J. P., “Taming the General-Purpose Vibration Test,” *Shock and Vibration Bulletin*, No. 33, Pt. III, pp. 221 - 217, 1964.

6.30 Scharton, T. D., and Chang, K., “Force Limited Vibration Testing of Cassini Spacecraft and Instruments,” *Proc., 17th Aerospace Testing Sem.*, pp 85-93, 1997.

6.31 Sweitzer, K. A., “A Mechanical Impedance Correction Technique for Vibration Tests,” *Proc., 33rd ATM, Inst. Envir. Sc.*, pp 73-76, May 1987.

6.32 Lee, Y. A., and Lee, A. L., “Recommended Practice for High Intensity Acoustic Test,” *Proc., 42nd ATM, Inst. Envir. Sc.,* Vol. PR/DTE, pp 200-204, May 1996.

6.33 Gatscher, J. A., and Kawiecki, G., “Review: Comparison of Mechanical Impedance Methods for Vibration Simulation,” *J. Shock and Vibration*, Vol. 3, No. 3, pp 223-232, 1966.

6.34 Smallwood, D. O., and Nord, A. R., “Matching Shock Spectra with Sums of Decaying Sinusoids Compensated for Shaker Velocity and Displacement Limitations,” *Shock and Vibration Bull.*, No. 44, Pt 3, pp. 43 - 56, 1974.

6.35 “Shock Testing on Shakers by using Digital Control,” *IES Technology Monograph*, Inst. of Envir. Sc., Mount Prospect, IL, 1986.

6.36 Nelson, D. B., “Parameter Specification for Shaker Shock Waveform Synthesis; Damped Sines and Wavelets,” *Proc., 60th Shock and Vibration Symp.*, Vol. III, pp. 151 - 193, 1989.

6.37 Hine, M. J., “Controlling Conservatism in Transient Vibration Testing,” *Proc., 15th Aerospace Testing Sem*., pp. 231 - 237, 1995.

6.38 Hine, M. J., “Transient Synthesis using a Fourier Transform Envelope,” *J., Inst. Envir.*, Vol. XXXIX, No. 5, pp. 17 - 22, 1996.

7. COMPUTATION OF ENVIRONMENT DURATION

From the viewpoint of exposure duration, the space vehicle dynamic environments summarized in Section 3 can be divided into three categories, as shown in Table 7.1. The transient (shock) environments are usually described by a time history (see Section 2.2.1) or a single spectral function that reflects a mixture of both the magnitude and duration of the entire event (see Sections 2.2.8 - 2.2.10). Nevertheless, the specific durations of transient events are of concern in the formulation of design and test criteria [7.1].

TABLE 7.1. Summary of Space Vehicle Dynamic Loads by Type.

Type of Dynamic Load	Source of Dynamic Load	Details (Section)
Transient or shock loads (less than one second)	Seismic loads**	3.2
	Motor ignition overpressure*	3.4
	Liftoff release*	3.5
	Engine/motor thrust transients	3.9
	Thrust vector loads	3.10
	Stage and fairing separations*	3.14
	Pyrotechnic events*	3.15
	Soil penetration transients**	3.19
	Meteoroid impacts**	3.20
Short duration acoustic or vibration loads (a few seconds to a few minutes)	Wind during ascent	3.3
	Engine/motor acoustic noise*	3.6
	Structureborne noise	3.7
	Aerodynamic noise*	3.8
	Pogo**	3.11
	Motor resonant burning**	3.12
	Fuel slosh in tanks	3.13
	Operations induced loads	3.16
	Planetary descent and entry*	3.18
Long duration acoustic or vibration loads (more than one hour)	Transportation**	3.1
	Wind on launch pad	3.3
	Onboard equipment operations	3.17

* Usually the dominant loads for a normal flight.
** Could be the dominant loads if they occur.

The acoustic and vibration loads, both short and long term, are described by spectra that may vary with time (see Sections 2.2.3 - 2.2.6). These time-varying spectra are commonly collapsed into a single maximax spectrum (see Section 2.2.7), which is then used to formulate design and test criteria. The problem is to determine a duration for the dynamic loads at the maximax levels that will produce the same damage to the hardware as the actual nonstationary dynamic environment. To arrive at an appropriate duration for all dynamic loads used to establish design and test criteria, it is first necessary to make assumptions concerning the modes and mechanisms for the potential failure of the hardware to be designed and/or tested.

7.1 Failure Models. A failure of an item of space vehicle hardware is defined as any deterioration of performance or any damage or malfunction that prevents the hardware from accomplishing its intended purpose. There are two basic types of failures that may be caused by a dynamic loads environment, as follows:

a. Hard failure: A hard failure involves permanent physical damage that makes the hardware unable to perform its intended purpose, even after the dynamic load is terminated. Hard failures generally result in observable damage, such as the fracture of a structural element or the permanent disability of an electronic element.

b. Soft failure: A soft failure involves a malfunction or deterioration of performance during the dynamic load exposure that makes the hardware unable to accomplish its intended purpose, but after the dynamic load is terminated, the hardware does not reveal any damage and functions properly. Soft failures occur most commonly in electrical, electronic, and/or optical elements, although soft failures occasionally occur in complex mechanical elements, such as gyroscopic devices.

A failure mechanism is the specific means by which an item of hardware is damaged by exposure to a dynamic load. All failure mechanisms are dependent on the magnitude of the dynamic load, but many are also dependent on the duration of the load as well. Those failure mechanisms that are dependent on both the magnitude and duration of the dynamic load are referred to as time-dependent failure mechanisms. Soft failures are rarely time-dependent, i.e., they usually occur immediately at the start of the dynamic load exposure. On the other hand, hard failures usually are time-dependent, although there are some exceptions. For example, if a shock or vibration load produces stresses that exceed the ultimate strength of a critical element in the hardware, a fracture will occur immediately at the start of the exposure.

For the purpose of establishing an appropriate duration for design and test purposes, time-dependent failure mechanisms (usually producing hard failures) are of greatest interest. Common examples of time-dependent failure mechanisms for equipment exposed to dynamic environments are fatigue damage, force contact wear, relative velocity wear, and the loosening of bolts or rivets [7.2 - 7.8]. There are several analytical models that have been used to relate the time-to-failure of hardware to the magnitude and duration of a dynamic load environment, including (a) the inverse power law model, (b) a fatigue damage model based upon peak stress versus number of cycles to failure, and (c) a fatigue damage model based upon the growth rate of an existing crack. There also is one purely magnitude dependent model that is sometimes assumed to determine the time-to-failure for hardware exposed to random vibration environments, namely, the first passage model.

7.1.1 Inverse Power Law Model. For a wide class of time-dependent failure mechanisms, the time-to-failure T_F for hardware exposed to a stationary dynamic load x(t) (periodic or random) with a mean value of zero and an rms value of σ_x can be approximated by the "inverse power law" [7.5] given by

$$T_F = c\,\sigma_x^{-b} \tag{7.1}$$

where b and c are constants dependent on the type of hardware. The inverse power law is commonly used to model the time-to-failure of mechanical and electrical equipment due to operational loads, but it is equally applicable to environmental loads, including dynamic loads.

Using Equation (7.1), it follows that the exposure times for two dynamic loads with the same spectral content but different rms values can be scaled to produce the same failure potential by

$$T_2 = T_1 \left(\frac{\sigma_1}{\sigma_2} \right)^b \tag{7.2}$$

For random vibrations defined in terms of autospectra, Equation (7.2) becomes

$$T_2 = T_1 \left(\frac{G_1(f)}{G_2(f)} \right)^{b/2} \tag{7.3}$$

The primary problem in using Equation (7.2) or (7.3) is to arrive at an appropriate value for the exponent b. A detailed experimental study of time-to-failure data for small guided missiles [7.9] indicates that b = 4 is reasonable for the time-to-failure of complex electrical and electronic equipment, although the value of b may vary widely for individual equipment items. A value of b = 4 is also used in [7.10] to arrive at the durations for stationary vibration tests that simulate the same damage as nonstationary vibration environments for general space vehicle hardware.

For example, assuming b = 4, if an item of electrical or electronic equipment is exposed to a stationary dynamic load with an rms value of $\sigma_1 = 1$, and that load is increased without a change in spectral content to have an rms value of $\sigma_2 = 1.5$, the duration T_2 for the increased load that would produce the same time-to-failure as the original load over a duration of T_1 is $T_2 = 0.20\ T_1$, or about 20% of the original exposure duration. The same result is obtained if the autospectrum of the load increases at all frequencies by a ratio of $(1.5)^2 = 2.25$.

7.1.2 Fatigue Damage Model Based Upon S-N Curve. Structural fatigue is a very complicated subject involving the principles of fracture mechanics [7.7]. In highly simplified terms, however, if a structural material is subjected to repeated applications of a load producing an adequate stress level, cumulative damage occurs that ultimately causes a crack to initiate and grow until the structure fails. The adequate stress level required to allow the accumulation of damage is referred to as the “fatigue limit” or “endurance limit” of the material. Fatigue data for various structural materials are commonly presented as peak stress (S) versus the total number of loading cycles-to-failure (N), i.e., the number of cycles needed to cause both a crack to initiate and grow to a critical length where a complete fracture occurs. Such data plots are referred to as S-N curves, and are widely published for many different materials [7.11 - 7.15]. Various functional forms have been proposed for the S-N curves of metals [7.16], but as a first order of approximation, an idealized S-N curve involving two straight lines on a plot of log S versus log N is commonly assumed, as illustrated in Figure 7.1. As a further simplification, if the fatigue limit of the material is ignored, the idealized S-N curve in Figure 7.1 can be defined by a single straight line on a plot of log S versus log N, leading to the relationship

$$N = c\,S^{-b} \tag{7.4}$$

where b and c are material constants. Note that if the number of cycles-to-failure N is proportional to the time-to-failure T, and the peak stress S is proportional to the rms value of the dynamic load σ_x, Equation (7.4) is simply a special case of the inverse power law in Equation

(7.1). Hence, assuming the spectrum of the dynamic load does not change, Equations. (7.2) and (7.3) apply.

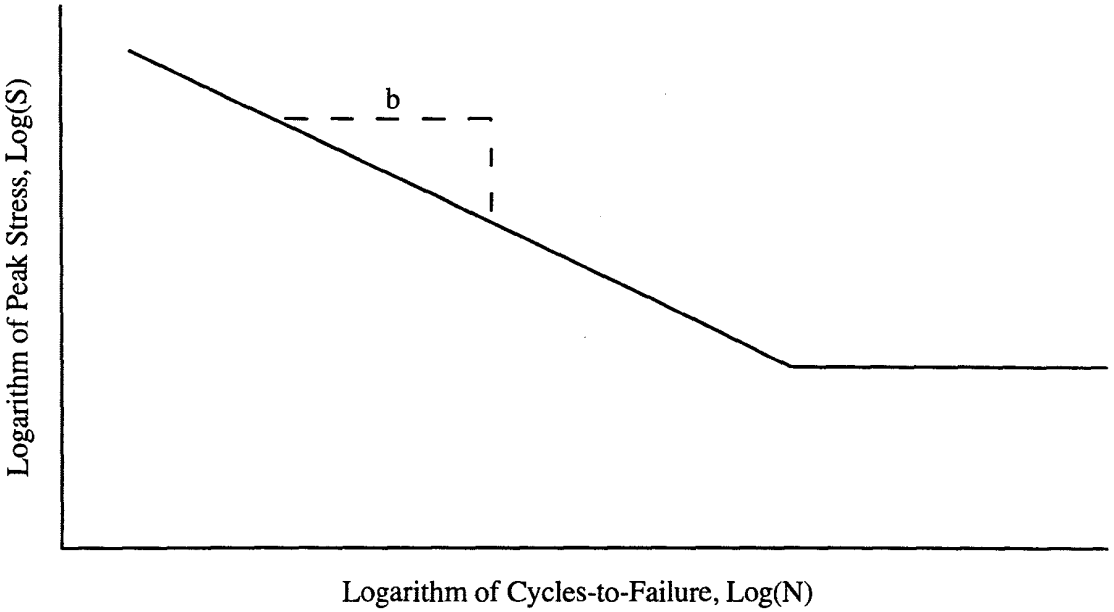

FIGURE 7.1. Idealized S-N Curve for Structural Materials.

The value of the exponent b (sometimes called the fatigue parameter) in Equation (7.4) can vary widely depending on the material, its geometry (notch factor), the mean stress level, other environmental factors (e.g., temperature and corrosion), and the characteristics of the vibration (e.g., periodic versus random), but 6 to 9 are the most commonly assumed values for unnotched steel and aluminum alloys. Specifically, b = 9 is recommended in [7.17], b = 6.4 is suggested in [7.18], and b = 6.4 for sinusoidal vibration and b = 8 for random vibration are specified in [7.19].

It should be mentioned that Equation (7.4) ignores the fatigue limit of the material; i.e., it assumes any dynamic stress peak will cause fatigue damage, no matter how small its magnitude. In practice, many of the stress peaks in the flight environment may fall below the fatigue limit of the structural material, while most or all of the stress peaks during a test at levels above the flight environment will be above the fatigue limit. It follows that Equations (7.2) and (7.3) are inherently conservative when the damage mechanism is structural fatigue. However, because most of the fatigue damage occurs at the highest stress peaks, which are probably above the fatigue limit of the structural material in both the test and the service environment, the degree of conservatism is not excessive in most situations. Nevertheless, more accurate results that account for the fatigue limit of the material can be obtained, if desired, by using the procedures detailed in [7.20].

7.1.3 Fatigue Damage Model Based Upon Crack Growth Rate. The greatest uncertainty in predicting the fatigue life of a material is in the crack initiation phase. Specifically, the time to initiate a crack is heavily influenced by the smoothness of the material surfaces and environmental factors, particularly those that accelerate corrosion [7.7]. However, once a crack has initiated, the growth of the crack can be quite accurately predicted using the principles of fracture mechanics [7.7]. It is for this reason that fatigue life predictions for load-carrying structures are commonly made by assuming a small crack exists, and then predicting the time required for the crack to become sufficiently large to cause a fracture using an appropriate crack

growth rate model. Two primary characteristics of the crack must be defined to arrive at an appropriate crack growth rate model, as follows:

a. The crack displacement mode, i.e., the relative movement of the two surfaces of the crack. The most common displacement mode for the types of fatigue cracks that commonly occur in aerospace vehicle hardware is where the displacement of the crack surfaces is normal to the crack length, as illustrated in Figure 7.2 and referred to as Mode I in [7.7].

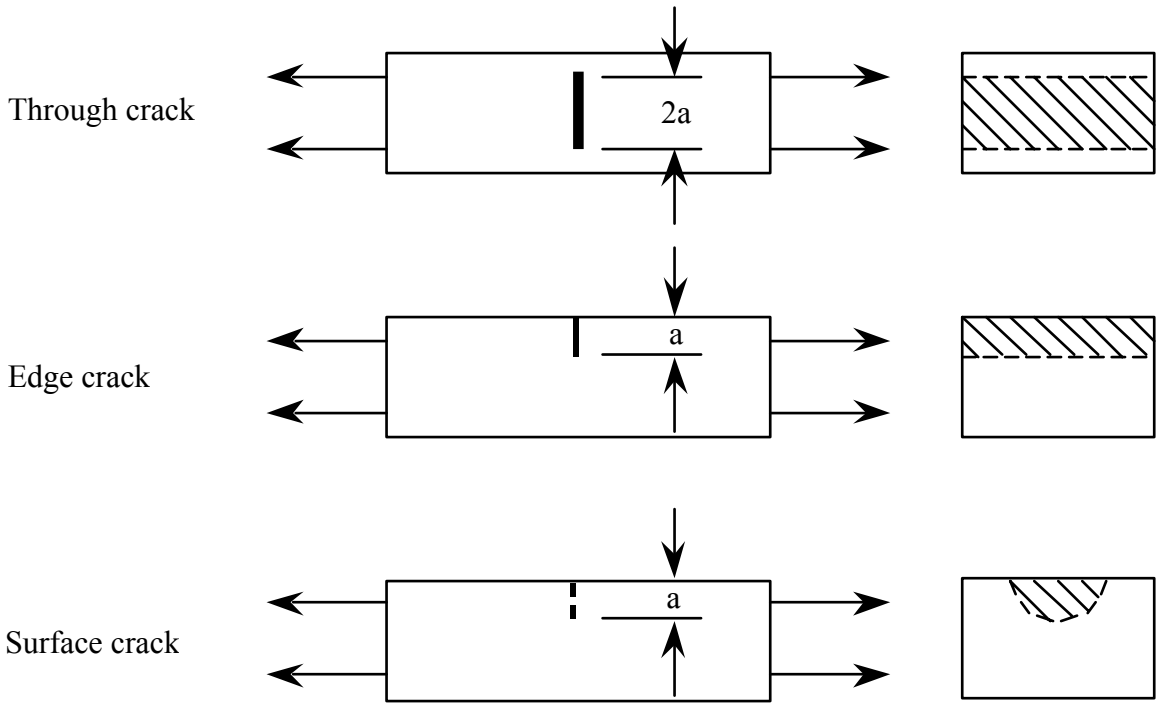

FIGURE 7.2. Common Crack Locations for Mode I Crack Displacement.

b. The location of the crack, i.e., a crack in the edge of a flat panel as opposed to a crack in one surface of the panel. An illustration of common crack locations is presented in Figure 7.2. Using the principles of fracture mechanics, the "stress-intensity factor range" for a crack in a structure exposed to dynamic loading is defined as

$$\Delta K = C \Delta S \sqrt{\pi a} \qquad (7.5)$$

where

ΔS = peak-to-peak range of the nominal stress in the vicinity of the crack
a = parameter of the crack length or depth (see Figure 7.2)
C = constant (for small through cracks, C = 1; for small edge cracks, C = 1.12; and for small surface cracks, C = 1.12 to 1.25 depending on the ratio of the peak stress to the yield stress of the material. See [7.7] for more exact values of C).

Based upon the stress-intensity factor range (ΔK), the crack growth rate (increased crack length per cycle denoted by da/dN) for any given material plots on log-log paper as shown in Figure 7.3.

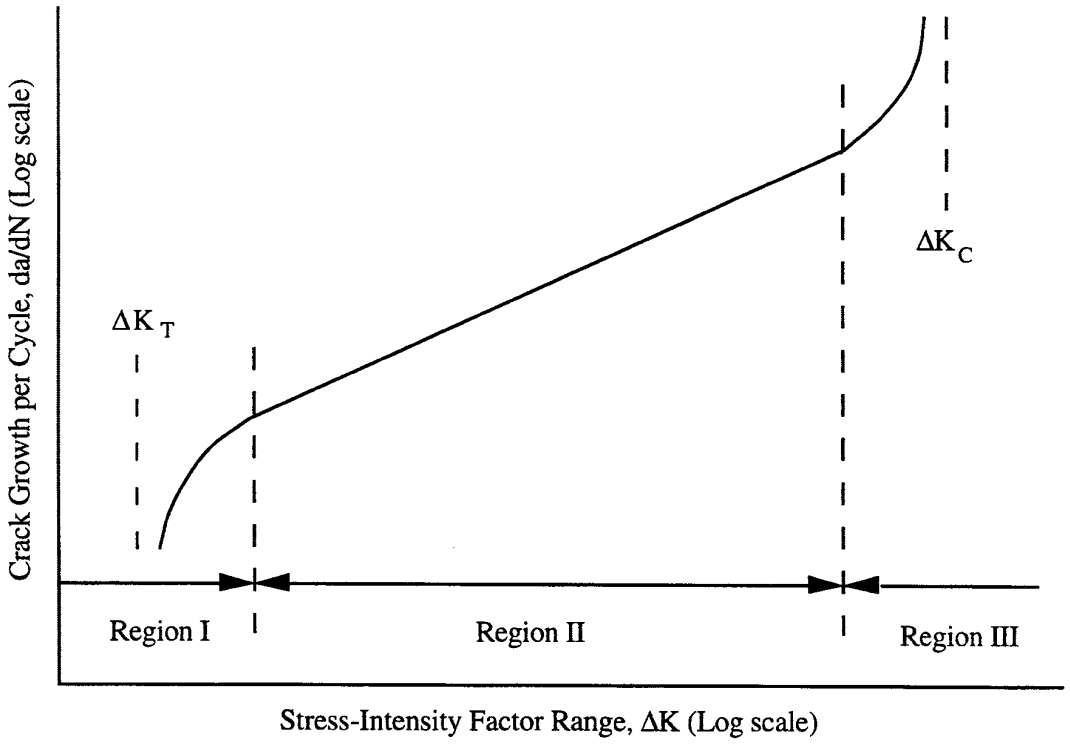

FIGURE 7.3. Crack Growth Rate Versus Stress-Intensity Factor Range for Typical Metal.

Note in Figure 7.3 that the plot of log (da/dN) versus log (ΔK) divides into three regions. Region I is the threshold region and defines the value of ΔK needed to cause the crack to increase in size, i.e., for $\Delta K \le \Delta K_T$, the crack will not grow (e.g., from [7.15], $\Delta K_T \approx 2.2$ MPa for aluminum alloy 2024-T3). Region III is the critical region and defines the value of ΔK where the crack growth rate accelerates to a complete fracture of the material, i.e., for $\Delta K = \Delta K_C$, the structure fails (e.g., from [7.15], $\Delta K_C \approx 153$ MPa for aluminum alloy 2024-T3). Region II is the intermediate region where log (da/dN) varies in a near-linear manner with log (ΔK) so that the crack growth rate can be approximated by

$$\frac{da}{dN} = A\left(\Delta K\right)^m \tag{7.6}$$

where A and m are constants (see [7.11 - 7.15] for more exact relationships between da/dN and ΔK). For complex or random stress time histories, it is shown in [7.7] that ΔK in Equation (7.6) can be replaced by the rms value of the stress-intensity factor ranges, i.e.,

$$\Delta K \approx \Delta K_{rms} = \sqrt{\sum_{i=1}^{N} \frac{\Delta K_i^2}{N}} \tag{7.7}$$

where $\Delta K_i = C\ \Delta S_i\ \sqrt{\pi a}$ and ΔS_i is the peak-to-peak value of the ith stress cycle in the stress time history; i = 1, 2, ..., N. A stress cycle and its peak-to-peak value is commonly determined using the "rain-flow" counting procedure [7.21], which reduces a complex or random stress time history to N individual stress cycles in a systematic manner that closely correlates with crack growth rates.

The values of the constants A and m in Equation (7.6) vary somewhat from one type of metal to another, but only slightly from one alloy to another of the same metal. For example, the crack growth rate data for various high strength aluminum alloys closely fit Equation (7.6) in the range $11\ \text{MPa} < \Delta K < 33\ \text{MPa}$, as follows:

$$\frac{da}{dN} \approx 1.5 \times 10^{-10} (\Delta K)^{2.5}\ \text{m/cycle} \tag{7.8}$$

Also, the values of the constants A and m are relatively insensitive to the static load on the structure (the mean stress level). However, the mean stress does strongly influence the onset of Region III in Figure 7.3, i.e., the larger the mean stress, the smaller the value of ΔK_C. See [7.7, 7.12 - 7.15] for more exact crack-growth rate models for specific materials including 2024-T3 and 7075-T6, which are widely used in aerospace vehicle structures and equipment.

Since the stress intensity factor range (ΔK) includes the square root of the crack length (a), Equation (7.6) must be solved in an iterative manner to predict the number of cycles required to increase the crack size to failure (see [7.7] for illustrations). It is easy to accomplish this iteration on a computer, and crack growth rate models are recommended to make conservative fatigue life predictions for aerospace vehicle structures. However, the dependence of ΔK on the crack length makes it impractical to use Equation (7.6) to scale the number of cycles at lower stress levels to the number of cycles at a higher stress level needed to produce equivalent damage in terms of a net crack growth.

7.1.4 First Passage Model. Certain types of failures occur because the stress in or the motion of a hardware element exceeds a critical value. For example, a switch or relay may open because the inertial load produced by an acceleration momentarily exceeds the force holding the switch or relay in its desired position, or two vibrating circuit cards in an electronic unit may collide because their separation distance momentarily becomes less than zero. In such cases, if the response of the hardware element to an applied dynamic load is periodic, failure will either occur during the first cycle of the response or it will never occur, i.e., the failure mechanism is not time dependent. For stationary random loads, however, the probability of exceeding a critical response value increases as the exposure duration increases, as illustrated in Figure 7.4. To be specific, let x(t) be the response parameter of concern (i.e., acceleration, displacement, stress, etc.), where the mean value of x(t) is zero ($\mu_x = 0$). Assuming the crossings of a critical level X are statistically independent (uncorrelated), the probability that a response will exceed a critical level X at least once in an exposure duration T_X is given by [7.3]

$$P(T_X) = 1 - \exp\left[-\nu_X^+ T_X\right] \approx \nu_X^+ T_X \text{ if } P(T_X) < 0.1 \tag{7.9}$$

where ν_x^+ is the average number of upper crossings per second of the level X. If it is further assumed the response x(t) is normally distributed (Gaussian) with an autospectrum (see Section 2.2.4) and a standard deviation (see Section 2.2.2) of $G_{xx}(f)$ and σ_x, respectively, then Equation (7.9) becomes [7.22]

$$P(T_X) \approx \nu_0^+ T_X \exp\left(\frac{-X^2}{2\sigma_x^2}\right) \tag{7.10}$$

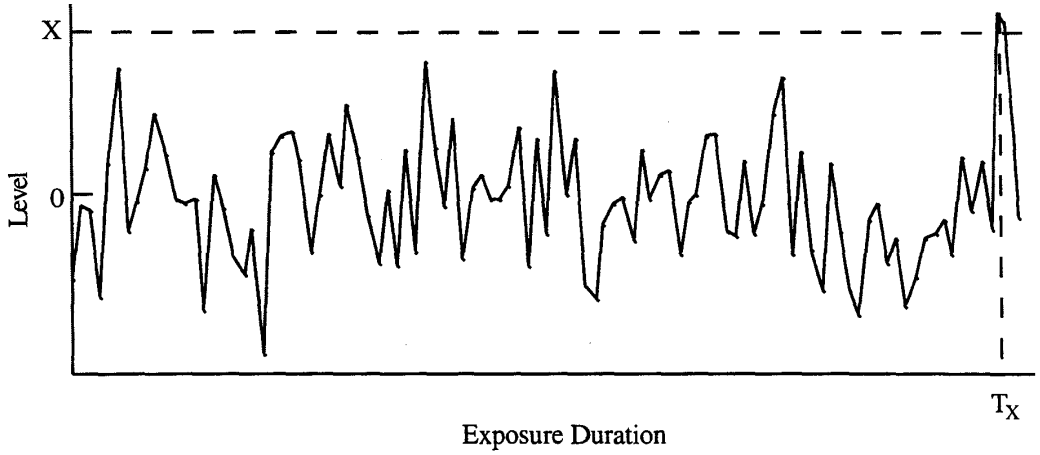

FIGURE 7.4. Exceedance of a Critical Level by a Random Load.

where ν_0^+ is the average number of upward crossings per second of zero [the mean value of x(t)], given by

$$\nu_0^+ = \left[\frac{\int_0^\infty f^2 G_{xx}(f)\,df}{\sigma_x^2}\right]^{1/2} \tag{7.11}$$

Hence, the expected time for x(t) to cross a critical level X is estimated by

$$T_X \approx \frac{P(T_X)}{\nu_0^+} \exp\left(\frac{X^2}{2\sigma_x^2}\right) \tag{7.12}$$

It is common to further reduce Equation (7.12) by assuming the response x(t) is dominated by a single resonant mode of the hardware element (corresponding to a simple oscillator) so as to produce a narrow bandwidth response centered at f_n, the natural frequency of the oscillator. For this case, $\nu_0^+ \approx f_n$ in Equation (7.11), and Equation (7.12) becomes

$$T_X \approx \frac{P(T_X)}{f_n} \exp\left(\frac{X^2}{2\sigma_x^2}\right) \tag{7.13}$$

In Equations (7.12) and (7.13), T_X is commonly interpreted as the time-to-failure, denoted by T_F. It should be mentioned that there is a basic conflict between the statistical independence assumption needed to arrive at Equation (7.12) and the narrow bandwidth response assumption leading to Equation (7.13), namely, the crossings of any level X by narrow bandwidth random signals are not statistically independent [7.3]. However, it has been demonstrated by unpublished studies using analog computer models of structures that Equation (7.13) makes an acceptable approximation for the probability of at least one crossing in a duration T_X, even for a narrow bandwidth response, if the critical level is at least four times the rms value of the response, i.e., $X \geq 4\sigma_x$. Empirical data for the first crossing of a critical level with $P(T_X) = 0.05$ by a simple oscillator with 5% damping is shown in comparison with the prediction of Equation (7.13) in Figure 7.5. For example, if a structural response is dominated by a single resonance with 5% damping at $f_n = 100$ Hz, Figure 7.5 states that the probability is 5% that the level $X/\sigma_x = 4$ will be exceeded in $T_X \approx 1.5$ seconds, or the level $X/\sigma_x = 5$ will be exceeded in $T_X \approx 134$ seconds.

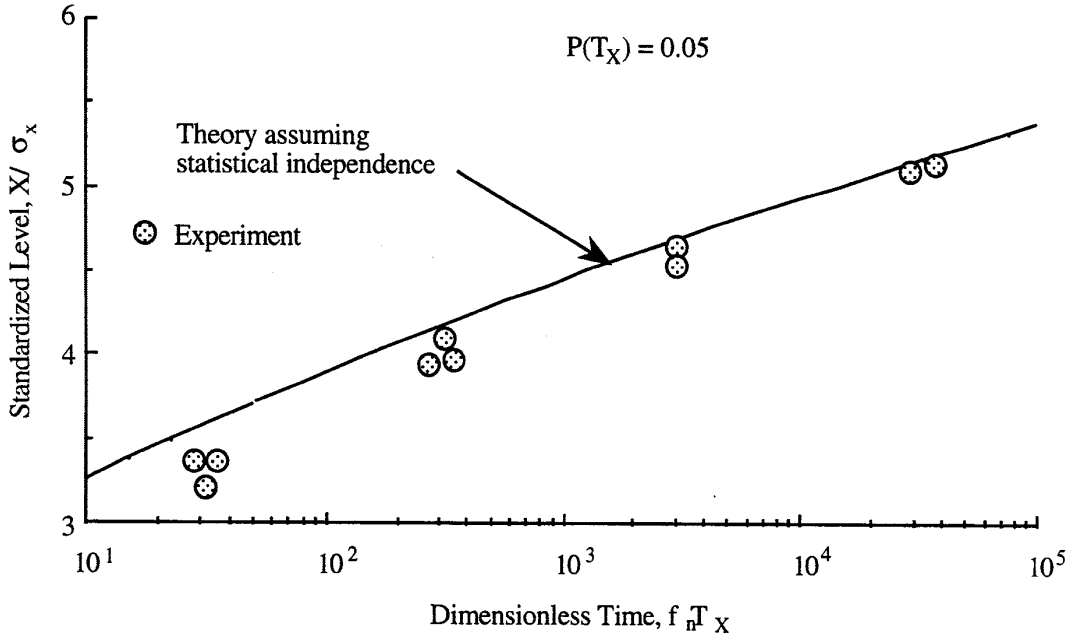

FIGURE 7.5. Time to First Crossing of a Critical Level with a Probability of 5%.

Using either Equation (7.12) or Equation (7.13), it follows that the exposure times for two random responses with the same spectral content (ν_0^+ or f_n constant), but different rms values, can be scaled to produce the same failure potential by

$$T_2 = T_1 \exp\left[\frac{K^2}{2}\left(\frac{\sigma_1^2}{\sigma_2^2} - 1\right)\right] \quad \text{where } K = X/\sigma_1 \tag{7.14}$$

For example, if a stationary random (Gaussian) vibration response with an rms value of $\sigma_1 = 1$ is increased to have an rms value of $\sigma_2 = 1.5$, and the level at which a failure will occur is $X = 4$, the duration T_2 for the increased response that would produce the same probability of failure as the original response over a duration of T_1 is $T_2 = 0.012\ T_1$, or about 1% of the original exposure duration.

Predictions of the time-to-failure based upon the first passage model using Equation (7.10) involve two major problems, as follows:

a. The model requires a knowledge of the value X that will cause a failure. Such information may be available in some cases, but not in others.

b. The model is vulnerable to the assumption that the structural response is Gaussian out to instantaneous values in excess of four standard deviations. The presence of even small periodic components in the response, or minor nonlinearities in the hardware, will cause substantial errors in the predicted time-to-failure.

7.1.5 Assessments. For the purposes of scaling the exposure durations for vibration environments, the fatigue damage model based upon crack growth rates (Section 7.1.3) and the first passage model (Section 7.1.4) are not recommended for the reasons detailed in those sections. For space vehicle hardware involving electrical or electronic equipment, the inverse power law model outlined in Section 7.1.1 is recommended with a value of b = 4 for all types of vibration, unless a different value can be justified by available data. For load carrying structures, the fatigue damage model based upon an S-N curve discussed in Section 7.1.2 is recommended with a value of b = 8 for all types of vibration, unless a different value can be justified by available data.

7.2 Durations of Short Term Acoustic and Vibration Loads. The launch events outlined in Table 7.1 consist of transients and short term acoustic and vibration loads. It is recommended that all transients loads be simulated for design and test purposes using a transient excitation with a conservative estimate of the magnitude of the service transient (see Section 6), and a spectral content and duration that are similar to the service transient. Launch events that produce short term acoustic or vibration environments are usually nonstationary, but the loads produced by such events are typically simulated by a stationary acoustic or vibration excitation with a level corresponding to the maximax spectrum (see Section 2.2.7) of the nonstationary event . The problem is to determine an appropriate duration for the stationary excitation simulating the nonstationary acoustic or vibration launch environment.

7.2.1 Approximate Procedure. The nonstationary acoustic and vibration environments associated with key launch events (liftoff and flight through the transonic and maximum dynamic pressure speed ranges) generally display a short time-averaged rms value versus time that first increases to and then decreases from a maximum value, as illustrated for typical Space Shuttle launch vibration data in Figure 7.6. To reduce the nonstationary event to a stationary excitation at the maximax level during the event, it is common to establish an equivalent stationary duration by computing the time between those points where the time-varying rms value of the nonstationary event is a specific number of dB below the maximum rms value, as illustrated in Figure 7.7. The number of dB below the maximum rms value used to establish the equivalent stationary duration is often determined somewhat arbitrarily, with 1, 2, or 3 dB being the most common selections. However, the selection can be made on a more quantitative basis using one of the damage models reviewed in Section 7.1.

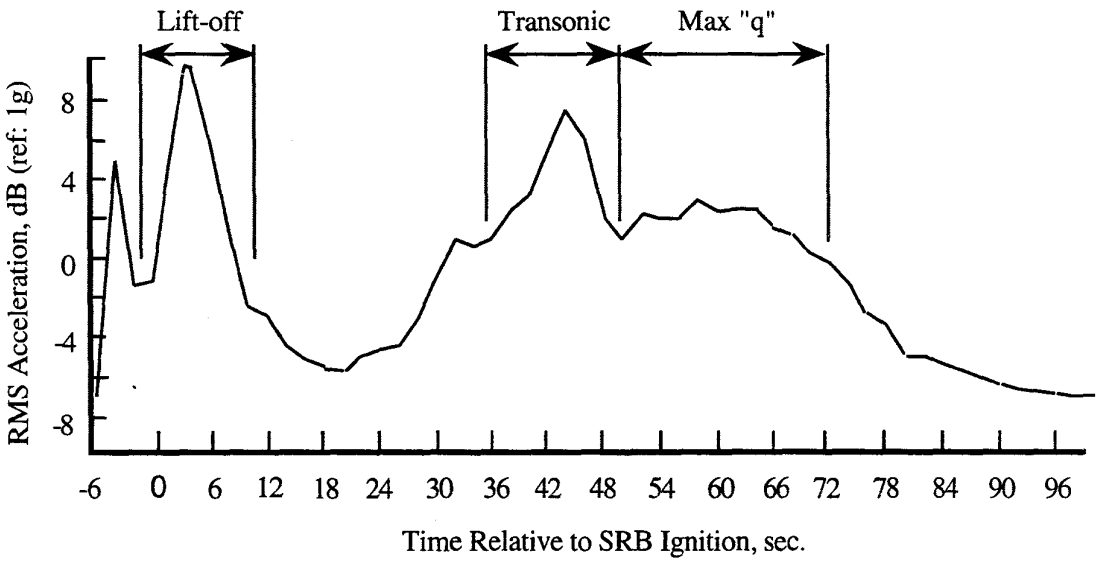

FIGURE 7.6. RMS Value of a Typical Vibration Measurement During a Space Shuttle Launch.

Specifically, let the following assumptions apply to the acoustic or vibration load with a zero mean value during a nonstationary launch event:

a. The time-varying rms value of the load, denoted by $\sigma_x(t)$, varies as a half-sine function through the nonstationary event, i.e.,

$$\sigma_x(t) = \sigma_{max} \sin\left[\frac{\pi t}{P/2}\right] \; ; \; 0 \le t \le P/2 \qquad (7.15)$$

where σ_{max} is the maximum rms value and P/2 is the half-period of the sine wave.

b. The spectral content of the dynamic load (the shape of the time-varying autospectrum) does not change through the nonstationary event.

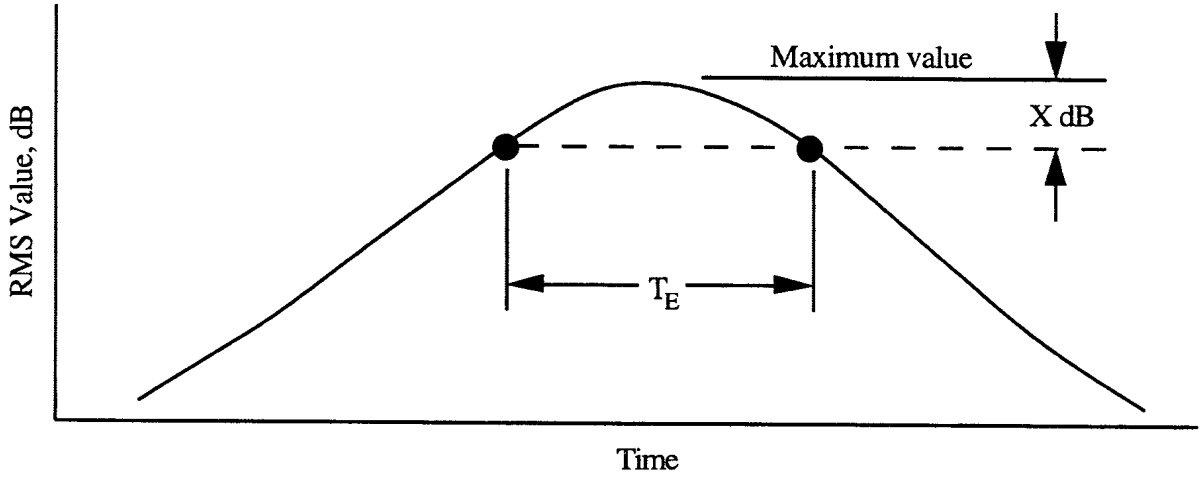

FIGURE 7.7. Determination of Equivalent Stationary Duration for Nonstationary Event.

Using either the inverse power law model in Equation (7.1) or the fatigue damage model in Equation (7.4), an equivalent duration for a stationary acoustic or vibration environment that will produce the same damage as the time-varying environment defined in Equation (7.15) can be expressed as

$$T_E = \int_0^{P/2} \left[\sigma_x(t)/\sigma_{max}\right]^b dt = \int_0^{P/2} \sin^b\left[\frac{\pi t}{P/2}\right] dt \qquad (7.16)$$

The solution of Equation (7.16) gives $T_E = 0.375\,P/2$ for b = 4 (the recommended exponent for equipment in Section 7.1.5) and $T_E = 0.273\,P/2$ for b = 8 (the recommended exponent for structures in Section 7.1.5). When centered on the maximum of the time-varying rms value in Equation (7.15), these durations correspond to the time between those rms values on either side of the maximum rms value that are below the maximum rms value by the number of dB summarized in Table 7.2.

TABLE 7.2. Values of Time-Varying RMS Acoustic or Vibration Environment that Bound the Duration of a Stationary Environment Producing Equivalent Damage.

Value of Exponent, b	Time-Varying RMS Values Relative to Maximum RMS Value	
	Exact Value	Recommended Conservative Value
b = 4	- 1.60 dB (83% of maximum value)	- 2 dB (79% of maximum value)
b = 8	- 0.83 dB (91% of maximum value)	- 1 dB (89% of maximum value)

From Table 7.2, if an equivalent stationary acoustic or vibration environment is desired for the design or test of electrical or electronic equipment (b = 4) exposed to a nonstationary flight environment, and the rms value of the stationary design or test environment equals the maximum rms value of the nonstationary flight environment, the duration between the rms values of the flight environment that are 2 dB below the maximum rms value should be used to establish the duration of the equivalent stationary environment. For structures (b = 8), the duration between the rms values of the flight environment that are 1 dB below the maximum rms value should be used.

In practice, the determination of the equivalent stationary durations for nonstationary flight events is based upon specific acoustic and/or vibration time history measurements, where a time-varying rms value for each measurement is computed by the procedures detailed in [7.23], which are based upon analytical developments in [7.24]. When several measurements are available for the same nonstationary event from several flights, the equivalent stationary duration should be estimated for all or a representative sample of the available measurements. To assure conservatism, the longest duration computed from the various measurements should be used to define the duration of the stationary acoustic or vibration environment for design and test purposes, assuming a longer duration is not specified (see Section 8.2).

7.2.2 Numerical Procedure. Rather than using an approximation for the time-varying characteristics of the nonstationary acoustic and/or vibration environment during various launch events, as given by Equation (7.15), a more accurate equivalent stationary duration can be determined by substituting the actual time-varying rms value during each flight event into Equation (7.16), and solving for the equivalent stationary duration T_E by numerical integration. Because of the large value of the exponent b in Equation (7.16), it is sufficient to perform the numerical integration over those rms values that vary by at least 2:1 about the maximum rms value. This approach is illustrated using a vibration measurement made inside the payload bay of Space Shuttle during lift-off, as shown in Figure 7.8. The time-varying rms value in this figure was computed using an exponentially-weighted average with an time constant of 0.5 sec, which corresponds to the optimum averaging time constant for Space Shuttle lift-off vibration data determined using the procedures in [7.23].

The numerical integration of the data in Figure 7.8 yields an equivalent duration of T_E = 2.6 sec for b = 4, and T_E = 1.9 sec for b = 8. Using the approximate procedure in Section 7.2.1 with the conservative values detailed in Table 7.2, the equivalent duration is T_E = 2.4 sec for b = 4, and T_E = 2.0 sec for b = 8. The agreement is rather good (within 8%), verifying that the approximate procedure in Section 7.2.1 generally produces acceptably accurate equivalent durations.

As discussed in Section 7.2.1, several measurements may be available for the same nonstationary event from several flights. Again, the equivalent stationary duration should be estimated for all or a representative sample of the available measurements, and the longest duration computed from the various measurements should be used to define the duration of the stationary acoustic or vibration environment for design and test purposes, assuming a longer duration is not specified (see Section 8.2).

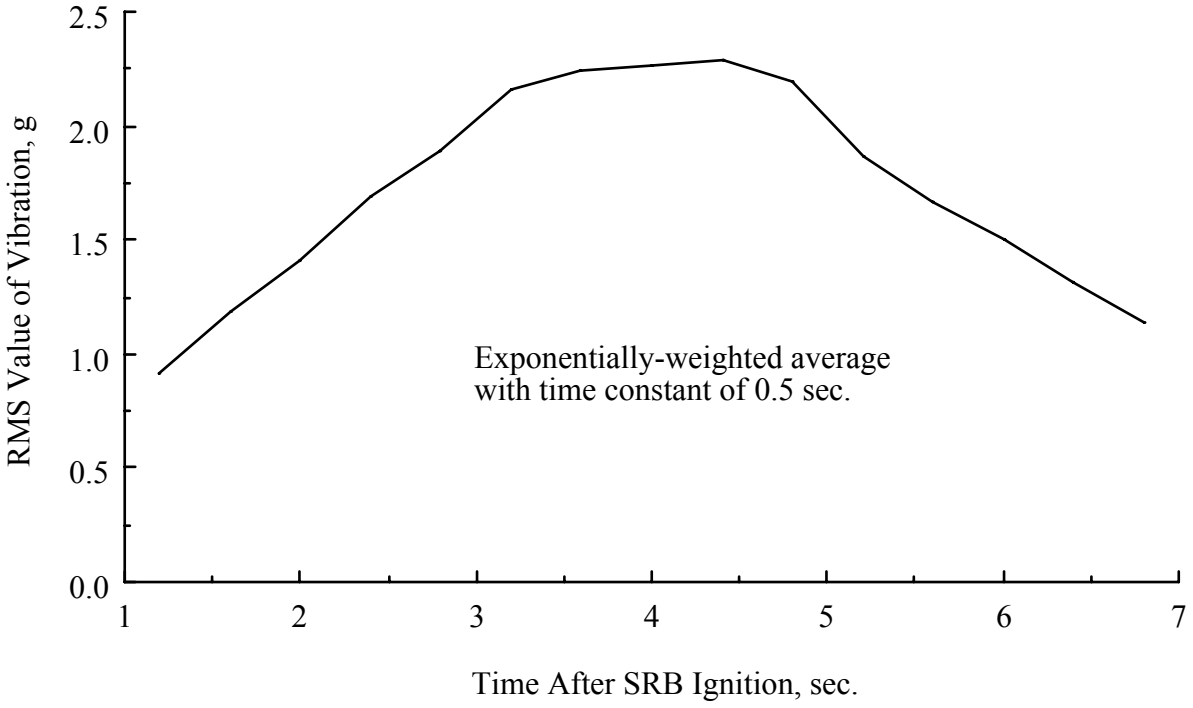

FIGURE 7.8. Time-Varying RMS Value of Space Shuttle Payload Bay Vibration During Lift-Off.

7.2.3 Procedure for Multiple Flight Events. The procedures detailed in Sections 7.2.1 and 7.2.2 for selecting an equivalent stationary duration for nonstationary flight events will usually be applied separately to each of several important flight events, e.g., lift-off, transonic flight, and flight through maximum dynamic pressure (see Figure 7.6). For design purposes, the maximax levels and equivalent stationary durations for the individual events can be evaluated separately to arrive at a final design. For testing purposes, however, it is usually desired to have only one acoustic or vibration test with a single test spectrum to represent the entire flight environment. A single test spectrum can be established by simply determining the maximax spectrum for all events together, i.e., the maximax of the maximax spectra for the individual events. A single equivalent duration can be established by the following procedure:

a. Compute the equivalent stationary duration and maximax spectrum for each of the individual events.

b. If the maximax spectra for the various events have a similar spectral content,

    1. compute the maximax rms value for each event (the square root of the area under the maximax spectrum),
    2. scale the equivalent stationary duration for each event to the largest maximax rms value of the various events using Equation (7.2) with the appropriate value for the exponent b, as recommended in Section 7.1.5, and
    3. sum the scaled equivalent stationary durations to obtain the total duration for the entire flight.

c. If the maximax spectra for the various events have significantly different spectral content,

    1. divide the frequency range of the maximax spectra for the various events into frequency increments where the maximax spectra have a similar spectral content,
    2. for each frequency increment, scale the equivalent stationary duration for each event to the largest maximax spectral value for the various events using Equation (7.3) with the appropriate value for the exponent b, as recommended in Section 7.1.5,
    3. sum the scaled equivalent stationary durations for each frequency increment, and
    4. select the longest total equivalent stationary duration among the various frequency increments to arrive at the total duration for the entire flight.

In many cases, the short term acoustic and/or vibration environments for space vehicle hardware is dominated by the environment during a single event. For example, the acoustic and/or vibration environment for a payload inside the fairing or payload bay of a launch vehicle is commonly most severe at all frequencies during lift-off, which usually has an equivalent stationary duration of less than 3 sec (see the example in Section 7.2.2). In this case, even after scaling the longer duration events (e.g., flight through maximum dynamic pressure) to the maximum flight levels, the total equivalent stationary duration for the entire flight may be only a few secs. Hence, for practical reasons associated with establishing a test spectrum, it may be necessary to use an actual test duration that is longer than the computed equivalent stationary duration for the entire flight. In no case, however, should the final test criteria exceed the design criteria for the space vehicle hardware.

7.2.4 Assessments. When estimates for nonstationary acoustic and/or vibration measurements during nonstationary flight events are available in numerical form, the numerical procedure detailed in Section 7.2.2 is recommended to arrive at an appropriate duration for a stationary excitation that will simulate the damage potential of the time-varying flight environment when the rms value of the stationary excitation is equal to the maximum rms value

of the time-varying environment. However, if the available nonstationary measurements are not available in a form convenient for the numerical integration required by the procedure in Section 7.2.2, the approximate procedure presented in Section 7.2.1 should provide acceptable results.

As a concluding comment on equivalent stationary durations for short term, nonstationary acoustic and vibration loads, when used for design and/or test criteria, the derived equivalent stationary durations should be multiplied by a scatter factor of four (see Section 8.1.1.1). In addition, it must be emphasized that NASA-STD-7001 specifies minimum durations for acoustic and vibration tests, which are detailed later in Section 8.2.4. These specified durations are highly conservative and generally will exceed the durations derived by the procedures detailed here, even after multiplying by a scatter factor of four. Hence, for most space vehicles and their components being developed for NASA programs, the specified durations in NASA-STD-7001 will prevail.

7.3 Durations of Long Term Acoustic and Vibration Loads. The long term acoustic and vibration environments listed in Table 7.1 may be stationary (e.g., loads due to continuous in-flight equipment operations), but it is more common for long term environments to be nonstationary. The duration of such environments can often be reduced for design and test purposes by using Equation (7.2) or (7.3) to scale the less severe acoustic and vibration levels to the most severe levels that occur during the entire exposure to the long term environment. Such scaling procedures are most applicable to acoustic and vibration loads that vary in overall level, but not substantially in spectral content, and where the dominant failure mechanism is anticipated to fit the inverse power law or fatigue damage model given by Equations. (7.1) and (7.4), respectively. For example, consider a payload that must be transported for 25 hrs by truck to a launch site for installation in a launch vehicle. Assume the anticipated vibration environment for the payload at its mounting points is as summarized in Table 7.3. Further assume b = 4 in Equation (7.2), and the spectra of the vibrations during the various transportation conditions have similar shapes. Table 7.3 indicates the damage potential of the 25 hour transportation vibration exposure can be simulated by a stationary vibration with a duration of 1.5 hrs (90 minutes) at the maximum transportation vibration level.

TABLE 7.3. Computations for Duration of Payload Transportation Vibration Environment.

Type of Road Segment	Duration on Road Segment (hrs)	RMS Vibration on Road Segment (g)	Equivalent Duration on Road Segment A (hrs)
A - Unpaved secondary roads	1	3	1.0
B - Improved secondary roads	4	1.6	0.3
C - Primary roads	8	1.0	0.1
D - Major highways	12	0.9	0.1
		Total equivalent duration on road segment A (hrs)	1.5

For those vibration environments where the spectral content, as well as the overall levels, change during the environmental exposure, the equivalent duration computations illustrated in Table 7.3 must be made on a frequency-by-frequency basis using Equation (7.3), or a similar expression for the appropriate spectral description in Section 3. This will result in a different equivalent stationary duration at each frequency, as discussed previously in Section 7.2.3. In most cases, to be conservative, the design or testing of the hardware should be based upon the longest equivalent stationary duration computed at all frequencies.

Whether or not the spectral content of the acoustic or vibration environment varies during a long term exposure, there is a potential error in the computation of an equivalent stationary duration due to an error in the assumed value for the exponent b in Equation (7.2) or (7.3). However, most of the time-dependent damage experienced by space vehicle hardware in a nonstationary acoustic or vibration environment occurs during exposure to the maximum level, which typically covers a small fraction of the total duration of the environment (see Table 7.3). In such cases, reducing the relatively long durations of the less severe vibrations by scaling to the maximum level according to Equation (7.2) or (7.3) does not introduce a major error, even if the exponent in the equation is inaccurate.

7.3.1 Accelerated Acoustic and Vibration Tests. From the viewpoint of testing, situations may arise where scaling the less severe segments of a nonstationary acoustic or vibration environment to a stationary level corresponding to the maximum level of the environment may yield a test duration that is still too long to be practical, e.g., the test duration of 90 minutes computed for the 25 hour transportation environment in Table 7.3 may still be too long for testing purposes. In such a case, it is common to further reduce the test duration by increasing the test level beyond the maximum level of the full environment [7.5]. Indeed, if no limit is placed on the rms test level in Equation (7.2), the test duration theoretically can be made as short as desired, provided the ultimate strength of the hardware being tested is not exceeded. However, increasing the test level beyond the maximum level produced by the service acoustic or vibration environment introduces major uncertainties in the test results, particularly if the hardware is fabricated using different materials and/or incorporates electrical, electronic, and/or optical elements. The problem is that the failure mechanisms of some elements may not comply with the scaling law in Equation (7.2). Furthermore, even if all failure mechanisms do comply with Equation (7.2), the exponent b may vary from one element to another within the hardware. Hence, increasing the test level to accelerate the test in compliance with Equation (7.2) may cause some elements of the hardware to be undertested and others to be overtested. The result could be the occurrence of unrepresentative failures during the accelerated test, as illustrated in [7.9].

7.3.2 Durability and Functional Tests. A common procedure to suppress unrepresentative failures that may be caused by accelerating a test of hardware with a long term acoustic or vibration environment is to perform two separate tests, namely, a durability test and a functional test. The durability test is intended to reveal only time-dependent failures, and is rapidly accelerated to produce the same damage as the entire duration of the long term acoustic or vibration environment based upon a specific damage model, e.g., Equation (7.2). The hardware is not required to function during the durability test, and any failures that are not time-dependent are ignored. The separate functional test is intended to reveal failures that are not time-dependent (i.e., failures related only to the acoustic or vibration level), and is not accelerated with test levels that exceed the maximum expected level during the long term acoustic or vibration environment. The hardware is required to function during the test, but since the failures of interest are not time-dependent, the test duration is not critical, e.g., the test duration is often fixed by the time required to fully operate the hardware and verify that it properly performs its intended purpose.

7.3.3 Environmental Durations for Design Criteria. When computing dynamic loads exposure durations for design purposes, the durations for all planned acoustic and vibration tests, as well as the number of transient loads, must be included in the total exposure duration. This is particularly important for hardware that may undergo repeated acceptance tests after refurbishing. For example, there probably will be many equipment items on Space Station that will be returned to Earth and refurbished at regular intervals, where certain parts and subassemblies are replaced but the basic structure of the equipment is maintained. Since such

equipment will undergo a flight acceptance test after each refurbishing, the total number of anticipated flight acceptance tests, as well as the launch environments to return the equipment to the Space Station, must include in the design criteria exposure duration for the basic structure of the equipment. This total exposure duration should also be reflected in the test duration for the qualification test of the equipment (see Section 8.2.4).

7.4 References

7.1 Hine, M. J., “Controlling Conservatism in Transient Vibration Testing,” *Proc., 15th Aerospace Testing Sem.,* Inst. Envir. Sc., pp 231-237, Oct. 1994.

7.2 Hu, J. M., Baker, D., Dasgupta, A., and A. Arora, "Role of Failure-Mechanism Identification in Accelerated Testing,” *J. IES*, Vol. XXXVI, No. 4, pp 39 - 45, July/Aug. 1993.

7.3 Crandall, S. H., and Mark, W. D., *Random Vibration in Mechanical Systems*, Academic Press, NY, 1963.

7.4 Preumont, A., *Random Vibration and Spectral Analysis*, Kluwer Academic, Dordrecht, The Netherlands, 1994.

7.5 Nelson. W., *Accelerated Testing*, Wiley, NY, 1990.

7.6 Stallmeyer, J. E., "Mechanical Properties of Metals Used in Equipment Design,” Ch. 35, *Shock and Vibration Handbook* (Ed: C. M. Harris), 4th ed., McGraw-Hill, NY, 1995.

7.7 Barsom, J. M., and Rolfe, S. T., *Fracture and Fatigue Control in Structures*, 2nd ed., Prentice-Hall, Englewood Cliffs, NJ, 1995.

7.8 Wirsching, P. H., Paez, T. L., and Ortiz, K., *Random Vibrations*, Wiley, NY, 1995.

7.9 Meeker, D. B., and Piersol, A. G., "Accelerated Reliability Testing Under Vibroacoustic Environments,” *Reliability Design for Vibroacoustic Environments* (Ed: D. D. Kana and T. G. Butler), AMD - Vol. 9, ASME, NY, 1974.

7.10 Anon., "Test Requirements for Booster, Upper-Stage, and Space Vehicles,” *MIL-STD-1540C*, 1994.

7.11 Frost, N. E., Marsh, K. J., and Pook, L. P., *Metal Fatigue*, Oxford Univ. Press, London, 1974.

7.12 Boyer, S. R., *Atlas of Fatigue Curves*, Amer. Soc. Metals, Metals Park, OH, 1986.

7.13 Anon., “Metallic Materials and Elements for Aerospace Vehicle Structures,” *Military Standardization Handbook MIL-HDBK-5E*, 1988.

7.14 Symonds, J., "Mechanical Properties of Materials", Ch. 5, *Marks' Standard Handbook for Mechanical Engineers* (Ed: E. A. Avallone and T. Baumeister III), 9th ed., p. 5-9, McGraw-Hill, NY, 1987.

7.15 Rice, R. C., et al, "Consolidation of Fatigue and Fatigue-Crack-Propagation Data for Design Use," *NASA CR-2586*, Oct. 1975.

7.16 Heywood, R, B., *Designing Against Fatigue*, Chapman and Hall, London, 1962.

7.17 Curtis, A. J., Tinling, N. G., and Abstein, H. T., "Selection and Performance of Vibration Tests," *SVM-8*, Shock and Vibration Info. Analysis Center, 1971.

7.18 Steinberg, D. S., *Vibration Analysis for Electronic Equipment*, 2nd ed., Wiley, NY, 1988.

7.19 Anon., " DOD Test Method Standard for Environmental Engineering Considerations and Laboratory Tests," *MIL-STD-810E*, Change Notice 3, July 31, 1995.

7.20 Himelblau, H., Fuller, C. M., and Scharton, T. D., "Assessment of Space Vehicle Aeroacoustic-Vibration Prediction, Design, and Testing," *NASA CR-1596*, July 1970.

7.21 Dowling, N. E., "Fatigue Failure Predictions for Complicated Stress-Strain Histories", *J. Materials*, Vol. 7, No. 1, pp v-1 - v-17, 1972.

7.22 Bendat, J. S., and Piersol, A. G., *Random Data: Analysis and Measurement Procedures*, 3rd ed., p. 161, Wiley, NY, 2000.

7.23 Himelblau, H., Piersol, A. G., Wise, J. H., and Grundvig, M. R., "Handbook for Dynamic Data Acquisition and Analysis," *IES-RP-DTE012.1*, Inst. Envir. Sc., Mt Prospect, IL, 1994.

7.24 Bendat, J. S., and Piersol, A. G., *Engineering Applications of Correlation and Spectral Analysis*, 2nd ed., Wiley, NY, 1993.

8. DESIGN AND TEST CRITERIA

The primary purpose of design and test criteria is to support a major objective of the system design, which is to ensure the integrity of the structure and hardware from the point(s) of manufacture to the termination of mission operations. Of course, the ultimate objective is the successful operation of the system throughout the mission life. The design criteria supports these objectives by requiring certain design stages to be completed during the design process prior to flight, such as shown in Figure 8.1 [8.1]. These stages are usually achieved by completing certain structural analyses and/or tests.

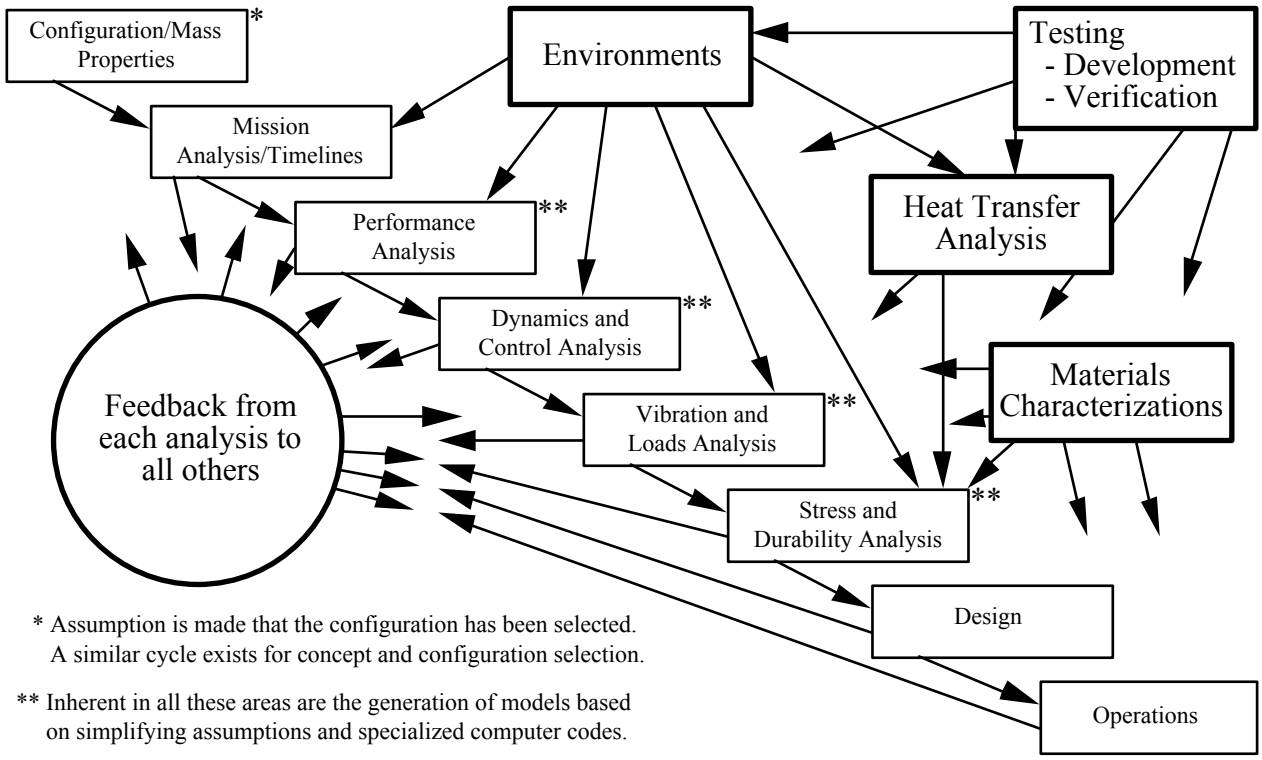

FIGURE 8.1. System Design Process for Aerospace Vehicles

8.1 Low Frequency Vibration and Transient Responses. The designer of aerospace vehicle structures and hardware must carefully consider all the loads and environments outlined in prior sections, especially Sections 4 through 7. How design criteria are integrated into the design process is often determined by the particular phase (early, interim, or late) of the vehicle or hardware design process. As illustrated in Figures 8.1 and 5.1, the design process is almost always iterative [8.1, 8.2], using a team approach required to achieve a weight-efficient and cost-effective design. Thus design and test criteria usually change as the design progresses. Most organizations intentionally use higher design margins initially when each load is considered separately, and then reduce them to minimum acceptable values later when various loads are considered in combination and/or sequence. Other organizations use alternative procedures to achieve system design goals. Transportation and handling loads, which are normally bounded by the limit load factors given in Table 8.1 [8.3], must also be included unless special protection is provided to assure that they contribute negligible damage compared to flight loads. The following subsections summarize design margins, followed by a discussion of

each end of the design process, namely, preliminary and early design, and late and final design. Lastly, test criteria and their relationship to design criteria are addressed.

TABLE 8.1. Transportation Limit Load Factors

Medium/Mode	Longitudinal Load Factors g	Lateral Load Factors g	Vertical Load Factors g
Water	±0.5	±2.5	+2.5
Air	±3.0	±1.5	±3.0
Ground			
Truck	±3.5	±2.0	+6.0
Rail (humping shocks)	±6.0 to ±30.0	±2.0 to ±5.0	+4.0 to +15.0
Rail (rolling)	±0.25 to ±3.0	±0.25 to ±0.75	+0.2 to +3.0
Slow-moving dolly	±1.0	±0.75	+2.0

8.1.1 Design Criteria.

8.1.1.1 Static and Dynamic Loads. The design and often the testing of aerospace structures and hardware must include consideration of the applicable static loads based on the mission profile and overall system performance, plus the predicted dynamic response loads occurring in sequence and/or combination with static and other dynamic loads as summarized in Section 5, multiplied by applicable deterministic safety factors. These safety factors are usually specified based on the type of material, usage for design and/or test, and/or criticality, as shown in Tables 8.2 through 8.6 [8.4]. (NASA projects that propose to use a “no-test” approach generally must employ larger factors of safety and develop project-specific criteria and rationale for review and approval by the responsible NASA center [8.4]). The resulting maximum stresses are then compared to allowable material strength properties, such as provided in [8.5, 8.6], to determine if a safe design is achieved. For fatigue, a design margin or “scatter factor” of four is specified in terms of the number of applied cycles [8.2] in lieu of applying a factor to the load. As indicated in Figures 5.1 and 8.1, this process is nearly always iterative to eventually obtain the desired cost and weight optimization.

TABLE 8.2. Minimum Design and Test Factors for Metallic Structures

Verification Approach	Ultimate Design Factor	Yield Design Factor	Qualification Test Factor	Acceptance or Proof Test Factor
Prototype	1.4	1.0*	1.4	NA or 1.05**
Protoflight	1.4	1.25	NA	1.2

* Structure must be assessed to prevent yielding during flight, acceptance, or proof testing.
** Propellant tanks and solid rocket motor cases only.

TABLE 8.3 Minimum Design and Test Factors for Fasteners and Preload Joints

Verification Approach	Design Factors			Test Factors	
	Ultimate Strength	Joint Separation		Qualification	Acceptance or Proof
		Safety Critical*	Other		
Prototype	1.4	1.4	1.2	1.4	NA
Protoflight	1.4	1.4	1.2	NA	1.2

* Joints that maintain pressures and/or hazardous materials in a safety-critical application.

TABLE 8.4 Minimum Design and Test Factors for Composite/Bonded Structures

Verification Approach	Geometry of Structure	Ultimate Design Factor	Qualification Test Factor	Acceptance or Proof Test Factor
Prototype	Discontinuities	2.0*	1.4	1.05
	Uniform Material	1.4	1.4	1.05
Protoflight	Discontinuities	2.0*	NA	1.2
	Uniform Material	1.5	NA	1.2

* Factor applies to concentrated stresses. For non-safety critical applications, this factor may be reduced to 1.4 for prototype structures and 1.5 for protoflight structures.

TABLE 8.5 Minimum Design and Test Factors for Glass

Verification Approach	Loading Condition	Ultimate Design Factor	Qualification Test Factor	Acceptance or Proof Test Factor
Protoflight	Nonpressurized	3.0*	NA	1.2
	Pressurized	3.0	NA	2.00
Analysis Only	Nonpressurized	5.0	NA	NA

TABLE 8.6 Minimum Design and Test Factors for Structural Glass Bonds

Ultimate Design Factor	Qualification Test Factor	Acceptance or Proof Test Factor
2.0	1.4	1.2

Metallic and composite material strength properties of [8.5] and [8.6], respectively, are usually given in terms of measured data in one of the following four categories: (1) raw data and/or typical values, (2) statistical analysis using the lower 99 percentile of the data with 95 percent confidence (called the A Basis), (3) statistical analysis using the lower 90 percentile of the data with 95 percent confidence (B Basis), (4) statistical analysis using some other percentile and confidence, which may not necessarily be identified (S Basis). Fatigue, crack propagation, fracture and creep data, as well as the primary tension, compression, and shear yield and ultimate strengths are included. Other established references should also be utilized as required, e.g., [8.7]. Stress concentrations (e.g., in the vicinity of fasteners and joints) must be included in the structural analysis unless it can be shown that local yielding will not adversely affect the fit, form, or integrity of the structure [8.4]

Probabilistic methods of structural analysis have been successfully implemented by the Air Force and its contractors on the same launch vehicles used by NASA and commercial customers, using either flight data to establish design factors with high statistical confidence or a variety of worst case loads to establish worst-on-worst case combinations for design purposes [8.2]. However, [8.4] states that the above deterministic design and test factors are adequate to compensate for uncertainties in the strength analysis and that a statistically-based loads analysis is unnecessary. Nevertheless, each NASA Center is given the option to approve a probabilistic criteria to supplement deterministic factors of safety on an individual case basis.

8.1.1.2 Instabilities. Potential instabilities in aerospace systems should be avoided whenever possible. However, this is not always practical. Sources of potential instability in aerospace systems include (a) structural buckling and crippling under static and/or dynamic loads, (b) combustion instability in solid motors and liquid engines, (c) rotor-dynamics in turbo machinery, (d) flutter of panels, wings, control surfaces, and turbine and compressor blades, (e) control system/fluid slosh interaction in tanks, (f) pogo interaction between liquid rocket engines and vehicle structure, and (g) wheel whirl and shimmy in landing gears, which are discussed in Section 3. In some cases the instability can be catastrophic and this is unacceptable, while in other cases a limit cycle may occur well below allowable design margins. In most cases, the oscillation appears sinusoidal and nearly steady-state or slowly-varying when the limit cycle is reached, rather than transient or random. In all cases, a stability analysis is required to determine if the system is (a) stable, (b) unstable but within acceptable load limits, or (c) unstable with a limit cycle exceeding acceptable load limits. It is critical to consider all uncertainties in these analyses, and to include them in the stability assessment.

8.1.2 Preliminary and Early Design

8.1.2.1 General Considerations. There are three possible situations encountered during the initial design phase of a new program:

a. The function and design of the new structure or hardware is similar or identical to those from a previous program.

b. The function and design of the new structure or hardware has some elements which are similar to those from a previous program.

c. The function and design of the new structure or hardware has no resemblance to those from any previous program.

The first situation is normally the easiest because of the availability and utilization of earlier design and test data. Scaling relationships are often used between the previous and new forcing functions and external environments and/or dynamic responses, as well as design margins and test results, to determine if an adequate design is achievable. The number of load cycle iterations can usually be greatly reduced as a consequence. Also, new tests may be considered unnecessary based on structure or hardware similarity, as well as a favorable comparison of new and previous design and test criteria.

The third situation is the most difficult to implement because members of the design team need to start from “scratch.” Often great care and a substantial amount of detail are needed early in the design phase. As a result, design time may be long and design costs large. Thus it is not uncommon to utilize multiple load cycles (typically three) to achieve an adequate design. In addition, a thorough test program is usually required, especially for newly-encountered mission

events, e.g., planetary landing or penetration. The second category is obviously somewhere between the above two categories.

The experience and perception of the design team is often the key to achieving a cost effective and weight efficient design. In general, more experienced team members have developed knowledge-based rules-of-thumb to avoid dynamic design problems, whereas newer members often must rely on computer-based design tools plus support from experienced members. Preliminary and early design traditionally culminates in one or more Preliminary Design Reviews (PDRs).

8.1.2.2 Specific Considerations. A payload is defined as an integrated system carried into space by a launch vehicle for space operations. A spacecraft is a self-contained payload able to operate completely independently for most or all of its mission life. Thus a spacecraft usually has many more on-board subsystems not found on other payloads, such as independent power, propulsion and control.

NASA has imposed specific requirements for NASA payloads [8.2], especially on the fidelity of math models used for loads analysis. For the preliminary load cycle, [8.2] recommends an ***additional*** minimum uncertainty factor of 1.5, to be gradually reduced in later cycles. The launch vehicle organization(s) is required to furnish forcing functions for launch vehicle-generated events, such as liftoff, motor/engine cutoff(s), wind loads, and staging transients. These forcing functions must envelope flight data and produce load responses which will not be exceeded with 99.87 percent (3σ) probability. For larger payloads, a minimum payload natural frequency is usually specified to avoid harmful structure/control system interactions or coupled resonance conditions.

Preliminary sizing of payload primary (load-carrying) structure is based on load factors furnished by the launch vehicle organization [8.2]. These load factors must be applied at the payload center of mass and are based on design load databases, analyses of similar payloads, and flight data. The preliminary design of payload hardware or equipment items commonly utilize load factors obtained from a physical mass acceleration curve (MAC), such as shown in Figure 8.2, or a table providing similar data. The MAC or table recognizes the fact that hardware response accelerations at lower frequencies usually vary inversely with hardware mass. They are usually based on a combination of prior flight and test data, analysis, and experience [8.2, 8.8]. It should be mentioned that MAC can be configuration sensitive.

Following the above preliminary sizing of the payload structure and hardware items, math models must then be developed to initiate the load cycle process in order to ensure structural integrity and minimize weight. At low frequencies, the math model of the payload is almost always a finite element method (FEM) model, whereas for larger payloads at somewhat higher frequencies, statistical energy analysis (SEA) or a boundary element method (BEM) model is often added [8.9]. Spectral overlap is common, usually in the intervening frequency range between 20 and 100 Hz. However, it has been observed that SEA is a good predictor of acceleration response but a poor predictor of load (stress) response [8.9, 8.10].

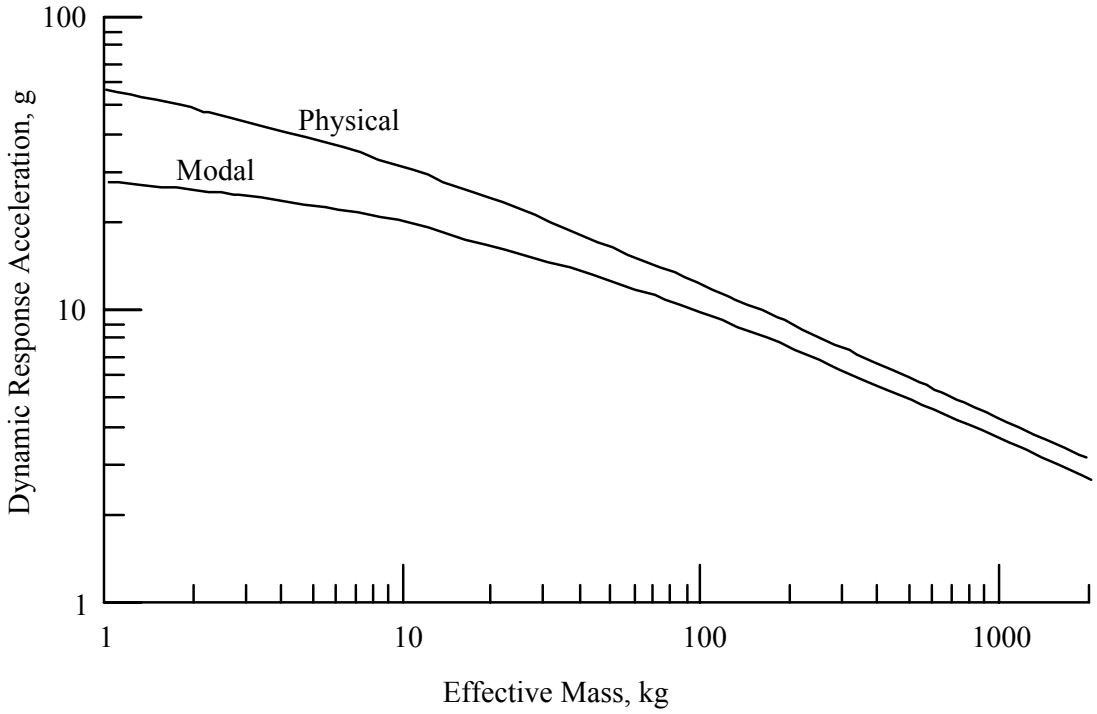

FIGURE 8.2. Physical and Modal MAC for the Galileo Spacecraft Launched on Shuttle and Inertial Upper Stage.

Specific requirements for payload math models at lower frequencies include the following [8.2]:

a. Finite elements must be used to model the structure and/or hardware.

b. Traditionally, a loads model must first be developed that has adequate fidelity to describe the payload dynamic behavior in a frequency range specified by the launch vehicle organization. Usually this range extends to 50 Hz, although a lower or higher maximum or cutoff frequency is sometimes specified for larger or smaller launch vehicles, respectively. For example, the cutoff frequency for the Shuttle is 35 Hz. Overall payload and subsystem modes must be accurately modeled up to an upper bound frequency, which must exceed 1.4 times the cutoff frequency of the loads analysis.

c. If reduction in the size of the model matrix is required, the reduced matrix must preserve the fidelity of the original model up to the upper bound natural frequency.

d. Model damping must be selected based on test measurements of the actual or similar structure at magnitudes representative of flight values. If measured damping data are unavailable, low damping must be assumed, e.g., one percent for transient responses in most cases.

e. Because the loads model will be used for predicting member loads, from which member stress analyses are performed, as well as natural frequencies and mode shapes, a good idealized model is normally required with varying mesh density as required to define a proper load distribution.

f. The main goal of the loads analysis is to identify structural members or elements which are liable to produce high stresses. Once identified, a separate stress analysis is traditionally performed. Historically, the vast majority of high stress points are found at fasteners, joints and connections. For simple loading on a simple member, a hand stress calculation may suffice. For more complicated loading on a complex member (e.g., combined bending and twisting on a triangular composite shell element), a stress model will probably be needed. In most cases, a stress model has already been developed for supporting the structural design under static loading. If so, this model may be utilized for combined static and dynamic stress analysis. In this case, a finer mesh may be required for the stress model in the vicinity of stress concentrations, unless stress risers are handled separately.

g. In addition, the loads model must be utilized to determine dynamic displacements or accelerations at the various interfaces between the structure and hardware items, in order to select preliminary design and test criteria for the hardware.

SEA and BEM models are traditionally used to predict internal acoustic noise in the frequency range of 20 Hz-10 kHz, and random vibration (acceleration) response within 20 Hz-2 kHz or higher, from an external acoustic field extending from 20 Hz to 10 kHz [8.12], with the lower of these frequencies most often utilized for large payloads. SEA or BEM models are popular for computing higher mode structural responses because they are much more cost effective than FEM models with no apparent loss in acceleration response accuracy, especially when the forcing function or environment is random. Nearly all SEA predictions are performed by averaging over wide bandwidths compared to FEM predictions. Usually 1/3 octave bands are selected. The large number of structural details usually necessary for FEM analysis are usually unnecessary for SEA and BEM. However, SEA accuracy is usually limited at the lower frequencies when errors are encountered due to averaging over an insufficient number of response modes [8.13]. On the other hand, FEM analyses often lose accuracy at their higher frequencies, so that adequate results may be achievable when both methods are applied.

Combined loads for environments and/or forcing functions occurring simultaneously, which usually generate simultaneous transient and random responses, require special treatment [8.2]. Often the responses to separate loads are SRSS combined in a time-consistent manner. Payloads may be required to be returnable to Earth on a reusable launch vehicle, such as Space Shuttle. For these cases, launch vehicle docking plus entry and landing loads must be included in the payload design [8.2, 8.14].

Once reasonably consistent modeling results of the payload has been established, the computed modal masses of the various modes may be used in conjunction with the modal MAC curve, such as shown in Figure 8.2, to modify and reduce the accelerations applied to hardware items. For each item, the total acceleration is computed by summing the modal acceleration contribution for each structural mode whose natural frequency is less than the upper bound frequency.

There are a variety of special requirements for spacecraft which are not applicable to other payloads [8.2], since a spacecraft often has a much greater number and variety of subsystems, operational phases and/or configurations that must be considered separately by the spacecraft organization. For example, math models need to be developed, reconfigured or extended to different frequency ranges and used with special operational forcing functions and load factors. After deployment, spacecraft operations do not involve the launch vehicle, so the launch vehicle interface boundaries must be replaced with free boundaries. Additional design uncertainty factors, load combinations, and sequences must also be considered [8.2]. Loads from various deployments and separations must be assessed and included in the spacecraft design. In

addition, some spacecraft missions may require separate atmospheric entry and/or exit, and possible operations under non-Earth conditions.

8.1.3 Late and Final Design

8.1.3.1 General Considerations. As program development continues from earlier stages, the design of the system should have progressed to the point where all design goals and requirements have been achieved or are about to be met, including cost and weight goals and strength requirements. Late design efforts are mainly directed to supporting one or more Critical Design Review (CDRs), after which manufacturing drawings are normally released and payload or spacecraft manufacturing is initiated. Thereafter, design changes usually involve physical rather than paper changes to the system, which may become very expensive and make weight increases impossible to avoid.

In most cases, there is little latitude given for waiving strength requirements, so that the overall weight goal is often sacrificed as a result. Sometimes a weight increase cannot be tolerated, so that the system may have to be redesigned. Often this redesign necessitates the removal of subsystems, the reduction of propellants, and/or the replacement of heavier materials with lighter materials or configurations. If this redesign does not produce the desired system goals, as a last alternative the mission may need to be modified, or the original launch vehicle may have to be replaced with a more powerful one, or the mission canceled. The economic consequences of any of these alternatives are obviously severe.

8.1.3.2 Specific Considerations. As the load cycle progresses, more attention is normally paid to the effects of load combinations and sequences on the design of the structure and hardware, with load combinations considered to pinpoint maximum stresses and load sequences considered to determine fatigue margins. Meanwhile, the uncertainty factor added earlier in the design process has hopefully been prudently reduced toward unity. One acceptable way of avoiding an excessive uncertainty factor is to utilize sensitivity analysis, by which systematic changes are analytically made to payload properties and design loads selected from (a) the worst case load or (b) statistical analysis of a variety of load cases. Frequency sensitivity, or tuning, may also be used, which permits artificial frequency shifts in the math model in order to determine potential load increases to the structural design [8.2]. These techniques are considered reasonable late-design substitutes for earlier uncertainty factors greater that unity.

Once the final payload structural design has been essentially established, the system natural frequencies, mode shapes, and damping values, and applicable forcing functions, can be used to compute the accelerations at the various interfaces between the structure and each hardware item, which may be used to refine hardware dynamic test criteria at lower frequencies

8.1.4 Modal Tests. At this stage, an engineering structural model is often built (called a prototype), or the actual payload used (called the protoflight), to perform modal test(s) in the applicable operational phase(s) of the system, as described in Section 5.1.5. The objective of the modal test is to provide an independent method of evaluating the accuracy of the math model used to compute the low frequency structural behavior of a dynamical system, such as a launch vehicle or payload, in its various mission configurations, rather than to determine if the structure can withstand the various applicable dynamic loads. Since modal tests are normally performed using low excitation conditions, they are considered design tools. Therefore, verification of the adequacy of primary structure to withstand the various static and dynamic loads occurring in combination and/or in sequence is achieved by analysis rather than by test. For modal tests, large or heavy hardware items are either installed or mass-simulated. Smaller or lighter hardware items, cables, tubing, etc are often omitted. This situation usually requires

the math model to be modified to reflect the modal test configuration. After the structure is modally tested and if the math model is adequately verified and the forcing functions finalized, all prior uncertainties in the analysis can be safely eliminated. However, if the model verification is inadequate, an appropriate uncertainty factor may be required in the last or verification load cycle [8.2].

8.1.5 Test Criteria. As described in Sections 8.1.3 and 8.1.4, primary structures are usually verified by analyses and modal tests, rather than by environmental tests. However, the structural integrity of hardware items is usually verified by static loads and/or low frequency testing. In addition, low frequency testing is sometimes performed on small payloads as a substitute or supplement to verification by analysis. In fact, it is not uncommon to specify test criteria rather than design criteria for hardware and small payloads. If test criteria (including test tolerances) exceed design criteria, the design criteria should be increased to avoid the possibility of achieving hardware that satisfies the design criteria but fails the test.

For low frequency random vibration, either of two test procedures are often utilized:

a. Simulating the acceleration time history for each random mission event computed in Section 8.1.3, plus a design or test margin, and performing a series of tests.

b. Computing the auto spectrum for each event , covering these spectra with a single spectral envelope, plus a design or test margin, and performing a single random test.

For low frequency transients, either of three test procedures are often utilized:

a. Simulating the acceleration time history for each transient mission event computed in Section 8.1.3, plus a design or test margin, and performing a series of tests (see Section 10.2).

b. Computing the shock response spectrum (SRS) for each event, covering these SRSs with a single spectral envelope, plus a design or test margin, and performing a single transient test.

c. Using swept-sine testing whose criteria is derived by matching the single-degree-of-freedom response to the SRS of (b), plus a design or test margin, and performing a single sine sweep [8.15]. Problems encountered in using swept-sine testing are discussed in Section 9.4.1.

Hydraulic and electrodynamic shaker systems are used for performing low frequency testing. The low frequency cutoff for hydraulic shakers is about 2 Hz, depending on its maximum stroke or displacement, whereas most electrodynamic shakers have a 5-20 Hz cutoff and a substantially lower allowable displacement (see Section 10.1). When low frequency test criteria is formulated in terms of acceleration, it is important to determine the maximum test displacement in order to avoid hard bottoming of the shaker system. If shaker displacement limits are computed to be exceeded, it is common practice to either (a) reduce the low frequency portion of the time history or spectrum, or (b) increase the cutoff frequency. The effects of these measures on test results should be negligible as long as the response at the fundamental resonance is unaffected.

8.2 High Frequency Vibration Responses. The low frequency dynamic responses described in Section 8.1 usually produce the loads of greatest concern to the design of space vehicle structures. The high frequency vibration responses may be of concern in the final design of thin panel sections or other structural elements susceptible to high frequency vibration damage, for example, sonic fatigue [8.16]. Nevertheless, the primary design concerns

associated with high frequency vibration environments involve the equipment or hardware items mounted on the vehicle structure. The criteria for the design of space vehicle equipment for their high frequency vibration environments are based upon the maximum expected environment computed in Section 6 and the equivalent stationary duration computed in Section 7, plus the appropriate margin detailed in Section 8.2.4. However, the vibration qualification test environment is also involved in arriving at the design criteria. The vibration qualification test levels are usually derived in the same way as the vibration levels used for design, and typically with the same margin, as discussed in Section 8.2.4. On the other hand, to account for the scatter in fatigue data, the vibration test is a stationary environment that often has a substantially longer duration than the equivalent stationary duration computed in Section 7. Hence, the qualification test durations detailed in Section 8.2.4 should be used as the minimum duration of the vibration environment for design purposes.

8.2.1 Preliminary Design – Equipment. The design of equipment for high frequency vibration excitations can be a demanding task, particularly for electronic equipment that may have a wide range of failure modes, including a degradation in functional performance. However, during the preliminary design phase, attention is usually restricted to the integrity of the equipment structure, specifically, the maximum stress that will occur in the equipment structure due to the vibration excitation. Simplified procedures to at least coarsely predict the maximum stress for preliminary design purposes will now be discussed.

8.2.1.1 Simplified Stress Model. It most cases, it can be assumed the maximum stress in the structure of an equipment item will be caused by the response at single dominant normal mode (resonance), usually the first normal mode of the structure. This dominant normal mode can be approximated by a base driven oscillator (single degree-of-freedom system) where the frequency response function between an acceleration excitation at the base and a relative (modal) displacement response of the mass is given by [8.17]

$$H_{a-d}(f) = \frac{1}{1 - (f/f_n)^2 + j2\zeta f/f_n} \left(\frac{1}{2\pi f_n}\right)^2 \qquad (8.1)$$

In Equation (8.1), ζ = damping ratio, f_n = undamped natural frequency (approximately equal to the resonance frequency for $\zeta < 0.1$), and $j = \sqrt{-1}$. Assume a random vibration excitation is applied at the base of the equipment with an acceleration autospectrum, $G_{xx}(f)$, having the units of g^2/Hz. Further assume the acceleration autospectrum is relatively constant at frequencies near the natural frequency of the equipment [i.e., $G_{xx}(f) \approx G_{xx}$ for f near f_n]. The standard deviation of the relative displacement response of the simple oscillator representing the equipment is given by [8.17, 8.18]

$$\sigma_d = \left[\frac{\pi f_n g^2 G_{xx}(f_n)}{4\zeta}\right]^{1/2} \left(\frac{1}{2\pi f_n}\right)^2 \qquad (8.2)$$

where g is the gravity unit (9.81 m^2/s). At frequencies below 2 kHz, it can be assumed the dominant normal mode response of the equipment will involve primarily the bending of structural elements. The bending stress at the natural frequency of a structure is proportional to the modal velocity response of the structure [8.19 - 8.22], specifically,

$$S = C\,V\,E/c_L = C\,V\,\sqrt{E\rho} \tag{8.3a}$$

where S = maximum stress
V = maximum modal velocity
E = Young's Modulus for material
c_L = longitudinal wave velocity in material
ρ = mass density of material
C = constant of proportionality

Assuming linearity and a Gaussian random response, the maximum stress and velocity in Equation (8.3a) can be replaced by the standard deviations of the instantaneous stress and velocity, respectively, at those points on the structure where the maximum stress and velocity occur, that is,

$$\sigma_S = C\,\sigma_V\,E/c_L \tag{8.3b}$$

To obtain a standard deviation of the stress, the standard deviation of the modal velocity can be approximated from Equation (8.2) by

$$\sigma_V = 2\pi f_n\,\sigma_d \tag{8.4}$$

Substituting Equations (8.3b) and (8.4) into Equation (8.2) yields an estimate for the standard deviation of the stress given by

$$\sigma_S = \frac{CE\sigma_V}{c_L} = \frac{CE}{4c_L}\left[\frac{g^2\,G_{xx}(f_n)}{\pi f_n\,\zeta}\right]^{1/2} \tag{8.5}$$

where all terms are as defined in Equations (8.1) through (8.4).

The value of the constant C in Equation (8.5) can vary widely depending upon the geometry of the structure [8.21, 8.22] and stress concentration factors, but a value of C = 8 is considered conservative for most equipment configurations, although this value might be relaxed to C = 4 for simple mechanical equipment items. For example, assume an item of equipment is constructed from an aluminum alloy where E = 6.9 x 10^4 MPa (10 x 10^6 psi) and c_L = 5100 m/s (2 x 10^5 in./s). Further assume the dynamic response of the equipment is dominated by a fundamental resonance at f_n = 50 Hz with a damping ratio of ζ = 0.05. If the equipment is exposed to a relatively severe random excitation with an acceleration spectral density (including margin) of $G_{xx}(f_n)$ = 0.4 g^2/Hz at the resonance frequency, then using a conservative value of C = 8, the standard deviation for the maximum stress produced by this resonance is given by Equation (8.5) as $\sigma_S \approx$ 60 MPa (8.7 ksi).

At least conservative values for f_n and ζ in Equation (8.5) can be estimated early in the design to obtain an estimate for the stress standard deviation σ_s. However, an estimate of a maximum stress is required. Given the computed σ_s, there are three basic ways to estimate a maximum stress, namely, (a) a maximum instantaneous stress, (b) a first passage stress, and (c) a shock response stress. Procedure (a) is most applicable to nonstationary vibration environments where the maximum rms stress predicted by Equation (8.5) occurs only momentarily, for example, the liftoff environment. Procedure (b) is most applicable to at least briefly stationary vibration environments. Procedure (c) is applicable to both stationary and nonstationary environments. Since the qualification vibration tests for all equipment are stationary for at least two minutes (see Table 8.12), fatigue damage must also be considered to arrive at an acceptable stress for preliminary design purposes. Note that for all procedures, static stresses due to assembly stresses or a static acceleration superimposed on the high frequency vibration are not accounted for. If such static stresses can be estimated, they should be added to the maximum predicted stress due to the random vibration.

8.2.1.2 Maximum Instantaneous Stress. The simplest approach to estimating a maximum stress for equipment exposed to a high frequency vibration excitation is to use that stress value corresponding to three times the standard deviation of the equipment stress [8.18]. Specifically, from Equation (8.5),

$$S_{max1} = 3\sigma_s = \frac{3CE}{4c_L}\left[\frac{g^2 G_{xx}(f_n)}{\pi f_n \zeta}\right]^{1/2} \tag{8.6}$$

Equation (8.6) may be interpreted as follows. If it is assumed the response of the equipment mounted to the space vehicle structure (or to the shaker table for a qualification test) is normally distributed (Gaussian), then the stress level S_{max1} in Equation (8.6) is that stress that will be exceeded with a probability of 0.13% by the maximum stress in the equipment at that instant when the standard deviation of the stress is a maximum. For example, consider the illustration in Section 8.2.1.1 where the standard deviation of the stress is $\sigma_s \approx 60$ MPa (8.7 ksi), it follows from Equation (8.6) that $S_{max1} \approx 180$ MPa (26 ksi), which is well below the yield stress for 2024-T3 aluminum.

The only advantage of the maximum instantaneous stress procedure is its simplicity. The primary disadvantages are as follows:

a. The procedure assumes that equipment items mounted to the vehicle structure or the shaker table have responses dominated by a single normal mode.

b. The procedure does not account for modifications in the vibration input to the equipment, as defined by the maximum expected environment, due to equipment loading of its mounting structure or the shaker table.

c. The procedure assumes a normal (Gaussian) response of the equipment mounted to the space vehicle structure or the shaker table. Even if the vibration of the space vehicle structure or the shaker table is not Gaussian, as long as it is random with a broad bandwidth, this assumption is usually acceptable for an equipment item that has a linear response dominated by a single normal mode because this situation suppresses deviations from the Gaussian form [8.23]. However, nonlinear characteristics in the equipment response may produce a highly non-Gaussian response.

d. The procedure does not account for the duration of the vibration response, i.e., it assumes the vibration excitation is nonstationary with a single, momentary maximum. This assumption may be valid for some launch events, but clearly is not valid for the vibration qualification test.

8.2.1.3 First Passage Stress. A procedure for estimating the maximum stress that includes the influence of the vibration exposure duration is to apply the first-passage model detailed in Section 7.1.4. Specifically, for equipment represented by a simple oscillator having a stationary random vibration response with a standard deviation of the stress given by σ_s in Equation (8.5), the probability that the maximum stress value S_{max2} will be exceeded at least once during an exposure period of T_S sec is approximated by

$$P(T_S) \approx f_n T_S \exp\left[\frac{-S^2_{max2}}{2\sigma_s^2}\right] \tag{8.7}$$

which yields

$$S_{max2} = \sigma_s \sqrt{2 \ln\left[\frac{f_n T_S}{P(T)}\right]} = \frac{CE}{4 c_L} \sqrt{2 \ln\left[\frac{f_n T_S}{P(T_S)}\right] \frac{G_{xx}(f_n)}{\pi f_n \zeta}} \tag{8.8}$$

where all terms are as defined in Equations (8.1) through (8.5). A common value assumed for the probability distribution in Equation (8.7) is 5%, i.e., $P(T_S) = 0.05$ (see Figure 7.5).

A problem in applying Equation (8.8) to space vehicle vibration data is that such data are often nonstationary. However, the vibration qualification test for the equipment will be stationary for at least two minutes (see Table 8.12). Hence, it can be assumed that $T_S \geq 120$ sec. For example, consider the illustration in Section 8.2.1.1 where the standard deviation of the stress is $\sigma_s \approx 60$ MPa (8.7 ksi), it follows from Equation (8.8) with C = 8 and $P(T_s) = 0.05$ that $S_{max2} = 4.8\ \sigma_s \approx 290$ MPa (42 ksi), which is below the yield stress for 2024-T3 aluminum. The fact that S_{max2} is 60 % greater than S_{max1} given by Equation (8.6) is not surprising since the first passage value represents the probability that a single value will exceed the level S_{max} over a time duration T_S, rather than at a single instant during that time duration.

The advantages of the first passage stress procedure are its simplicity and the fact that it accounts for the duration of the vibration environment. On the other hand, the procedure has the first three disadvantages summarized for the maximum instantaneous stress procedure in Section 8.2.1.2.

8.2.1.4 Shock Response Stress. Another procedure for estimating the maximum stress in an equipment item that includes the influence of the vibration exposure duration is to compute the maximum expected environment in terms of a maximax shock response spectrum (SRS), as defined in Section 2.2.10. The SRS for the velocity response of the oscillators is desired, but if a conventional acceleration SRS given by $S_x(f_n,\zeta)$ in g versus f_n is computed, a pseudo-velocity SRS in (m/s) versus f_n can be estimated from

$$S_v(f_n,\zeta) = g\, S_x(f_n,\zeta)/(2\pi f_n) \tag{8.10}$$

For equipment with any estimated resonance frequency f_n and damping ratio ζ, since $S_v(f_n,\zeta)$ represents the maximum velocity of the equipment response, the maximum stress is given directly by Equation (8.3) as

$$S_{max3} = C\ E\ S_v(f_n,\zeta)/c_L = C\ E\ g\ S_x(f_n,\zeta)/(2\pi\ f_n\ c_L) \qquad (8.11)$$

The advantages of the shock response spectrum procedure are as follows:

a. Since the SRS for a stationary random signal depends on the duration of the signal, the procedure accounts for the duration of the vibration environment.

b. The procedure properly accounts for both the potential nonstationary and non-Gaussian characteristics of the vibration environment.

On the other hand, the procedure has the first two disadvantages summarized for the maximum instantaneous stress procedure in Section 8.2.1.2.

8.2.1.5 Fatigue Damage Considerations. As noted earlier, all equipment items will be exposed to a random vibration environment with a duration of at least two minutes during the vibration qualification test. Furthermore, during equipment transportation or operations in orbit, or for equipment that is installed on a reusable launch vehicle such as Space Shuttle, the random vibration environment might be substantially longer than two minutes. Hence, the possibility of fatigue damage must be considered during preliminary design. This can be accomplished by estimating the standard deviation of the stress using Equation (8.5), and then using a random S-N curve (see Section 7.1.2) or a crack propagation model (see Section 7.1.3) for the primary equipment material to determine if the equipment will fail in $N = f_n\ T$ cycles where T is the anticipated duration of the environment. For example, consider the illustration in Section 8.2.1.1 where the standard deviation of the stress in the equipment is $\sigma_s \approx 60$ MPa (8.7 ksi). A random S/N curve for 2024-T3 aluminum is shown in Figure 8.3, which is taken direct from [8.24] with an appropriate change of units. Referring to Figure 8.3, a random stress with the above standard deviation corresponds to a fatigue life of about 8×10^6 cycles or about 44 hours for $f_n = 50$ Hz.

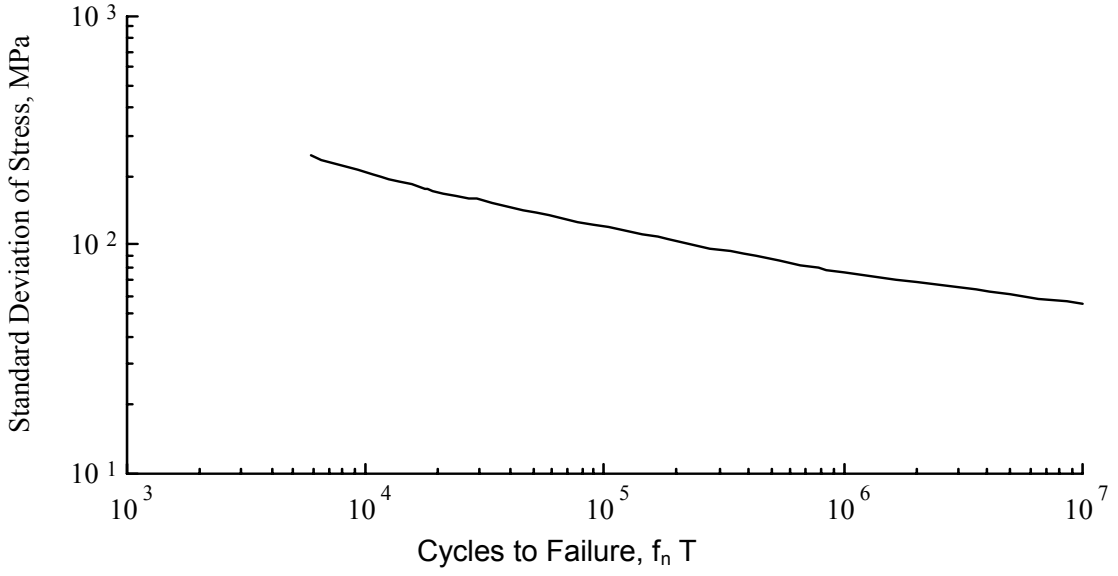

FIGURE 8.3. Narrowband Random S-N Curve for AL 2024-T3 with Zero Mean Value [8.24].

8.2.1.6 Assessments. The merits of the various procedures for predicting the maximum stress in space vehicle equipment items due to high frequency vibration excitations at their mounting points are summarized in Table 8.7. All of the procedures have a number of limitations, and no one procedure is decisively superior to the others.

TABLE 8.7 Summary of Merits of Various Procedures for Establishing Preliminary Design Loads for High Frequency Vibration Environments.

Merit	Maximum Inst. Value	First Passage Value	SRS Value	Fatigue Damage
Relatively easy to apply	Yes	Yes	Yes	Yes
OK for multi-mode response	No	No	No	No
OK for non-Gaussian response	No	No	Yes	No
OK for nonstationary response	Yes	No	Yes*	Yes**
Accounts for vibration duration	No	Yes	Yes	Yes

* Assuming the equipment response is linear.
** Assuming the vibration environment can be reduced to at least piece-wise stationary segments.

8.2.2 Final Design – Equipment. The final design criteria for equipment subjected to high frequency vibration environments should be based upon vibration response predictions, including maximum stress predictions, obtained using a finite element method (FEM) model, as detailed in Section 5.2.3. If needed to support predictions at the higher frequencies, a statistical energy analysis (SEA) model should also be used, as outlined in Section 5.2.2. Four important factors should be included in the final predictions, as follows:

8.2.2.1 Mass Loading Effects. Since the details of the structure to which the equipment is mounted are better known at the time of final design, the possible modifications of the input motion to the equipment due to the mass loading of the equipment on its mounting structure should be included. The corrected input motion is given by Equation (6.20). For all vibration testing, one of the procedures summarized in Sections 6.5.2 through 6.5.5 should be employed to account for mass loading effects.

8.2.2.2 Multi-Mode Responses. If the final predictions produce response values only for individual, widely-spaced modes, the multi-modal response of the equipment at two or more natural frequencies should be computed to obtain more accurate estimates for the overall dynamic response. The overall standard deviation of the modal stresses can be estimated by taking the square root of the sum of squares of the standard deviations of the stresses for each natural frequency, that is

$$\sigma_{OA} \approx \sqrt{\sum_{i=1}^{M} \sigma_i^2} \qquad (8.12)$$

where M is the number of natural frequencies of the equipment with a substantial response to the excitation.

8.2.2.3 Combined Loads. The low frequency loads detailed in Section 8.1 usually do not produce a substantial dynamic stress in space vehicle equipment items and, hence, normally do not have to be considered in the final design of equipment items for their high frequency vibration environment, except perhaps as an added static load, as discussed in Section 8.2.2.4. However, there are exceptions, in particular when an equipment item is sufficiently large to have a dominant normal mode below about 50 Hz, i.e., in a frequency range where a dominant normal mode can be excited by both low and high frequency excitations as defined in Section 3. In such cases, the predicted high frequency vibration responses must be combined with the predicted responses to the low frequency loads detailed in Section 8.1 to arrive at a final design requirement.

8.2.2.4 Static Loads. Static loads can also increase the possibility of an equipment failure due to high frequency dynamic excitations if the static load is large compared to the vibration experienced by the equipment. Included here are the peak loads due to the low frequency dynamic responses, since they will appear to the equipment as a repeated, momentary static load. The influence of the static load on the probability of failure is heavily dependent on the mode of failure [8.18, 8.25]. Their possible influence on the total stress should be considered, although in most cases, they can be accounted for by appropriate design and test margins.

8.2.3 Design and Test Margins. Because of the difficulties in applying analytical methods to high frequency random vibration problems, it is unusual to specify a design margin for high frequency loads. However, it is common practice to specify a test margin. The minimum design criteria (explicit or implied) is usually the same as the prototype (qualification) test criteria. Test margins may vary widely between organizations and even programs, but two key test criteria documents for space vehicles, one issued by NASA [8.12] and the other issued by USAF [8.26], give the test level margins summarized in Table 8.8 for both high frequency random vibration and acoustic tests. A third key document issued by NASA GSFC [8.27] presents test criteria that are broadly consistent with [8.12]. NASA defines flight acceptance (FA), protoflight, and qualification (prototype) test level margins relative to the maximum expected environment (MEE), as given in Table 8.8, but specifies that the test levels shall also envelope minimum workmanship levels. NASA minimum workmanship random vibration levels are given in Table 8.9 for components (units) with a mass of less than 50 kg (110 pounds). NASA minimum workmanship acoustic levels are 138 dB overall, with the test spectrum shape identical to the expected flight spectrum for all hardware levels of assembly. USAF [8.26] defines FA test level margins relative to the MEE, and protoflight and prototype (qualification) test level margins relative to the FA, as given in Table 8.8, but specifies that FA test levels shall also envelope minimum workmanship levels. USAF minimum workmanship random vibration levels are given in Table 8.10 for units (components) with a mass of less than 23 kg (50 pounds) and for vehicles of any mass. USAF minimum workmanship acoustic levels are given in Table 8.11 for all hardware levels of assembly. For both NASA and the USAF, the maximum expected environment is determined using a 95/50 normal tolerance limit, as defined in Section 6.1.2.

The test level margins given in [8.12] are applicable to all NASA programs. For non-NASA programs, the test level margins given in [8.12] are recommended as the minimum acceptable margins. Higher margins might be used if justified by specific program requirements, but margins in excess of those specified in [8.26] are not recommended. Also, as mentioned in Section 8.1.5, if a design margin is specified, and if the test criteria (including the test tolerances detailed in Section 10) exceed the design criteria, then the design criteria should be increased to at least equal or exceed the prototype or protoflight test criteria so as to avoid the possibility of producing hardware that might satisfy the design criteria but fail the prototype or protoflight test.

TABLE 8.8. Summary of High Frequency Random Vibration and Acoustic Test Level Margins.

Type of Test	NASA-STD-7001 [8.12]	MIL-STD-1540C [8.26]
Prototype (Qualification)	MEE* + 3 dB**	FA + 6 dB
Protoflight	MEE* + 3 dB**	FA + 3 dB
Flight Acceptance (FA)	MEE* - 3 dB**	MEE* + 0 dB**

* Maximum expected environment defined by 95/50 normal tolerance limit (see Section 6.1.2).
** But not less than a specified minimum workmanship level.

TABLE 8.9. NASA Component Minimum Workmanship Random Vibration Test Levels [8.12].

Units with a Mass Less than 50 kg	
Frequency, Hz	Minimum Power Spectral Density, g^2/Hz
20 20 to 80 80 to 500 500 to 2000 2000	0.01 +3 dB/octave slope 0.04 -3 dB/octave slope 0.01
Overall	6.8 g_{rms}

TABLE 8.10. USAF Minimum Workmanship Random Vibration Test Levels [8.26].

Units (mass less than 23 kg)		Vehicles	
Frequency, Hz	Minimum Level	Frequency, Hz	Minimum Level
20 20 to 150 150 to 600 600 to 2000 2000	0.0053 +3 dB/octave slope 0.04 -6 dB/octave slope 0.0036	20 20 to 100 100 to 1000 1000 to 2000 2000	0.002 +3 dB/octave slope 0.01 -6 dB/octave slope 0.0025
Overall	6.1 g_{rms}	Overall	3.8 g_{rms}

TABLE 8.11. USAF Minimum Workmanship Acoustic Test Levels [8.26].

Units and Vehicles			
1/3 Octave Band Center Frequency, Hz	Minimum Sound Pressure Level, dB	1/3 Octave Band Center Frequency, Hz	Minimum Sound Pressure Level, dB
31	121	630	125
40	122	800	124
50	123	1000	123
63	124	1250	122
80	125	1600	121
100	125.7	2000	120
125	126.5	2500	119
160	126.7	3150	118
200	127	4000	117
250	127	5000	116
315	126.7	6300	115
400	126.5	8000	114
500	125.7	10000	113
Overall 138 dB			

The durations for high frequency vibration and acoustic tests specified in [8.12, 8.26] are summarized in Table 8.12. The test durations specified in [8.12], which include a test margin, should be considered the minimum acceptable test durations. However, if the equivalent duration of the environment computed using the procedures in Section 7.3 exceeds the requirements in [8.12], a longer test duration should be considered. Also, the retest criteria in [8.26] apply.

TABLE 8.12. Summary of High Frequency Random Vibration and Acoustic Test Durations.

Type of Test*	NASA-STD-7001 [8.12]	MIL-STD-1540C [8.26]
Prototype (Qualification)	Single mission: 2 min. N missions: 2 + 0.5N min.	For units: 3 min. For vehicles: 2 min.
Protoflight	1 min.	For units: 3 min. For vehicles: 2 min.
Flight Acceptance	1 min.	1 min.

*For uniaxial vibration tests, the specified test durations apply to the individual tests along each of the three orthogonal axes. For simultaneous three-axis vibration tests and acoustic tests, the specified durations apply to the total test.

8.3 High Frequency Transient Responses. As discussed in Section 5.3, the high frequency transient responses of spacecraft structures are due primarily to the activation of pyrotechnic (explosive) devices. Assuming no net velocity change occurs, such transients, commonly referred to as pyroshocks, produce little low frequency energy. Hence, they pose no significant damage threat to the basic spaceraft structure beyond that localized damage the pyrotechnic device is intended to produce. The primary design concerns associated with pyroshocks involve the equipment items that are mounted on the spacecraft structure.

The maximum expected environments for pyroshock excitations to equipment are usually defined in terms of a maximax shock response spectrum (SRS), as discussed in Section 6, which in turn is computed from response predictions, as detailed in Section 5.3. These maximax SRS are needed to establish test criteria for equipment mounted on the spacecraft structure. However, they are less useful for design purposes. Specifically, for equipment items that have a first natural frequency below 500 Hz, the predicted responses of the equipment structure will generally correspond to stresses well below those needed to cause a failure, even though small elements in the equipment with resonance frequencies above 1 kHz may fail. To be more specific, the primary threat posed by pyroshocks is to small elements, primarily in optical and electronic equipment, that are composed of brittle materials such as glass or ceramics. Pyroshocks have also been known to cause malfunctions of surface mounted elements on electronic circuit boards and computer memory elements. At the time this document was written, the prediction procedures in Section 5.3 do not provide sufficient detail to establish the local inputs to those small elements in the equipment that are most vulnerable to high frequency transient excitations. However, with the rapidly increasing capabilities of computer hardware and software, it is possible that finite element method (FEM) models may be developed in the future that can successfully predict these local inputs with sufficient accuracy for design applications.

8.3.1 General Design Considerations. Although there are no accurate analytical procedures for the design of equipment for pyroshock environments at this time, general design guidelines are presented in [8.28]. Also, considerable insight into good design practices can be gained from studies of documented pyroshock failures, for example, [8.29, 8.30]. Those involved in the design of equipment for pyroshock environments should acquaint themselves with these references, as well as any other documented studies of confirmed pyroshock induced equipment failures. A few of the more important general design guidelines that have evolved from experience are as follows:

a. Always mount equipment that is sensitive to high frequency excitations, particularly optical and electronic equipment, as far away as feasible from pyrotechnic devices.

b. Referring to Figure 5.8, if there is a choice, avoid locating sensitive equipment on structures that provide a good transmission path for high frequency energy, for example, honeycomb structures.

c. Referring to Section 5.3.4.2, if there is a choice, attempt to locate sensitive equipment on structures that are separated from pyrotechnic devices by structural joints and/or discontinuities.

d. When feasible, avoid hard-mounting elements composed of brittle materials to the basic structure of the equipment.

In summary, the main defense against pyroshock induced flight failures is the careful testing with an appropriate margin of individual equipment items using one of the laboratory simulation procedures outlined in Section 10.4, and in particular, a full pre-flight system test in the laboratory where all pyrotechnic devices are activated in sequence or in combination, as will occur in flight.

8.3.2 Design and Test Margins. Since the design procedures for pyroshock environments are generally qualitative, design margins are not applicable. However, test margins are common, although they often vary widely between organizations and even between programs. Nevertheless, specific test margins are recommended in two key environmental test criteria

documents for space vehicle equipment, one issued by NASA [8.31] and the other issued by USAF [8.26], which give the test level margins for high frequency transient environments summarized in Table 8.13. A third key document issued by NASA GSFC [8.27] presents test criteria that are broadly consistent with [8.31]. The maximum expected environment in Table 8.13 (called the maximum expected flight level in [8.31]) is usually defined in terms of a shock response spectrum (see Section 2.2.10). As for high frequency random vibration environments discussed in Section 8.2.4, it is recommended that the maximum expected environment be determined using a 95/50 normal tolerance limit, as defined in Section 6.1.2.

The test level margins given in [8.31] are applicable to all NASA programs. For non-NASA programs, the test level margins given in [8.31] are recommended as the minimum acceptable margins. Higher margins might be used if justified by specific program requirements, but margins in excess of those specified in [8.26] are not recommended. Also, the retest criteria in [8.26] apply.

TABLE 8.13. Summary of High Frequency Transient Test Margins.

Type of Test	NASA-STD-7003 [8.31]	MIL-STD-1540C [8.26]
Prototype (Qualification)	MEE* + 3 dB 2 applications per axis	FA + 6 dB 3 applications in each direction per axis
Protoflight	MEE* + 3 dB 1 application per axis	FA + 3 dB 2 applications in each direction per axis
Flight Acceptance	MEE* + 0 dB 1 application per axis	MEE* + 0 dB 1 application in each direction per axis

* Maximum expected environment defined by 95/50 normal tolerance limit (see Section 6.1.2).

8.4 References

8.1 Ryan, R. S., “Structural Design/Margin Assessment,” *NASA TP 3410,* Sep. 1993.

8.2 Anon., “Loads Analysis of Spacecraft and Payloads,” *NASA Technical Standard NASA-STD-5002,* June 21, 1996.

8.3 Anon., “Transportation and Handling Loads,” *NASA SP-8077,* Sep. 1977.

8.4 Anon., “Structural Design and Test Factors of Safety for Spaceflight Hardware,” *NASA Technical Standard NASA-STD-5001,* June 21, 1996.

8.5 Anon., “Metallic Materials and Elements for Aerospace Vehicle Structures,” *Military Handbook MIL-HDBK-5G*, Chge Notice 1, Dec. 1, 1995.

8.6 Anon., “Polymer Matrix Composites”, *Military Handbook MIL-HDBK- 17D* (Vol. I - Guidelines; Vol. II - Material Properties; Vol. III - Data Utilization), Chge Notice 1, Sep. 29, 1995.

8.7 Fuchs, H. O., and Stephens, R. I., *Metal Fatigue in Engineering*, Wiley, NY, 1980.

8.8 Trubert, M. R., “Mass Acceleration Curve for Spacecraft Structural Design,” *JPL Pub. D-5882,* Nov. 1 ,1989.

8.9 Tanner, C. S., “Lessons Learned in Predicting Launch Vehicle Vibroacoustic Environments,” *Proc. 16th Aerospace Testing Sem.,* pp 129-135, Mar. 1996.

8.10 Chung, Y. T., and Foist, B. L., “Prediction of Payload Random Vibration Loads,” *Proc. 13th Intern. Modal Analysis Conf.,* pp 934-9940, Feb. 1995.

8.11 Leung, K., and Foist, B. L., “Prediction of Acoustically Induced Random Vibration Loads for Shuttle Payloads,” *AIAA Paper 95-1200-CP,* 1995.

8.12 Anon., “Payload Vibroacoustic Test Criteria,” *NASA Technical Standard NASA-STD-7001,* June 1996.

8.13 Hughes, W. O., McNelis, M. E., and Manning, J. E., “NASA LeRC’s Acoustic Fill Effect Test Program and Results,” *Proc., 15th Aerospace Testing Sem.,* Inst. Envir. Sc., pp 205-221, Oct. l994. (Also *Proc. 65th Shock and Vibration Symp.*, Vol. 1, pp 459-474, Nov. 1994.)

8.14 Anon., “Space Shuttle System Payload Accommodations,” *NSTS 07700,* Vol. XIV, Rev. I, Sep. 16, 1986.

8.15 Barrett, S., “The Development of Sine Vibration Test Requirements for Viking Lander Capsule Components,” *Proc. 20th ATM*, *Inst. Envir. Sc.*, pp 77-82, 1974.

8.16 Blevins, R. D., “An Approximate Method for Sonic Fatigue Analysis of Plates and Shells,” *J. Sound and Vibration*, Vol. 129, No. 1, pp. 51-71, 1989.

8.17 Bendat, J. S., and Piersol, A. G., *Random Data: Analysis and Measurement Procedures*, 3nd ed., Wiley, NY, 2000.

8.18 Wirshing, P. H., Paez, T. L., and Ortiz, H., *Random Vibrations: Theory and Applications*, Wiley, NY, 1995.

8.19 Hunt, F. V., "Stress and Strain Limits on the Attainable Velocity in Mechanical Vibration,” *J. Acoust. Soc. Amer.*, Vol. 32, No. 9, pp 1123-1128, 1960.

8.20 Ungar, E. E., "Maximum Stresses in Beams and Plates Vibrating at Resonance,” *Trans. ASME, J. Engrg Ind.*, Vol. 82B, No. 1, pp 149-155, 1962.

8.21 Crandall, S. H., "Relation between Strain and Velocity in Resonant Vibration,” *J. Acoust. Soc. Amer.,* Vol. 34, No. 12, pp 1960-1961, 1962.

8.22 Gaberson, H. A., and Chalmers, R. H., "Modal Velocity as a Criterion of Shock Severity,” *Shock and Vibration Bull.*, No. 40, Pt 2, pp 31-40, 1969.

8.23 Papoulis, A., "Narrow-Band Systems and Gaussianity,” *RADC-TR-71-225,* Rome Air Dev. Ctr, Griffis AFB, NY, 1971.

8.24 Brown, W. G., and Ikegami, R., "The Fatigue Life Of Aluminum Alloys Subjected to Random Loading,” *SCL-CR-69-164,* Sandia National Labs, Livermore, CA, 1969.

8.25 Piersol, A. G., “Study of the Interaction of Combined Static and Dynamic Loads,” *J. Sound Vib.*, Vol. 7, No. 3, pp. 319-332, 1968.

8.26 Anon, “Military Standard: Test Requirements for Launch, Upper-Stage, and Space Vehicles,” *MIL-STD-1540C*, 1994.

8.27 Milne, J. S., “General Environmental Verification for STS & ELV Payloads, Subsystems, and Components,” *NASA GSFC Doc. GEVS-SE, Rev. A*, 1996.

8.28 Bement, L. J., and Schimmel, M. L., “A Manual for Pyrotechnic Design, Development and Qualification”, *NASA TM 110172*, June 1995.

8.29 Moening, C. J., “A View of the World of Pyroshock”, *Institute of Environmental Sciences Pyrotechnic Shock Tutorial Program*, 31 ATM, Inst. Envir. Sc., 1985.

8.30 Moening, C. J., “Pyrotechnic Shock Flight Failures”, *Shock and Vibration Bull.*, No. 56, Part 3, pp. 3-28, 1986..

8.31 Anon., “Pyroshock Test Criteria,” *NASA Technical Standard NASA-STD-7003,* May 1999.

9. GENERAL TESTING CONSIDERATIONS

There are many considerations involved in the selection and performance of appropriate dynamic tests for space vehicle hardware including, (a) the purpose of the test, (b) the event(s) simulated by the test, (c) the level of assembly to be tested, (d) the type of simulation used for the test, (e) test fixtures, and (f) the determination of a failure during test. For a few long duration events, such as pre-flight transportation, there is an additional consideration, namely, the possible use of accelerated testing procedures. The type of dynamic tests to be performed and the criteria for the tests are heavily dependent upon these considerations.

9.1 Test Purpose. Dynamic tests are commonly divided into six broad categories [9.1], namely, (a) development tests, (b) qualification tests, (c) acceptance tests, (d) screening tests, (e) statistical reliability tests, and (f) reliability growth tests. Development tests support the design effort and may involve something as simple as determining the dominant resonance frequency of a constituent component of a space vehicle, or a substantially more elaborate test to determine the normal modes and damping of a space vehicle structure for use in analytical models, as discussed in Section 5.1.5. In any case, such tests are too specific to be covered by a general test specification and, hence, are not addressed in this document. Screening, statistical reliability, and reliability growth tests apply to mass-produced hardware. Since space vehicle hardware is rarely mass-produced, they are also omitted from consideration. On the other hand, space vehicles are sometimes constructed from one-of-a-kind hardware, where the purposes of the qualification and acceptance tests must be combined into a single test performed on flight hardware. Such a test is referred to as a "protoflight test".

9.1.1 Qualification Tests. The purpose of a qualification test is to demonstrate with margin that a hardware design is adequate to perform as are required throughout the mission (pre-flight and flight) environmental exposures. It is usually applied to a single item of prototype hardware that will not be flown, and is commonly a contractual requirement where a well documented test specification is involved. Developmental tests are sometimes carried out on prototype hardware to identify and correct design problems before the formal qualification test is performed. Also, qualification test requirements might be based upon a general environmental test specification, e.g., NASA GEVS-SE [9.2]. However, contracts usually allow deviations from the specified test levels and/or durations in general environmental test documents, if it can be established that different test conditions would be more suitable for the given hardware. In any case, the basic purpose of a qualification test requires that the test conditions conservatively simulate the basic characteristics of the anticipated dynamic excitations in the service environments.

In earlier days when test facilities were more limited, it was argued that a dynamic environment for aerospace hardware could be simulated for qualification test purposes in terms of the damaging potential of the environment, without the need for fidelity of the test excitation to the detailed characteristics of the environment [9.3], e.g., the random vibration during liftoff could be simulated with a swept sinusoidal vibration designed to produce the same mechanical damage. Such equivalent damage concepts require the assumption of a specific mode of failure and a damage model to arrive at an appropriate excitation level and duration [9.4]. Since the assumed mode of failure and damage model might be incorrect for the equipment of interest, there is a substantial increase in the risk that the resulting test criteria will severely undertest or overtest the equipment. With the increasing size and flexibility of modern test facilities, the use of equivalent damage concepts to arrive at test criteria is rarely required and is not recommended. Specifically, when feasible, qualification tests should be performed using an excitation that has the same basic characteristics as the dynamic environment of concern, e.g., random vibration environments should be simulated with random vibration excitations, transient environments should be simulated with transient excitations of similar duration, etc.

As previously discussed in Section 8.1.5, the qualification of large space vehicle structures is often accomplished by analysis coupled with static load tests. The analysis procedures used for this approach to the qualification of space vehicle structures, including the use of data from normal mode and static load tests, are detailed in Section 5.1.

9.1.2 Acceptance Tests. An acceptance test is applied to all items of flight hardware, whose design integrity has previously been verified by a qualification test on a prototype item. The goal is to detect workmanship errors and/or material defects in the manufacture and assembly of the hardware, and to demonstrate that the hardware is representative of the qualified design. There are two basic approaches to acceptance testing for dynamic environments. The first approach is to devise a test that will quickly reveal common workmanship errors and/or material defects as determined from prior experience and studies of failure data for similar hardware, independent of the dynamic excitations in the service environments. For example, if a specific type of electrical equipment has a history of malfunctions induced by scrap-wire or poorly soldered wire junctions, then the application of a sinusoidal vibration at the resonance frequencies of wire bundles will quickly reveal such problems and, hence, constitutes a good test excitation even though there may be no sinusoidal vibrations in the service environment. The second and more common approach for space vehicle hardware is to apply an excitation that simulates the dynamic environments anticipated during service, similar to the qualification test, but usually at a less conservative (lower) level and a shorter duration.

9.1.3 Protoflight Tests. A protoflight test is applied to one-of-a-kind flight hardware to meet the goals of both qualification and acceptance testing. For space vehicle hardware, the criteria for such tests are commonly the same as for a qualification test, except the test level and/or duration are reduced to minimize possible wearout damage to the hardware.

9.2 Events Producing Dynamic Excitations. From Section 3, the dynamic excitations experienced by a space vehicle during various pre-flight and flight events, and the basic characteristics of these dynamic excitations, are summarized in Table 9.1. Of course, all the dynamic excitations in Table 9.1 should be predicted and evaluated, but the excitations followed by an asterisk usually determine the test criteria. Note that the excitations followed by a double asterisk (transportation, pogo, resonant burning, meteoroid impacts, and soil penetration) could be the dominant dynamic excitations, if they occur.

9.2.1 Short Duration Events. The events listed in Table 9.1 produce relatively short duration dynamic excitations (i.e., excitations with a duration of less than a few minutes), with three exceptions as follows:

a. The vibration and/or acoustic pressure excitations produced during pre-flight transportation of the vehicle or its constituent hardware.

b. The fluctuating pressure excitation produced by the wind on the launch pad prior to launch.

c. The vibration produced by onboard equipment operations during flight.

The other events in Table 9.1 produce dynamic excitations that are sufficiently short in duration to be simulated in real-time without causing unreasonable test durations, as discussed in Section 7.

TABLE 9.1. Summary of Dynamic Excitations During Various Events.

Event	Source of Dynamic Load	Basic Characteristics of Dynamic Load	Details (Section)
Pre-Flight	Transportation**	Various	3.1
	Seismic loads**	Low frequency mechanical transient	3.2
	Wind on launch pad	Low frequency fluctuating pressure	3.3
Liftoff	Motor ignition overpressure*	Low frequency pressure transient	3.4
	Liftoff release*	Low frequency mechanical transient	3.5
	Engine/motor acoustic noise*	Broadband random acoustic pressure	3.6
Ascent	Wind during ascent	Low freq. random fluctuating pressure	3.3
	Structureborne noise	Broadband random mechanical vibration	3.7
	Aerodynamic noise (including vent noise)*	Broadband random fluctuating pressure and possible periodic pressure	3.8
	Engine/motor thrust transients	Low frequency mechanical transient	3.9
	Thrust vector loads	Low frequency mechanical transient	3.10
	Pogo**	Low freq. periodic mechanical vibration	3.11
	Motor resonant burning**	Mid freq. periodic mechanical vibration	3.12
	Fuel slosh in tanks	Low freq. random fluctuating pressure	3.13
Staging	Stage and fairing separations*	Low frequency mechanical transient	3.14
	Pyrotechnic events*	High frequency mechanical transient	3.15
Free-flight	In-flight operations	Low frequency mechanical transients	3.16
	Onboard equip. operations	Various	3.17
	Meteoroid impacts**	High frequency mechanical transients	3.20
Entry	Wind during entry	Low freq. random fluctuating pressure	3.3
	Aerodynamic noise	Broadband random fluctuating pressure	3.8
	Planetary descent and entry**	Broadband random fluctuating pressure	3.18
	Soil penetration**	Low frequency mechanical transient	3.19

* Usually the dominant excitations for a normal flight.
** Could be the dominant excitations if they occur.

9.2.2 Long Duration Events. The three long duration events in Table 9.1, as listed in Section 9.2.1, may have a duration that is too long to be simulated by a real-time test. Assuming the magnitude of the dynamic excitations produced by the long duration events is less than the magnitude of the maximum excitation produced by flight events, the tests for the dynamic excitations produced by these long duration events might be accelerated using the procedures applied in Section 7.3. Specifically, under appropriate assumptions, the times required to produce equivalent fatigue damage in (a) the dynamic test, and (b) the dynamic environment, are related by

$$T_t = \left(\frac{\sigma_e}{\sigma_t}\right)^b T_e \qquad (9.1)$$

where σ_t and σ_e are the standard deviations of the dynamic excitations during the test and the service environment, respectively, T_t and T_e are the durations of the dynamic excitations during the test and the service environment, respectively, and b is a fatigue-related material constant (see Section 7.1.2). If the dynamic excitations for the test and the environment are defined in terms of autospectra, Equation (9.1) becomes

$$T_t = \left(\frac{G_e(f)}{G_t(f)} \right)^{b/2} T_e \qquad (9.2)$$

Again from Section 7.1.2, values of b = 4 for equipment and b = 8 for load carrying structures are recommended in these relationships, although larger values of b can be used if justified by a careful evaluation of the hardware to be tested.

Equation (9.1) or (9.2) can be used to accelerate a dynamic test simulating a long duration environment under the following important restrictions:

a. The test level for the accelerated vibration and/or acoustic test must never exceed, at any frequency, the maximum expected environment determined in Section 6.

b. The accelerated test should be used only to evaluate the durability of structures where a fatigue damage model applies; no operation or functional performance of the hardware being tested should be required.

9.3 Level of Assembly. From Section 2.3, there are five basic levels of assembly for space vehicle hardware ranging from individual parts to an entire system (space vehicle). Of course, the parts and subassemblies that form a unit (component) will be naturally tested when the component is tested for its anticipated dynamic excitations. Similarly, all components are naturally tested when dynamic tests are performed on the final subsystems and/or system. Nevertheless, because of the long lead times necessary to design and fabricate the parts, subassemblies, components, and subsystems used to produce a system, the hardware items at each level of assembly are usually tested separately to provide confidence that they will function properly at the next level of assembly. However, the types of dynamic excitations of concern from a testing viewpoint are different for different levels of assembly. For example, the lowest resonance frequency for parts and subassemblies is usually well above 50 Hz, meaning they see the low frequency dynamic excitations in Table 9.1 essentially as static loads that are easily simulated using a centrifuge. Also, parts, subassemblies, and components will experience vibration excitations caused by the aeroacoustic excitation of the structures that support them, but because of their relatively small size, usually will not respond to the direct aeroacoustic pressures over their surfaces.

Based upon the above considerations, the dominant dynamic excitations identified in Table 9.1 (those followed by a single asterisk) that are of concern in arriving at dynamic test criteria at each level of assembly are broadly summarized in Table 9.2. It should be emphasized that the list of excitations for each level of assembly in Table 9.2 is very general and might be incomplete in certain situations. For example, a component that has a large surface area, but is light in weight, might be susceptible to substantial dynamic excitation from the direct impingement of acoustic noise over its exterior surface, as well as the aeroacoustic-induced vibration of its supporting structure. Also, the excitations identified with a double asterisk in Table 9.1 are excluded but must be considered if they might occur. The dynamic environment for every system and its constituent elements must be carefully evaluated to establish the excitations that are relevant at each level of assembly.

TABLE 9.2. Dominant Dynamic Loads that Drive Test Criteria Versus Level of Assembly.

Level of Assembly	Dynamic Load Driving Test Criteria	Prediction (Section)
Parts and Subassemblies	1. Vibration produced by engine/motor acoustic noise during liftoff and/or aerodynamic noise during transonic and max q flight. 2. Mechanical transients produced by pyrotechnic events.	5.2 5.3
Unit (Components, Equipment)	1 Mechanical transients produced by stage and fairing separations. 2. Vibration produced by engine/motor acoustic noise during liftoff and/or aerodynamic noise during transonic and max q flight. 3. Mechanical transients produced by pyrotechnic events.	5.1 5.1 5.3
Subsystems	1. Mechanical transients produced by motor ignition overpressure and liftoff release. 2. Engine/motor acoustic pressures. 3. Aerodynamic fluctuating pressures during transonic and/or max q flight. 4. Mechanical transients produced by stage and fairing separations. 5. Mechanical transients produced by pyrotechnic events, if feasible.	5.1 4.3, 4.5 4.4 5.1 5.3
Systems (Vehicles)	1. Pressure transient produced by motor ignition overpressure. 2. Mechanical transient produced by liftoff release. 3. Engine/motor acoustic pressures. 4. Aerodynamic fluctuating pressures during transonic and/or max q flight. 5. Mechanical transients produced by stage and fairing separations. 6. Mechanical transients produced by pyrotechnic events, if feasible.	4.1 5.1 4.3, 4.5 4.4 5.1 5.3

9.4 Types of Simulation. There are certain types of dynamic tests where the test excitation need not resemble the anticipated dynamic excitations during flight. For example, swept-sine excitations are commonly used for development tests performed to determine the basic dynamic characteristics of a test item (see Section 5.1.5). Low frequency swept-sine or dwell-sine tests are sometimes also used in lieu of static loads tests for structural integrity verification (see Section 8.1.5). However, for dynamic environments qualification, acceptance, and protoflight tests of space vehicle hardware, there is a broad consensus that the test excitations should simulate the basic characteristics, as well as the magnitudes and durations, of the dynamic excitations anticipated during flight, as discussed in Section 9.1.1. This means that sine-wave tests should be used to simulate only those flight environments that are approximately periodic in character. A few examples are as follows:

a. Resonant burning of rocket engines/motors, usually during ascent.

b. Vehicle pogo and other limit cycle instabilities of vehicle, usually during ascent.

c. Aeroacoustic instabilities such as payload bay or fairing vent noise during ascent.

d. Periodic excitations due to onboard rotating equipment in payloads during in-flight operations.

Since the above environments are rare, the vast majority of the testing of space vehicle hardware at all levels of assembly (see Table 9.2) should be accomplished using stationary random or transient excitations, i.e., no sine-wave excitations, with the possible exception discussed in Section 9.4.1.

9.4.1 Swept-Sine Excitations to Simulate Transients. Low level sine-wave excitations are commonly used in various types of development tests, as discussed earlier in Section 9.1. There are situations where more intense sine-wave excitations are sometimes used for qualification and protoflight testing of space vehicle hardware, even though the dynamic exicitation being simulated is not periodic. In particular, the liftoff transient due to both the motor ignition overpressure and the liftoff release (see Section 5.1) is often simulated at the subsystem and system assembly level using a swept-sine vibration test [9.2, 9.5 - 9.7] over a frequency range up to about 50 to 100 Hz. The swept-sine excitation is achieved by driving an electrodynamic or hydraulic shaker with an oscillator, where the frequency of the oscillator is increased in a linear or logarithmic manner. The magnitude and sweep rate for the resulting vibration are selected supposedly to cause the hardware response to be similar to the response predicted for the transient. A common procedure to derive such a test is as follows:

a. A shock response spectrum (SRS) for the transient to be simulated is computed using a damping ratio ζ (see Section 2.2.10) that is similar to the anticipated damping ratio of the test item.

b. The magnitude of the SRS at each natural frequency is divided by $Q = 1/(2\zeta)$ to obtain an envelope that defines the peak values for a swept-sine test.

c. The sweep rate for the swept-sine test is selected to cause approximately the same number of vibration cycles at each frequency that is anticipated due to the transient being simulated [9.7]. It should be mentioned that this limitation on the number of vibration cycles at each frequency is sometimes difficult to achieve with a reasonable sweep rate.

d. To avoid overtesting, the envelope of the peak values for the swept-sine test determined in Step b. are often limited to the maximum response values at significant modes of the test item based upon analytical predictions.

The use of a swept-sine excitation to simulate a transient excitation can result in the unique situation of causing a simultaneous undertest and overtest of the hardware. The undertest is due to exciting only one hardware resonance at a time during the sweep-sine test, as opposed to the simultaneous excitation of multiple resonances of the hardware, as would be induced by the transient excitation. The potential overtest is due to applying a larger number of stress cycles to the hardware during the swept-sine test than occurs during the transient excitation. Of course, the amount of overtesting can be reduced by increasing the sweep rate, as detailed in [9.7]. Also, swept-sine excitation is performed closed-loop, whereas direct transient tests currently must usually be performed open-loop. Nevertheless, it is recommended that the practice of using swept-sine tests to simulate low frequency transient excitations for qualification test purposes be phased-out in favor of direct transient tests, as detailed in Section 10.2.

9.4.2 Multiple-Axis Excitations. The dynamic environments for space vehicle hardware are typically multiple-axis, i.e., the excitations occur simultaneously along all three orthogonal axes of the hardware. Acoustic tests naturally simulate a multiple-axis excitation, but shock and vibration test facilities are commonly uniaxial (see Section 10). Multiple axis test facilities designed to simulate low frequency shock and vibration environments (generally below 50 Hz), such as earthquake motions, are widely available [9.8]. Also, multiple-axis vibration test facilities have been developed for higher frequency shock and vibration excitations (up to 2 kHz) [9.9, 9.10]. For space vehicle hardware, however, it is more common to perform shock and vibration tests using machines that apply the excitation sequentially along one axis at a time. The potential error caused by simulating a multiple-axis shock and/or vibration excitation with sequentially applied single-axis excitations is widely debated and the subject of ongoing study [9.11]. Due to the relatively high cost of such facilities, their use for the shock and/or vibration testing of space vehicle hardware is not considered essential at this time. However, if such facilities are available, their use is recommended.

9.5 Test Fixtures. Acoustic tests of space vehicle hardware generally require no special fixtures. However, for almost all shock and vibration tests, a fixture between the test item and the test machine is required because the mounting hole locations on the test item and the test machine table probably do not correspond. For the usual case where the test machine generates rectilinear motion normal to the table surface, a test fixture is also necessary to reorient the test item relative to the table so that vibratory motion can be delivered along the lateral axes of the test item, i.e., the axes parallel to the plane of the test item mounting points. This requires a versatile test fixture between the table and the test item, or perhaps three different test fixtures.

9.5.1 Small Test Items. For test items that are small relative to the test machine table, excitation along the vertical axis of the test item can be applied by attaching the test item to the test machine table through a thin mounting plate with hole patterns appropriate for both the test item and the table. To deliver excitation along the lateral axes of the test item, "L-shaped" test fixtures with side gussets are commonly used, as illustrated in Figure 9.1. Unless designed with great care, such fixtures are likely to have resonances in the test frequency range. In principle, the resulting spectral peaks and valleys due to fixture resonances can be flattened out by the electronic equalization of the test machine table motion (see Section 10.1.1.3), but this is difficult to accomplish if the damping of the fixture is low. The best approach is to design the fixture to have few or, if possible, no resonances in the test frequency range. The design of good shock and vibration test fixtures is an important engineering effort that deserves careful attention [9.3, 9.12, 9.13].

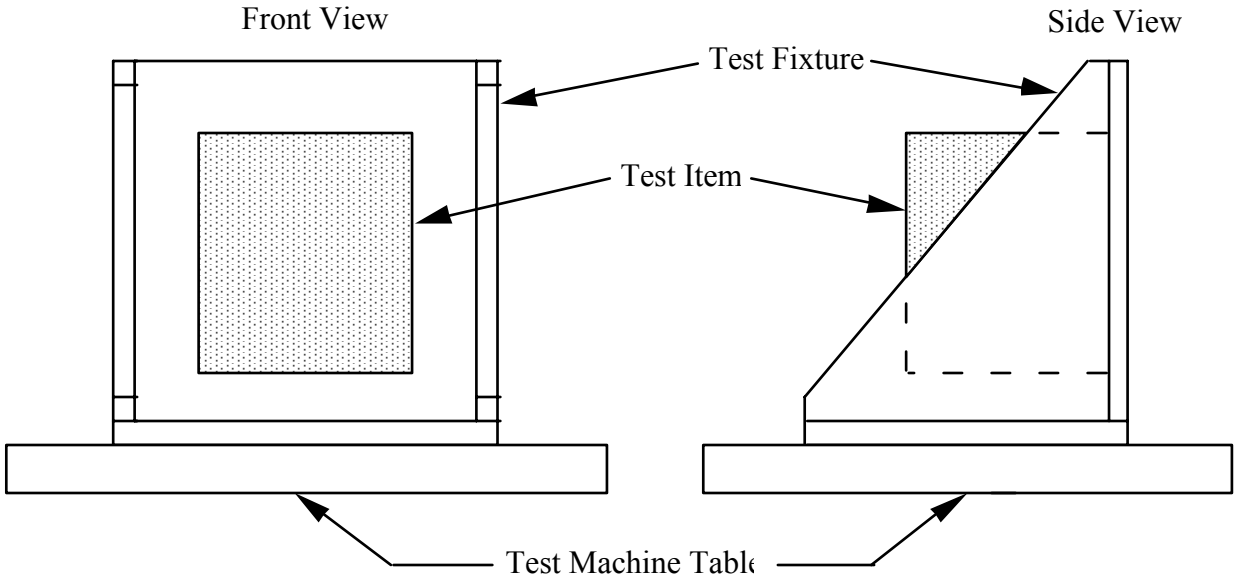

FIGURE 9.1. Typical Fixture for Shock and Vibration Testing of Small Test Items Along their Lateral Axes.

9.5.2 Large Test Items. For test items that are large relative to the test machine table, expansion fixtures that are supported from above to help carry the weight of the test item are often used to apply excitation along the vertical axis, as illustrated in Figure 9.2. Excitation along the lateral axes is commonly achieved by mounting the test item on a horizontal plate driven by the test machine rotated into the horizontal plane, where the plate is separated from the flat opposing surface of a massive block by an oil film or hydrostatic oil bearings, as shown in Figure 9.3. The oil film or hydrostatic bearings provide little shearing restraint, but give great stiffness normal to the surface, the stiffness being distributed uniformly over the complete horizontal area. Accordingly, a relatively light moving plate can be vibrated that has the properties of the massive rigid block in the direction normal to its plane.

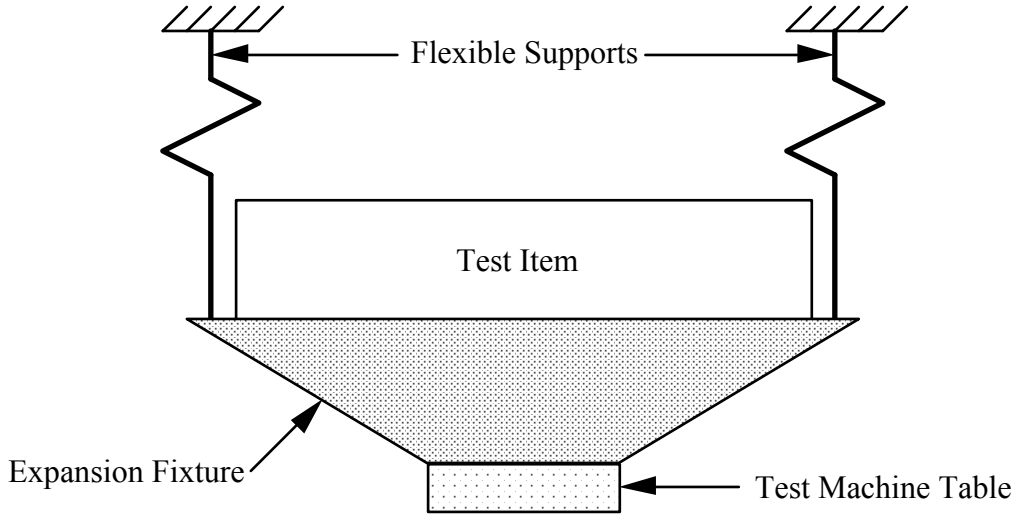

FIGURE 9.2. Typical Fixture for Shock and Vibration Testing of Large Test Items Along their Vertical Axis.

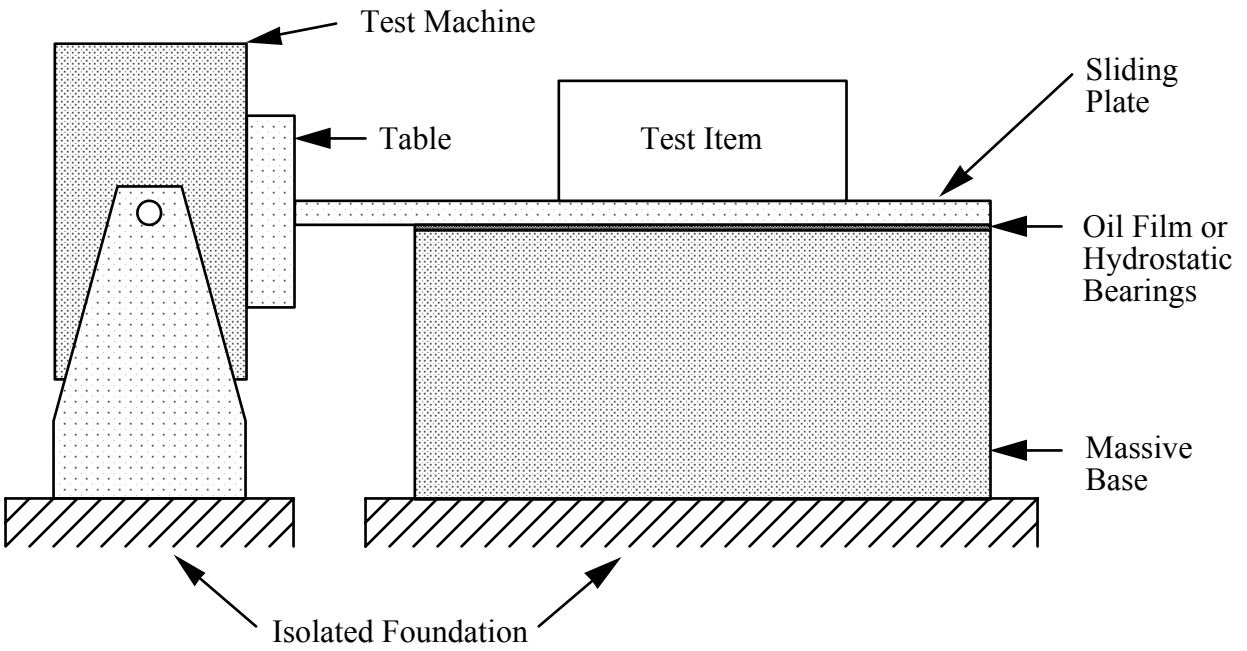

FIGURE 9.3. Typical Fixture for Shock and Vibration Testing of Large Test Items Along their Lateral Axes.

9.6 Determination of Test Failures. In all dynamic tests of space vehicle hardware, it is important to carefully establish what types of hardware malfunctions or deterioration of performance will be considered a failure. This determination depends heavily on the purpose of the test and sometimes the judgments of the customer who is purchasing the hardware. The recommended rules for defining failures as a function of the type of test are summarized in Table 9.3.

Beyond the general definitions in Table 9.3, more specific definitions of what constitutes a test failure must be established and specified for qualification and protoflight tests, including the following:

a. If a fatigue crack forms in the hardware structure that does not propagate to a fracture within the duration of the test, whether the mere existence of a fatigue crack constitutes a failure, or a crack with a specific length is needed to constitute a failure, must be specified.

b. If there is measurable deterioration in the performance of electrical, electronic, and/or optical hardware during the test, the exact degree of deterioration that constitutes a failure must be specified.

TABLE 9.3. General Definition of Failures for Various Types of Tests.

Type of Test	Definition of Failure
Qualification	Any malfunction that is the direct result of a design deficiency only. All malfunctions that are clearly due to a workmanship error or material defect should be repaired and the test should be continued.
Acceptance	Any malfunction that is due to a workmanship error or material defect. Since the hardware has already passed a qualification test prior to acceptance tests, there should be no failures related to a design deficiency.
Protoflight	Any malfunction due to either a design deficiency, or a workmanship error or material defect. However, all malfunctions that are clearly due to a workmanship error or material defect should be repaired and the test should be continued.

9.7 References

9.1 Piersol, A. G., "Test Criteria and Specifications," Ch. 20, *Shock and Vibration Handbook* (Ed: C. M. Harris), 4th ed., McGraw-Hill, NY, 1995.

9.2 Milne, J. S., "General Environmental Verification for STS & ELV Payloads, Subsystems, and Components," *NASA GSFC Doc. GEVS-SE*, Rev. A, 1996.

9.3 Curtis, A. J., Tinling, N. G.,and Abstein, H. T., "Selection and Performance of Vibration Tests," *SVM-8,* Shock and Vibration Info. Analysis Ctr, Arlington, VA , 1972.

9.4 Fackler, W. C., "Equivalence Techniques for Vibration Testing," *SVM-9,* Shock and Vibration Info. Analysis Ctr, Arlington, VA , 1972.

9.5 Barrett, S., "The Development of Sine Vibration Test Requirements for Viking Lander Capsule Components," *Proc. 20th ATM*, *Inst. Envir. Sc.*, pp 77-82, 1974.

9.6 Hine, M. J., "Evaluation of Conservatism in Low Frequency Vibration Test Control," *Proc., 14th Aerospace Testing Sem.*, pp. 223 - 233, 1993.

9.7 Hine, M. J., "Swept Sine Vibration Test Conservatism," *J. Inst. Envir. Sc.*, Vol. XXXVIII, No. 6, pp. 13 - 17, 1995

9.8 Shipway, G. D., and Kana, D. D., "Seismic Qualification of Equipment," Chap. 24 , Pt II, *Shock and Vibration Handbook* (Ed: C. M. Harris), 4th ed., McGraw-Hill, NY, 1995.

9.9 Freeman, M. T., "3-Axis Vibration Test System Simulates Real World," *Test Engrg and Mgt*, Vol. 52, No. 6, pp 10-14, 1990/1991.

9.10 Stroud, R. C., and Hamma, G. A., "Multiexciter and Multiaxis Vibration Exciter Control System," *Sound and Vibration*, Vol. 22, No. 4, pp 18-28, 1988.

9.11 Himelblau, H., Hine, M. J., Frydman, A., and Barrett, P. A., "Effects of Triaxial and Uniaxial Random Excitation on the Vibration Response and Fatigue Damage of Typical Spacecraft Hardware," *Proc. 66th Shock and Vibration Symp.*, Vol. I, pp 15 - 32, 1995.

9.12 Klee, B. J., Kimball, D. V., and Tustin, W., *Vibration and Shock Test Fixture Design,* 2nd ed., Tustin Technical Inst., Santa Barbara, CA, 1994.

9.13 Anon., "Vibration and Shock Test Fixturing", *IEST-RP-DTE013.1*, Institute of Environmental Sciences and Technology, Mount Prospect, IL, 1998

This Page Left Blank Intentionally

10. PERFORMANCE OF TESTS

The facilities and procedures used to perform qualification, acceptance, and protoflight dynamic tests (as defined in Section 9.1) on space vehicle hardware are conveniently divided into five categories, namely, those facilities and procedures appropriate for (a) low frequency vibration tests, (b) low frequency transient tests, (c) high frequency vibration tests, (d) high frequency transient tests, and (e) acoustic tests. Low frequency vibration and transient tests, as well as acoustic tests, are usually performed only on entire space vehicles (payloads) or major subsystems thereof, while high frequency vibration and transient tests are generally performed only on space vehicle components or major subassemblies thereof. The criteria for these various types of tests are detailed in Section 8.

It should be mentioned that the qualification of space vehicles for low frequency dynamic excitations is often accomplished by analytical procedures rather than tests that simulate the anticipated low frequency vibration and transient environments, as discussed in Section 8.1. However, with the introduction of force limiting procedures (see Section 6.5.2), low frequency dynamic tests, as outlined in Sections 10.1 and 10.2, are now more practical and less threatening to flight vehicles.

10.1 Low Frequency Vibration Tests. Referring to Table 4.1, the low frequency vibration environment for space vehicles or major subsystems thereof is due primarily to transportation, wind on the launch pad, atmospheric turbulence and buffet during ascent and entry through the atmosphere, and pogo during ascent. Depending upon the mode of transportation, some periodic excitations may occur in transportation, but the dominant transportation vibration excitations are usually random in character, as are wind, atmospheric turbulence, and buffet excitations. Pogo is periodic, but its occurrence is launch vehicle specific. Hence, a random excitation is usually desirable for low frequency vibration tests. However, the low frequency vibration testing of space vehicle payloads is often accomplished using a swept-sine excitation in order to also envelope the effects of the low frequency transient events, in spite of the technical deficiencies described in Section 9.4.1. Whether a random or sine excitation is used, the upper frequency limit for low frequency vibration tests varies depending upon the details of the specific environments (see Table 3.1), but is usually 100 Hz or less. The lower frequency limit for such tests is often determined by the low-frequency capabilities of the test facility.

10.1.1 Test Facility. There are two types of test facilities that are used to perform low frequency vibration tests on space vehicles and/or major subsystems thereof, namely, (a) electrodynamic vibration test systems and (b) hydraulic vibration test systems.

10.1.1.1 Electrodynamic Vibration Test Systems. An electrodynamic vibration test system consists of an electrodynamic vibration machine (shaker), an amplifier, including a field coil power supply, a signal controller, and one or more acceleration monitoring transducers (control accelerometers), as schematically illustrated in Figure 10.1. The shaker consists of a mounting table for the test item that is rigidly attached to a drive coil armature whose movement is restricted by bearings and flexures to rectilinear motion. The armature is surrounded by a large electromagnetic field coil in the body of the shaker. The field coil power supply delivers the current for the electromagnet (field current), and the amplifier provides the signal to the drive coil (armature signal) that produces the desired motion of the shaker table. The controller creates the armature signal needed to produce the desired shaker table motion by repeatedly comparing the spectrum of the signal(s) from the control accelerometer(s) to a specified reference spectrum and eliminating the discrepancies, as described in Section 10.1.1.3. The controller may further modify the armature signal to achieve force limiting, as discussed in Section 10.1.1.4.

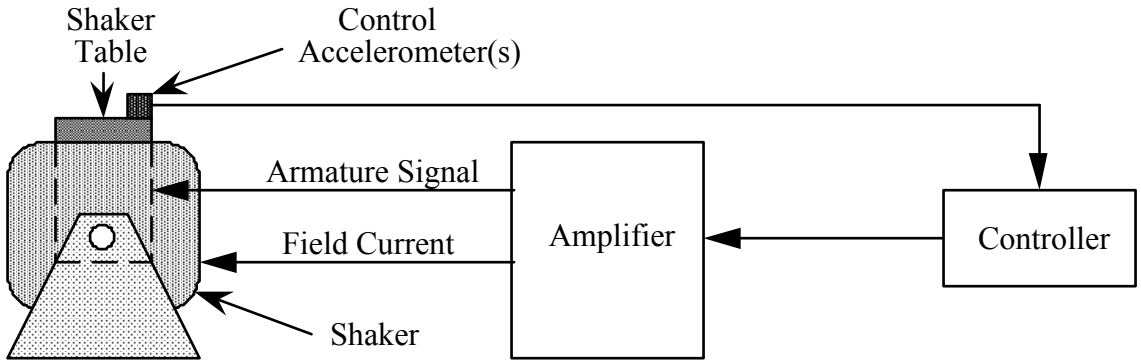

FIGURE 10.1. Diagram of Electrodynamic Vibration Test System.

Most electrodynamic vibration test systems can provide vibration excitations up to 2 kHz with no significant shaker table resonances (table resonances below 2 kHz may occur if the test item and/or its fixture are unusually heavy). The largest systems provide an rms force of about 50,000 lb (222 kN). On the negative side, the maximum displacement of the shaker table is usually limited to 2 inch, (±5 cm), which severely restricts the acceleration that can be delivered at frequencies below 20 Hz. See [10.1] for details on the design features of typical electrodynamic vibration test systems. It should be mentioned that multiple-axis electrodynamic vibration testing systems and controllers have been developed that provide vibration excitations simultaneously along all three orthogonal axes of a test item [10.2, 10.3]. If such a multiple-axis system is available and has an adequate capacity, its use for low frequency vibration tests is recommended.

10.1.1.2 Hydraulic Vibration Test Systems. The latest hydraulic vibration test systems consist of a hydraulic vibration machine (shaker), a source of high pressure fluid flow (hydraulic power supply), an electrical power supply (amplifier), an electrodynamic-controlled two-way valve (valve), a controller, and one or more acceleration monitoring device(s) (control accelerometers), as schematically illustrated in Figure 10.2. The shaker consists of a mounting table for test items that is rigidly attached to a piston whose movement is intended to be restricted to rectilinear motion. The piston is driven up or down by a fluid pressure generated by a two-way valve on a hydraulic power supply, where the valve is driven by a small electrodynamic shaker. An amplifier provides the field current to the valve electrodynamic driver, as well as the armature signal that causes the valve to modulate the fluid flow as required to produce the desired motion of the shaker table. The controller creates the armature signal needed to produce the desired shaker table motion by repeatedly comparing the spectrum of the signal(s) from the control accelrometer(s) to a specified reference spectrum and eliminating discrepancies, described in Section 10.1.1.3. The controller may further modify the armature signal to achieve force limiting, as discussed in Section 10.1.1.4.

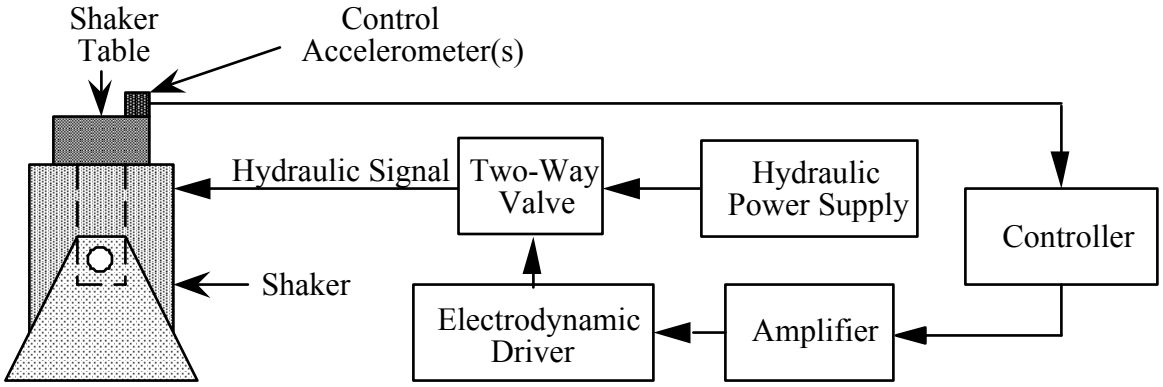

FIGURE 10.2. Diagram of Hydraulic Vibration Test System.

Due to fluid column resonances in the hydraulic lines, most hydraulic vibration test systems can provide vibration excitations up to only about 100 Hz, although higher frequency systems have been developed [10.4]. The largest systems can provide an rms force in excess of 50,000 lb (222 kN). A major advantage of hydraulic vibration test systems is that they provide a better performance than electrodynamic machines at frequencies below 20 Hz, primarily because they can produce large displacements (several inches) and, hence, substantial accelerations at very low frequencies. This fact makes hydraulic vibration test systems desirable for low frequency vibration tests. See [10.1] for details on the design features of typical hydraulic vibration test systems.

It should be mentioned that multiple-axis hydraulic vibration test systems have been developed that provide vibration excitations simultaneously along all three orthogonal axes of a test item at frequencies up to 500 Hz [10.4]. If such a multiple-axis system is available and has an adequate capacity, its use for low frequency vibration tests is recommended.

10.1.1.3 Controller for Vibration Test Systems. For random vibration tests, most modern vibration test machine controllers operate broadly as follows:

a. The desired shaker table motion given in terms of a one-sided autospectrum (see Section 2.2.3) in g^2/Hz is entered into the controller, and is digitized into (N/2) + 1 spectral values (the first value is at zero frequency) separated by a frequency increment of Δf Hz to cover a frequency range from 0 to $(N/2)\Delta f$ Hz.

b. The controller multiplies the desired one-sided autospectrum of the table motion by Δf, computes the square root of the scaled autospectrum to obtain a series of (N/2) + 1 Fourier coefficient magnitudes, denoted by $|X(n\Delta f)|$; n = 0, 1, ..., (N/2), and finally adds on an additional N - 1 redundant Fourier coefficients [10.5] to obtain a two-sided array of N Fourier coefficient magnitudes $|X(n\Delta f)|$; n = 0, 1, ..., N - 1.

c. The controller then assigns a phase $\phi(n\Delta f)$ to each Fourier coefficient magnitude to obtain the complete Fourier coefficients $X(n\Delta f)$; n = 0, 1, ..., N - 1, where the phase is randomly selected from a uniform probability density function bounded by $\pm\pi$, i.e., $p(\phi) = 1/(2\pi)$; $-\pi \le \phi \le \pi$.

d. The Fourier coefficients computed in c. are inverse Fourier transformed using a fast Fourier transform (FFT) algorithm [10.5] to obtain a time history, $x(n\Delta t)$; n = 0, 1, ..., N - 1, called a signal block, where $\Delta t = 1/(N\Delta f)$. The randomly selected phase angles assure that each signal block will have a normal (Gaussian) distribution function [10.5]. The repeatedly computed signal

blocks are appropriately tapered and overlapped to obtain one long time history signal without truncation errors.

e. To correct for the nonuniform frequency response function of the shaker, the controller generated signal is applied at a reduced level (usually 20 dB down from the desired test level) to the shaker, and the autospectrum of the shaker table motion, as measured by the control accelerometer(s), is computed. The computed autospectrum is compared to the desired autospectrum, and the controller-generated Fourier coefficients are altered to make the measured autospectrum agree with the desired autospectrum. This step is repeated as the test level is increased (usually in 6 dB increments) until the desired autospectrum for the shaker table motion is obtained, and is continued to maintain that desired autospectrum.

f. The frequency resolution of the signal generated by the controller, as given by $\Delta f = 1/(N\Delta t)$, is a key parameter that can be selected on most vibration test systems. This frequency resolution selection directly impacts the time required for the controller to recompute a corrected autospectrum, called the "loop time" of the controller.

For sinusoidal vibration tests involving either a dwell or swept-sine excitation [10.6], a sweep oscillator with a feedback amplitude control can be used as the controller. Such an oscillator is often incorporated in the controllers for random vibration tests.

10.1.1.4 Dual Controllers (Motion and Force) for Vibration Test Systems. Most controllers allow a second control signal from a second transducer to be processed and applied to limit the spectral values of the primary control signal. This second control signal can be used to apply a test item response limit on the shaker table motions that would otherwise be produced by the primary input motion specification (see Section 6.5.4), but it can also be used to create an input force limit (see Section 6.5.2). Ideally, the controller will allow a test item response or input force specification, as well as the input motion specification, to be programmed so that the output of a response transducer on the test item or the net output of force transducers between the test item and the shaker table would be used directly to produce the second control signal. However, older controllers, as well as some newer ones, do not allow two specifications with different spectral shapes to be simultaneously programmed. This problem can be circumvented by properly filtering a parallel signal from the controller to make it have the desired spectrum for a test item response limit or input force limit signal, and then using this fabricated signal as the second control signal [10.7]. See [10.8] for details on force limiting procedures.

10.1.2 Test Procedure. Assuming a uniaxial vibration test system is used, the general procedure for performing low frequency vibration tests on space vehicles or major subsystems thereof is as follows:

a. Attach the test item to the vibration test machine (see Section 10.1.1) using an appropriate test fixture (see Section 9.5) and safety-approved procedures so as to provide the desired vibration excitation along one of the three orthogonal axes of the test item. For those cases where the low frequency vibration test specification includes input force limiting (see Section 6.5.2), the test item should be mounted to the fixture through force transducers.

b. Attach one or more control accelerometers to the vibration test fixture at locations near the input to the test item. For vibration excitations below 100 Hz, the vibration test machine table and fixture should be sufficiently rigid to allow one control accelerometer to represent the input motions at all mounting points of the test item, but even in this case, two control accelerometers are often used to provide redundancy. If there is concern over the rigidity of the test machine table and/or the test fixture, two or more control accelerometers mounted near

individual equipment mounting points should be used. In this situation, it is recommended that the average of the outputs of the two or more control accelerometers be used as the control signal. An alternate procedure that is sometimes employed is to use the maximum output of the two or more control accelerometers as the control signal. If test item response limiting is used, the output of an accelerometer mounted at an appropriate response location on the test item should be used as the response control signal. If input force limiting is used, the sum of the outputs of the force transducers should be used as the force control signal.

c. For functional tests (see Section 7.3.2), power-up the test item to function as it would during the exposure to the vibration excitations being simulated.

d. Apply stationary random and/or periodic vibration with the spectral levels (as modified by the test item response or input force limits) determined in Section 6 and the duration determined in Section 7 or 8, plus the margins detailed in Section 8.1.

e. During the test, accomplish the following:

1. record or make an on-line hard copy of the spectrum of the table motion as measured by the control accelerometer, or the average of the control accelerometers if multiple accelerometers are used for control purposes,

2. record or make an on-line hard copy of the spectra for other accelerometers mounted on the test item and/or the force transducers between the test item and the test fixture,

3. monitor or record all relevant functional performance data for the test item, and

4. monitor and verify that the specified spectral levels (at frequencies where test item response or input force limits do not prevail) have been achieved to within ±1.5 dB. If this verification is accomplished using an independent spectrum analyzer, compute the average spectrum for the control accelerometer(s) using the same resolution as the controller for the test machine.

f. Terminate the test as follows:

1. after reaching the end of the test duration determined in Section 7 or 8,

2. when a relevant failure of the test item is identified (see Section 9.6), or

3. when there is an indication that the specified test level is being exceeded.

g. Assuming no failure occurs, reattach the test item to the vibration test machine using an appropriate test fixture and safety-approved procedures so as to provide the vibration excitation along the second of the three orthogonal axes of the test item, and repeat Steps b. through f.

h. Again assuming no failure occurs and three-axis testing is required by the test specification, reattach the test item to the vibration test machine using an appropriate test fixture and safety-approved procedures so as to provide the vibration excitation along the third of the three orthogonal axes of the test item, and repeat Steps b. through f.

If a multiple-axis vibration test facility is available, a customized test procedure must be established that is appropriate for the specific test facility.

10.2 Low Frequency Transient Tests Referring to Table 4.1, low frequency transient tests of space vehicles or major subsystems thereof are usually performed to simulate rocket motor ignition overpressures, liftoff release, engine/motor thrust transients, vector induced loads, stage and fairing separation, and perhaps transportation, seismic, in-flight operations, landing (including soil penetration), and/or onboard equipment induced excitations. The upper frequency limit for such transient tests varies depending on the details of the specific environments (see Table 3.1), but is usually below 100 Hz.

10.2.1 Test Facility. The test facilities used to perform low frequency transient tests on space vehicles and/or major subsystems thereof are the same as described for low frequency vibration tests in Section 10.1.1. Hydraulic systems are often preferred because of their high displacement capability, but large displacement electrodynamic shakers can also be used. However, the controllers for low frequency transient tests are somewhat different from the type of controller described for low frequency vibration tests in Section 10.1.1.3.

10.2.1.1 Controller for Low Frequency Transient Waveform Tests. For those low frequency transient tests that simulate a specified transient waveform, most modern transient test machine controllers operate broadly as follows:

a. The desired shaker table motion given in terms of a waveform x(t) in g versus time in seconds is entered into the controller, and is digitized into N discrete values separated by a time increment of Δt sec to obtain $x(n\Delta t)$; n = 0, 1, 2, ..., (N - 1). See Section 6.6 for details on the computation of an appropriate waveform x(t) for a maximum expected transient environment defined in terms of a Fourier spectrum.

b. The controller applies a low-level version (no more than 20% of full value) of the desired table motion waveform x(t) to the test machine, and the actual table motion waveform y(t) is measured with the control accelerometer and digitized to obtain $y(n\Delta t)$; n = 0, 1, 2, ..., (N - 1).

c. The controller computes the Fourier transforms of the desired and actual table motion waveforms to obtain $X(k\Delta f)$ and $Y(k\Delta f)$; k = 0, 1, 2, ..., (N - 1), and then computes the frequency response function for the transient test machine from $H(k\Delta f) = Y(k\Delta f)/X(k\Delta f)$.

d. The controller then constructs the Fourier transform of a corrected input waveform by computing $X_c(k\Delta f) = X(k\Delta f)/H(k\Delta f)$; k = 0, 1, 2, ..., (N - 1).

e. Finally, the controller computes the inverse Fourier transform of $X_c(n\Delta f)$ to obtain the corrected waveform $x_e(n\Delta t)$, i.e.,

$$x(n\Delta t) = \Delta f \sum_{k=0}^{N-1} X(k\Delta f) \exp(j2\pi kn/N)\ ;\ n = 0, 1, \ldots, (N-1)$$

f. Since the controller is operating open-loop, Steps a through e might be repeated at several reduced levels (i.e., 5%, 10%, and 20% of full level) to identify possible nonlinearities that might influence the full level results.

10.2.1.2 Controller for Low Frequency Swept-Sine Vibration Tests. As discussed later in Section 10.2.3, swept-sine vibration tests are sometimes performed to acquire structural response data that are then used to determine the structural integrity of payloads or major subsystems thereof by analytical computations, or perhaps even to simulate the damaging potential of the transient (see Section 9.4.1), in lieu of an actual low frequency transient test.

For this case, the controller for the vibration test system is the same as described for sinusoidal vibration tests in Section 10.1.1.3.

10.2.2 Test Procedure. Assuming a uniaxial vibration test system (either electrodynamic or hydraulic) is used, the general procedure for performing low frequency transient tests on space vehicles or major subsystems thereof is as follows:

a. Attach the test item to the test machine (see Section 10.1.1) using an appropriate test fixture (see Section 9.5) and safety-approved procedures so as to provide the transient excitation along one of the three orthogonal axes of the test item.

b. Attach a control accelerometer to the test fixture at a location near the input to the test item (two control accelerometers are often used to provide redundancy). For large test items, additional accelerometers should also be mounted on the test item at key locations where limit loads have been defined.

c. For functional tests (see Section 7.3.2), power-up the test item to function as it would during the exposure to the transient events being simulated.

d. Apply a transient excitation with the waveform determined in Section 6 plus the margins detailed in Section 8.1.

e. During the test, accomplish the following:

1. record or make an on-line hard copy of the table motion time history as measured by the control accelerometer,

2. record or make an on-line hard copy of the time histories for all other accelerometers mounted on the test item, and

3. monitor or record all relevant functional performance data for the test item.

f. After the test, accomplish the following:

1. compute the energy spectra (see Section 2.2.9) for all of the accelerometer outputs, and
2. verify that the energy spectral levels for the control accelerometer agree with the energy spectral levels for the specified transient to within ±1.5 dB.

g. Assuming no failure occurs (see Section 9.6), reattach the test item to the test machine using an appropriate test fixture and safety-approved procedures so as to provide the transient excitation along the second of the three orthogonal axes of the test item, and repeat Steps b through f.

h. Again assuming no failure occurs and three-axis testing is required by the test specification, reattach the test item to the test machine using an appropriate test fixture and safety-approved procedures so as to provide the transient excitation along the third of the three orthogonal axes of the test item, and repeat Steps b through f.

If a multiple-axis vibration test facility is available, customized test procedures must be established that are appropriate for the specific test facility.

10.2.3 Alternate Procedure. Instead of performing a direct low frequency transient test on space vehicles or major subsystems thereof, an alternate procedure is to perform a swept-sine vibration test either to (a) determine key structural response characteristics of the test item, and then use analytical techniques to verify the ability of the test item to survive its anticipated low frequency transient environment, or (b) simulate the damaging potential of the transient environment (see Section 9.4.1). It should be mentioned that swept-sine tests are sometimes designed to simultaneously verify the design integrity of the hardware for the low frequency vibration excitations discussed in Section 10.1.

Assuming a uniaxial vibration test system (either electrodynamic or hydraulic) is used, the general procedure for performing swept-sine vibration tests on space vehicles or major subsystems thereof is as follows:

a. Attach the test item to the test machine (see Section 10.1.1) using an appropriate test fixture (see Section 9.5) and safety-approved procedures so as to provide the swept-sine excitation along one of the three orthogonal axes of the test item. For those cases where the swept-sine vibration test specification includes input force limiting, the test item should be mounted to the fixture through force transducers. See Section 6.5.2 for a discussion of dual control techniques to achieve force limiting.

b. Attach a control accelerometer to the test fixture at a location near the input to the test item (two control accelerometers are often used to provide redundancy). For large test items, additional accelerometers should also be mounted on the test item at key locations where limit loads have been defined. One or more of the accelerometers mounted on the test item might be used to impose a test item response limit, as detailed in Section 6.5.3. If force limiting is also used, the sum of the outputs of the force transducers should be used as the force control signal.

c. For functional tests (see Section 7.3.2), power-up the test item to function as it would during the exposure to the transient events being simulated.

d. Apply a swept-sine excitation with the magnitude (as modified by the test item response and/or input force limits) and an appropriate sweep rate, as discussed in Section 9.4.1.

e. During the test, accomplish the following:

1. record or make an on-line hard copy of the swept-sine magnitude versus frequency for the table motion,

2. record or make an on-line hard copy of the time histories for all other accelerometers mounted on the test item, and

3. monitor or record all relevant functional performance data for the test item.

f. Terminate the test as follows:

1. after reaching the end of the test duration determined in Section 8,

2. when a relevant failure of the test item is identified (see Section 9.6), or

3. when there is an indication that the specified test level is being exceeded.

g. After the test, verify that the vibration level versus frequency for the control accelerometer (at frequencies where test item response or input force limits do not prevail) agrees with the specified swept-sine vibration level versus frequency to within ±10 percent.

h. Assuming no failure occurs, reattach the test item to the test machine using an appropriate test fixture and safety-approved procedures so as to provide the swept-sine excitation along the second of the three orthogonal axes of the test item, and repeat Steps b through g.

i. Again assuming no failure occurs and three-axis testing is required by the test specification, reattach the test item to the test machine using an appropriate test fixture and safety-approved procedures so as to provide the swept-sine excitation along the third of the three orthogonal axes of the test item, and repeat Steps b through g.

If a multiple-axis vibration test facility is available, customized test procedures must be established that are appropriate for the specific test facility.

10.3 High Frequency Vibration Tests. Referring to Table 4.1, high frequency vibration tests of space vehicle components or major subassemblies thereof are usually performed to simulate the mounting point vibrations of the vehicle structure produced by the aeroacoustic excitations during liftoff and/or flight through transonic and maximum flight dynamic pressure (max q). These high frequency excitations are typically random in character, but certain other high frequency excitations may occur that are approximately periodic in character, i.e., motor resonant burning (see Section 3.12). From Section 6.5.5, final space vehicle assemblies or large subsystems thereof, with all components and equipment in place, are usually tested for their high frequency dynamic environments using an acoustic test facility, rather than a direct mechanical vibration test facility. An acoustic test provides a more accurate simulation of the high frequency vibration excitations for all components and equipment, and under certain circumstances can be used as a substitute for high frequency vibration tests (see Section 6.5.5). In most cases, however, the individual components of a space vehicle must be individually tested prior to their installation in the vehicle to verify they will function properly during exposure to high frequency vibration excitations. This is accomplished by direct random vibration tests of the individual components or large subassemblies, typically over the frequency range from 20 Hz to 2 kHz.

10.3.1 Test Facility. The most common test facility used to perform high frequency (up to 2 kHz) random vibration tests is an electrodynamic vibration test system, as described in Section 10.1.1.1 and illustrated in Figure 10.1. The controller for the vibration test system is the same as described in Section 10.1.1.3. It should be mentioned that multiple-axis electrodynamic vibration test systems have been developed that provide vibration excitations simultaneous along all three orthogonal axes of a test item at frequencies up to 2 kHz [10.2]. If such a multiple-axis system is available and has an adequate capacity, its use for high frequency vibration tests is recommended.

10.3.2 Test Procedure. The test procedure for high frequency vibration tests is essentially the same as detailed for low frequency vibration tests in Section 10.1.2, except the verification requirement is ± 1.5 dB below 1000 Hz and ± 3 dB from 1000 Hz to 2000 Hz.

10.4 High Frequency Transient Tests. Referring to Table 4.1, high frequency transient tests of space vehicle components or major subassemblies thereof are usually performed to simulate pyroshocks caused by the activation of pyrotechnic devices (see Section 3.15), although the same tests could be used to simulate the shocks produced by high velocity metal-to-metal impacts, if such an environment occurs. From Section 3.15, pyroshocks can be broadly

divided into (a) near-field, (b) mid-field pyroshocks, and (c) far-field pyroshocks, which require different test facilities and procedures. In some cases, space vehicle components can be tested for their pyroshock environments by a laboratory test where the pyrotechnic devices are activated on a prototype of the space vehicle, or a dynamically similar model of the space vehicle or a major subsystem thereof, as discussed in [10.9]. Such laboratory tests on actual space vehicles or dynamically similar models provide highly accurate simulations of the pyroshock environments seen by the space vehicle components. However, they do not allow the convenient addition of a test margin, as discussed in Section 8.3. Hence, the test facilities and procedures discussed here are only those involving laboratory test machines that permit the convenient addition of test margins.

10.4.1 Test Facility. Different types of test facilities are commonly used for near-field, mid-field, and far-field pyroshock tests (see Section 3.15 for distinctions between near-, mid-, and far-field). Hence, they are summarized separately. In all cases, however, it should be emphasized that conventional drop test machines, where the test item is mounted on a table that free-falls to an arresting device, should never be used to simulate pyroshocks. Such machines subject the test item to a large net velocity change, which produces a shock with substantial low frequency energy that can damage basic structures. On the other hand, pyrotechnic devices generally produce little or no net velocity change [10.10, 10.11] and, hence, rarely constitute a threat to basic structures with a first normal mode below 100 Hz.

10.4.1.1 Near-Field Tests. It is recommended that all tests for near-field pyroshock environments be performed using ordnance devices. The most commonly used ordnance facility consists of a flat plate (usually constructed of steel) excited by an explosive material (usually primacord) attached to the edges and/or the bottom side of the plate; edge charges are used to generate motions in the component mounting plane and bottom charges are used to generate motions normal to the component mounting plane. The component to be tested is mounted to the top side of the plate, as illustrated in Figure 10.3. The magnitude of the resulting pyroshock is controlled by the size and location of the explosive material, and the location of the component on the plate. It must be remembered that the operation of an ordnance test facility usually requires a special permit and sometimes a remote test location. See [10.10, 10.11] for details.

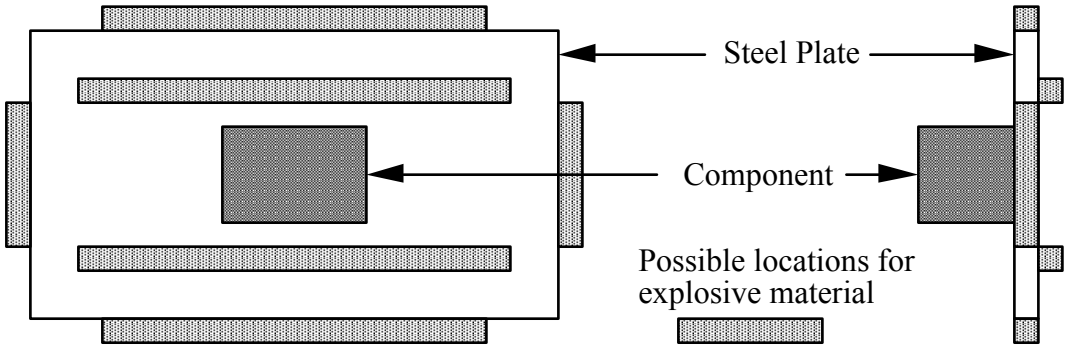

FIGURE 10.3. Diagram of Near-Field Pyrotechnic Test Facility.

10.4.1.2 Mid-Field Tests. A wide range of facilities are available for mid-field pyroshock tests including [10.10, 10.11]

a. bounded impact shock test machines, (10.4.1.2.1)
b. mechanical impact pyroshock (MIPS) simulators, (10.4.1.2.2) and
c. mechanically excited resonant test fixtures, (10.41.2.3).

10.4.1.2.1 Bounded Impact Shock Test Machine. A typical bounded impact shock test machine is illustrated in Figure 10.4. The test item is attached to a spring supported fixture. The shock is delivered to the test item by dropping a heavy table onto a spring attached to a fixture. The excitation terminates when the drop table rebounds off the spring and is captured. The magnitude, duration, and frequency range of the shock can be controlled by the table drop height and weight, and the stiffness and damping of the springs. Such facilities deliver a shock in the form of a decaying sinusoid with a magnitude of up to 5,000 g and a duration of a few cycles with a dominant frequency of up to 2 kHz. See [10.10, 10.11] for details.

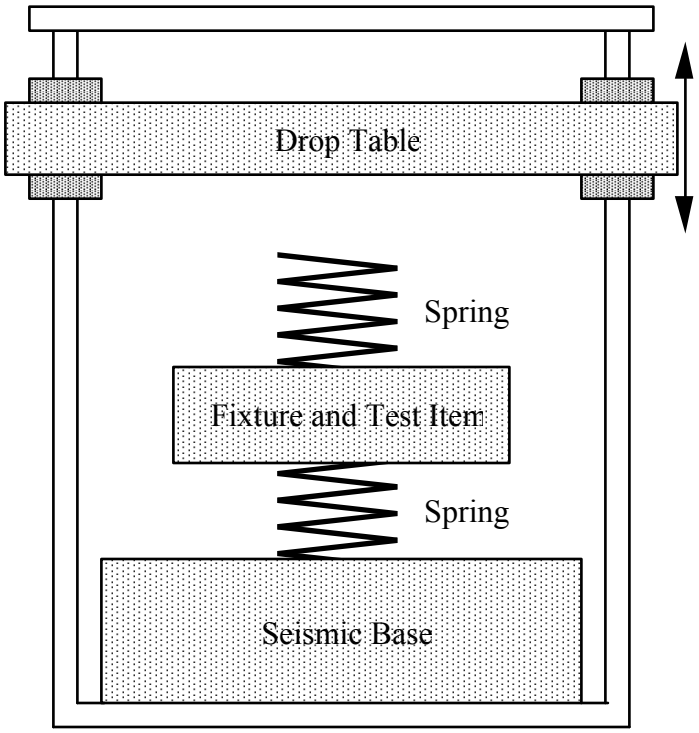

FIGURE 10.4. Diagram of Bounded Impact Shock Test Machine.

10.4.1.2.2 Mechanical Impact Pyroshock (MIPS) Simulators. A typical MIPS simulator is illustrated in Figure 10.5. The test item is mounted to an aluminum plate resting on a foam pad. The shock is delivered to the test item by a pneumatic propelled impactor that strikes the aluminum plate with a high velocity. The magnitude, duration, and frequency range of the shock can be controlled by the impactor velocity, the impactor material, and the impact point on the plate. MIPS simulators deliver a complex shock with a magnitude of up to 5,000 g and a duration of less than 10 ms over a frequency range up to 10 kHz. See [10.10, 10.11] for details.

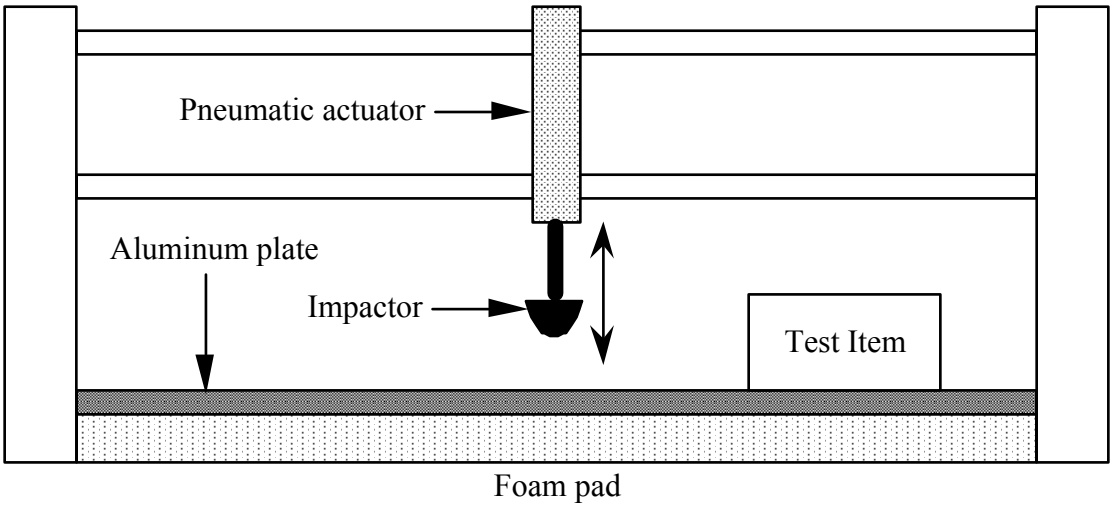

FIGURE 10.5. Diagram of Mechanical Impact Pyroshock (MIPS) Simulator.

10.4.1.2.3 Mechanically Excited Resonant Test Fixtures. Mechanically excited resonant test fixtures operate on the same principle as MIPS simulators (a structure supporting the test item is excited by a mechanical impact), except the structure is designed to respond primarily at its first normal mode frequency. A wide range of structural configurations can be used, including plates and beams excited into either a longitudinal axis response or a bending response. In some cases, the first normal mode frequency of the structure can be varied so that the frequency of the dominant response is tunable. The excitation can be a pneumatic activator, as illustrated in Figure 10.5, or some other device such as a projectile or a pendulum hammer. The magnitude, duration, and frequency range of the shock can be controlled by the velocity and weight of the impact device, the impact point on the resonant structure, and the first normal mode of the resonant structure. Such facilities deliver a shock in the form of a decaying sinusoid with a magnitude of up to 5,000 g and a duration of a few cycles with a dominant frequency of up to 3 kHz. See [10.10, 10.11] for details.

10.4.1.3 Far-Field Tests. All of the testing machines discussed in Section 10.4.1.2 for mid-field pyroshock tests also can be used for far-field tests. Beyond these machines, an electrodynamic vibration test system, as illustrated in Figure 10.1, can be used to simulate far-field pyroshocks with any desired waveform at frequencies up to about 3 kHz. Peak magnitudes of up to about 5,000 g can be achieved, depending on the force rating of the shaker and the weight of the test item and its fixture. If the specific wave form to be simulated is known (see Section 6.6), the controller for this application is the same as discussed for low frequency transient tests in Section 10.2.1.1. However, if the test requirements are specified in terms of a shock response spectrum (see Section 2.2.10), then the test signal is usually constructed using either decaying sine waves or wavelets, as discussed in Section 6.6 and described with sample FORTRAN programs in [10.12].

10.4.2 Test Procedure. The detailed test procedure for near-field pyroshock simulations using ordnance test facilities is dependent on the specific design of the facility and local government regulations related to safety. Similarly, the detailed test procedures for mid-field and far-field pyroshock simulations are dependent on the type of facility used, as outlined in Sections 10.4.1.2 and 10.4.1.3. Nevertheless, the general procedure in all cases is as follows:

a. Attach the test item to the test machine (see Section 10.4.1) using an appropriate test fixture (see Section 9.5) and with safety-approved procedures so as to provide the high frequency transient excitation along one of the three orthogonal axes of the test item.

b. Attach an accelerometer to the test fixture at a location near the input to the test item. For large test items with multiple attachment points, additional accelerometers should be mounted at several of the mounting point locations for the test item to allow the computation of an average input excitation to the test item.

c. For functional tests (see Section 7.3.2), power-up the test item to function as it would during the exposure to the transient events being simulated.

d. Apply the high frequency transient with the wave form or shock response spectrum determined in Section 6, plus the margins detailed in Section 8.3.2. Note that some test facilities (e.g., MIPS tables and ordnance excited plates) may require considerable trial-and-error effort using a simulated test item to achieve the specified SRS for the excitation into the test item.

e. During the test, accomplish the following:

1. record or make an on-line hard copy of the motion time histories measured by the input accelerometers, and

2. monitor or record all relevant functional performance data for the test item.

f. Compute the SRS (see Section 2.10) for all input accelerometer signals.

g. After the test, verify that the SRS levels for the input accelerometer, or the average of multiple input accelerometers, agree with the specified SRS levels to within ±6 dB at or below 3 KHz, and +9/-6 dB above 3 KHz, with the further requirement that at least half of the SRS values at the various natural frequencies exceed the specified SRS levels.

h. Assuming no failure occurs, reattach the test item to the test machine using an appropriate test fixture and safety-approved procedures so as to provide the high frequency transient excitation along the second of the three orthogonal axes of the test item, and repeat Steps b through g.

i. Again assuming no failure occurs and three-axis testing is required by the test specification, reattach the test item to the test machine using an appropriate test fixture and safety-approved procedures so as to provide the high frequency transient excitation along the third of the three orthogonal axes of the test item, and repeat Steps b through g.

Note that some pyroshock test facilities produce substantial off-axis excitations, e.g., ordnance excited panels. If the test facility can be adjusted to produce the specified shock response spectra along all three axes of the test item simultaneously, then this can be accepted as equivalent to a sequential test along all three axes of the test item.

10.5 Acoustic Tests. Acoustic tests of space vehicles or major subsystems thereof are usually performed to simulate the acoustic excitations during liftoff (see Section 3.6), and sometimes the aerodynamic-induced fluctuating pressure excitations during ascent and entry through the atmosphere (see Section 3.8). In both cases, the excitations are random in character, cover a wide frequency range (up to about 10 kHz), and are applied over the exterior

surface area of the space vehicle. It follows that a test that directly simulates these pressure excitations over the exterior surface of the vehicle or a major subsystem thereof is desirable. Such tests are usually performed as a final step in the dynamic testing of a space vehicle, and provide the most accurate simulation of the high frequency vibration environments for all components in the space vehicle (see Section 6.5.5).

10.5.1 Test Facility. The acoustic pressure field during the liftoff of a space vehicle propagates forward over the vehicle structure, while the aerodynamic-induced fluctuating pressure field during ascent and entry convects aft over the vehicle structure. Hence, a facility that generates a propagating pressure field excitation along the longitudinal axis of the vehicle (i.e., a propagating wave test facility) would provide the most accurate simulation. Such propagating wave test facilities have been constructed for special applications, e.g., the Apollo spacecraft [10.13]. Nevertheless, due to the complexity and high cost of large, general purpose propagating wave test facilities, most acoustic tests of space vehicles or major subsystems thereof are performed in large, high intensity acoustic reverberation rooms [10.14]. For space vehicle structures that have a surface exposed to the atmosphere, it is understood that reverberant acoustic noise does not have the same spatial correlation characteristics as the propagating acoustic noise during liftoff or the convecting aerodynamic noise during ascent or entry through the atmosphere [10.15] and, hence, for the same acoustic noise level, the response of the space vehicle structure to the reverberant acoustic noise excitation will be different from the response to the liftoff and flight environments (see Section 5.2.1). Some experimental studies have indicated that this difference in structural responses may be substantial at frequencies below the first normal mode of the structure [10.16 - 10.18], but other studies do not reveal a significant difference [10.19]. In most cases, however, the potential error due to differences in the spatial correlation characteristics of the test and flight environments is ignored as long as an adequate margin is added to the specified 1/3 octave band levels for the test. For payloads enclosed in a fairing or payload bay, acoustic reverberation rooms provide a more accurate simulation since the payload will experience a reverberant acoustic noise excitation during flight. Even in this case, however, the accuracy of the simulation deteriorates at the low frequencies where the pressure field is heavily influenced by the acoustic modes inside the reverberation room versus the fairing or payload bay.

A typical high intensity acoustic reverberation test facility is illustrated in Figure 10.6. The basic element of the facility is a large room with thick walls and a smooth interior surface that provides a high reverberation time (usually about 5 sec) inside the room [10.20]. As a rule of thumb, the volume of the room should be at least ten times the volume of the largest payload to be tested. Random acoustic noise inside the room is usually provided by air modulators, each consisting of a valve on a high pressure air supply where the valve is opened and closed by a small electrodynamic actuator. The acoustic levels inside the room are established by a controller that functions broadly as follows:

a. The desired sound pressure spectrum given in terms of 1/3 octave band sound levels in dB (ref: 20 μPa) is entered into the controller.

b. The controller generates and applies a low-level version (no more than 20% of full value) of an acoustic signal with the desired 1/3 octave band sound levels to the air modulators, and the actual 1/3 octave band sound levels inside the room are measured by two or more control microphones, where the average of the 1/3 octave band sound levels is used as the control signal.

c. The controller determines the discrepancy between the desired and measured 1/3 octave band sound levels in the room, and applies a corrected acoustic signal to the air modulators. This adjustment of the control signal may be made automatically or manually.

d. The above procedure may be repeated as the 1/3 octave band sound levels in the room are brought up to the desired levels to suppress the effects of nonlinearities in the air modulators and/or the acoustic response of the room.

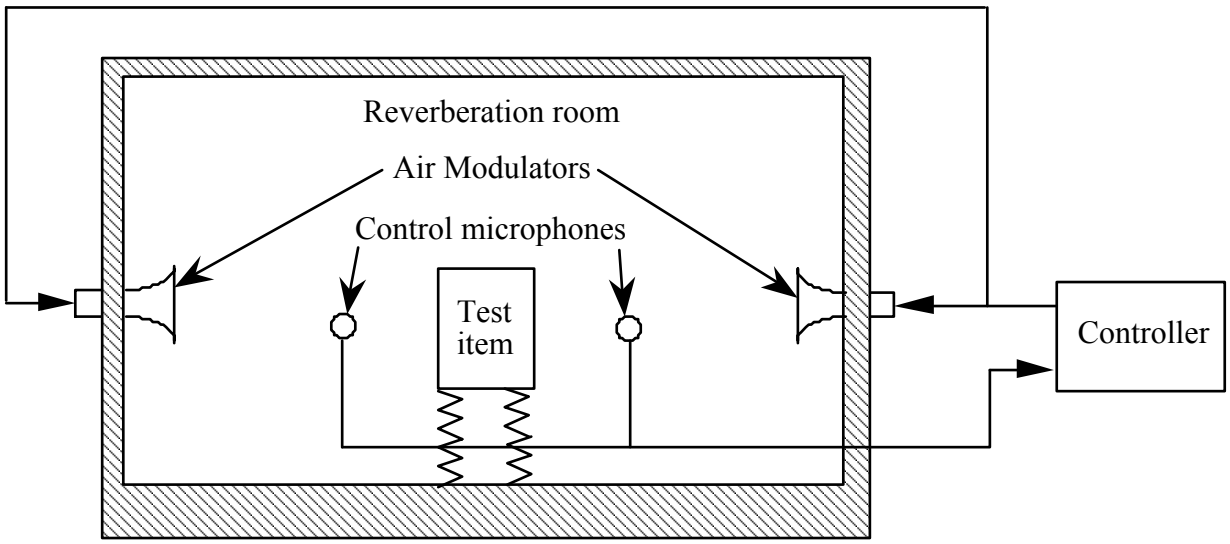

FIGURE 10.6. Diagram of Typical High Intensity Acoustic Reverberation Room.

The sound pressure level that can be generated in a high intensity acoustic reverberation room is dependent on the sound power capabilities of the air modulators and the reverberation time of the room, while the lower frequency limit for the sound pressure levels is determined primarily by the room volume [10.20]. Large test articles can also influence both the high and low frequency capabilities of reverberation rooms. Current high intensity acoustic reverberation rooms designed for the acoustic testing of space vehicles typically have a volume of 200 to 1000 m^3 and produce overall sound pressure levels in an empty room of 150 to 160 dB over a frequency range from about 100 Hz to 10 kHz. See [10.14] for further discussions of acoustic test facilities, [10.20] for general details on the design of high intensity acoustic reverberation rooms, and [10.21] for a specific illustration.

It should be mentioned that any high intensity acoustic reverberation room intended for the acoustic testing of space vehicle hardware should be thoroughly evaluated before any acoustic tests are performed to establish the empty room's acoustic characteristics. Of particular interest are

a. the reverberation time of the room as a function of frequency,
b. the homogeneity of the sound field within the room, and
c. the spacial correlation function of the sound field within the room.

10.5.2 Test Procedure. The general procedure for performing a high intensity acoustic test on a space vehicle or a major subsystem thereof is as follows:

a. Mount the test item in the high intensity acoustic reverberation room (see Section 10.5.1) using an appropriate supporting structure that isolates the test item from the room structure, e.g., support on the floor through a soft mount or from the ceiling using "bungee cord" in a safety-approved manner. The distance between the test item and the nearest surface of the room should be no less than the maximum dimension of the test item.

b. Install the control microphones inside the room near the test item. Two to four control microphones are usually installed at different locations within the room to provide a spatial average of the acoustic levels within the room. In such cases, the average of the 1/3 octave band spectra for the microphone signals is used as the control signal. It is recommended that each control microphone be separated from the test item by a distance at least equal to the maximum dimension of the test item, but never further than one-half the separation distance between the test item and the closest surface of the room.

c. For functional tests (see Section 7.3.2), power-up the test item to function as it would during the exposure to the acoustic excitations being simulated.

d. Apply a stationary random acoustic signal to the air modulators so as to produce 1/3 octave band sound pressure levels in the room with the levels determined in Section 6 and the duration determined in Section 7 or 8, plus the margins detailed in Section 8.2.4, using the average of the 1/3 octave band spectra measured by the control microphones as the control signal. It is wise to approach the specified 1/3 octave band sound pressure levels in discrete steps (e.g., -12 dB, -9 dB, -6 dB, -3 dB, and then the full level) to detect any potential problems in the test setup early.

e. During the test, accomplish the following:

1. record or make an on-line hard copy of the 1/3 octave band spectrum for the sound levels in the room as measured by each control microphone,

2. record or make a hard copy of the spectra for other transducers, such as accelerometers and/or strain gages mounted on the test item,

3. monitor or record all relevant functional performance data for the test item, and

4. verify that the specified 1/3 octave band sound levels have been established to within ± 3 dB for the 1/3 octave bands from 50 Hz to 3 kHz, and ±5 dB (or the best the test facility can provide) for the 1/3 octave bands below 50 Hz and above 3 KHz, using the average of the 1/3 octave band sound levels measured by the control microphones(s).

f. Terminate the test as follows:

1. after reaching the end of the test duration specified in Section 7 or 8.2,
2. when a relevant failure of the test item is identified (see Section 9.5), or
3. when there is an indication that the specified test level is being exceeded.

See [10.14] for further discussions of high intensity acoustic testing practices.

10.6 Alternative Dynamic Tests. Several alternative dynamic testing techniques have been recently developed, primarily in response to the need to make testing “faster, better and cheaper”. While most of these techniques are somewhat abbreviated and involve compromises when compared with the conventional tests they replace, the alternative techniques sometimes offer certain technical advantages, in addition to cost and schedule savings. Two alternative dynamic testing techniques are discussed herein.

10.6.1 Combined Dynamic Tests. A combined dynamic test consists of a structural loads test, an environmental vibration test, a modal test, and sometimes a direct acoustic test all conducted sequentially while the test item is base-mounted on a vibration test machine (a shaker). This sequence of dynamic tests replaces the four individual mechanical tests that are typically conducted in different time frames, at different places, with different personnel, and sometimes with different test hardware. The combined dynamic testing approach can cut test time by a factor of four or more [10.22].

In addition to saving cost and schedule, combined vibration tests are sometimes more realistic than conventional tests. For example, consider a spacecraft vibration test on a shaker. On a shaker, the structural loads are applied at the spacecraft base and reacted through the center-of-gravity, which better simulates the launch loading than does a conventional loads test that involves pulling or pushing on individual structural elements. Similarly, the global modes excited with a base drive may be more representative of those excited by the launch vehicle than are the local modes excited in conventional modal tests when individual structural elements are excited. Also the vibration levels in shaker tests better represent the launch conditions, so that better estimates of damping may be obtained. However, base drive tests can not simulate complex loading configurations, which might result from local loading, such as with a parachute bridle; and conventional translation shaker tests cannot excite purely rotational modes.

10.6.2 Direct Field Acoustic Tests. Small satellite manufacturers may not have convenient access to a reverberant acoustic chamber, such as that used for conventional acoustic tests in the aerospace industry. In the past, they have had to choose between two options: 1. Packing up the satellite and doing a reverberant acoustic test in the facility of a larger company, often a competitor, or 2. Not conducting an acoustic test. Neither of these choices is very attractive, given the risks and time associated with moving a complex flight system and the uncertainties associated with a vibroacoustic analysis. Recently an alternative approach, the direct field acoustic test, has been utilized [10.23, 10.24].

In a direct field acoustic test, the test item is surrounded by a large number of electro-dynamic speakers. The speakers, comprised of an appropriate mix of woofers, mid-ranges, and tweeters, and the associated audio amplifier and control system may be rented or purchased from one of the many concert sound system companies, which also provide the system design, equipment handling, and operator. In a direct field acoustic test, sometimes called an insitu acoustic test, the test item may be located in any convenient area, which will accommodate the high acoustic test levels, without injuring personnel or damaging the facility or test item. Typical locations are a clean room, used for assembly and functional testing, or a vibration test facility. A number of omni-directional microphones, e.g. eight, are placed at various elevations around the satellite about one foot from the surface to monitor the environment. The microphone response is averaged, monitored by a frequency analyzer, and controlled to the reference test spectrum, manually or with a closed loop system.

There are a number of concerns associated with the direct field acoustic test approach. The maximum level which can be achieved with conventional audio equipment is limited, and it is questionable whether acoustic levels high enough to envelop the noisiest launch vehicles can be reliably obtained and controlled. (The first direct field acoustic test of a flight spacecraft had an overall SPL of 137 dB [10.23].) In order to achieve these SPL's with electro-dynamic speakers, it is necessary to position the speakers relatively close to the test item (approximately 4 feet away in the first test), which results in the test item being in the near field of the speakers. With the test item this close to the speakers, the spatial coverage is non-uniform, particularly at the higher frequencies where the speakers are very directional. Also one may question the efficiency of the direct, primarily normally incident waves in exciting the structure, as compared with a reverberant field. There is some evidence that normal incidence sound waves are more efficient in exciting the fundamental modes of a structure, and that conversely a reverberant field is more efficient at high frequencies, above the structure's coincidence frequency. The directionality of the flight environment is also open to question, but grazing incident waves are probably more dominant than normal ones, particularly at the fairing ring frequency where the interior levels are highest.

10.7 References

10.1 Smallwood, D. O., "Vibration Testing Machines", Ch. 25 , *Shock and Vibration Handbook* (Ed: C. M. Harris), 4th ed., McGraw-Hill, NY, 1995.

10.2 Freeman, M. T., "3-Axis Vibration Test System Simulates Real World," *Test Engrg and Mgt*, Vol. 52, No. 6, pp 10-14, Dec. 1990/Jan. 1991.

10.3 Stroud, R. C., and Hamma, G. A., "Multiexciter and Multiaxis Vibration Exciter Control Systems," *Sound and Vibration*, Vol. 22, No. 4, pp 18-28, 1988.

10.4 Hamma, G. A., Stroud, R. C., Underwood, M. A., Woyski, W. B., Tauscher, R. C., and Cappel, K. L.,"A Review of Multiaxis/Multiexciter Vibration Technology," *Sound and Vibration Mag.,* Vol. 30, No. 4, pp 20-27, Apr. 1996.

10.5 Bendat, J. S., and Piersol, A. G., *Random Data: Analysis and Measurement Procedures*, 3rd ed., Wiley, 2000.

10.6 Piersol, A. G., "Test Criteria and Specifications," Ch. 20, *Shock and Vibration Handbook* (Ed: C. M. Harris), 4th ed., McGraw-Hill, NY, 1995.

10.7 Worth, D. B., "A Method for Implementing Force-Limited Vibration Control," *J., Inst. Envir. Sc.*, Vol. XL, No. 4, pp. 34-41, 1997.

10.8 Scharton, T. D., "Force Limited Vibration Testing Monograph," *NASA Reference Publication RP-1403*, 1997.

10.9 Anon., "Pyroshock Test Criteria," *NASA Technical Standard NASA-STD-P010,* August 15, 1997.

10.10 Anon., "Pyroshock Testing Techniques," *IEST-RP-DTE032.1,* Institute of Environmental Sciences and Technology, Mount Prospect, IL., 2000.

10.11 Davie, N. T., and Bateman, V. I., "Pyroshock Testing," Ch. 26, Pt II, *Shock and Vibration Handbook* (Ed: C. M. Harris), 4th ed., McGraw-Hill, NY, 1995.

10.12 Nelson, D. B., "Parameter Specification for Shaker Shock Waveform Synthesis - Damped Sines and Wavelets," *Proc. 66th Shock and Vibration Symp.,* Vol. III, pp 151 - 193, 1989.

10.13 Wren, R. J., Dorland, W. D., and Eldred, K. M., "Concept, Design, and Performance of the Spacecraft Acoustic Laboratory," *Shock and Vibration Bull.,* No. 37, Pt 5, pp 25-54, Jan. 1968.

10.14 Lee, Y. A., and Lee, A. L., "High Intensity Acoustic Tests - Recommended Practice 2.0," *Proc., 44th ATM, Inst. Envir. Sc.*, pp. 152 - 164, 1998.

10.15 Hughes, W.O., McNelis, A.M., and Himelblau, H., "Investigation of Acoustic Fields for the Cassini Spacecraft: Reverberant Versus Launch Environments", AIAA-99-1985, 5th AIAA/CEAS Aeroacoustics Conference and Exhibit, Bellevue, WA, May 1999.

10.16 Wilby, J. F., and Piersol, A. G., "Analytical Prediction of Aerospace Vehicle Vibration Environments," *ASME Paper 81-DET-29*, 1981.

10.17 Barnoski, R. L., et al, "Summary of Random Vibration Prediction Procedures," *NASA CR-1302*, p. 66, 1969.

10.18 Bradford, L., and Manning, J. E., "Acoustic Blanket Effect on Payload Acoustic Environment," *Proc., 42nd ATM, Inst. Envir. Sc.*, pp. 244 - 253, 1996.

10.19 Cap, J. S., "A Comparison of the Response of a Captive Carried Store to Both Reverberant and Progressive Wave Acoustic Excitation," *Proc., 66th Shock and Vibration Symp.*, Vol. I, pp 277 - 286, Oct./Nov. 1995.

10.20 Hodgson, M., and Warnock, A. C. C., "Noise in Rooms," Ch. 7, *Noise and Vibration Control Engineering* (Ed: L. L. Beranek and I. L. Ver), Wiley, NY, 1992.

10.21 Rogers, J. D., and Hendrick, D. M., "Sandia National Laboratories' New High Level Acoustic Test Facility," *Proc.36th ATM*, *Inst. Envir. Sc.,* pp 574 - 579, Apr. 1990.

10.22 Vujcich, M. and Scharton, T., "Combined Loads, Vibration, and Modal Testing of the QuikSCAT Spacecraft", Paper 1999-01-5551 presented at 1999 SAE World Aviation Congress, San Francisco, CA, Oct. 20, 1999.

10.23 Anthony, D., Scharton, T., and Leccese, A., "Direct Acoustic Test of QuikSCAT Spacecraft", Paper 1999-01-5550 presented at 1999 SAE World Aviation Congress, San Francisco, CA, Oct. 20, 1999.

10. 24 Larkin, P., "Direct, Near Field Acoustic Testing", Paper 1999-01-5553 presented at 1999 SAE World Aviation Congress, San Francisco, CA, Oct. 20, 1999.